Towards Molecular Systems Capable of Self-Assembly on Gold Surfaces: Synthesis and Characterisation of Ruthenium and Osmium Based Terpyridine Complexes

by Stefania Tasca

A Thesis presented to Dublin City University

for the

Degree of Doctor of Philosophy

under the supervision of Professor Johannes G. Vos

School of Chemical Sciences

Dublin City University

2005

Dedicated to my parents Lucia and Giuseppe

and my sister Simona

Authors Declaration

I hereby certify that this material, which I now submit for assessment on the programme of study leading to the award of Doctor of Philosophy by research and thesis, is entirely my own work and has not been taken from work of others, save and to the extent that such work has been cited within the text of my work.

Signed: Stefania Tasca

Stefania Tasca

Student I.D. No.: 52150941

Date: 17 Novembre 2005

Abstract

The synthesis, spectroscopic and electrochemical characterisation of Ru(II) and Os(II) mononuclear complexes are described. Special attention is paid to the synthesis of a new series of terpyridine complexes capable of self-assembled on gold surfaces such as pyridine or thiol group.

Chapter 1 is an introductory chapter in that the basic concepts regarding Ru(II) polypyridyl chemistry are introduced and explained. The parent complex $[Ru(bpy)_3]^{2+}$ is examined along with its photochemical and photophysical properties. The replacement of a bpy ligand with terpyridine is discussed, as are several examples of terpyridine systems investigated in the last few years.

Chapter 2 introduces the instrumental methods and the synthetic procedures used in the preparation of all the Ru(II) and Os(II) complexes, including the synthesis of the ligands. The synthesis and purification of starting and reference materials used throughout the thesis are discussed.

Having introduced Ru(II) and Os(II) complexes in the opening chapter, Chapter 3 takes a practical look at the various synthetic strategies used to synthesise such complexes. The prototypes $[Ru(tpy)_2]^{2+}$ and $[Os(tpy)_2]^{2+}$ are examined along with their synthesis and ^{1}H-NMR measurements. The synthesis and the ^{1}H-NMR spectra of all the Ru(II) and Os(II) complexes investigated in this thesis are compared to the archetypes before mentioned.

Starting from the basic complexes $[Ru(tpy)_2]^{2+}$ and $[Os(tpy)_2]^{2+}$, photophysical and electrochemical properties are described in Chapter 4. The absorption and emission properties of the complexes investigated are described and compared to those of the two prototypes $[Ru(tpy)_2]^{2+}$ and $[Os(tpy)_2]^{2+}$.

Chapter 5, takes a practical look at the various synthetic strategies attempted to synthesise Ru(II) and Os(II) terpyridine complexes with thiol group substituents. Suzuki coupling reactions used to attempt these syntheses are described. Finally, the synthesis and purification of starting and reference materials used for the Suzuki coupling reactions are discussed.

Results of the work undertaken are summarised with suggestions on further possible research directions in Chapter 6.

Finally three appendices are included in this thesis. In the first appendix the ^{1}H-NMR spectra of the ligands and all the complexes are reported. The second appendix is a literature survey which synopsises the last five years scientific papers on metal terpyridine complexes. The third appendix shows oral presentations and posters made during the course of the research.

Acknowledgements

I would like to thank all those people who helped me throughout this thesis.

My best supporters, the three most important people in my life: *Lucia*, ("Lucy"), *Giuseppe* ("Pirata") and *Simona* ("the sweetest daughter").

My supervisor: *Han* for giving me the possibility to work in his lab. Three years in Ireland, helped me to learn not only about chemistry, but also about life.

To the Italian corner:

Marco, (the brother I never had), first flat mate and great friend, who helped me so much from my first month in Dublin. *Eze* (one day, we will laugh about it!) and *Enrico* ("big eyes") for the great time spent together in "Dùblin" (la città delle arance") and for supporting me during my bad days! *Andrea Balducci* from Pennabilli, one of the nicest people ever met, always ready to go out for a couple of Irish pints!

To the people passed in the HVRG:

Fiona L., my lab mate, who was always looked after me, I never feel lost with her! *Noel O'Boyle*, even if I could not understand a word from his strong Ballina's accent, he has been always so patient with me. *Claire*, who gave me the possibility to know Dundulk and what is an Irish family. *Johan*, my favourite Swedish guy, when are we going for skiing? *Bill*, "the vinegar man", we started together and we had the best laugh, especially in Holland! *Tony*, "where is the chocolate?".the swetest guy ever. *Mohamed,* always smiled and encouraged me "Take it easy, Stefania!" *Fiona F.*, the last Post Doc in the group who was still eating with PhD students! *Lynda*, the little one, always so happy and in a good mood, thanks God I met you, I will miss you! *Roby and Eric,* good guys, but I would never go to a concert with you! *Johnny*, always so nice CD and cinema expert! Finally, thanks to *Shane* ("Ta cha!") and *Yann* ("the ferm guy") and *Ger* (best Italian speaker ever!) for supporting me during my writing.

To my Irish friends outside DCU:

Dervla, first Irish person I met: a wonderful woman. If I'm in Ireland it's because of you and because of Howth.

My ex-flat mates, *Caroline* (alias Demi) and *Christine S.* (alias Dido), for being my Irish family for two wonderful years and for still being very good friends, I will miss you! *Christine O.* (alias Aguilera), to help me so much especially at the very beginning; *Eileen*, for all the deep conversations we had about life, I enjoyed it! My flatmate *Gillian*, a perfect person to share a flat with, the little one, *Sinead*, always so enthusiastic! With you, never a fight!

To my Italian friends:

Simona, the best sister ever! *Fabrizio* and *Simone*, I'll be always there for you. *Polly*, my best friend, thanks to be so good to me. *Richi*, I don't know how many mails and how many travels together. *Carlo* and *Mile*, see you in Rome the 29th!. My favourite and only cousin *Christian* (alias Totti) for being so present during these three years.

To the technicians, in DCU:

Firstly the two brothers: *Mick* and *Maurice*, *Ambrose* (I finished in DCU, are you happy, aren't you?) *Damian*, *Vinnie*, *John*, and the two girls, *Veronica* and *Ann*. Without you this thesis would not have been possible. Special thanks to *Julie*, who helped me to solve so many practical problems.

Outside of college

Finally I would like to thank S.U.S.A.N.A. European project for the financial support. Special thanks to all the people involve in S.U.S.A.N.A. project, in particular to *Anthony D'Aleo*, University of Amsterdam and *Jeroen van Heyst*, University of Bonn for the collaboration at my thesis and to everyone in the group for the great experience we shared all around Europe!

Table of Contents

Table of Contents

Abbreviations and Symbols

Bpy	2,2' - bipyridine
BuLi	butyl lithium
$CHCl_3$	chloroform
CHN	carbon, hydrogen, nitrogen analysis
CH_3CN	acetonitrile
CT	charge transfer
CV	cyclic voltammetry
DMF	dimethylformamide
DMSO	dimethylsulphoxide
Et_3N	triethylamine
EtOAc	ethyl acetate
EtOH	ethanol
Fc/Fc^+	ferrocene/ferricinium redox couple
GS	ground state
H_2L1	2,6-bis-([1,2,4]triazol-3-yl)pyridine
H_2L2	2,6-bis-(5-phenyl-[1,2,4]triazol-3-yl)pyridine
H_2L3	2,6-bis-([1,2,3,4]tetrazol-5-yl)pyridine
HOMO	highest occupied molecular orbital
ic	internal conversion
isc	intersystem crossing
k_f	fluorescence rate costant
k_p	phosphorescence rate costant
λ	absorption wavelength
λ_{em}	emission wavelength
L	ligand
LC	ligand centred
LMCT	ligand to metal charge transfer
LUMO	lowest occupied molecular orbital

Mass Spec	mass spectroscopy
MC	metal centred
MeOH	methanol
^{1}MLCT	singlet metal to ligand charge transfer
^{3}MLCT	triplet metal to ligand charge transfer
m/z	mass to charge ratio (MS)
NMR	nuclear magnetic spectroscopy
(py)	pyridine
(py-tpy)	4'(pyrid-4"'-yl) 2,2'; 6', 2" - terpyridine
TLC	thin layer chromatography
(tpy)	2,2'; 6', 2" - terpyridine
(tpy-ph-Br)	4'(4-bromo-phenyl) 2,2'; 6', 2" - terpyridine
(tpy-ph-SH)	4'–(4"'–mercaptophenyl)-2,2': 6',2" - terpyridine
(tpy-ph-ph-SH)	[4'–(4"'–mercaptophenyl) benzene]-2,2': 6', 2" - terpyridine
[tpy-$(ph)_2$-SCH_3]	[4'-(4"'-methylmercaptophenyl)benzene]-2,2':6',2" - terpyridine
UV/Vis	ultraviolet/visible

Chapter 1

Introduction

This Chapter introduces the principles of supramolecular systems, with special emphasis on their photophysics and intercomponent transfer processes such as optical electron transfer, photoinduced electron transfer and energy transfer. Examples of such processes are discussed in some detail for terpyridine complexes. An introduction of self-assembled monolayers is also presented.

1 Introduction

1.1 Molecular electronics: "Supramolecular chemistry"

Whereas the 20th century is generally regarded as the era of the silicon revolution and of micro-scale electronics, the 21st century is becoming known as the nano-age. One of the most important challenges in modern technology is the need to decrease, in the field of electronics, sizes of devices and components. Molecular or nanoscale building blocks are hundreds of time smaller than the smallest features that may be attained using present semiconductor technology and identical individual molecules and particles may be massively produced. As microelectronic devices approach their technological and physical limits[1], molecular electronics, i.e., the information technology at the molecular-scale, becomes more and more investigated and envisioned as a promising candidate for the nanoelectronics of the future[2].

Originally, the term "supramolecular" was used for multicomponent systems, where molecular components were held together by weak intramolecular forces such as hydrogen bonds, electrostatic or host-guest interaction, and donor acceptor interactions. Inter- and intramolecular non- covalent interactions are very important for biological processes such as highly selective catalytic reactions and information storage[3][4]. Different non – covalent interactions are present in proteins, giving them their specific structures. DNA represents one of the most famous examples, where the self-recognition of the complementary base – pairs by hydrogen bonding leads to the self – assembly of the double helix. Now it is possible to generalise the definition of supramolecular systems, to include systems in which molecular units are covalently bound, but where the intercomponent forces would only have a structural role and would not change the essential individual component properties[5]. Molecules constructed of units, which do not have well defined properties, are simply defined as large molecules. What differentiates a supramolecule from a large molecule is the presence of additional features in the assembling[6]. Using this definition, the properties of a supramolecule would not be a simple superposition of those of the component molecules but they will possess new processes, which can include energy and

electron transfer or complexation of new species. Taking transition metal complexes as building blocks, it is possible to govern the direction of electronic energy transfer in supramolecular arrays and design and synthesise artificial supramolecular systems that act as photochemical molecular devices, which may perform a variety of useful functions[4].

An example of electronic energy transfer in polynuclear metal complexes may be observed in the exploitation of light harvesting: the "antenna effect". An artificial antenna may be described as a multicomponent system (see Figure 1.1) in which several molecular components absorb the incident light and channel the excitation energy to a common acceptor component.

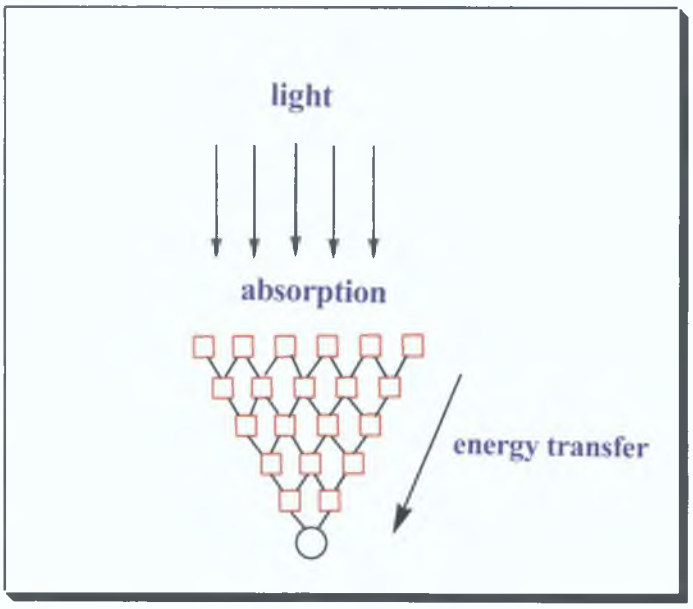

Figure 1.1: Schematic representation of an artificial antenna for light harvesting

Toward the development of artificial antenna systems based on transition metal complexes, one trend noticed is the assembly of large numbers of molecular components in more or less statistical ways. For example photon-harvesting polymers are being developed in which rapid energy migration among chromophoric groups is observed under certain conditions. Recent development in the field of classic polynuclear complexes have shown that synthetic control of the position of the various components in the supramolecular array may be used to create a gradient for energy transfer in a predetermined direction[7][8][9].

Cyano-bridged complexes of d^6 metals have been used in the design of some simple antenna systems. An example is the trinuclear complex shown below in Figure 1.2.

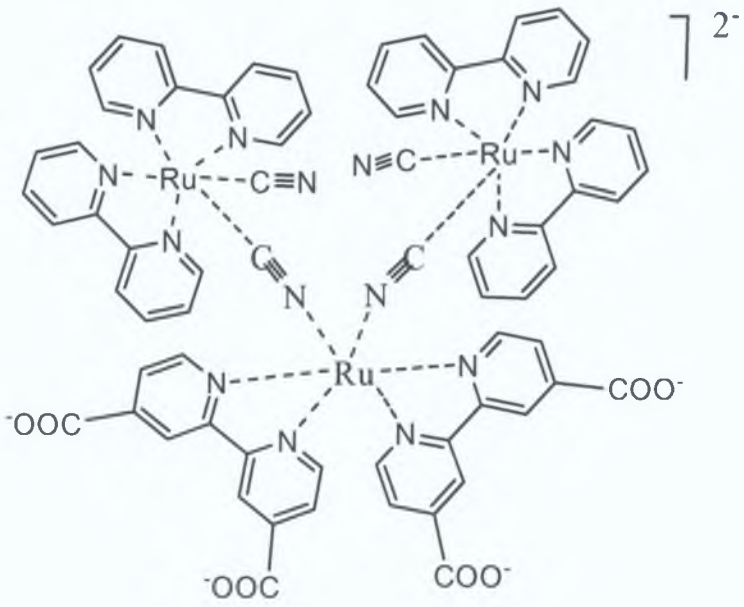

Figure 1.2: An example of an antenna made of a trinuclear compound[8]

In this system, because of the combined effects of the N-bonded bridging cyanides and the carboxylate groups on the ligands, the lowest energy excited state is that of the central unit. Light energy absorbed by the peripheral units is efficiently funnelled to the central metal, as demonstrated by emission measurements [10]. These type of antennas have proven useful in a practical system for conversion of solar energy into electricity[10][11][12].

Today many synthetic supramolecular systems are known[13][14]. The resulting compounds are expected to reveal new chemical and physical as well as biological properties. Starting from biomimetic systems, the concept was extended to "molecular machines" and supramolecular polymers[15]. Among the approaches to supramolecular polymers is the use of self complementary multiple hydrogen bonding units that are characterised by increased stability compared to single hydrogen bonds[16][17][18][19]. Supramolecular assemblies and fully reversible polymers have already been prepared in the past.

Another type of interaction, which has been used extensively in supramolecular chemistry, is metal coordination. In particular, chelating ligands are of interest, since they allow the construction of defined supramolecular architectures and possess an increased stability compared to hydrogen bonding.

Besides bi-pyridines, terpyridines have been utilized extensively. Terpyridine – ruthenium complexes of the type $[Ru(tpy)_2]X_2$ (where X = Cl^-, ClO_4^-, PF_6^-) are already well-known[20]. A main characteristic is the strength of the metal-ligand coordinative bond in these complexes. With many transition metal ions in low oxidation states a bis-complex is formed, with pseudo octahedral coordination at the metal centre. The stability of this type of complex can be explained by a strong metal – ligand (d-π*) back donation. The common hexacoordination geometry leads to a strong chelate effect being present in such complexes. The distorted octahedral coordination geometry has been investigated in detail by X-ray structure analysis[21]. A variety of terpyridines, functionalised at different positions, has been prepared over the past years, in particular, the most common functionalisation procedures used 4'-functionalised terpyridine, that are versatile building blocks for supramolecular assemblies and polymers.

1.2 Molecular switches: photochemical and photophysical behaviour

The assembly of metal centres covalently linked in supramolecular structures has been object of several investigations in the last few years[22][23][24][25][26][27]. Metal complexes are suitable as molecular switches [28] by virtue of electronic properties associated with the metal centre[29]. In particular the study of the luminescence and redox properties of transition metal complexes is of great interest for a variety of fundamental and practical reasons. In recent years, it has been realised that the energy and the information properties carried by photons will more likely be exploited by photoinduced processes in suitably designed supramolecular multicomponent systems rather than in intermolecular photoreactions[7][8b][30].

On going from mononuclear to dinuclear and polynuclear systems, as expected the photochemical and photophysical behaviour is expected and found to be more complex and interesting for two principal reasons:

1 - The properties of each metal containing subunit may undergo perturbations upon incorporation into the multicomponent system.

2 - A number of new processes involving different metal-containing units may take place in the polynuclear complex.

There are three possible functions that may be performed by molecular device: photoinduced electron transfer, electronic energy transfer and photoinduced structural change.

A suitable choice of components is shown in Figure 1.3.

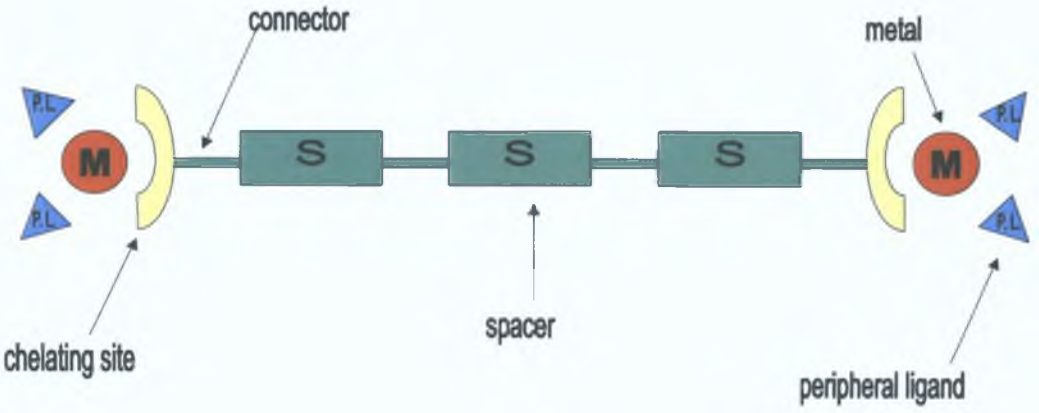

Figure 1.3: example of dinuclear metal complexes

Metal centre, peripheral ligands (acceptor and donor ligands) and bridging ligands (multi chelating site to connect dinuclear systems) lead to the possibility of controlling the overall structure (geometry, electronic interaction and distance between the chromophores) and also allow the occurrence of interesting and useful photoinduced processes such electronic charge, charge separation, etc.

Figure 1.3 described an example of a dinuclear system, where:

- M is the metal, ruthenium or osmium.
- P.L. (peripheral ligand) are bpy or terpyridine.
- S is the spacer , saturated or conjugated molecules.
- Connector is a single or double bond.
- Chelating site is bpy or terpyridine.

1.3 Bonding and excited states properties of Ruthenium (II) polypyridyl complexes

In the last few years, it has been found that transition metal complexes containing aromatic ligands such as 2,2'-bipyridine (bpy), 1,10-phenanthroline (phen), or their derivatives are attractive candidates for excited state electron-transfer processes [31-35]. The complexes have an octahedral structure and may be obtained with a variety of transition metal ions.

Among the numerous luminescent transition - metal complexes, Ruthenium (II)-based polypiridyl chromophores are the most commonly studied because they usually exhibit fairly strong luminescence in the visible region also the photo physical properties are relatively easily tuned by simply modifying the coordinated or ancillary ligands. These compounds have the advantage of being relatively stable with respect to photodecomposition. Compared to organic molecules, coordination compounds of transition metals exhibit a variety of electronically excited state types[36][37][38][39][40]. In particular, complexes of the $[Ru(bpy)_3]^{2+}$ family have been widely studied and used in covalent linked multicomponent systems because of their chemical stability, redox properties, excited state reactivity, luminescence emission and excited state lifetime. For these complexes, it is possible to assign the molecular orbitals as predominantly localised on either metal or ligands, as a consequence it may be easier to classify the molecular orbitals as the excited states of the metal centre complexes. The molecular orbitals involved in the electronic transitions for Ruthenium (II) complexes with octahedral symmetry are:

- Strongly bonding, ligand centred σ_L orbitals.
- Bonding, ligand centred π_L orbitals.
- Metal centred essentially π_M (t_{2g}), predominantly d orbitals.
- Antibonding σ_M^* (e_g) metal centred, predominantly d orbitals.
- Ligand centred antibonding π_L^* orbitals.
- Strongly antibonding, metal centred σ_M^* orbitals.

A molecular orbital diagram of the energy levels of the principal orbitals involved in the electronic transitions for an octahedral complex of Ru (II), is shown in Figure 1.4 (M = metal, L = ligand).

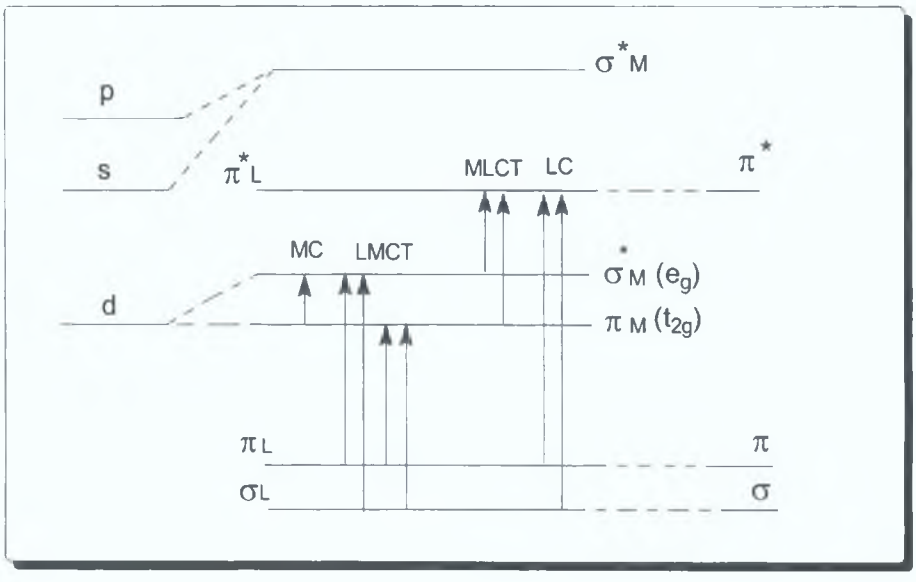

Figure 1.4: Schematic of molecular orbitals and electronic transitions involved for an octahedral transition metal complex (M = metal, L = ligand)

The variety of excited state types, photochemical and photo physical behaviour[37][39], exhibited by coordination compounds is clearly related to the nature of these molecular systems. The assignment of the various bands that appear in the absorption spectra of transition metal complexes is often difficult, as the absorption spectra reflect the complexity of the electronic structure of the molecules. Using the diagram in Figure 1.4 it is possible to classify the electronic transitions according to the localization of the molecular orbitals involved. The diagram in Figure 1.4 shows the three possible types of electronic transitions, which may occur in the configuration state for an octahedral metal complex [31].

Ruthenium (II) is a stable d^6 species and forms octahedral coordination complexes with a diamagnetic t_{2g}^6 electronic configuration. Ru (II) compounds can be oxidised (removal of a metal-localised electron) or reduced (addition of an electron in a ligand π^* orbital). The electronic transitions shown in the molecular orbitals diagram for a octahedral metal complex are:

- Transitions localised on the ligand, LC, electron moves from orbital π_L to π_L^* are equivalent to that observed for the free ligand.
- Transitions localised on the metal, MC, electron moves from orbital of type $\pi_M (t_{2g})$ to orbitals of type $\sigma_M^* (e_g)$.
- LMCT transitions, from ligand to metal charge transfer, the electron passes from a ligand-based orbital to a metal–based one: π_L to $\pi_M (t_{2g})$.
- MLCT transitions, metal to ligand charge transfer, the electron moves from an orbital metal- based to one that is ligand-based: $\pi_M (t_{2g})$ to π_L^*.

All excited states may have singlet or triplet multiplicity. It is important to note however that for ruthenium complexes, spin orbit coupling causes singlet-triplet mixing in the MC and MLCT excited states[32][33][44][45]. Other types of transitions not shown in Figure 1.4 are also possible, but less frequently encountered; those from a metal-centred orbital to a solvent orbital, charge-transfer to solvent, CTTS, or between two orbitals predominantly localised on different ligands of the same metal centre, ligand-to-ligand charge transfer and LLCT. The chemical and physical properties of these excited states have been also object of several studies [35][36][46][47].

1.4 Electronically excited states as redox reactants

Electronically excited states are excellent reactants for redox processes. It is known that an excited state formed by light absorption, is a high energy, unstable species which must undergo some deactivation (see Figure 1.5). The first step of any photochemical and photophysical process is the absorption of a photon by a molecule. Excited state deactivation may occur via disappearance of the original molecule (photochemical reaction, constant k_p), with emission of light (luminescence, constant k_L), degradation of the excess energy into heat (radiationless deactivation, constant k_d) and interaction with species in the solution (quenching process).

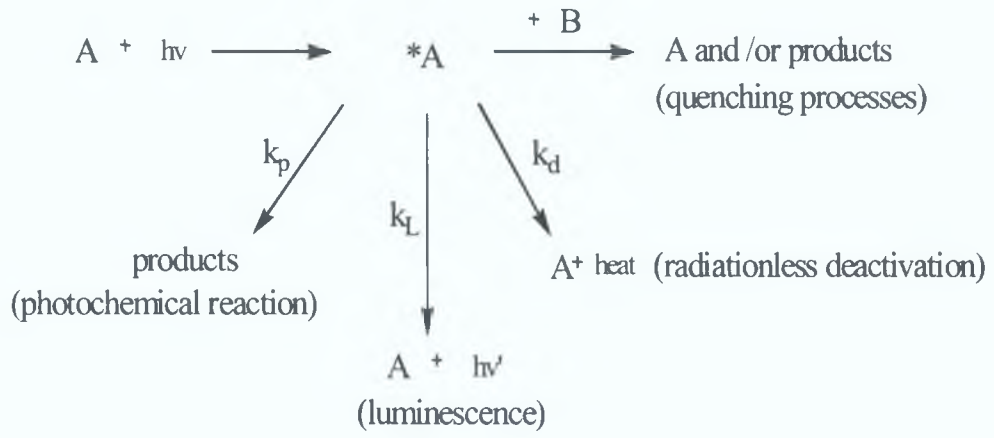

Figure 1.5: Deactivated processes of an electronically excited molecule

The probability of light absorption is correlated to the characteristics of the states involved and in particular to their spin state. Transition from the ground state to excited states having the same spin value are allowed and give rise to intense bands, whereas transitions to excited states of different spin value are forbidden and may hardly be observed in the absorption spectra. For most molecules the ground state is a singlet and the lowest excited state is a triplet that can not be directly populated by light absorption but may be obtained from deactivation of upper excited states. As shown in Figure 1.6, three typical states are involved in a photochemical process: ground state, excited singlet state and excited triplet state. The process of emission of light (luminescence) is called fluorescence (rate constant, k_f) or phosphorescence (rate constant, k_p) depending on whether the excited state has the same or different spin compare to the ground state. Radiationless deactivation is called internal conversion when it occurs between states of the same spin (rate constant, k_{ic}) and intersystem crossing when it occurs between states of different spin (rate constant, k_{isc}). Finally, fluorescence and internal conversion are spin allowed steps, whereas phosphorescence and intersystem crossing are spin forbidden steps.

Each intramolecular decay step is characterised by its own rate constant and each excited state is characterised by its lifetime,

$$\tau = 1 / \sum_i k_I \qquad [0]$$

where k_i, is the first order rate constant for a generic unimolecular process that causes the disappearance of the excited state[48][49].

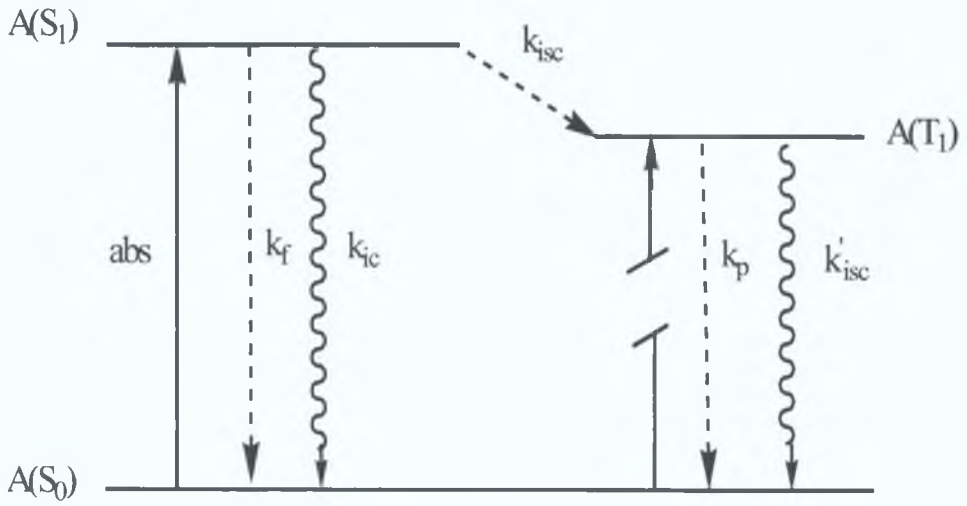

Fig.1.6: Jablonski diagram showing the different deactivation processes

If a process does not involve interactions with other molecules it is called intramolecular process. When the intramolecular deactivation steps are not too fast, for example when the lifetime of the excited state is sufficiently long, the excited molecules have a chance to meet a molecule of another solute, B (see Figure 1.7) and eventually to undergo a quenching process in a bimolecular process. Even when high quencher concentrations are used only those excited states that have lifetimes longer than 10^9 s may be involved in encounters with other solute molecules [48b][49b]. For transition metal complexes the only excited state that may be involved in bimolecular processes is usually the lowest spin-forbidden excited state, but even these states are often too short-lived owing to their high reactivities, lack of rigidity and strong spin-orbit coupling. Once an excited state is involved in an encounter with another molecule, different processes may occur depending on the nature of the interaction (Figure. 1.7).

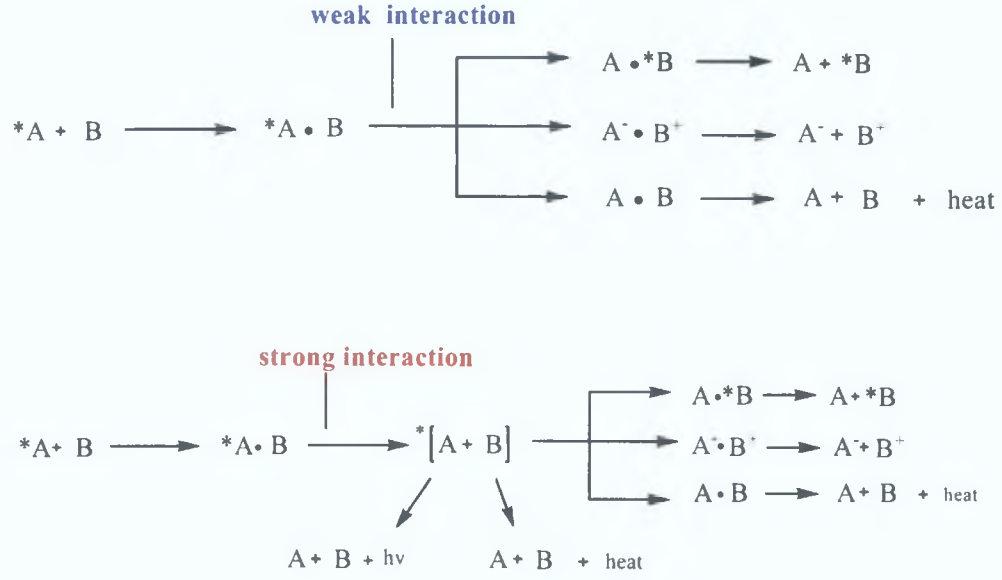

Fig.1.7: Schematic diagram of the possible interactions between excited state and a quencher

Weak interaction may lead to energy transfer via an exchange mechanism, to electron transfer or to simple deactivation of the excited state, catalysed in some way by the quencher. Strong interactions lead to the formation of new chemical species which may undergo radiative or non-radiative deactivation, or may also lead to energy or electron transfer as well as to other kinds of chemical reactions. When the excited state and / or the reaction partner are transition metal complexes and the solvent is a polar solvent, the interaction is generally weak.

The most important bimolecular processes are energy transfer and electron transfer[48b][49b][50][51]; with the latter process involving either oxidation or reduction of the excited state:

$$A + B \longrightarrow A^+ + B^- \quad \text{energy transfer} \qquad [1]$$

$$*A + B \xrightarrow{k_{en}} A + *B \quad \text{energy transfer} \qquad [2]$$

$$*A + B \xrightarrow{k_{ox}} A^+ + B^- \quad \text{oxidative electron transfer} \qquad [3]$$

$$*A + B \xrightarrow{k_{red}} A^- + B^+ \quad \text{reductive electron transfer} \qquad [4]$$

From the energy point of view, the only difference between reactions [1] and [2] is that the excited state reactant of [2] possesses some additional energy with respect to the ground state reactant of [1]. The excited states have extra free-energy content, which is approximately equal to E^{o-o}. The ability of the excited state to intervene in energy transfer processes is related to this energy, E^{o-o}. For the electron transfer processes, the relevant thermodynamic parameters are the oxidation (equation [3]) and reduction (equation [4]) potentials of the $^{*}A/A^{+}$ and $*A/A^{-}$ couples. Because of the higher energy content, an excited state is stronger reductant and stronger oxidant than the corresponding ground state. To a first approximation, the redox potentials for the excited state molecule can be given as:

$$E(A^{+} / A) = E(A^{+} / A) - E^{o-o}(*A / A) \quad [5]$$

$$E(*A / A^{-}) = E(A / A^{-}) + E^{o-o}(*A / A) \quad [6]$$

The redox reactions of electronically excited states can be used for three fundamental types of applications schematically represented in Figure 1.8.

- Photocatalysis
- Conversion of light into chemical energy
- Conversion of chemical energy into light (chemiluminescence)

When light is used as a reactant and:

$$A+hv \longrightarrow *A$$

$$*A+B \longrightarrow A^{+} + B^{-}$$

type (a) and (b) are the two possible pathways for electron transfer reactions.

(a) Photocatalysis

The tendency of excited states to undergo redox processes is used to obtain products for catalytic purposes, otherwise that would have been obtained with much lower efficiency by a thermal reactions. The scheme corresponds to an exergonic dark reaction which is slow for kinetic reasons (high activation energy).

Upon light excitation, the reductant A is transformed into the much stronger reductant *A, so that the reaction between *A and B is much more exergonic than the reaction between A and B. Since the activation energy generally decreases with increasing exergonicity, the reaction involving the excited state will be much faster than that involving the ground state. In a system of this kind light is simply used to overcome a kinetic barrier and plays the role of a catalyst.

(b) Conversion of light into chemical energy

The conversion of light into chemical energy is an example of photochemical transformation of lower energy reactants into higher energy products.

In the case of a dark reaction, the scheme is:

$$A + B \longrightarrow A^{+} + B^{-} \qquad [1]$$

This process can not take place because of thermodynamic reasons. Light excitation causes the formation of *A and if

*A is a much stronger reductant than A, resulting in the reaction:

$$*A + B \longrightarrow A^{+} + B^{-} \qquad [3]$$

becomes thermodynamically allowed. Light favours reaction [3] over reaction [1] and in such process a fraction of light energy is converted into the chemical energy of the products. The converted energy is released when A^{+} and B^{-} undergo the back electron transfer reaction leading to A + B.

(c) Chemiluminescence

In electron transfer reactions, light may also be involved as a product (chemiluminescence reactions), for example in the conversion of chemical energy into light. The process may be schematically represented as in Figure 1.8 (c), which differs from the other two systems (a) and (b) because the energy content of the product of reaction [1] is not only higher than that of its starting materials, but also than that of starting materials of reaction [3]. In such case, the reaction [1] can not be driven thermally or photochemically. However when A^{+} and B^{-} can be prepared in some other way (for example, electrochemically) and are mixed, their electron transfer reaction can lead either to A + B, with complete dissipation of

the excess free energy into heat, or to *A + B with dissipation of a smaller amount of energy. In the latter case *A can undergo radiative deactivation (luminescence) so that in this reaction a fraction of the available chemical energy is converted into light energy. The chemiluminescent process may be considered as the reverse of a photochemical process:

$$A + B \xrightarrow[\text{chemiluminescence}]{+h\nu} A^+ + B^- \rightleftharpoons A^+ + B^- \qquad [7]$$

and the equilibrium represented by equation [7] may be displaced from left to right or from right to left, depending on the energetic situation described in Figure 1.8 (a) or (b).

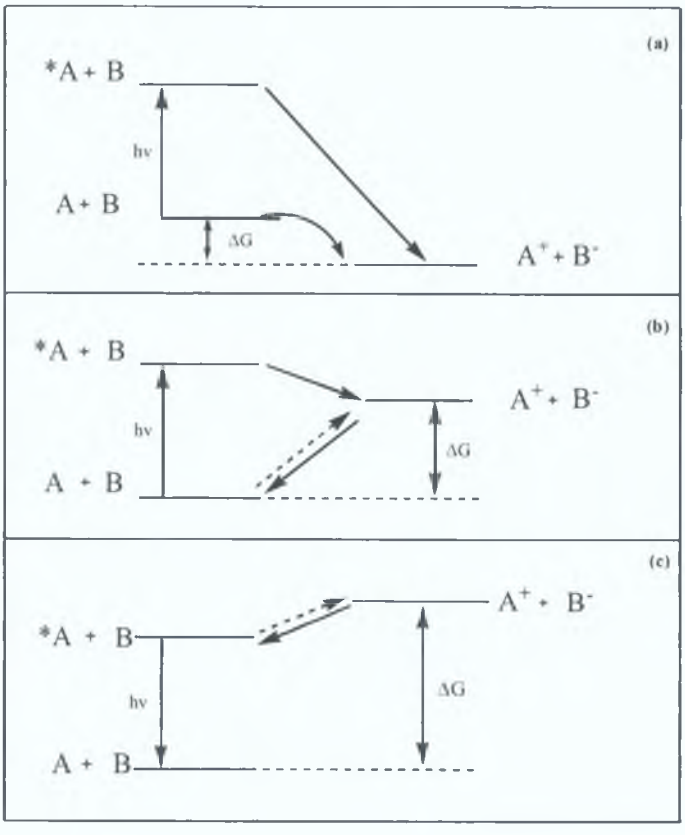

Figure 1.8: Schematic diagram of the three types of applications of excited states electron-transfer processes, (a) photocatalysis, (b) conversion of light into chemical energy, (c) chemiluminescence

To be a useful redox reactant for solar energy conversion, an excited state should meet several specific requirements[48][49]:

- Have a reasonably high energy content, but at the same time excitation with a low energy excitation wavelength.
- Be formed with high efficiency upon light absorption, regardless of the excitation wavelength.
- Have a sufficiently long lifetime.
- Should not be strongly distorted with respect to the ground state.
- Be a good oxidant and/or reductant.
- Be stable towards photodecomposition.

Moreover, the resulting oxidation and reduction products should themselves be good oxidants and reductants respectively and they should be stable towards side reactions. Many of these requirements are more easily met by transition metal complexes than by organic molecules or simple metal ions. For example metal ions do not exhibit intense absorption bands in the visible region and their lowest excited states often lie at very low energy and are strongly distorted and short-lived. The lowest spin-allowed excited state in organic molecules may often be reached only with high energy photons and are usually rather short-lived, while the lowest spin forbidden excited state which is long-lived, may be obtained only via singlet absorption sometimes with low efficiency. Transition metal complexes of metals of the second and third transition rows with suitable organic ligands exhibit intense charge transfer bands in the visible region; moreover, their lowest excited states are undistorted because they involve promotion of an electron to a delocalised π^* orbital[48][49][50][51]. They can be populated efficiently because of the spin orbit coupling induced by the heavy metal atom and can still be sufficiently long-lived to be involved in bimolecular processes. Another important advantage of transition metal complexes is the presence of redox sites on both the metal and the ligands, which offers additional redox possibilities not available for either simple metal ions or organic molecules.

1.5 Photophysical properties of polypyridine complexes

The reactions that play the most important role in the connection between chemistry and light are the electron and energy transfer reactions. Ru (II) polypyridine complexes have contributed greatly to the development of the understanding of such reactions. To understand the photophysical properties of ruthenium polypiridyl complexes, the prototype $[Ru(bpy)_3]^{2+}$ complex will be considered as a representative example. In Figure 1.9 is shown the Jablonski diagram for $[Ru(bpy)_3]^{2+}$, with the states involved in the photochemical process.

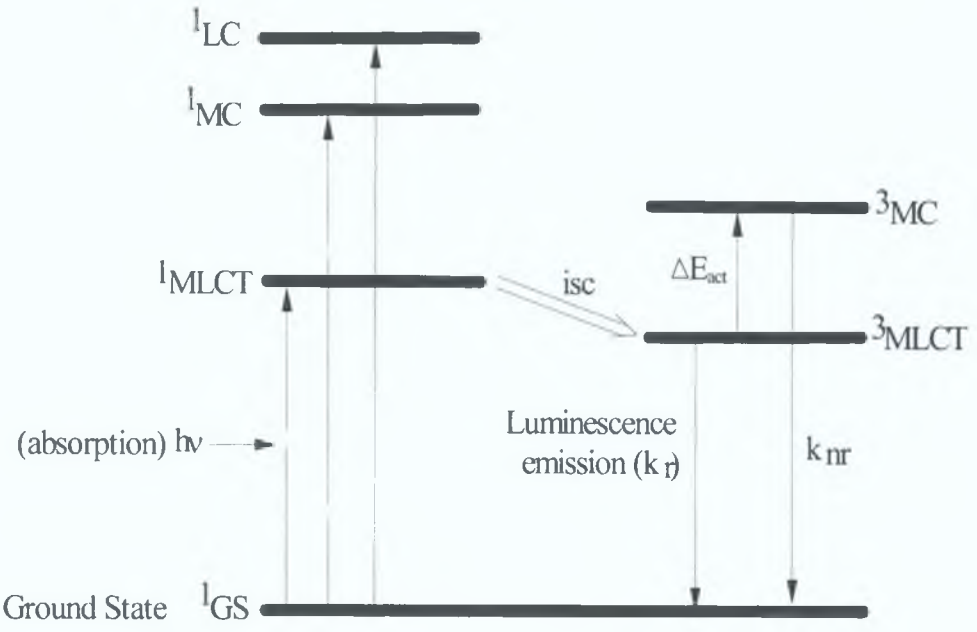

Fig.1.9: Molecular orbital diagram of the energy levels of the principal orbitals and transitions which occur for an octahedral complex of Ru (II)

The three bipyridyl ligands of $[Ru(bpy)_3]^{2+}$, contain σ-donor orbitals localised on the nitrogen atoms and π-donor and π^* acceptor orbital, delocalised on the aromatic rings. The ligand- centred π^* orbitals are lower in energy than the metal-centred $\sigma^*(e_g)$ orbitals. When $[Ru(bpy)_3]^{2+}$ absorbs the energy of an incident light beam, an electron from the ground state orbital (π_M) of ruthenium is promoted to a ligand orbital (π_L^*) localised on one of the bipyridyl rings, resulting in a MLCT excited state. The excited state can be represented as:

$$[Ru^{II}(bpy)_3]^{2+} + h\nu \rightarrow [Ru^{III}(bpy)_2(bpy^{-\bullet})]^{2+*} \qquad [8]$$

The other important excited states are metal centred (MC) excited state, between π_M and σ_M^* orbitals, and ligand-centred excited state (LC), between π_L and π_L^* orbitals. The relative ordering of these excited states, together with the possible radiative, non-radiative and deactivation pathways are shown in Figure 1.9. The singlet state ^{1}MLCT has a very short lifetime and converts into a triplet excited state (^{3}MLCT) by fast intersystem crossing. This is a spin forbidden transition but is made possible by spin orbit coupling. Electronically excited molecules may return to the ground state by their emission from the triplet state to the ground state (k_r) or by radiationless deactivation to the ground state (k_{nr}). The symmetry and spin of the molecule govern the deactivation process. When the emission is a spin allowed process, it is called fluorescence. When the process is spin forbidden, it is called phosphorescence. This latter process is the most common type of radiative decay for our compounds.

Another important deactivating pathway for Ru(II) type metal complexes is population of the metal centred (^{3}MC) excited state, resulting in either radiationless deactivation or a thermally activated decomposition of complex or non-radiative decay. Radiative or radiationless processes don't cause any chemical change in the light absorbing molecule and can therefore be classified as photophysical processes. These transitions are responsible for the absorption and emission of spectral patterns in complexes. It is important to consider that the excited states energy ordering is sensitive to the type of ligands and to the nature of the metal centre. For example, the lowest excited state for the complexes $[Ru(bpy)_3]^{2+}$ and $[Os(bpy)_3]^{2+}$, is MLCT, whereas for $[Ru(bpy)_3]^{3+}$ and $[Os(bpy)_3]^{3+}$, is LMCT[46]. Other complications arise from the energy splitting between the spin states, for example singlet and triplet state. In the case of the orbital configuration, for the MC and LC excited states, the energy splitting is very large, whereas for the CT states the energy splitting is smaller.

1.6 ^{3}MLCT-^{3}MC interactions

In d^6 transition metal complexes the MC excited states are strongly distorted compared with the ground state geometry. This causes fast radiationless deactivation which prevents luminescence from occurring and precludes the

participation of the excited state in bimolecular processes. LMCT excited states behave in the same way. By contrast, the LC and MLCT excited states, being relatively undistorted, undergo slow radiationless decay processes to give rise to luminescence and may be involved in bimolecular reactions. It follows that the ability to determine the orbital nature of the lowest excited state is a key step toward the design of useful compounds. The orbital nature of the lowest excited state can be revealed by examination of the luminescence behaviour [42][46][53]. Luminescence arising from a ^{1}MC excited state appears as a gaussian – shaped emission band that is devoid of structure and considerably red-shifted compared with the lowest energy absorption bands. The excited state lifetime is relatively long in rigid matrix at 77 K but decreases rapidly with increasing temperature as does the luminescence intensity.

Luminescence from a ^{3}MLCT excited state is generally highly structure at low temperature[42][46][54][55][56][57][58][59]. On increasing temperature, the luminescence intensity decrease relatively slowly. Usually it is possible to distinguish the two types of energy emission on lifetime grounds[42][46][53][59][60][61][62]. ^{3}LC emission occurs quite close to the emission of the free ligand, whereas ^{3}MLCT emission may occur, at much lower energies. It has been known for a long time[42][43][46] that in complexes of the same metal ion, the orbital nature of the lowest excited state may be determine by a suitable choice of ligand. The energy of the MC excited states depends on the ligand field strength, which in turn depends on the σ - donor and π – acceptor properties of the ligand, the steric crowding around the metal and the bite angle of the polydentate ligands. The energy of the MLCT excited states depend on the reduction potential of the ligand involved in the MLCT transition, the oxidation potential of the metal in the complex, which is affected by the electron donor and acceptor properties of all the ligand and finally, by the charge separation caused by the transition. The energy of the LC excited state depends on intrinsic properties of the ligands, such as the HOMO-LUMO energy gap and the singlet-triplet splitting. The luminescence of $[Ru(bpy)_3]^{2+}$ is a typical ^{3}MLCT emission: it occurs at much lower energy than the phosphorescence of free (bpy) and the luminescence spectrum is structured at low temperature. Most of the known Ru(II) polypyridine

complexes exhibit a luminescent behaviour quite similar to that of $[Ru(bpy)_3]^{2+}$, indicating that their lowest excited state is also a ^{3}MLCT state. By an appropriate choice of the ligands, however, it has been possible to change the orbital nature of the lowest excited state. ^{3}MC emission may be obtained decreasing the ligand field strength, for example replacing one or two polypyridine ligands by Cl^- ions [62]. The π–donor ability of the Cl^- ligand also lowers the energy of the MLCT state by increasing the negative charge on the metal. When a $[Ru(LL_3)]^{2+}$ compound has a ^{3}MLCT excited state at very low energy, substitution of LL by $2Cl^-$ does not cause an inversion on the excited state energy ordering. ^{3}LC emission may be obtained using polypyridine ligands, which satisfy the following requirements:

- Presence of a relatively low-lying ^{3}LC level
- Sufficiently high ligand field strength to keep ^{3}MC at high energy
- Sufficiently negative reduction potential to keep ^{3}MLCT at high energy.

Figure 1.10 (a) and Figure 1.10 (b) show representation of two limiting cases for position of ^{3}MC and ^{3}MLCT excited states

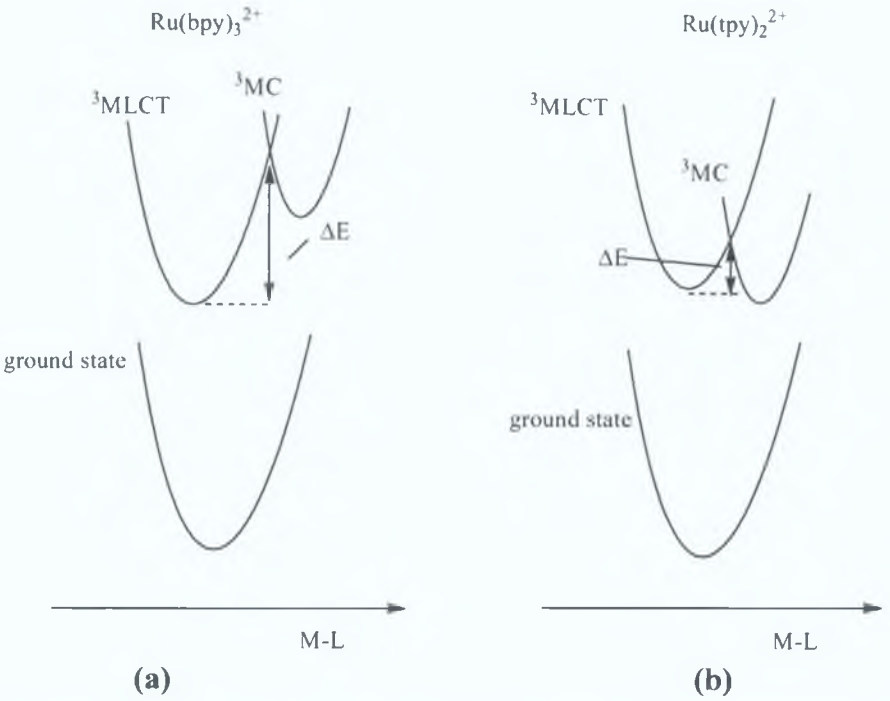

Figure 1.10: Schematic representation of two limiting cases for positions of ^{3}MC and ^{3}MLCT excited states

LC or MLCT transitions (see Figure 1.10 (a)) do normally not undergo such fast radiationless decay to the ground state and luminescence may be observed. When the lowest excited state is MC, it undergoes fast radiationless deactivation to the ground state and / or ligand dissociation (see Figure 1.10(b)).

Terpyridine complexes tend to have relatively short-lived ^{3}MLCT state and to be weak emitters as compared to analogues bpy complexes. While the ^{3}MLCT state of the $[Ru(bpy)_3]^{2+}$ is long-lived, the luminescence lifetime is 890 ns, $[Ru(tpy)_2]^{2+}$ is a very weak luminescence and lifetime at room temperature is extremely short: 0.25 ns. The lifetime of the luminescent ^{3}MLCT state depends on their energy and also on the higher-energy of the metal centred excited states ^{3}MC. The possibility to populate such state by thermal activation is one of the main radiationless deactivation paths of the luminescent excited state. Tris-chelating ligand such as terpyridine is not ideally suited for octahedral coordination. This results in a low energy of the ^{3}MC state that may be thermally populated from the luminescent ^{3}MLCT state (see Figure 1.10 (b)). The smaller ΔE value for $[Ru(tpy)_2]^{2+}$ leads to very efficient deactivation of the luminescent excited state. Strategy may be devised to increase the excited state lifetime of Ru(II) terpyridine complexes. The main origins of the short lifetime is the small gap between the emitting ^{3}MLCT state and the upper – lying ^{3}MC state, increasing this energy gap would be beneficial. The use of electron withdrawing substituents or groups that effect electronic delocalisation[61][62b] over the terpyridine fragment has made possible to obtain long lived excited Ru (II) terpyridine type units. Electron donor and electron acceptor substituents are found to decrease the energy of the ^{3}MLCT state but their effect on the energy of the ^{3}MC state is such that the largest gap and the longer lifetime are obtained when the two substituents X and Y are the opposite type. With this strategy lifetimes as long as 40-50 ns can be obtained. With this range of lifetime, Ru(II) terpyridine units may be used as photosensitizer molecular components in supramolecular devices.

1.7 Terpyridine - metal complexes as molecular wires

The complexes of the $[Ru(bpy)_3]^{2+}$ family have been used as photosensitizers in covalently –linked multicomponent systems in order to obtain photoinduced migration of electronic energy and / or charge separation[7][9]. Therefore, these complexes are not suitable from the geometric viewpoint for the construction of supramolecular systems. In the design of well – defined supramolecular systems by synthetic assembly of mononuclear building blocks, the occurrence of isomers is a major problem. At difference with most species containing bidentate ligands, ochtahedral terpyridine complexes are achiral (no complications due to stereoisomers) and they can be connected to other molecular components thought the terpyridine 4' – position while maintaining the C_{2v} symmetry of the ligand (no complications due to geometrical isomerism) (see Figure 1.11).

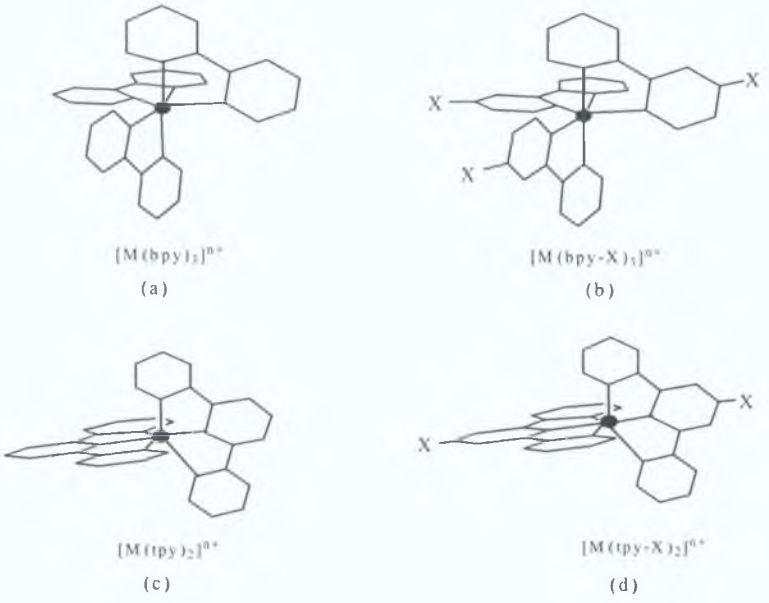

Figure 1.11: Schematic representation of (a) one of the chiral isomers of $[M(bpy)_3]^{n+}$; (b) the mer geometrical isomer of an $[M(bpy\text{-}X)_3]^{n+}$ complex; (c) the unique achiral form of an $[M(tpy)_2]^{n+}$ complex and (d) the unique form of an $[M(tpy\text{-}X)_2]^{n+}$ complex

2,2' – bipyridines give rise to stereoisomerism at six-coordinated centres due to its bidentate nature and therefore an $[M(bpy)_3]^{n+}$ complex exists in two enantiomeric forms.

If the two coordinating nitrogen are not equivalent, as happens for monosubstituted bpy, two geometrical isomers, fac. and mer., are possible; furtheremore each of them can exist as one of two enantiomers.

In contrast to this behaviour, a six coordinate metal forms an achiral $[M(tpy)_2]^{n+}$ complex upon reaction with tpy (example (c) in Figure.1.11). The introduction of a single substituent in 4' – position of each (tpy) ligands presents no additional problems (example (d) Figure.1.11).

A significant amount of research is being performed on mononuclear terpyridine complexes. A huge potential lies in these compounds regarding the fine-tuning of optical properties or the use as precursors for supramolecular architectures. For example ligands modified with carboxy group play an important role as substituents on terpyridine ligands due to their potential use as an anchoring group on surfaces such as TiO_2, which is widely used in solar cell applications[63].

Terpyridine ruthenium complexes, attached to TiO_2, may be used as sensitizers in novel solar cells. Carboxy groups have been introduced into the 4 – position of terpyridines [64] (Figure 1.12).

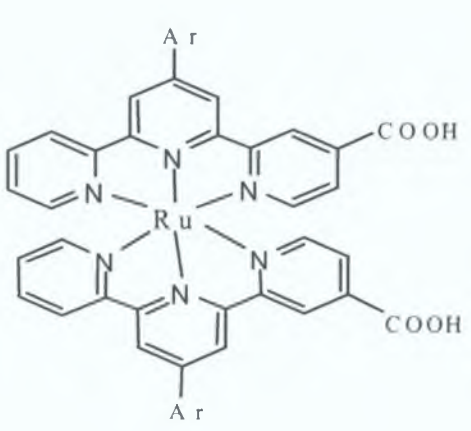

Figure 1.12: Carboxy functionalised terpyridine complexes

Due to their spatial orientation, they may easily coordinate by ionic interactions providing a photo – induced electron transfer. In order to increase the electron injection efficiency and to reduce the chance of desorption of the complexes from the TiO_2 surface, asymmetric bis(terpyridinyl)-ruthenium (II) complexes carrying vicinal carboxylic acid were developed[65] (see Figure. 1.13).

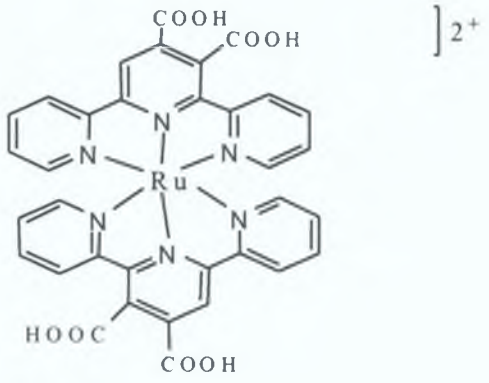

Figure 1.13: Example of terpyridine complexes carrying vicinal carboxylic acids

Because of the complexation of the free ligand di-acid resulted in the loss of one carboxylic group (decarboxylation), the protection of the acid groups by ester-formation was necessary. The resulting compounds show room temperature luminescence and efficient sensitization of nanocrystalline TiO_2 films. Electron withdrawing groups in the 4' – position of terpyridine have been shown to result in room temperature phosphorescent ruthenium (II), complexes[66]. The introduction of π – system of the ligand by one or more aromatic rings is a promising approach. One strategy towards such system is the use of connected benzoic aromatic rings. In the case shown in Figure 1.14, a pyrimidine moiety has been introduced into the 4' – position of a terpyridine.

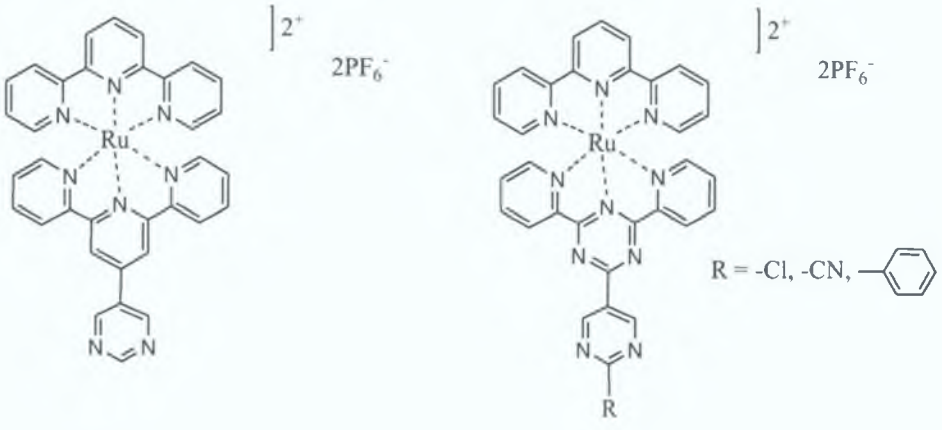

Fig.1.14: pyrimidine into the 4' – position of terpyridine complexes

In addition, analogous terpyridines bearing a second pyrimidine, phenyl, or group in the para position of the first aromatic ring, have been prepared to extend the conjugated π-system[67]. A luminescence at room temperature is obtained

Other examples of luminescent ruthenium complexes include complexes involving the ligand 2-(4'-pyriyl)-4,6-bis(2'-pyridyl)-1,3,5-triazine. The bis(2'-pyrimidyl)-1,3,5-triazines may be considered as heteroterpyridines which have the potential for room temperature luminescence (see Figure 1.15).

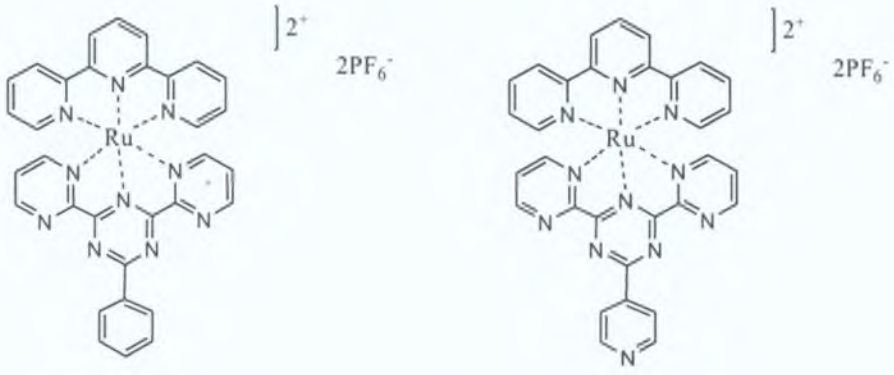

Figure 1.15: Phenyl and pyridyl functionalised complexes of hetero-terpyridine complexes

An interesting feature of the 2,4,6-tris(2-pyrimidyl)-1,3,5-triazine ligands is that it is composed of three pyridine subunits resulting in complex containing two vacant complexing units. This architectural feature makes this system interesting for the construction of supramolecular assemblies. Anellated or fused aromatiques have also been introduced into terpyridines, where the corresponding ruthenium complexes show the ability for room temperature luminescence[68]. Besides photo-physical properties originating from delocalisation phenomena, the intermolecular interactions of such compounds are also of interest. Extended aromatic systems are known to give rise to $\pi - \pi$ interactions, which could be relatively strong for large molecules. Such π – stacking could be exploited for the 3-dimensional arrangement of terpyridine complexes[69] (see Figure 1.16).

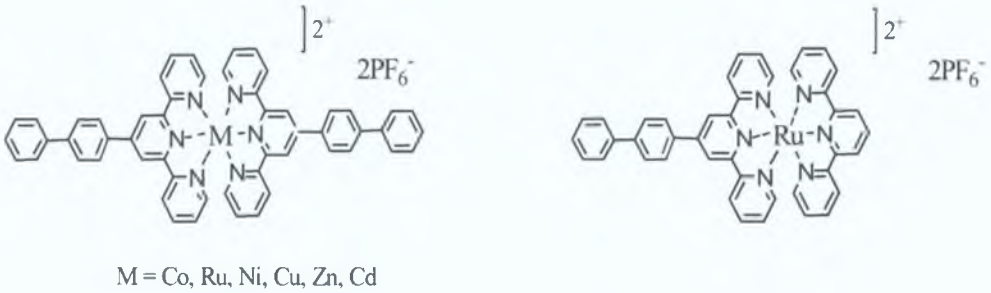

M = Co, Ru, Ni, Cu, Zn, Cd

Figure 1.16: π – stacking of 4'-(4-biphenyl) terpyridine-ruthenium complexes

The group of Alcock reported the synthesis of 4' – biphenyl functionalised terpyridines and the preparation of the corresponding complexes using a variety of metal ions[69]. Depending on the metal ion, different structures were found: for cobalt, ruthenium, nickel and copper, biphenylene – biphenylene interactions lead to linear rod-like arrays; for complexes of zinc and cadmium, biphenylene – pyridyl interactions lead to two dimensional sheets. Moreover ruthenium, zinc and cadmium complexes showed room temperature luminescence both in solid state as well as in solution.

Many multinuclear systems containing two or three terpyridine complex units, linked by different spacers, have been synthesised. Both homodyads (same metal ion) and heterodyads (different metal ion) are known. Interesting example is represented by the combination of the metals ruthenium and osmium. A variety of such compounds and their properties[70]. If a ruthenium complex is connected to an osmium complex, then an energy transfer from ruthenium to osmium may be observed when exciting the ruthenium (II) complex unit. Energy and also electron transfer process make such complex-arrays interesting for use as "molecular wires". Starting from a dyad with directly connected terpyridines, various spacer groups have been introduced. Intensive work has been performed on a wide range of conjugated spacers of different length and composition, allowing the photo-physical properties of the corresponding complexes to be fine-tuned. Along with homometallic ruthenium complexes, ruthenium-osmium dyads have been prepared using bridging ligands[70]. Multinuclear terpyridine complexes, especially those capable of energy and / or electron transfer, are promising compounds for future applications in optical nano-devices or solar cells.

The field of devices and molecular switches, where electrochemical or optical activities may be switched simply and reversibly, is of special importance. The mono ruthenium (II) complex of a bridging ligand could not only be used for further complexation, it also possesses other interesting properties. By protonation of the non-coordinating free terpyridine moiety, the luminescence properties could be modulates in a reversible manner. A non luminescent complex became luminescent after addition of different metal ions like iron (II), or zinc (II), to result in triads[70], (see Figure 1.17). The almost non luminescent ruthenium (II),

terpyridine chromophore, functionalised with an uncoordinated terpyridine fragment, has been complexed with Zn (II) ions[71], leading to a luminescent rod-like complex array revealing a luminescence enhancement factor larger than 10. Due o the reversible, relatively weakly coordinated zinc complex, this system also gives rise to "switchable" emitters.

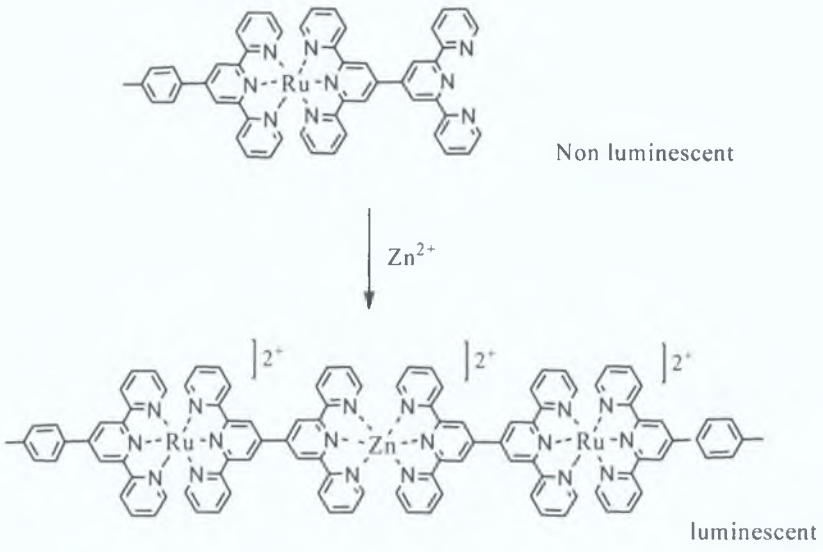

Figure 1.17: Switching of luminescence by complexation with zinc (II) ions

A different approach to tunable metal complex arrays includes the incorporation of a different complexing moiety such as bipyridine ligands. One of the first compounds to be synthesised was a dyad, bridged by a 2,2'-bipyridine-5,5'-diethynyl group[72][73]. The bipyridine moiety in the bridging ligand has been complexed with various metal ions. By this method the luminescence properties of the parent complex may be tuned. Whereas weakly binding ions cause an increase in the luminescence of the $[Ru(tpy)]_2$ units, strong binders like Ag^+ or Hg^{2+} decrease the luminescence. The cause for this behaviour is the reducibility of these metal centres, making a photo-induced electron transfer possible which results in luminescence quenching. In a recently reported dyad[74], the terpyridine complexes were attached directly to a brinding bipyridine moiety (Figure 1.18). An enhancement of the luminescence was found for protonation of the bipyridine by addition of acids as well as complexation with Zinc (II).

Utilizing cyclic voltammetry, it has been found that the electronic interaction between the peripheral chromophores in enhanced by zinc coordination.

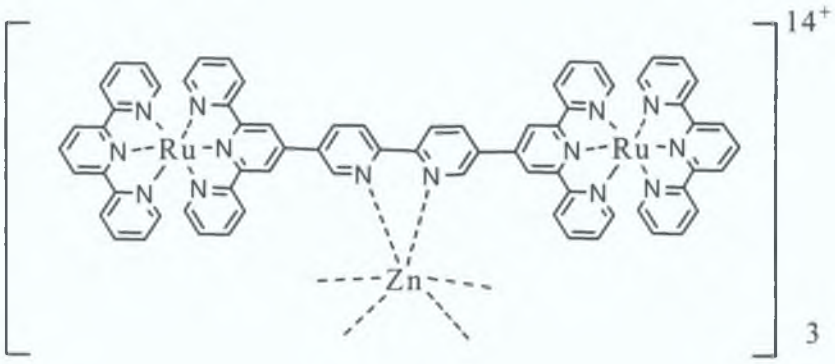

Figure 1.18: Switchable dyad, containing a bipyridine fragment in the bridging ligand

A promising approach towards switchable luminescent chromophores are azo-linked ruthenium-osmium dyads[75] (Figure 1.19).

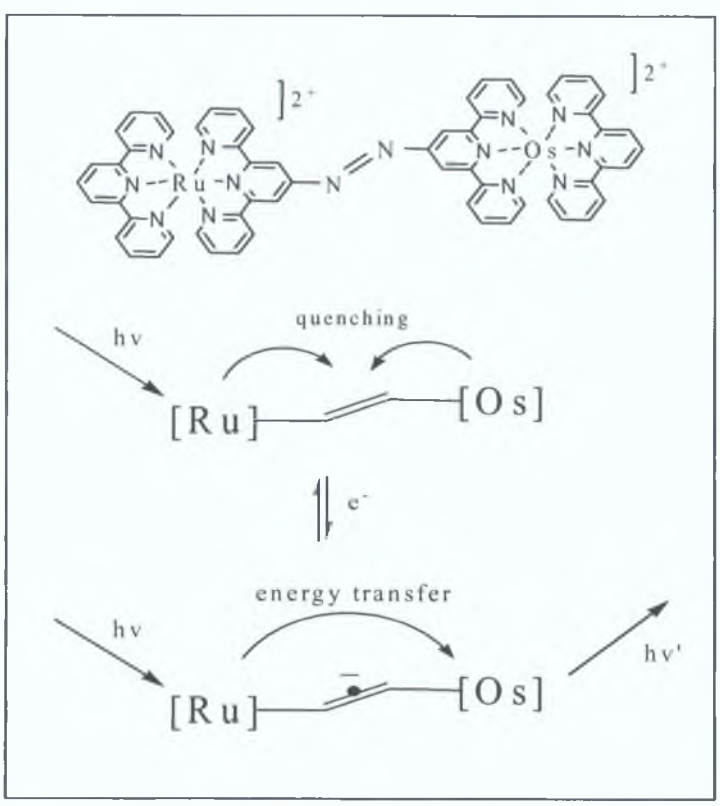

Figure 1.19: Luminescence switching by reduction of azo-linked ruthenium-osmium dyads

In these systems, the energy transfer may be switched, triggered by a redox reaction. In its natural state, the azo – group quenches the luminescence of both the ruthenium and osmium. Reaction of the linker, however, leads to a luminescent homodinuclear Os(II) complex at room temperature. The corresponding homodinuclear Ru(II) complex shows a luminescence at 77 K. In the heterodinuclear complex, an energy transfer from ruthenium to osmium may take place, resulting in a strong osmium luminescence. This approach has been extended to dyads and triads where the ruthenium complexes have been combined with osmium complexes in order to study energy and electron transfer processes[76]. These mixed complexes are also luminescent and an energy transfer process from ruthenium to osmium could be observed. As a result, luminescence in enhanced when compared to the homometallic complexes.

Another possibility for constructing extended complex architectures involves ligands where two or more terpyridine motives are combined with sharing one or more nitrogen. Because the geometry is well defined, these kinds of ligands have been used as building blocks for the construction of extended supramolecular architectures. One example is the ligand tetra-2-pyridyl-1,4-pyrazine (tppz). This molecule may be considered as consisting of two fused terpyridines sharing the central aromatic ring. This allows the construction of rigid rod-like structures [77] (Figure 1.20).

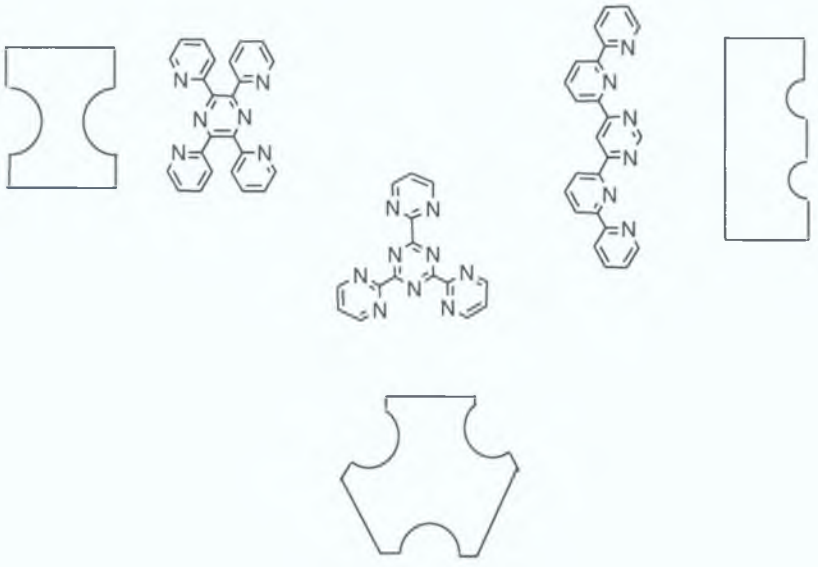

Figure 1.20: Building blocks for supramolecular architectures

Pyrazine ligands have been also used to synthesise mixed Ru(II) /Rh(III) complexes. In this case, a mono-metallic tppz-tpy ruthenium complex has been further complexed with rhodium (III) trichloride. With the rhodium complex known to be an electron acceptor, quenching of luminescence takes place in 80% efficiency via an electron transfer.

1.8 Nanotechnology: self-assembled monolayers

Although gold is the subject of one of the most ancient themes of investigation in science, it is also particulary relevant in the emerging areas of nanoscience, nanotechnology and nanoparticles [78]. In particular gold nanoparticles present fascinating aspects such as their assembly of multiple types involving materials science, the behaviour of the individual particles, size-related electronic, magnetic and optical properties and their application to catalysis and biology. Because of its overwhelming importance in the above mentioned fields gold will continue to be a key material and building block in the 21st century.

Self-assembled monolayers of thiol substituted materials on gold surface have been the subject of several researches in the last few years[79]. Due to the flexibility in the design of molecular structures and simple preparation methods, monolayers of thiol based organic molecules have been well recognised as convenient systems to control charge transfer at metal electrodes[80]. Mostly self-assembled aliphatic thiols have been studied[81][82] whereas experiments on monolayers of conjugated thiolates or even single molecules[83][84] are still relatively scarce but are rapidly increasing due to recent interest in the molecules electronics. Charge transfer trought the organic systems are either studied by electrochemical techniques or by direct measurement of the conductivity using scanning probe techniques or macroscopic electrode/self-assembled monolayer/electrode sandwich structures [85]. The organisation of monomolecular assemblies at solid surfaces provides a rational approach for fabricating interfaces with a well-defined composition, structure and thickness. Such assemblies may provide a means to control the chemical and physical properties of interfaces for a variety of heterogeneous phenomena including catalysis[86], corrosion and adhesion[87]. The ability to control interfacial processes has important implications

from the point of view of both fundamental and technological advances; in particular, the study of fundamental chemical and physical interactions that control the formation, structure and reactivity of chemically modified surfaces. This consists of selecting molecular systems that provide the means to probe those interactions that govern the attachment, orientation and packing density of the surface species and in part, of searching for informative characterization tools to apply to these systems. Further, it has become increasingly clear that characterisation of defect structures, as well as average molecular structures, is an important issue, which needs to be addressed in many applications. The types of interactions which are most relevant to these structural aspects include the bonding interactions and between the head group and the intermolecular interactions between adjacent adsorbate molecules[88].

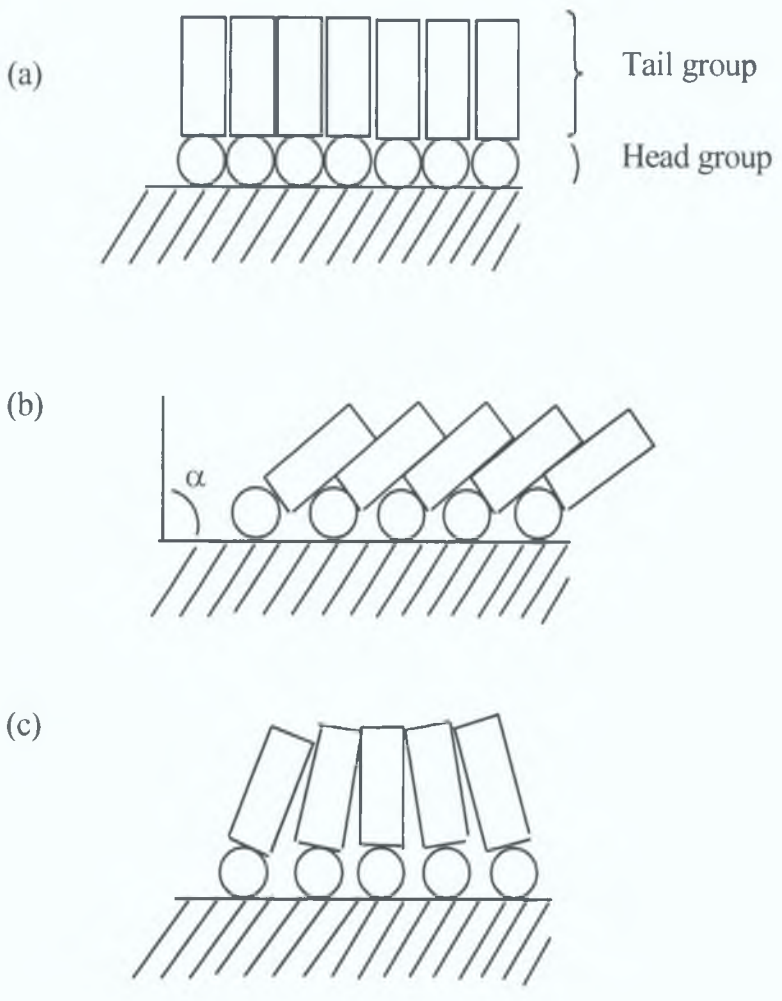

Figure 1.21: Structural models of an organised monolayer assembly

Figure 1.21 are describes three examples of idealised structures for organised monolayers assembled, based on various studies, particularly those using electron diffraction[89]. In Figure 1.21 (a), shows the closest packed arrangement of tail groups orientated normal to the substrate surface; Figure 1.21 (b) shows the closest packed arrangement of head groups with the tail groups uniformly orientated at an angle α from the surface. Finally, Figure 1.21 (c) reports the closest packed arrangement of head groups with a distribution of tilted tail groups. Several systems possess the requisite properties on an experimental model. Previous studies have shown the utility of charge transfer [90][91][92] chemistry for attaching a variety of molecules at both metallic and non metallic surfaces. A particularly detailed series of studies has examined the effects of the size and functionality of substituent groups on the orientation, surface concentration and electrochemical reactivity of aromatic molecules adsorbed, for example at platinum[90][91][92].

Other investigations have shown the importance of the alkyl chain length of alkanoic acids on the orientation and bonding at ambient surfaces of aluminium, silver [93] and at metal copper [94]. Many systems are based on the adsorption of organosulfur compounds on noble metals such as gold[95][96]. Systems based on the adsorption of sulfur compounds on gold surfaces have several advantages as a model. These advantages include the choice of thiol, sulfide, or disulfide functionalities to study head-group / substrate interactions and the variation of the chain length to study the importance of tail interactions. In addition, a metallic substrate with a low chemical reactivity, such as gold, provides the opportunities to apply both vibrational spectroscopic and electrochemical techniques. In particular thiol compounds are easily absorbed on metallic surface, allowing for the preparation of chemically modified electrodes, molecular devices and sensors, where they may be used as supports for other adsorbates.

1.9 Scope of the thesis

One of the scientific objectives of the SUSANA (Supramolecular Self-Assembly of Interfacial Nanostructures) project is the preparation of switchable junctions in which nanoparticles are linked via molecular bridges whose electron transfer barrier properties can be chemically and electrochemically switched. Transition metal complexes containing aromatic ligands are attractive candidates for excited state electron transfer processes in fluid solution. In particular the aim of this study is to prepare metal complexes functionalised with groups that can be used to connect the metal complex to a solid surface. For this purpose, I worked for one month in collaboration with the University U.V.A. in Amsterdam and one month in collaboration with the Kekule' Institute in Bonn. Two different approaches have been attempted in this thesis, with different purposes:

1. Introduction of functional groups as pyridine and thiol groups as linkers in terpyridine systems (see self-assembled scheme in Figure 1.22).
2. Study of the electrochemical properties: low oxidation and potentials; use of osmium as metal centre to study redox properties of the complexes.

1 - Special attention was paid to the thiol end groups that have been well recognised as convenient systems to control charge transfer at metal electrodes [4], especially because of their flexibility in the design of molecular structures. Mostly self-assembled monolayers have been studied [81][82] and experiments on monolayers of conjugated thiolates are rapidly increasing due to recent interest in molecular electronics. Synthesis of thiol - terpyridine complexes have been attempted starting from 4' - (4-bromo-phenyl) 2,2'; 6', 2" - terpyridine (tpy-ph-Br) and boronate groups by a palladium – catalysed Suzuki coupling reactions.
Pyridyl groups have been also used as substituents in terpyridine complexes. In particular, the ligand 4' - (pyrid-4"'-yl) 2,2'; 6', 2" - terpyridine (py-tpy) that can provide anchoring on nanoparticles and on surfaces, has been used for the synthesis of Ru(II) and Os(II) mixed complexes.

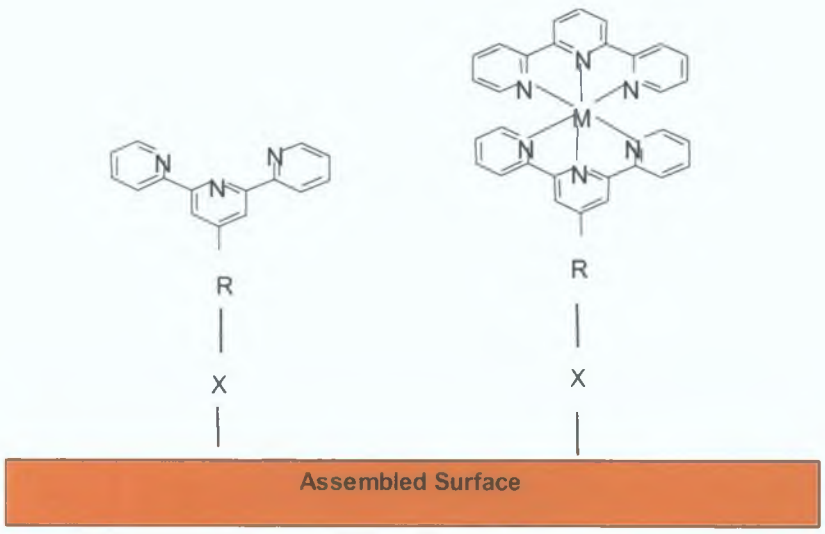

Figure 1.22: Self – assembled monolayers of Metal (II) terpydine complexes onto surface; X = - SH, - pyridine

2 – Synthesis of ruthenium and osmium terpyridine complexes incorporating tetrazole ligand [2,6-bis-([1,2,3,4]tetrazol-5-yl)pyridine] (H_2L3) has been investigated with the purpose of vary the electrochemical properties of this class of complexes. An interesting point is the possibility of the application of such compounds in photoinduced processes in suitably supramolecular systems. Particular attention has been paid to the use of osmium as metal centre to improve the redox properties of the complexes (low oxidation and potentials).

A range of complexes with 4'(pyrid-4"'-yl) 2,2'; 6', 2" - terpyridine (py-tpy)l and 4'(4-bromo-phenyl) 2,2'; 6', 2" - terpyridine (tpy-ph-Br) ligands have been prepared. Pyridyl groups were introduced because of their ability to provide well-defined anchoring points on nanoparticles and on a range of surfaces. Complexes with (tpy-ph-Br) groups were also prepared as precursors for the thiol analogues. (tpy-ph-Br) was prepared and then reacted, with boronic acid compounds in cross-coupling Suzuki reactions, Pd-catalysed, for the synthesis of thiol substituted terpyridine complexes.

Synthesis of ruthenium and osmium terpyridyl complexes, with (py-tpy) and (tpy-ph-Br) group has been investigated in this thesis.

$[Ru(py\text{-}tpy)]_2[PF_6]_2$, $[Ru(py\text{-}tpy)(tpy\text{-}ph\text{-}Br)][PF_6]_2$, $[Ru(tpy)(tpy\text{-}ph\text{-}Br)][PF_6]_2$, $[Os(py\text{-}tpy)]_2[PF_6]_2$ and $[Os(py\text{-}tpy)(tpy\text{-}ph\text{-}Br)][PF_6]_2$ and $[Os(tpy)(tpy\text{-}ph\text{-}Br)][PF_6]_2$, have been prepared and characterised. To vary redox and photophysical properties of terpyridine complexes, ligands such as [2,6-(2,3 phenyl-4-methyl pyrazol) pyridine] (H_2L3) and 2,6-(2,3 phenyl-4-methyl pyrazol) pyridine [2,6-(2,3-ph-4-CH_3-pyrazol)py] have been introduced and used for synthesising ruthenium and osmium complexes.

In Chapter 2, all the instrumental methods used for the characterisation of the compounds are described, including ^{1}H-NMR, UV/Visible spectroscopy, electrochemistry, chromatographic techniques and mass spectroscopy. The synthesis of the ligands and of the mononuclear ruthenium, osmium and cobalt complexes are also presented in this Chapter.

In Chapter 3, characterisation by ^{1}H-NMR spectroscopy of ruthenium (II) and osmium (II) terpyridine substituted complexes are described. A practical look at the various synthetic strategies used to synthesise these complexes is also described in this Chapter.

Chapter 4 attempts to rationalise the absorption, emission spectroscopy, lifetime and electrochemical data collected for all the complexes synthesised in this thesis. The correlation between spectroscopic and electrochemical data has been also reported.

Chapter 5 describes synthesis investigated for ruthenium and cobalt thiol - terpyridine substituted complexes. Attempted Suzuki coupling reactions, synthesis and characterisations of boronic acid compounds, used as starting materials for the coupling processes have been also described in Chapter 5.

Finally, Chapter 6 will bring this thesis to a close by discussion of the conclusions of the experimented data and some suggestions on future work, with possible research directions. Particular attention has been paid to the comparison between the luminescence and electrochemistry results obtained for ruthenium and osmium complexes investigated in this thesis.

1.10 Bibliography

[1] Campano, R., Molenkamp, L., Paul, D.J., Technology for Nanoelectronics, European Commission, IST programme, Future and Emering Technologies, *2000.*

[2] Vuillaume, D., Lenfant S., Microelectronic Engineering, *2003*, 70, 2-4, 539.

[3] Philip, D., Stoddart, F. J. Angew. Chem. Int. Ed., *1996*, 35, 1154.

[4] (a) Darnell, J., Lodish, H., Baltimore, B., Molecular Cell. Biology, Scientific American Books, New York, 1990; (b) Magennis, S. W., Craig, J., Gardner A., Fucassi, F., Cragg, P. J., Robertson, N., Parsons, S., Pikramenou, Z., Polyhedron 22, *2003*, 745.

[5] Balzani, V., Scandola, F., Supramolecular Photochemistry Harwood, *1991*, 12.

[6] Hush, N.S., Supramolecular photochemistry (Ed. Balzani, V) *1987,* 455.

[7] Scandola, F., Indelli, M.T., Chioroboli, C., Bignozzi, C.A., Top. Curr. Chem. *1990*, 158, 73.

[8] (a) Balzani, V., Credi, A., Scandola, F., In Transition Metals in Supramolecular Chemistry; (b) Fabbrizi, L., Poggi, A., (Eds), Transition Metals in Supramolecular Chemistry, Kluwer, Dordrecht, the Netherlands, *1994*.

[9] Balzani, V., Scandola, F., Supramolecular Photochemistry Harwood, *1991*, 6.

[10] Amadelli, R., Argazzi, R., Bignozzi, C. A., Scandola, F.,J. Am. Chem. Soc., *1990*, 112, 7099.

[11] (a) O'Regan, B., Gratzel, M., Nature, *1991*, 353, 737; (b) Gratzel, M., Comments Inorg. Chem., *1991*, 12, 93; (c) Hagfeldt, A., Gratzel, M., Chem. Rev., *1995*, 95, 49.

[12] Argazzi, R., Bignozzi, C. A., Heimer, T. A., Castellano, F., N., Meyer, G., J. Inorg. Chem., *1994*, 33, 5741.

[13] Lehn. J.M., Supramolecular Chemistry, Concepts and Perspectives, *1995*.

[14] Schubert, U. S., in Tailored Polymers and Applications, eds. Yagci, M. K. M. Y., O. Nuyken, O., Ito, K., Wnek, G., VPS Publishers, Utrecht, *2000*, 63-85.

[15] Schubert, U. S., Eschbaumer, C., Angew. Chem., Int. Ed., *2002*, 41, 2892-2926.

[16] Brunsveld, L., Folmer, B.J.B., Mejjer, E.W., Sijbesma, R. P., Chem. Rev., *2001*, 101, 4071.

[17] Cooke, G., Rotello, V.M., Chem. Soc. Rev., *2002*, 31, 275-286.

[18] Yamauchi, K., Lizotte, J.R., Hercules, D.M., Vergne, M.J., Long, T.E., J. Am. Chem. Soc., *2002*, 124, 8599.

[19] Yamauchi, K., Lizotte, J.R., Long, T.E., Macromolecules, *2003*, 36, 1083.

[20] Constable, E.C., Thompson, W.C., New J. Chem., *1992*, 16, 855.

[21] Lashgari, K., Kritikos, M., Norrestam, R., Norrby, T., Acta Crystallogr. Sect. C.: Cryst. Struct. Commun., *1999*, 55, 64.

[22] Lehn, J. M., Science *1985*, 227, 849.

[23] Lehn J.M., Supramolecular Chemistry, VCH, Weinheim, Germany, *1995.*

[24] Reinhoudt, D.N. (Ed) Comprehensive Supramolecular Chemistry, Pergamon, New York, *1996.*

[25] Schneider, H.-J., Durr H. (Eds), Frontiers in Supramolecular Organic Chemistry and Photochemistry, VCH, Weinheim, Germany, *1990.*

[26] Vogtle, F., Supramolecular Chemistry, Wiley, New York, *1991.*

[27] Balzani, V., De Cola, L., (Eds.), Supramolecular Chemistry, Kluwer, Dordrecht, The Netherlands, *1992.*

[28] Fabbrizi, L., Licchelli, M., Pallavicini, P., Acc. Chem, Res.*1999*, 32, 846.

[29] Di Bella, S., Chem. Soc. Rev. *2001*, 30, 355.

[30] Bissel, R.A., de Silva, A.P., Gunaratne, H.Q.N., Lynch, P.L.M., Maguire, G.E.M., McCoy, C.P., Sandanayake, K.R.A.S.Top. Curr. Chem., *1993*, 168, 223 Gust, D., Moore, T.A., Moore, A.L., Acc. Chem. Res., *1993*, 26, 198.

[31] Balzani, V., Bolletta, F., Gandolfi, M. T., Maestri, M., Top. Curr. Chem., *1978*, 75, 1.

[32] Sutin, N., J. Photochem. *1979*, 10, 19.

[33] Sutin, N., Creutz, C., Inorganic and Organometallic Photochemistry, Advances in Chemistry Series, 168, American Chemical Society, *1978*, 1.

[34] (a) Meyer, T.,J., Israel J. Chem. *1977*, 15, 200; (b) DeLaive, P. J., Giannotti, C., Whitten, D. G., J. Am. Chem. Soc., *1978*, 100, 7413.

[35] (a) Creutz, C., Chou, M., Netzel, T. L., Okumura, M., Sutin, N., J. Am. Chem. Soc., *1980*, 102, 1309; (b) Ballardini, R., Varani, G., Balzani, V., J. Am. Chem. Soc., *1980*, 102, 1719.

[36] Balzani, V., Carassiti, V., Photochemistry of coordination compounds, *1970.*

[37] Adamson, A. W., Flischauer, P. D., Concepts of inorg. photochemistry, *1975.*

[38] Special issue, J. Chem. Educ., *1983*, 60, 814.

[39] Ferraudi, G., J., Elements of inorganic photochemistry, *1988*.

[40] Scandola, F., Balzani, V., In Serpone, N., Pellizzetti, E., Photocatalysts, *1989*.

[41] Cotton, F.A., Wilkinson, G., Gaus, P.L., Basic Inorg. Chem., *1994*, 3rd Edition.

[42] Crosby, G. A., Acc. Chem. Res., *1975*, 8, 231.

[43] Crosby, G. A., Adv. Chem. Ser., *1976*, 150, 149.

[44] Kober, E. M., Meyer, T. J., Inorg. Chem., *1982*, 21, 3967.

[45] Mandal, K., Pearson, T. D. L., Krug, W. P., Demas, J. N., J. Am. Chem. Soc., *1983*, 105, 701.

[46] Crosby, G. A., Watts, R. J., Carstens, D. H. W., Science, *1970*, 170, 1195.

[47] Yeung, P. K.Y., Cheung, K. K., J. Chem. Soc. Commun., *1995*, 267.

[48] (a) Birks, J. B., Photophysics of Aromatic Molecules, Wiley-interscience, *1970*; (b) Turro, N. J., Mod. Molecules Photoch., Benjamin, Menlo Park, *1978*.

[49] (a) Porter, G. B., Balzani, V., Moggi, L., Adv. Photochem., *1974*, 9, 147; (b) Balzani, V., Moggi, L., Manfrin, M. F., Bolletta, F., Laurence, G. S., Coord. Chem. Rev., *1975*, 15, 321.

[50] Kavarnos, G. J., Turro, N. J., Chem. Rev., *1986*, 86, 401.

[51] Sutin, N., Creutz, C., J. Chem. Educ., *1980*, 60, 809.

[52] Kalyanasundaram, K., Photoch. of polypyridine and porphyrins complexes, *1992*, 8.

[53] DeArmond, M. K., Acc. Chem. Res., *1974*, 7, 309.

[54] Sprouse, S., King, K. A., Spellane, P. J., Watts, R. J., J. Am. Chem. Soc., *1984*, 106, 6647.

[55] Maestri, M., Balzani, V., Sandrini, D., Chassot, L., Jolliet, P., von Zelewsky, A., Chem. Phys. Lett., *1985*, 122, 375.

[56] Casper, J. V., Meyer, T. J., Inorg. Chem., *1983*, 22, 2444.

[57] King, K. A., Finlayson, M. F., Spellane, P.J., Watts, R. J., Riken, Q., *1984*.

[58] Casper, J. V., Westmoreland, T. D., Allen, G. H., Bradley, P.G., Meyer, T. J., Woodruff, W. H., J. Am. Chem. Soc., *1984*, 106, 3492.

[59] Ohsawa, Y., Sprouse, S., King, K. A., DeArmond, M. K., Hanck, K. W., Watts, R. J., J. Phys. Chem., *1987*, 91, 1047.

[60] Chassot, L., von Zelewsky, A., Sandrini, D., Maestri, M., Balzani, V., J. Am. Chem. Soc., *1986*, 108, 6084.

[61] Maestri, M., Sandrini, D., Balzani, V., Mader, U., von Zelewsky, A., Inorg. Chem., *1987*, 26, 1323.

[62] (a) Belser, P., von Zelewsky, A., Juris, A., Berigelletti, F., Balzani, V., Gazz. Chim. Ital., *1983*, 113, 731; (b) Benniston, A.C., grosshenny, V., Harriman, A., Ziessel, R., Angew. Chem. Int. Ed. Engl. 33, *1994*, 1884.

[63] Gratzel, M., Prog. Photovoltaics, *2000*, 8, 171.

[64] Mikel, C., Potvin, P.G., Polyhedron, *2002*, 21, 49

[65] Beley, M., Bignozzi, C.A., Kirsch, G., Alebbi, M., Raboin, J.C., Inorg. Chem. Acta, *2001*, 318, 197.

[66] Maestri, M., Armaroli, N., Balzani, V., Constable, E.C., Thompson, A.M.W.C., Inorg. Chem., *1995*, 34, 2759.

[67] Fang, Y.Q., Taylor, N.J., Hanan, G.S., Loiseau, F., Passalacqua, R., Campagna, S., Nierengarten, H., van Dorsselaer, A., J. AM. Chem. Soc., *2002*, 124, 7912.

[68] Constable, E.C., Smith, D.R., Supramol. Chem., *1994*, 4, 5.

[69] Alcock, N.W., Barker, P.R., Haider, J.M., Hannon, M.J., Painting, C.L., Pikramenou, Z., Plummer, E.A., Rissanen, K., Saarenketo, J. Chem. Soc. Dalton Trans., *2000*, 1447.

[70] Sauvage, J.P., Collin, J.P., Chambron, J.C., Guillerez, S., Coudret, C., Balzani, V., Berigelletti, F., De Cola L., Flamigni, L., Chem. Rev., *1994*, 94, 993.

[71] Berigelletti, F., Flamigni, L., Balzani, V., Collin, J.P., Sauvage, J.P., Sour, A., Constable, E.C., Thompson, M.W.C., J. AM. Chem. Soc., *1994*, 116, 7692.

[72] Ziessel, R., Synthesis, *1999*, 1839.

[73] Hissler, M., El-ghayoury, A., Harriman, A., Ziessel, R., Angew. Chem. Int., Ed., *1998*, 37, 1717.

[74] Loiseau, F., Passalacqua, R., Campagna, S., Polson, M.I.J., Fang, Y.Q., Hana, G.S., Photochem. Photobiol., *2002*, 1, 982.

[75] Akasaka, T., Otsuki, J., Araki, K., Chem. Eur.J., *2002*, 8, 130.

[76] Encinas, S., Flamigni, L., Berigelletti, F., Constable, E.C., Housecroft, C.E., Schofield, E.R., Figgemeier, E., Fenske, D., Neuburger, M., Vos, J.G., Zehnder, M., Chem. Eur. J., *2002*, 8, 137.

[77] Islam, A., Ikeda, N., Nozaki, K., Okamoto, Y., Gholamkhass, B., Yoshimura, A., Ohno, T., Coord. Chem. Rev., *1998*, 171, 355.

[78] Daniel, M.C., Astruc, D., Chem. Rev., *2004*, 104, 293.

[79] Swalen, J.D., Allara, D.L., Amdrade, J.D., Chandross, E.A., Garoff, S., Isrealachvili, J., McCarthy, T.J., Murray, R., Pease, R.F., Rabolt, J.F., Wynne, K.J., Yu, H., Langmuir, *1987*, 3, 932.

[80] Finklea, H.O., Electroanalytical Chemistry, *1996*, 19, 109.

[81] Porter, M.D., Bright, T.B., Allara, D.L., Chidsey, C.E.D., J. Am. Chem. Soc., *1987*, 109, 3559.

[82] Xu, J., Li, H., Zhang, J. Phys. Chem., 1993, 97, 11497.

[83] Reed, M.A., Zhou, C., Muller, C.J., Burgin, T.P., Tour, J.M., Science, *1997*, 278, 252.

[84] Zhitenev, N.B., Meng, H., Bao, Z., Phys. Rev. Lett., *2002*, 88, 226801.

[85] Slowinsky, K., Fong, H.K.Y., Majda, M., J. Am. Chem. Soc., *1999*, 121, 7257.

[86] Murray, R.W., Electroanalytical Chemistry, *1984*, 13.

[87] Kaelble, D.H., Physical Chemistry of Adhesion, *1971*.

[88] Langmuir, I. J. Chem. Phys., *1933*, 1, 756.

[89] Garoff, S., Deckman, H.W., Dunsmuir, J.H., Alvarez, M.S., J. Phys., *1986*, 47, 701.

[90] Soriaga, M.P., Hubbard, A.T., J. Am. Chem. Soc., *1982*, 104, 3937.

[91] Soriaga, M.P., Hubbard, A.T., J. Am. Chem. Soc., *1982*, 104, 2735.

[92] Chia, V., Soriaga, M.P., Hubbard, A.T., J. Electroanal. Chem., *1984*, 169, 97.

[93] Allara, D.L., Nuzzo, R.G., Langmuir, *1985*, 1, 45

[94] DuBois, L.H., Zagarski, B.R., Nuzzo, R.G:, Langmuir, *1986*, 2, 412.

[95] Nuzzo, R.G., Allara, D.L., J. Am. Chem. Soc., *1983*, 105, 4481.

[96] Li, T.T., Weaver, M.J., J. Am. Chem. Soc., *1984*, 106, 6107.

Chapter 2

Experimental Procedures and Synthesis of Ligands and Ru(II) and Os(II) Terpyridine Complexes

An introduction to the instrumental methods used throughout this thesis is described in chapter 2. Methods of characterisation such as ^{1}H-NMR, UV-Visible Spectroscopy, Electrochemistry, Mass Spectrometry are presented for all the complexes. A description of the synthetic methods for the preparation of starting materials, ligands and terpyridine complexes is also reported in this chapter.

2.1 Introduction

In this chapter experimental and basic synthetic procedures used are described. All synthetic reagents were of commercial grade and no further purification was employed, unless otherwise stated. All solvents employed in spectroscopic measurement were HPLC or spectroscopic grade. All solvents were used as purchased from Aldrich.

2.1.1 Nuclear Magnetic Resonance

^{1}H-NMR spectra were recorded on a Bruker AC400 (400 MHz) instrument. The solvent used for the complexes was mainly deuteriated acetonitrile and dimethyl sulphoxide. Deuteriated dimethyl sulphoxide and chloroform were used for the ligands. The chemical shifts were recorded relative to the standard tetramethylsilane (TMS). The spectra were converted from their Free Induction Decay (FID) profiles using a Bruker WINNMR software package. The 2-D cosy (correlated spectroscopy) experiments involved the accumulation of 128 FIDs of 16 scans.

2.1.2 Absorption and Emission Spectroscopy

UV/Vis absorption spectra were carried out on a Shimadzu UV/Vis-NIR 3100 spectrophotometer interfaced with an Elonex-466 PC using UV-Vis data manager software. Emission spectra were obtained using a Perkin Elmer LS50-B luminescence spectrophotometer, equipped with a red sensitive Hamamatsu R928 PMT detector; that was interfaced with an Elonex-466 PC using Windows based fluorescence software.

2.1.3 Electrochemistry

Electrochemical measurements were performed in acetonitrile. In particular for solution phase electrochemistry anhydrous acetonitrile HPLC grade was used as solvent. The supporting electrolyte was Tetrabutylammonium tetrafluoroborate whose concentration was typically of 0.1 M. Prior any measurements the solution was deoxygenated by purging it with pre-purified nitrogen for at least 10 minutes. Then cyclic voltammetry of the blank (no complex in solution) was ran in order to

check the purity of the electrolyte solution. The redox active couple was then dissolved in the electrolyte and electrochemical measurements were performed. The cell was a three-electrode cell containing:

- Working macro electrode, 3 mm diameter, Teflon shrouded glassy carbon or platinum electrode, each of which was previously polished with 0.3 micron allumina. The polishing material was then removed by rinsing and sonicating the electrode for at least 10 min in water.·
- A reference electrode Ag/Ag^{+} previously calibrated against the ferrocene/ferrocenium redox couple.
- A Platinum wire as a counter electrode.

2.1.4 Chromatographic techniques

High performance liquid chromatography (HPLC) was carried out on a Waters 510 HPLC using a Waters 990 photodiode array detector equipped with a NEC PAC III computer, a 20 μl injector loop and a Partisil SCX radial PAK cartridge. The detection wavelength used was 280 nm. The chromatography was achieved using a mobile phase, which consisted of acetonitrile / water, 80/20 (v/v) containing 0.08 M $LiClO_4$. The flow rate for routine work was 1.8 cm^3 min^{-1}. Semi-preparative HPLC was performed using an ACS pump, a 1 cm^3 injection loop and a Waters Partisil SCX 10 μm cation exchange column (25 x 100 mm). The mobile phase used 0.12 M Ammonium Acetate in methanol. The flow rate used 2.0 cm^3/min.

2.1.5 Luminescent lifetime

Luminescent lifetimes were carried out on a Q-switched Nd-Yag System. Room temperature measurements were carried out in deaerated acetonitrile. Samples were degassed by bubbling dry argon through the sample for at least 20 minutes. Lifetimes conforming to single exponential decays were analysed with Microcal Origin Software. The lifetime errors are estimated to be less than 8%. Short-lived measurements were carried out with a Single Photon Counter. Analytical Instrument in a T setting. The lamp were a nF900, in a Nitrogen setting, the monochromators were J-yA models, the detector was a Single Photon

Photomultiplier Detection System, model S 300, with a MCA card type Norland N5000 and a PC interface Cd900 serial. The program used for the data correlation and manipulation is F900 Program, Version 5.13.

2.1.6 Mass Spectroscopy

The experiments were performed on an electro spray interface (ESI) in DCU University with the assistance of Mr. Maurice Burke. Spectra are collected by constant infusion of the analyte dissolved in a mixture of 80:20, methanol: water, in presence of Acetic Acid (1%). ESI is a soft ionisation technique, resulting in protonated, sodiated species in positive ionisation mode and deprotonated, chlorinated or acetate salt in negative ionisation mode.

2.1.7 Elemental analysis

Carbon, hydrogen and nitrogen elemental analyses were carried out an Exador Analytical CE440 by the Microanalytical Department, University College Dublin and in Kekule' Institute in Bonn, Germany.

2.2 Synthetic methods

2.2.1 General

All synthetic reagents were of commercial grade and no further purification was employed. All solvents were used as purchased from Aldrich. Column chromatography was performed using neutral activated aluminium oxide or silicon oxide (35–70 μm).

2.3 Synthesis of ligands

The ligand 2,2'; 6', 2" - terpyidine (tpy) and [2,6-(2,3 phenyl-4-methyl pyrazol) pyridine] were used without any other purification. Compound 2,2'; 6', 2" - terpyidine (tpy) is commerciale available, whereas [2,6-(2,3 phenyl-4-methyl pyrazol) pyridine] was obtained form Prof Sally Brooker, University of Otago. Synthesis and purification of all the ligands used for the preparation of the mononuclear terpyridine complexes are described below. ^{1}H-NMR spectra of the ligands and of the metal complexes are shown in Appendix I.

2.3.1 Synthesis of 4'(pyrid-4-yl) 2,2'; 6' , 2" - terpyridine (py-tpy)

The three step synthetic procedure for the preparation of 4'(pyrid-4-yl) 2,2'; 6', 2" - terpyridine (py-tpy) were used as a procedure described in the literature[1].

Step 1: Synthesis of [1-(2-pyridyl)-3-(4-pyridyl)-2-propenone]

A solution of 2-acetylpyridine (8.40 cm^3, 70.0 mmol), pyridine-4-carbaldehyde (3.00 cm^3, 30.0 mmol) and sodium hydroxide (2.02 g, 50.0 mmol) in water (25 cm^3) and ethanol (35 cm^3) was stirred for 1 hour at room temperature. After this period water (30 cm^3) was added and a white precipitate obtained. This precipitate was collected by filtration, washed well with cold ethanol and dried to give the product as a white solid. Yield: 4.50 g, 67%.

Step 2: Synthesis of 1-(2-pyridylcarbonyl) pyridinium [PF_6]

A solution of 2-acetylpyridine (2.24 cm^3, 20.0 mmol) in 5 cm^3 of dry pyridine and I_2 (5.12 g, 20.0 mmol) in 15 cm^3 of dry pyridine, was heated to 100° C, under argon, and stirred for three hours. After this period, the solution was cooled overnight. A black precipitate occurred and was collected by vacuum filtration. The product 1-(2-pyridylcarbonyl) pyridinium iodide was dissolved in H_2O. The solution was heated and stirred. Then NH_4PF_6 dissolved in water was added and a light brown product precipitated. The precipitate was filtered by vacuum filtration and used without any other purification. Yield: 4.12 g, 60%.

Step 3: Synthesis of 4'(pyrid-4-yl) 2,2'; 6', 2" - terpyridine (py-tpy)

A solution of the enone (400 mg, 2.0 mmol), 1-(2-pyridylcarbonyl) pyridinium [PF_6] (650 mg, 2.0 mmol) and ammonium acetate (1.46 g, 2.0 mmol) in water was heated at reflux for 2 hours. After this period, the pale coloured solution was cooled to give an off-white precipitate, which was collected by filtration. Recrystallisation from ethanol gave small white needles of 4'(pyrid-4-yl) 2,2'; 6', 2" - terpyridine. Yield: 0.38 g, 65 %. ^{1}H-NMR (CD_3CN): 8.72 (s) 1H, 8.70 (d) 1H, 8.68 (d) 1H, 8.62 (d) 1H, 7.85 (dd) 1H, 7.78 (d) 1H, 7.33 (dd) 1H (Figure 1, Appendix I).

2.3.2 Synthesis of 4'(4-bromo-phenyl) 2,2'; 6', 2" - terpyridine (tpy-ph-Br)

4'(4-Bromo-phenyl) 2,2'; 6', 2" - terpyridine (tpy-ph-Br) was prepared as a procedure described in the literature [2]. Three steps are required for the synthesis of this ligand.

Step 1: Synthesis of 1-(2-pyridyl)-3-(4-bromophenyl)-2-propenone

The synthesis of the 1-(2-pyridyl)-3-(4-bromophenyl)-2-propenone was a modification of the preparation described in the literature [3]. 4-Bromoacetaldehyde (1.41 g, 80.0 mmol) and NaOH (544 mg, 14.0 mmol) were dissolved in a solution of ethanol/H_2O (1:1). A solution of 2-acetylpyridine (2.06 cm^3, 20.0 mmol) in ethanol (5 cm^3) was slowly added to the solution. After 10 minutes, a yellow solid was precipitated and was stirred for 40 minutes. The yellow precipitate was collected by vacuum filtration, washed well with cold ethanol and H_2O. Yield: 1.90 g, 86%. The complex was used without any further purification.

Step 2: Synthesis of 1-(2-pyridilcarbonyl) pyridinium [PF_6]

A solution of 2-acetylpyridine (2.24 cm^3, 20.0 mmol) in 5 cm^3 of dry pyridine and I_2 (5.12 g, 20.0 mmol) in 15 cm^3 of dry pyridine, was heated to 100° C, under argon, and stirred for three hours. After this period, the solution was cooled overnight. A black precipitate occurred and was collected by vacuum filtration. The product 1-(2-pyridylcarbonyl) pyridinium iodide was dissolved in H_2O. The solution was heated and stirred. Then NH_4PF_6 dissolved in water was added and a light brown product precipitated. The precipitate was filtered by vacuum filtration and used without any other purification. Yield: 4.12 g, 60%.

Step 3: Synthesis of 4'(4-bromo-phenyl) 2,2'; 6', 2" - terpyridine (tpy-ph-Br)

A solution of 1-(2-pyridyl)-3-(4-bromophenyl)-2-propenone (1.21 g, 40.0 mmol), 1-(2-pyridylcarbonyl) pyridinium [PF_6] (1.44 g, 40.0 mmol) and ammonium acetate (3.23 g, 42.0 mmol) in methanol, was heated at reflux for 7 hours. After this period, the solution was cooled overnight to give an off-white precipitate that

was collected by vacuum filtration and washed with cold methanol. Yield: 410 mg, 26%.

^{1}H-NMR ($CDCl_3$): 8.66 (d) 1H, 8.63 (s) 1H, 8.59 (d) 1H, 7.82 (dd) 1H, 7.72 (d) 1H, 7.57 (d) 1H, 7.30 (m) 1H (Figure 2, Appendix I).

2.3.3 Synthesis of 2,6-bis-([1,2,4]triazol-3-yl)pyridine (H_2L1)

The ligand 2,6-bis-([1,2,4]triazol-3-yl)pyridine (H_2L1) was prepared as a procedure described in the literature[3]. Five steps are involved in the synthetic route of this ligand.

Step 1: Synthesis of pyridine-2,6-dicarboxylic acid diethyl ester

Pyridine-2,6-dicarboxylic acid (10.02 g, 60.0 mmol) was dissolved in 70 cm^3 of EtOH containing 1.3 cm^3 concentrated H_2SO_4. The reaction mixture was heated at reflux overnight. The excess ethanol was removed in vacuo and the residue neutralised with a $NaHCO_3$ saturated solution and extracted with CH_2Cl_2. The organic layer was washed twice with NaCl saturated aqueous solution. After removal, the product was obtained as oil, which solidified on standing. Yield: 10.89 g, 81%.

Step 2: Synthesis of pyridine-2,6-dicarboxy diamide

Pyridine-2,6-dicarboxylic acid diethyl ester (3.50 g, 20.0 mmol) was dissolved in 3 cm^3 MeOH and added to 15 cm^3 of a stirring aqueous solution of NH_3 (d = 0.88 g / cm^3), immersed in an ice-bath. Precipitation occurred after a half-hour. Another 7 cm^3 of MeOH was added and the resulting mixture stirred overnight at room temperature. The product was collected by filtration and washed with cold methanol. Yield: 2.22 g, 72%.

Step 3: Synthesis of pyridine-2,6-dicarbonitrile

Pyridine-2,6-dicarboxy diamide (2.03 g, 10.0 mmol) and 50 cm^3 DMF were warmed up. 5 cm^3 of $POCl_3$ was slowly added. The solution was stirred for 3h at room temperature. The residue was diluted with CH_2Cl_2 and mixed with H_2O. The organic layer was collected. The solvent was reduced under vacuum. The product

was crashed out from the resulting thick mixture by adding a small amount of ice, filtered off, washed with H_2O. Yield: 0.78 g, 60%.

Step 4 Synthesis of pyridine-2,6-diimidrazone

An excess of hydrazine monohydrate (25 cm^3) was added to a stirring solution of (3.60 g, 30.0 mmol) of pyridine-2,6-dicarbonitrile and 60 cm^3 of EtOH. The resulting solution was stirred for two hours at 60°C. A precipitation occurred which was collected by filtration, washed with a small portion of MeOH and dried. Yield: 4.27 g, 75%.

Step 5 Synthesis of 2,6-bis-([1,2,4]triazol-3-yl)pyridine (H_2L1)

Pyridine-2,6-diimidrazone (3.03 g, 20.0 mmol) was added step wise to 40 cm^3 of formic acid at 0 °C. The resulting mixture was stirred for three hours, after which the acid was removed under reduced pressure. The resulting oil was dissolved in 25 cm^3 of 1,2-ethandiol and heated at reflux for 1 hours. The solution was allowed to cool. The precipitate was filtered and washed with water. Yield: 2.36 g, 56%.

^{1}H-NMR (d^6-DMSO): 8.00-8.15, (m), 2H; 8.20-8.50, (s), 1H.

2.3.4 Synthesis of 2,6-bis-(5-phenyl-[1,2,4]triazol-3-yl)pyridine (H_2L2)

The preparation of the ligand (H_2L2) was a modification of the synthesis described in literature [3]. Five steps are involved in the synthetic route of this ligand. For the first four steps see the procedure described in Section 2.3.3.

Step 5 Synthesis of 2,6-bis-(5-phenyl-[1,2,4]triazol-3-yl)pyridine (H_2L2)

Diimidrazone (2.01 g, 10.0 mmol) obtained from step 4 (see preparation of H_2L1) was dissolved in 20 cm^3 of THF, 2 cm^3 triethylamine and 40 cm^3 of EtOH. The mixture was stirred overnight. The intermediate was collected by filtration. The resulting solid was dissolved in 1,2-ethandiol and heated at reflux for 2 hours. The solution was allowed to cool down, mixed with ice water. Precipitation occurred, which was collected by filtration and washed with diethylether. The material was used as obtained. Yield: 2.70 g, 74%.

^{1}H-NMR (d^6-DMSO): 7.40-7.65, (m), 6H, 8.10-8.20, (d), 4H, 8.20-8.40, (s), 3H.

2.3.5 Synthesis of 2,6-bis-([1,2,3,4]tetrazol-5-yl)pyridine (H_2L3)

The preparation of the ligand (H_2L3) was carried out as synthesis described in the literature [3]. Pyridine-2,6-dicarbonitrile (2.03 g, 20.0 mmol), NaN_3 (2.10 g, 30.0 mmol), NH_4Cl (1.81 g, 30.0 mmol) and LiCl (1.90 g, 50.0 mmol) were mixed. DMF (20 cm^3) was added and the stirred suspension was heated for 10 hours, under nitrogen atmosphere. After cooling at room temperature, evaporation of the solvent afforded a residue that was dissolved in H_2O. By adding HCl (1M) a white product precipitated; it was collected by filtration and dried under vacuum. The product obtained in quantitative yield was recrystallised from H_2O/EtOH (1:1) solution. Yield: 3.02 g, 70%.

^{1}H-NMR (d^6-DMSO): 8.30-8.40, (m) (Figure 3, Appendix I).

2.4 Synthesis of precursor metal complexes

The syntheses of ruthenium starting materials [Ru(tpy)Cl_3], and H[Ru(py-tpy)Cl_3] [PF_6], are reported in literature [4][5]. A modification of the same preparation was used for the synthesis of [Ru(tpy-ph-Br)Cl_3]. Syntheses of [Os(tpy)Cl_3] and [Os(py-tpy)Cl_3] are a modification of synthesis reported in literature [6]. Because of their paramagnetic properties, it was not possible to characterise these compounds by ^{1}H-NMR. To confirm the formation of these precursors they have been reacted with terpyridine and the complexes resulted were characterised by ^{1}H-NMR.

2.4.1 Synthesis of [Ru(tpy)Cl_3]

[($RuCl_3$)2H_2O] (1.00 g, 4.0 mmol) were dissolved in 150 cm^3 of ethanol. The solution was refluxed and 2,2'; 6',2" - terpyridine (1.41 g, 6.0 mmol) dissolved in 20 cm^3 of EtOH, was added wise. The reaction was heated at reflux for 2 hours and filtered hot. A brown product was collected and washed with ethanol, water and diethyl ether. Yield: 1.65 g, 94%. The complex was used without any further purification.

2.4.2 Synthesis of H[Ru(py-tpy)Cl_3][PF_6]

(Py-tpy) (304 mg, 1.0 mmol), was dissolved in an acid solution of HCl, in water (pH=2). A concentrate solution of NH_4PF_6 salt was added to precipitate out the protonated ligand. The product was collected by vacuum filtration and dried using diethyl ether, then dissolved in EtOH (15 cm^3). [($RuCl_3$)$2H_2O$] (239 mg, 1.0 mmol), was added and the solution was heated at reflux for 2 hours. A dark green precipitate was collected by vacuum filtration and dried using diethyl ether. Yield: 150 mg, 36%. The complex was used without any further purification.

2.4.3 Synthesis of [Ru(tpy-ph-Br)Cl_3]

[($RuCl_3$)$2H_2O$] (238 mg, 1.0 mmol) was dissolved in 200 cm^3 of EtOH. The solution was refluxed and 1 equivalent of 4'(4-bromo-phenyl) 2,2'; 6', 2" - terpyridine (380 mg, 1.0 mmol) dissolved in 25 cm^3 of EtOH, was added dropwise. The reaction was heated for 2 hours and filtered hot. A dark brown product was collected and washed with EtOH, H_2O and diethyl ether. Yield: 437 mg, 75%. The complex was used without any further purification.

2.4.4 Synthesis of [Os(tpy)Cl_3]

[$(NH_4)_2OsCl_6$] (428 mg, 1.0 mmol) and 1 equivalent of 2,2'; 6',2" - terpyridine (227 mg, 1.0 mmol) were dissolved in 10 cm^3 of DMF. The solution was heated at reflux under argon for four hours. The reaction was cooled and NH_4Cl was filtered off. Ethanol (15 cm^3) was added to the solution and afterwards, ethyl ether (40 cm^3). The reaction mixture was cooled in the fridge overnight A dark green-brown product precipitated. It was collected and washed with EtOH, H_2O and diethyl ether. It was used without any other purification. Yield: 346 mg, 67%.

2.4.5 Synthesis of [Os(py-tpy)Cl_3]

[$(NH_4)_2OsCl_6$] (100 mg, 0.20 mmol) and 1 equivalent of 4'(pyrid-4-yl) 2,2'; 6', 2" - terpyridine (62 mg, 0.20 mmol) were dissolved in 4 cm^3 of DMF. The solution was heated at reflux under argon for six hours. The reaction was cooled and a NH_4Cl was filtered off. EtOH (10 cm^3) was added to the solution and afterwards, ethyl ether (30 cm^3). The reaction mixture was left in the fridge overnight. A dark green-brown product precipitated. It was collected and washed with ethanol, water and diethyl ether. The product was used without any other purification. Yield: 90.0 mg, 71%.

2.5 Synthesis of target complexes

Ruthenium complexes described below have been synthesised in according to the literature [7] for similar compounds. Syntheses of osmium complexes were used as a procedure described in the literature [8][9][10].

2.5.1 Synthesis of [Ru(tpy)$_2$][PF_6]$_2$

A solution of [($RuCl_3$)$2H_2O$] (188 mg, 0.80 mmol), and two equivalent of 2,2';6', 2" - terpyridine (373 mg, 1.6 mmol), in 15 cm^3 of EtOH, were added to a round bottomed flask and heated at reflux for 6 hours. The solution was filtered and the filtrate was treated with NH_4PF_6 salt and water. The red precipitate was collected by vacuum filtration and dried using diethyl ether. Yield: 411 mg, 60%.

^{1}H-NMR (CD_3CN): 8.70 (d) $H^{3'}$, 8.43 (d) H^3, 8.34 (dd) $H^{4'}$,7.83 (dd) H^4, 7.28 (d) H^6, 7.18 (dd) H^5 (Figure 4, Appendix I).

2.5.2 Synthesis of [Ru(py-tpy)$_2$][PF_6]$_2$

This complex was prepared with two different methods.

Method 1:

A solution of [($RuCl_3$)$2H_2O$] (54.0 mg, 0.20 mmol), and two equivalent of 4'(pyrid-4-yl) 2,2';6', 2" - terpyridine (138 mg, 0.40 mmol), in ethylene glycol (8 cm^3), were added to a round bottom flask and heated at reflux for 6 hours. The solution was filtered using a Buchner funnel and the filtrate was treated with

NH_4PF_6 in water. The precipitate was collected by vacuum filtration and dried using diethyl ether. The complex was purified on a silica column, using acetonitrile/H_2O (8:2) and KNO_3 (0.5%) as eluent. Yield: 67.0 mg, 33%. Mass spectrometry (m/z) for M^{2+} ion calcd. at 361, found 361. Anal. Calcd.: $C_{40}H_{28}N_8Ru_1P_2F_{12}$ C: 47.49%; H:2.79%; N: 11.08 %. Anal. Found: C: 47.00%; H: 2.59%; N: 10.8%.

^{1}H-NMR (CD_3CN): 9.10 (s) $H^{3'}$, 8.98 (d) H^b, 8.68 (d) H^3, 8.18 (d) H^a, 8.00 (dd) H^4, 7.43 (d) H^6, 7.23 (dd) H^5 (Figure 5, Appendix I).

Method 2

A solution of H[Ru(py-tpy)Cl_3][PF_6] (160 mg. 0.20 mmol) and $AgBF_4$ (117 mg. 0.60 mmol) in dry acetone (30 cm^3) was refluxed for 2 hours. The solution was filtered to remove AgCl. DMF was added and the acetone was evaporated. (Py-tpy) (62 mg, 0.20 mmol) was dissolved in DMF (with nitrogen bubbled through the solution). The solution of [Ru(py-tpy)$(OAc)_3$] was added to the ligand and heated at reflux under nitrogen, for 2 hours. NH_4PF_6 in water was added to precipitate [Ru(py-tpy)$_2$][PF_6]. The precipitate was collected by vacuum filtration and recrystallised from acetonitrile. Yield: 60.0 mg, 29%. Mass spectrometry (m/z) for M^{2+} ion calcd. at 361, found 361. Anal. Calcd.: $C_{40}H_{28}N_8\ Ru_1P_2F_{12}$ C: 47.49%; H:2.79%; N: 11.08 %. Anal. Found: C: 47.00%; H: 2.59%; N: 11.06%.

^{1}H-NMR (CD_3CN): 9.10 (s) $H^{3'}$, 8.98 (d) H^b, 8.68 (d) H^3, 8.18 (d) H^a, 8.00 (dd) H^4, 7.43 (d) H^6, 7.23 (dd) H^5 (Figure 5, Appendix I).

2.5.3 Synthesis of [Ru(tpy)(tpy-ph-Br)][PF_6]$_2$

[Ru(tpy-ph-Br)Cl_3] (267 mg, 0.40 mmol) and $AgBF_4$ (233 mg, 1.2 mmol) were heated at reflux for 2 hours in dry acetone (20 cm^3). The solution was filtered in order to remove AgCl. DMF (10 cm^3) was added and the acetone was evaporated. A suspension of terpyridine (93.0 mg, 0.40 mmol) in DMF (10 cm^3) was heated till complete dissolution of the ligand. The DMF solution containing ruthenium complex was slowly added and the resulting solution was heated at reflux, under N_2, for four hours. The complex was precipitated by addition of a concentrated aqueous solution of ammonium hexafluorophosphate and then filtered by vacuum filtration. The orange precipitate was dried with diethyl ether. Yield: 168 mg,

41%. Mass spectrometry (m/z) for M^{2+} ion calcd. at 362, found 362. Anal. Calcd. $C_{36}H_{25}N_6Ru_1Br_1P_2F_{12}$ C: 42.70%; H: 2.49%; N: 8.30 %. Anal. Found: C: 42.78%; H: 2.40%; N: 7.58%. ^{1}H-NMR (CD_3CN): 9.10 (s) $H^{3'}$, 8.81 (d) H^b, 8.69 (d) H^3, 8,55 (d) H^6, 8.42 (dd) $H^{4''}$, 8,18 (d) H^a, 7.90-8.00 (m) H^4, $H^{3'''}$, $H^{3''}$, 7.48 (d) $H^{2'''}$, 7.40 (d) $H^{5'''}$, 7.20 (m) H^5, $H^{4'''}$ (Figure 6, Appendix I).

2.5.4 Synthesis of [Ru(py-tpy)(tpy-ph-Br)][PF_6]$_2$

This complex was prepared with two different methods.

Method 1:

[Ru(tpy-ph-Br)Cl_3] (100 mg, 0.20 mmol) and $AgBF_4$ (117 mg, 0.60 mmol) were refluxed for 2 hours in dry acetone (20 cm^3). The solution was filtered in order to remove AgCl, DMF (10 cm^3) was added and the acetone was evaporated with rotary evaporated. A suspension of ligand (py-tpy) (62.0 mg, 0.20 mmol) in DMF (15 cm^3) was heated till complete dissolution of the ligand. Then, the DMF solution containing ruthenium complex was slowly added and the resulting solution was heated at reflux, under N_2, for 4h. The product was precipitated by addition of a concentrated aqueous solution of ammonium hexafluorophosphate and then filtered by vacuum filtration. The residue mixture was purified with silica column using acetonitrile/H_2O (18:20) and KNO_3 (0.5%) as eluent. The fifth fraction contained the desired complex. Yield: 49.0 mg, 23%. Mass spectrometry (m/z) for M^{2+} ion calcd. at 399, found 399. Anal. Calcd. $C_{41}H_{28}N_7Ru_1Br_1P_2F_{12}$ C: 45.19%; H: 2.59%; N: 8.99%. Anal. Found: C: 45.21%; H: 2.48%; N: 9.01%. ^{1}H-NMR ($CDCl_3$): 8.98 (s) $H^{3'pytpy}$, 8.90 (m) $H^{3'}$, H^3, 8.58 (dd) H^{6pytpy}, 8.08 (m) H^6, H^{3pytpy}, 7.90 (m) H^{4pytpy}, H^4, H^5, 7.62 (d) H^d, 7.55 (d) H^a, 7.37 (d) $H^{c\ pytpy}$, 7.31 (d) $H^{b\ pytpy}$, 7.15 (m) H^5, H^{5pytpy} (Figure 7, Appendix I).

Method 2:

A solution of H[Ru(py-tpy)Cl_3][PF_6] (200 mg, 0.30 mmol), was added to $AgBF_4$ (175 mg, 0.90 mmol) in acetone (30 cm^3) and was heated at reflux for two hours. The resulting solution was filtered to remove precipitated AgCl. DMF (10 cm^3), was added and acetone was evaporated off, using a rotary evaporator. 2, 2': 6', 2" -

terpyridine (70.0 mg, 0.30 mmol), was dissolved in DMF (15 cm^3), under nitrogen. The ligand was added and heated at reflux for 3 hours under nitrogen. The solution was allowed to cool, a saturated solution of NH_4PF_6 in water were added to precipitate $[Ru(py\text{-}tpy)(tpy\text{-}ph\text{-}Br)][PF_6]_2$. The precipitate was collected by vacuum filtration and purified with silica column using acetonitrile/H_2O (8:2) and KNO_3 (0.5%) as eluent. Yield: 220 mg, 67%. Mass spectrometry (m/z) for M^{2+} ion calcd. at 399, found 399. Anal. Calcd. $C_{41}H_{28}N_7Ru_1Br_1P_2F_{12}$ C: 45.19%; H: 2.59%; N: 8.99%. Anal. Found: C: 45.22%; H: 2.50%; N: 8.88%.

^{1}H-NMR ($CDCl_3$): 8.98 (s) $H^{3'pytpy}$, 8.90 (m) $H^{3'}$, H^3, 8.58 (dd) H^{6pytpy}, 8.08 (m) H^6, H^{3pytpy}, 7.90 (m) H^{4pytpy}, H^4, H^5, 7.62 (d) H^d, 7.55 (d) H^a, 7.37 (d) $H^{c\ pytpy}$, 7.31 (d) $H^{b\ pytpy}$, 7.15 (m) H^5, H^{5pytpy} (Figure 7, Appendix I).

2.5.5 Synthesis of [Ru(tpy-ph-Br)(L3)(H_2O)]

The complex was obtained by heating $[Ru(tpy\text{-}ph\text{-}Br)Cl_3]$ (140 mg, 0.20 mmol) and a stoichiometric amount of the ligand (H_2L3), 2,6-bis-([1,2,3,4]tetrazol-5-yl)pyridine, (43.1 mg, 0.20 mmol), in 20 cm^3 of ethylene glycol containing a slight molar excess of NaOH and few drops of N-ethylmorpholine. The reaction mixture was heated at reflux for 6 hours. Water was added to precipitate out the brown solid complex. The product was recrystalised from DMF/H_2O solution (1:1). Then it was purified on a silica column with acetonitrile/H_2O (3:1) as the eluent. The first fraction contained the desired complex Yield: 50.0 mg, 35%. Mass spectrometry (m/z) for M^{2+} ion calcd. at 722, found 722. Anal. Calcd. $C_{28}H_{21}N_{12}O_1Ru_1Br_1$ C: 46.55%; H: 2.93%; N: 23.26%. Anal. Found: C: 46.49%; H: 2.91%; N: 23.20%.

^{1}H-NMR (CD_3CN): 9.55 (s) $H^{3'}$, 9.18 (d) H^b, 8.70 (m) H^3, $H^{3''}$, $H^{4''}$, 8.48 (d) H^a, 8.15 (m) H^4, 7.53 (d) H^6, 7.28 (dd) H^5 (Figure 8, Appendix I).

2.5.6 Synthesis of [Ru(tpy)[2,6-(2,3-ph-4-CH_3-pyrazol)py][PF_6]$_2$

The complex was obtained by heating $[Ru(tpy)Cl_3]$ (210 mg, 0.50 mmol) and a stoichiometric amount of ligand [2,6-(2,3 phenyl-4-methyl pyrazol) pyridine], (165 mg, 0.50 mmol) in H_2O containing a slight molar excess of NaOH and few drops of N-ethylmorpholine. The reaction mixture was heated at reflux for two

hours. The solution was concentrated with rotary evaporator, acidified to pH 2 with HCl and an excess of NH_4PF_6 was added. A dark brown solid precipitated was collected by vacuum filtration and recrystallised from EtOH. Yield: 180 mg, 40%. Mass spectrometry (m/z) for M^{2+} ion calcd. at 337, found 337. Anal. Calcd. $C_{36}H_{28}N_8Ru_1P_2F_{12}$ C: 44.87%; H: 2.93%; N: 11.63%. Anal. Found: C: 44.81%; H: 2.90%; N: 11.20%.

^{1}H-NMR (d^6-DMSO): 9.43 (d) $H^{6'}$, 9.10 (d) H^{3tpy}, 8.83 (d) $H^{3'tpy}$, 8.78 (dd) H^{4tpy}, 8.53 (dd) $H^{4'tpy}$, 8.18 (d) H^3, 8.10 (dd) H^4, 7.90 (d) $H^{3'}$, 7.45 (d) H^{6tpy}, 7.28 (dd) H^5 tpy, 7.10 (dd) $H^{4'}$, 7.00 (dd) $H^{5'}$, 2.6-3.00 (m) CH_3 (Figure 9, Appendix I).

2.5.7 Synthesis of $[Os(tpy)_2][PF_6]_2$

$[(NH_4)_2OsCl_6]$ (71.1 mg, 0.20 mmol) and 2 equivalents of (tpy) (93.0 mg, 0.40 mmol) were dissolved in 7 cm^3 of ethylene glycol, containing few drops of N-ethylmorpholine. The reaction mixture was heated at reflux under nitrogen, for 6 hours. An aqueous solution of NH_4PF_6 was added. The product was filtered by vacuum filtration and purified by column chromatography, using silica gel and acetonitrile/H_2O (18:20) and KNO_3 (0.5%) as eluent. Yield: 60.0 mg, 32%.

^{1}H-NMR (CD_3CN): 8.80 (d) $H^{3'}$, 8.50 (d) H^3, 7.95 (dd) $H^{4'}$, 7.81 (dd) H^4, 7.23 (d) H^6, 7.10 (dd) H^5 (Figure 10, Appendix I).

2.5.8 Synthesis of $[Os(py\text{-}tpy)_2][PF_6]_2$

$[(NH_4)_2OsCl_6]$ (71 mg, 0.20 mmol) and 2 equivalents of (py-tpy) (124 mg, 0.40 mmol) were dissolved in 7 cm^3 of ethylene glycol, containing few drops of N-ethylmorpholine. The reaction mixture was heated at reflux under nitrogen, for 6 hours. An aqueous solution of NH_4PF_6 was added. The product was filtered by vacuum and recrystallised from acetonitrile. Yield: 53 mg, 24%.

^{1}H-NMR (CD_3CN): 9.10 (s) $H^{3'}$, 8.88 (d) H^b, 8.59 (d) H^3, 8.05 (d) H^a, 7.76 (dd) H^4, 7.23 (d) H^6, 7.05 (dd) H^5 (Figure 11, Appendix I).

2.5.9 Synthesis of $[Os(tpy)(tpy\text{-}ph\text{-}Br)][PF_6]_2$

$[Os(tpy)Cl_3]$ (137 mg, 0.30 mmol) and 1 equivalent of (tpy-ph-Br) (116 mg, 0.30 mmol) were dissolved in 10 cm^3 of ethylene glycol, containing few drops of N-ethylmorpholine. The reaction mixture was heated at reflux under nitrogen, for 6

hours. An aqueous solution of NH_4PF_6 was added. A dark brown product precipitated and was purified with silica column using acetonitrile/H_2O (18:20) and KNO_3 (0.5%) as eluent. Yield: 74.0 mg, 22%. Mass spectrometry (m/z) for M^{2+} ion calcd. at 810.9, found 810.6. Anal. Calcd. $C_{36}H_{25}N_6Os_1Br_1P_2F_{12}$ C: 39.25%; H: 2.29%; N: 7.63 %. Anal. Found: C: 39.19%; H: 2.32%; N: 7.59%. ^{1}H-NMR ($CDCl_3$): 8.70 (d) H^3, 8.63 (s) $H^{3'}$, 8,60 (d) H^6, 7.85 (dd) H^4, 7.64-7.61 (m) $H^{3''}$, $H^{3'''}$, $H^{2'''}$, 7.52 (d) H^b, 7.58 (d) H^a, 7.45-7.42 (m), H^5, H^4, $H^{5'''}$, $H^{4'''}$ (Figure 12, Appendix I).

2.5.10 Synthesis of [Os(py-tpy)(tpy-ph-Br)][PF_6]$_2$

[Os(tpy-ph-Br)Cl_3] (117 mg, 0.20 mmol) and 1 equivalent of (py-tpy) (62.0 mg, 0.20 mmol), were dissolved in 10 cm^3 of ethylene glycol, containing a few drops of N-ethylmorpholine. The reaction mixture was heated at reflux under nitrogen, for 8 hours. A saturated aqueous solution of NH_4PF_6 was added. A dark brown product precipitated. The product was filtered by vacuum filtration and dried with diethyl ether. Then it was purified with silica column using acetonitrile/H_2O (8:2) and KNO_3 (0.5%) as eluent. Yield: 75.0 mg, 32%. Mass spectrometry (m/z) for M^{2+} ion calcd. at 888.8, found 888.8. Anal. Calcd. $C_{41}H_{28}N_7Os_1Br_1P_2F_{12}$ C: 41.78%; H: 2.39%; N: 8.32 %. Anal. Found: C: 41.70%; H: 2.37%; N: 8.40%. ^{1}H-NMR (CD_3CN): 8.65 (s) $H^{3'pytpy}$, 8.50-8.57 (m) $H^{3'}$, H^3, 8.58 (dd) H^{6pytpy}, 7.90 (m) H^{4pytpy}, H^4, H^5, 7.88 (m) H^6, H^{3pytpy}, 7.62 (d) H^d, 7.55 (d) H^a, 7.62 (d) $H^{c\ pytpy}$, 7.31 (d), 7.52 (d), $H^{b\ pytpy}$, 7.40 (m) H^5, H^{5pytpy} (Figure 13, Appendix I).

2.5.11 Attempted Synthesis of [Os(tpy)(L1)(PF_6)(H_2O)]

[Os(tpy)Cl_3] (130 mg, 0.20 mmol) and 1 equivalent of ligand (H_2L1), 2,6-bis-([1,2,4]triazol-3-yl)pyridine, (43.2 mg, 0.20 mmol) were dissolved in 3.0 cm^3 of ethylene glycol, containing a slight molar excess of NaOH and few drops of N-ethylmorpholine. The reaction mixture was heated at reflux for 5 hours and then acidified to pH = 2 with HCl (2M). An aqueous solution of NH_4PF_6 was added. A dark brown product precipitated. Recrystallisation from (acetonitrile/metanol. 1:1) and alumina column chromatography, using acetonitrile/MeOH 1:1 as eluent, afforded a mixture of three isomers: N2N2 and N2N4 and N4N4.

2.5.12 Attempted Synthesis of [Os(tpy)(L2)(H_2O)][PF_6]

[Os(tpy)Cl_3] (160 mg, 0.30 mmol) and 1 equivalent of ligand (H_2L2), 2,6-bis-(5-phenyl-[1,2,4]triazol-3-yl)pyridine, (110 mg, 0.30 mmol) were dissolved in 2.8 cm^3 of ethylene glycol, containing a slight molar excess of NaOH and few drops of N-ethylmorpholine. The reaction mixture was heated at reflux for 6 hours and then acidified to pH = 2 with HCl (2M). An aqueous solution of NH_4PF_6 was added. A dark brown product precipitated. It was recrystallised from acetone and then purification with alumina column using acetonitrile/MeOH 1:1 as eluent. The product contained the two isomers: N2N2 and N2N4.

^{1}H-NMR (DMSO): 9.80 (d), H^3, 8.90 (d), $H^{4''}$, 8.80 (d), $H^{3'}$, 8.58 (dd) H^4, 8.30 (d), $H^{3''}$, 8.20 (d) H^6, 7.92 (dd), $H^{4'}$, 7.70 (dd), H^5, 7.65-7.60 (m) H^a, H^b, H^c.

2.5.13 Synthesis of [Os(tpy)(L3)(H_2O)]

[Os(tpy)Cl_3] (190 mg, 0.40 mmol) and 1 equivalent of ligand (H_2L3), 2,6-bis-([1,2,3,4]tetrazol-5-yl)pyridine, (86.0 mg, 0.40 mmol) were dissolved in 3 cm^3 of ethylene glycol, containing a slight molar excess of NaOH and few drops of N-ethylmorpholine. The solution was heated at reflux under argon for four hours. Water was added to the solution and a brown solid product precipitated. The product was filtered by vacuum filtration and dried with diethyl ether. It was dissolved in acetone and the black insoluble precipitate was filtered off. The product was purified with silica column using acetonitrile/H_2O (8:2) and KNO_3 (0.5%) as eluent. The brown product was dried under vacuum overnight. Yield: 196 mg, 75%. Mass spectrometry (m/z) for M^{2+} ion calcd. at 655, found 655. Anal. Calcd. $C_{22}H_{16}N_{12}O_1Os_1$ C: 40.36%; H: 2.46%; N: 25.68%. Anal. Found: C: 40.28%; H: 2.43%; N: 25.72%.

^{1}H-NMR (d^6-DMSO): 8.95 (d) $H^{3'}$, 8.70 (d) H^3, 8.43 (d) $H^{3''}$, 7.90 (d) $H^{4''}$, 7.78 (m) $H^{4'}$, H^4, 7.28 (d) H^6, 7.18 (dd) H^5 (Figure 14, Appendix I).

2.5.14 Synthesis of [Os(tpy)[2,6-(2,3-ph-4-CH_3-pyrazol)py][PF_6]$_2$

The complex was obtained by heating [Os(tpy)Cl_3] (72.1 mg, 0.10 mmol) and a stoichiometric amount of [2,6-(2,3 phenyl-4-methyl pyrazol) pyridine], (45.0 mg, 0.10 mmol) dissolved in 6 cm^3 of ethylene glycol, containing a slight molar excess of NaOH and few drops of N-ethylmorpholine. The reaction mixture was heated at reflux under nitrogen, for 4 hours. The solution was concentrated using a rotary evaporator, acidified to pH 2 with HCl and an excess of NH_4PF_6 was added. A dark brown solid precipitated was collected by vacuum filtration and dried with diethyl ether. The product was purified with silica column using acetonitrile/H_2O (8:2) and KNO_3 (0.5%) as eluent. Recrystallisation from acetonitrile afforded the pure product. Yield: 60.0 mg, 58%. Mass spectrometry (m/z) for M^{2+} ion calcd. at 751, found 751. Anal. Calcd. $C_{36}H_{28}N_8Os_1P_2F_{12}$ C: 41.07%; H: 2.68%; N: 10.64 %. Anal. Found: C: 41.07%; H: 2.66%; N: 10.62%.

^{1}H-NMR (d^6-DMSO): 9.55(d) $H^{6''}$, 9.38 (d) H^{3tpy}, 9.18 (d) $H^{3'tpy}$, 8.88 (dd) H^{4tpy}, 8.80 (dd) $H^{4'tpy}$, 8.20 (m) H^3, H^4, 8.00 (d) $H^{3'}$, 7.88 (d) H^{6tpy}, 7.10 (dd) H^5 tpy, 6.98 (dd) $H^{4''}$, 7.00 (dd) $H^{5''}$, 2.6 (m) CH_3 (Figure 15, Appendix I).

2.5.15 Synthesis of [Co(py-tpy)$_2$][PF_6]$_2$

[$CoCl_2(6H_2O)$] (101 mg, 0.40 mmol) and 2 equivalents of ligand (py-tpy) (263 mg, 0.80 mmol) were dissolved in a solution of EtOH / H_2O. The reaction mixture was heated at reflux under stirrer for 4 hours. The solution was filtered and the filtrate was treated with NH_4PF_6 salt and water. The dark red precipitate was collected by vacuum filtration and dried using diethyl ether. Yield: 140 mg, 36%. Anal. Calcd. $C_{40}H_{28}N_8Co_1P_2F_{12}$ C: 43.93%; H: 2.58%; N: 10.25%. Anal. Found: C: 43.63%; H: 2.49%; N: 10.51%.

^{1}H-NMR (CD_3CN): 9.08(s) $H^{3'}$, 8.88 (d) H^b, 8.57 (d) H^3, 8.15 (d) H^a, 8.00 (dd) H^4, 7.40 (d) H^6, 7.21 (dd) H^5

2.6 Bibliography

[1] Constable E.C., Cargill Thompson, A.M.W., J. Chem. Soc. Dalton Trans. *1992*, 2947.

[2] (a) Case, F.H., Butte, W.A., J. Chem. Soc., *1961*, 4415; (b) Spahni, W., Calzaferri, G., Helv. Chem. Acta, *1984*, 67, 450.

[3] (a) Sugiyarto, K. H., Craig, D. C., Rae, A. D.; Goodwin, H. A., Aust. J. Chem., *1993*, 46, 1269; (b) Finnegan, W. G., Henry, R. A., Lofquist, R., J. Am. Chem. Soc., *1958*, 80, 3908.

[4] Constable, E.C., Cargill Thompson, Tocher, D.A., Daniels, M.A.M., New J. Chem, *1992*, 16, 855.

[5] Constable, E.C., Cargill Thompson, J. Chem. Soc. Dalton Trans. *1992*, 2947.

[6] Buckingham, D.A., Aust. J. Chem., *1994*, 17, 622.

[7] Duati, M,. Ph D Thesis, *2001*, Dublin City University, Dublin.

[8] Arana, C., Abruna, H.D., Inorg. Chem., *1993*, 32, 194.

[9] Duati, M., Tasca, S., Lynch, F., Bohlen, H., Vos, J. G., Inorg. Chem., *2003*, 42, 8377.

[10] Collin, J. -P., Guillerez, S., Sauvage, J. -P., Barigelletti, F., Flamigni, L., De Cola L., Balzani, V., Coord.Chem. Rev., 111, *1991*, 291.

Chapter 3

Ru(II) and Os(II) Terpyridine Complexes: Synthesis and ^{1}H-NMR Characterisation

Chapter 3 describes synthetic methods and characterisation by ^{1}H-NMR spectroscopy of a series of terpyridyl ligands and their ruthenium terpridine complexes, such as [Ru(py-tpy)]$_2$[PF$_6$]$_2$, [Ru(tpy)(tpy-ph-Br)][PF$_6$]$_2$, [Ru(py-tpy)(tpy-ph-Br)][PF$_6$]$_2$, [Ru(tpy-ph-Br)(L3)(H$_2$O)] (where (H$_2$L3) = [2,6-bis-([1,2,3,4]tetrazol-5-yl)pyridine]) and the [Ru[2,6-(2,3-ph-4-CH$_3$-pyrazol)py](tpy)[PF$_6$]$_2$. The corresponding osmium complexes, such as [Os(py-tpy)]$_2$[PF$_6$]$_2$, [Os(py-tpy)(tpy-ph-Br)][PF$_6$]$_2$, [Os(tpy)(tpy-ph-Br)][PF$_6$]$_2$, [Os(tpy)(L3)(H$_2$O)] and [Os[2,6-(2,3-ph-4-CH$_3$-pyrazol)py](tpy)[PF$_6$]$_2$, have been also synthesised and fully characterised. All the metal centre complexes have been here compared with the prototype, [Ru(tpy)$_2$][PF$_6$]$_2$ and [Os(tpy)$_2$][PF$_6$]$_2$.

3.1 Introduction

Since the tridentate ligand 2, 2': 6', 2" - terpyridine, (tpy), was first prepared over 70 years ago [1] its coordination chemistry, along with that of its substitutent (X-tpy) analogues, has been widely studied [2]. More recently terpyridines have found increasing favour as coordination chemistry has started to shift from molecular to supramolecular levels. The ability of terpyridine to chelate to a wide range of metal ions has lead to its incorporation in macrocyclic ligands. The synthesis of complexes capable of self-assembly [3][4] is of particular interest. There have been many reports of multinuclear molecular species with (tpy) ligands[5][6][7][8]. A structurally important advantage of terpyridine compounds over species containing bidentate ligands, is that octahedral (tpy) type complexes are achiral (no complications due to stereoisomers) and can be connected to other molecular components through the terpyridine 4'-position while maintaining the C_{2v} symmetry of the ligand (no complications due to geometrical isomerism). Therefore the geometry of terpyridine metal complexes offers the possibility to design linear supramolecular species in which R and R' components are trans to one another [9] (Figure 3.1).

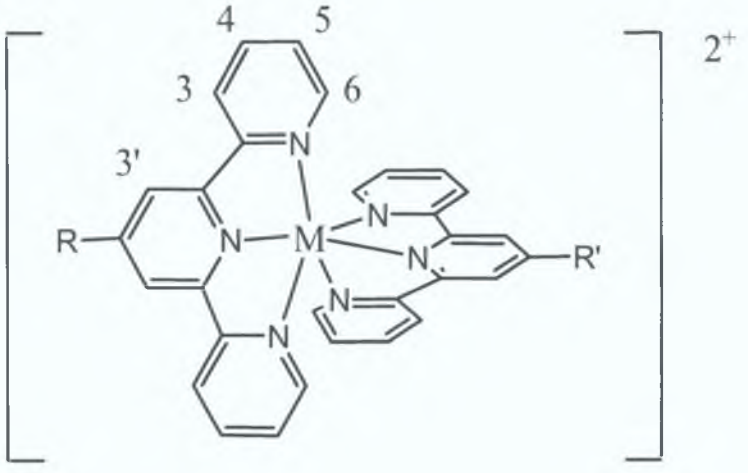

Figure 3.1 Unique form of $[M(tpy)_2]^{2+}$ complex

A disadvantage is that tridentate coordination of 2,2': 6',2" - terpyridine results in complexes, which are generally considerabled distorted. The distortion is evident

in the geometry of both the coordinated ligand and the coordination environment of the metal ion.

For example, Thummel and Jahng [10] have drawn attention to the acute N-M-N angles (60°) that would result from the coordination of the three nitrogen atoms of unperturbed terpyridine, in which the angles within and between the pyridine rings are normal. Such deviation from the 90° of a regular octahedron is not adopted and angles close to 80° are usually observed in six- coordinate compounds. These angles can be attained only by tightening the angles about the bonds of the ligands within the chelate rings, thereby imparting distortion within the terpyridine moiety.

The geometry about the metal atoms is typical for bis (terpyridine) metal complexes; the distortion of the ligand geometry is most pronounced in the angles about the 2- and 6 - positions of the central pyridine ring. Distortion about the bonds is evident even in uncoordinated terpyridine, which has the expected trans, trans configuration of the terminal nitrogen atoms, with respect to the central atom, as distinct from the cis, necessary for tridentate coordination [11]. The nature of this distortion involves a reduction in the N-C-C bridge angles from the ideal 120° to about 116°. The relatively short nitrogen-hydrogen distances (c. 2.45 Å), which accompany this distortion, suggest weak hydrogen bonding involving the terminal nitrogen atoms with the hydrogen atoms at the 3- and 5- positions of the central ring and the nitrogen atom of the central ring with the hydrogen atoms at 3-position of the terminal rings. It seems likely that such forces influence the geometry of a number of related polypyridine systems, where the trans configuration appears to be fairly generally adopted. In both the ruthenium and osmium complexes the M-N $_{central}$ distances are significantly shorter then the N-N $_{terminal}$ distances, which again is typical for coordination of conjugated terpyridine systems[10][11]. Both the bond angles and the metal-nitrogen distances are comparable to those reported for systems in which a single terpyridine molecule is coordinated to ruthenium (II) or osmium (II) or to those in the bis (ligand) ruthenium (II) derivative of a 4'-substituted terpyridine system.

The structure and atom numbering schemes for $[M(tpy)_2]^{2+}$ are shown in Figure 3.2.

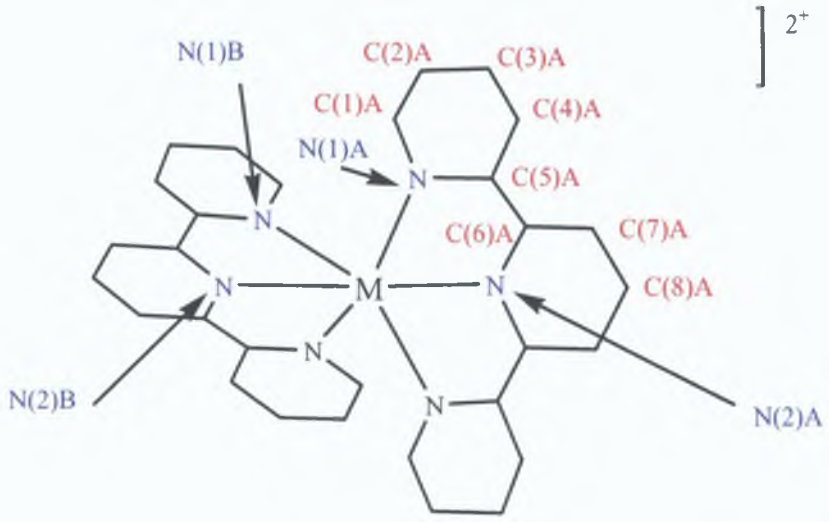

Figure 3.2: Structure of the complex cation in $[M(tpy)_2]^{2+}$, where M=Ru (II) and Os(II)

Bond lengths for the two terpyridine prototype, $[Ru(tpy)_2]^{2+}$ and $[Os(tpy)_2]^{2+}$ are not significantly different. The corresponding data [12] are collected in Table 3.1.

Atoms	**Bond lengths (Å)**	
	$[Ru(tpy)_2]^{2+}$	**$[Os(tpy)_2]^{2+}$**
M-N(1)	2.073	2.070
M-N(2)	1.977	1.978
N(1)-C(1)	1.339	1.321
N(1)-C(5)	1.376	1.362
N(2)-C(6)	1.346	1.371
C(1)-C(2)	1.381	1.385
C(2)-C(3)	1.386	1.393
C(3)-C(4)	1.381	1.384
C(4)-C(5)	1.387	1.402
C(5)-C(6)	1.470	1.475
C(6)-C(7)	1.382	1.385
C(7)-C(8)	1.380	1.379

Table 3.1: Bond lengths (Å) in $[Ru(tpy)_2]^{2+}$ and $[Os(tpy)_2]^{2+}$

Bond angles for the two compounds $[Ru(tpy)_2]^{2+}$ and $[Os(tpy)_2]^{2+}$ [12] are also similar as shown below in Table 3.2.

Atoms	Angle (degrees)	
	$[Ru(tpy)_2]^{2+}$	$[Os(tpy)_2]^{2+}$
N(1)A-M-N(2)A	78.7	79.3
N(1)A-M-N(1)B	91.2	91.1
N(1)A-M-N(2)B	101.3	102.6
N(1)A-M-N(1)A[a]	157.5	157.8
N(1)A-M-N(1)B[a]	93.3	92.2
N(2)A-M-N(1)B	101.6	102.0
N(2)A-M-N(2)B	180	177.5
N(1)B-M-N(2)B	78.4	79.5
N(1)B-M-N(1)B[a]	156.8	157.7

Table 3.2: Bond angle (degrees) in $[Ru(tpy)_2]^{2+}$ and $[Os(tpy)_2]^{2+}$

As already shown in Chapter 1, the scope of this thesis is making metal complexes for the preparation of junctions in which nanoparticles may be linked to a metal contact or electrode, through molecular bridges. These functionalised molecular systems may act as molecular bridges between the metal centre and the surface and electron transfer barrier properties may be used as chemical switches. In this thesis, different approaches have been attempted with different purposes:

- Introduction of functional groups as pyridine and thiol groups as linkers.
- Introduction of tetrazolate ligand that may improve photophysical properties of the complexes (stronger emission and longer lifetime).
- Electrochemical control: low oxidation and potentials; use of osmium as metal centre to improve redox properties of the complexes.

Terpyridine complexes with substituents in position 4 on the central pyridine ring have been studied. In particular, the synthesis of thiol terpyridine complexes has been attempted using (tpy-ph-Br) as starting material and reacting it with boronic acid compounds in cross-coupling Suzuki reactions, Pd-catalysed.

The precursor (tpy-ph-Br) has been also used for making ruthenium and osmium complexes: $[Ru(tpy)(tpy\text{-}ph\text{-}Br)][PF_6]_2$, $[Ru(py\text{-}tpy)(tpy\text{-}ph\text{-}Br)][PF_6]_2$, $[Ru(tpy\text{-}ph\text{-}Br)(L3)(H_2O)]$, $[Os(tpy)(tpy\text{-}ph\text{-}Br)][PF_6]_2$, $[Os(py\text{-}tpy)(tpy\text{-}ph\text{-}Br)][PF_6]_2$ and $[Os(tpy)(L3)(H_2O)]$.

Synthesis of metal complexes with pyridines substituted terpyridine ligands. Pyridyl group can provide well-defined anchoring points on nanoparticles and on a range of surfaces. Synthetic routes of redox centre linkers ruthenium and osmium terpyridyl complexes, modified with (py-tpy) group, have been investigated in this thesis: $[Ru(py\text{-}tpy)]_2[PF_6]_2$, $[Ru(py\text{-}tpy)(tpy\text{-}ph\text{-}Br)][PF_6]_2$, $[Ru(tpy)(tpy\text{-}ph\text{-}Br)][PF_6]_2$, $[Os(py\text{-}tpy)]_2[PF_6]_2$ and $[Os(py\text{-}tpy)(tpy\text{-}ph\text{-}Br)][PF_6]_2$ and $[Os(tpy)(tpy\text{-}ph\text{-}Br)][PF_6]_2$, have been prepared (Figure 3.3).

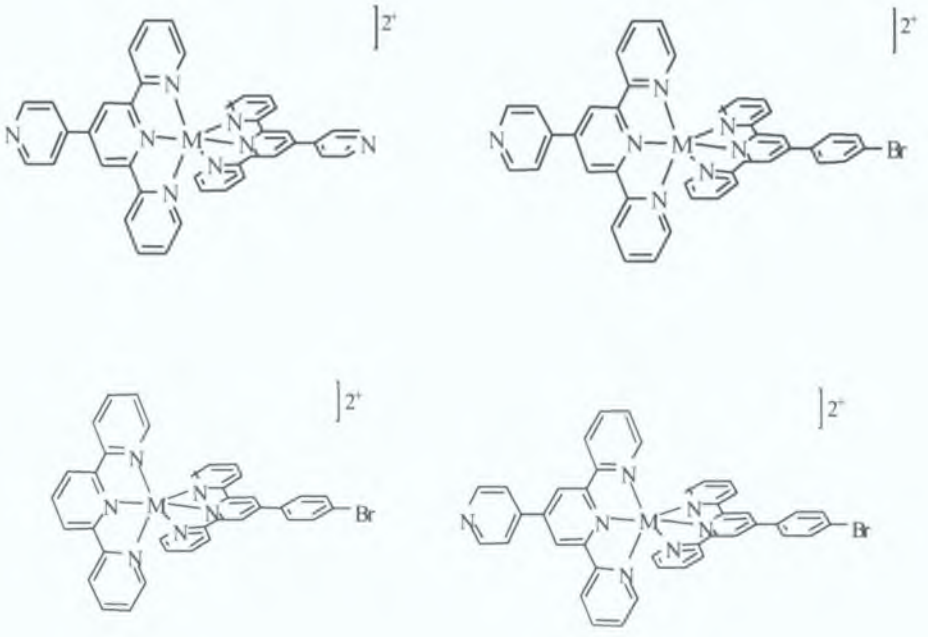

Figure 3.3: Structures of metal (M= Ru, Os) terpyridyl complexes synthesised in this thesis, functionalised with (py-tpy) and (tpy-ph-Br) groups

To improve redox and photophysical properties, other ligands have been introduce and used for synthesising ruthenium and osmium complexes: [2,6-bis-([1,2,3,4]tetrazol-5-yl)pyridine] (H_2L3) and [2,6-(2,3-ph-4-CH_3-pyrazol)py], (see Figure 3.4).

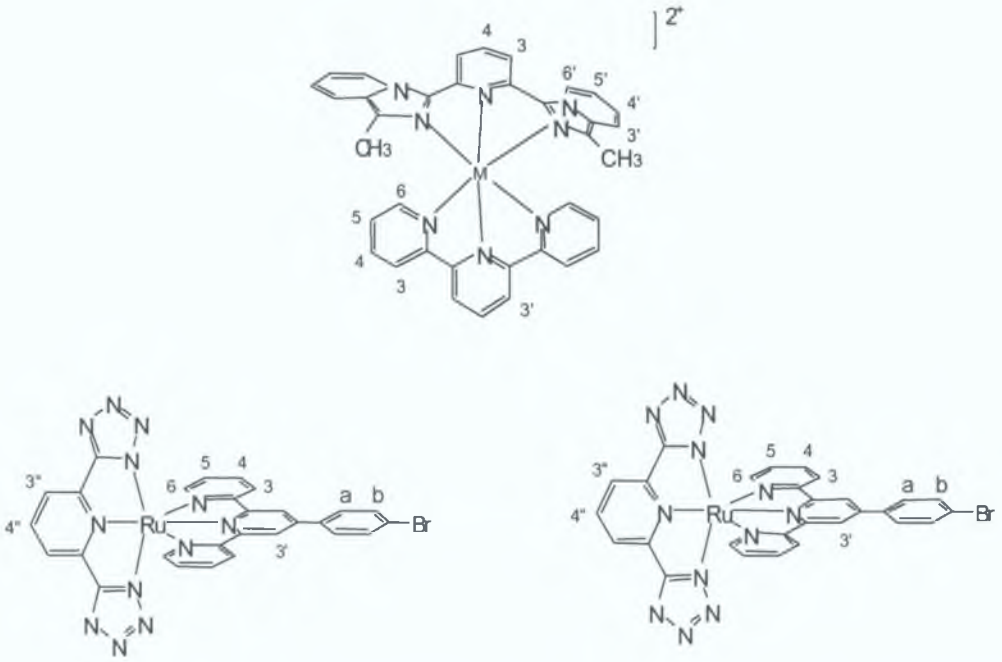

Figure 3.4: Structures of metal (M= Ru, Os) terpyridyl complexes synthesised in this thesis, functionalised with (1) and (H_2L3) groups

3.2 Synthesis of terpyridine ligands

All the terpyridine ligands were prepared using the Krohnke[14] procedure involving the condensation of two ketones with an aldehyde to give a 1,5-diketone with subsequent ring closure (Figure 3.5). Detailed synthetic conditions for all compounds are given in Chapter 2. Further characterisation of the metal complexes is given in Chapter 4. The purity of the compounds was checked by elemental analysis, ^{1}H-NMR as previously shown in chapter 2.

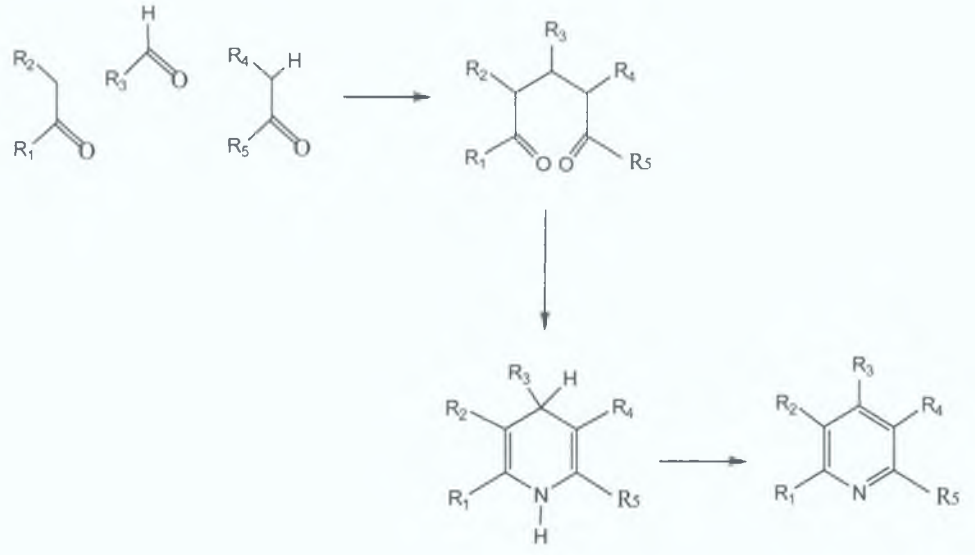

Figure 3.5: General synthesis of 2, 2': 6', 2'' - terpyridine ligand

For the synthesis of 2, 2': 6', 2" - terpyridine ligands R_1 and R_5 are 2 pyridyl groups, while R_2, R_3 and R_4 are substituents as desired.

3.2.1 Synthesis of 4'(pyrid-4-yl) 2,2'; 6', 2" - terpyridine (py-tpy)

For the synthesis of 4'(pyrid-4-yl) 2,2'; 6', 2" - terpyridine (py-tpy), firstly [1-(2-pyridyl)-3-(4-pyridyl)-2-propenone] was prepared by reacting 2-acetylpyridine and pyridine-4-carbaldehyde in a basic etanol/H_2O mixture solution. The enone obtained was reacted with [1-(2-pyridilcarbonyl) pyridinium][PF_6] and ammonium acetate in aqueous solution. The reaction scheme is shown in Figure 3.6. The first step of the reaction was somewhat problematic, because instead of the desired white solid, an orange gum was obtained. The gum was dissolved in a minimum amount of methanol. The solution was heated 50 °C and finally afforded a white product that was recrystallised from ethanol. The yield of the reaction is 65%.

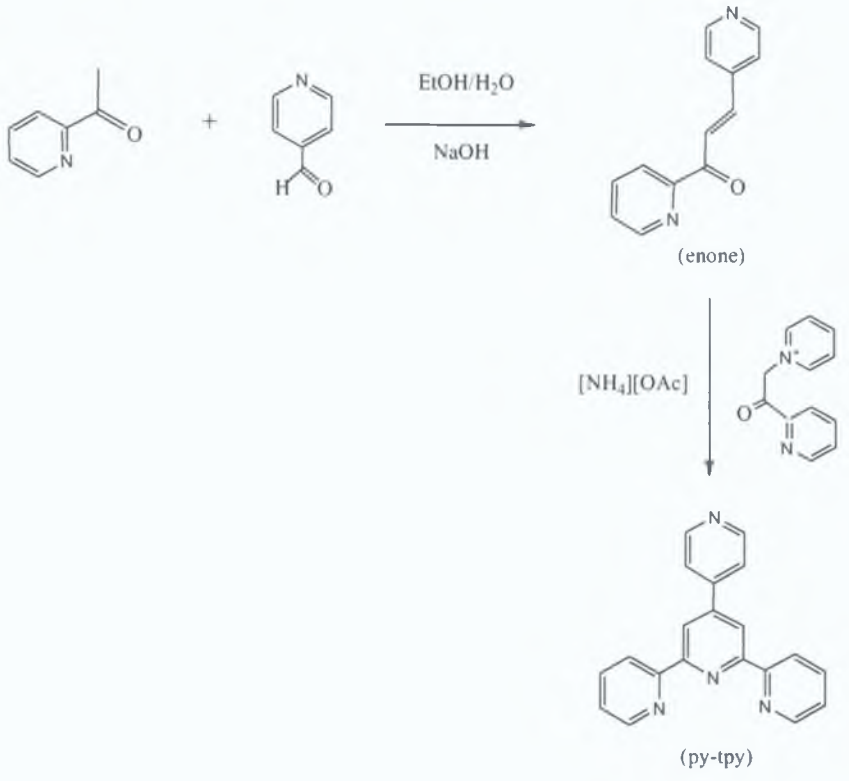

Figure 3.6: Synthesis of 4'(pyrid-4-yl) 2,2'; 6', 2" - terpyridine (py-tpy)

3.2.2 Synthesis of 4'(4-bromo-phenyl) 2,2'; 6', 2" - terpyridine (tpy-ph-Br)

As already described in Section 3.1, one of the purposes of this thesis was the preparation of complexes with substituents that may act as linkers to surface. Particular attention has been paid on the preparation of thiol complexes, by starting with 4'(4-bromo-phenyl) 2,2'; 6', 2" - terpyridine (tpy-ph-Br), as starting material. 4'(4-bromo-phenyl) 2,2'; 6', 2" - terpyridine was synthesised using the same procedure carried out for the synthesis of 4'(pyrid-4-yl) 2,2'; 6', 2" - terpyridine (py-tpy). In this synthesis, 2-acetylpyridine was reacted with 4-bromoacetaldeyde in basic ethanol/H_2O mixture solution to obtain the enone:

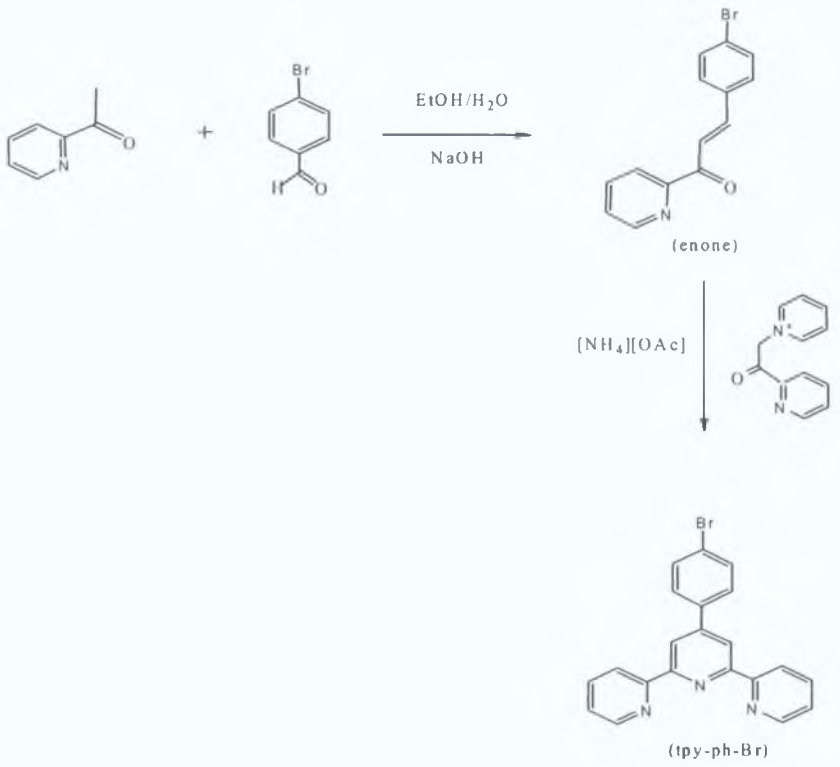

Figure 3.7: Synthesis of 4'(4-bromo-phenyl) 2,2'; 6', 2" - terpyridine (tpy-ph-Br)

A subsequent reaction with 1-(2-pyridilcarbonyl) pyridinium iodide (which is effectively a stabilised enolate of 2-acetylpyridine) generates a 1,5-dicarbonyl, which is ring-closed in situ with a large excess of ammonium acetate to give the terpyridine product. Unfortunately the yield is relatively low, 26%.

3.2.3 Synthesis of [2,6-bis-([1,2,4]triazol-3-yl)pyridine] (H_2L1) and [2,6-bis-(5-phenyl-[1,2,4]triazol-3-yl)pyridine] (H_2L2)

For the synthesis of the ligand [2,6-bis-([1,2,4]triazol-3-yl)pyridine] (H_2L1) the procedure reported in the literature[16] has been followed (Figure 3.8).

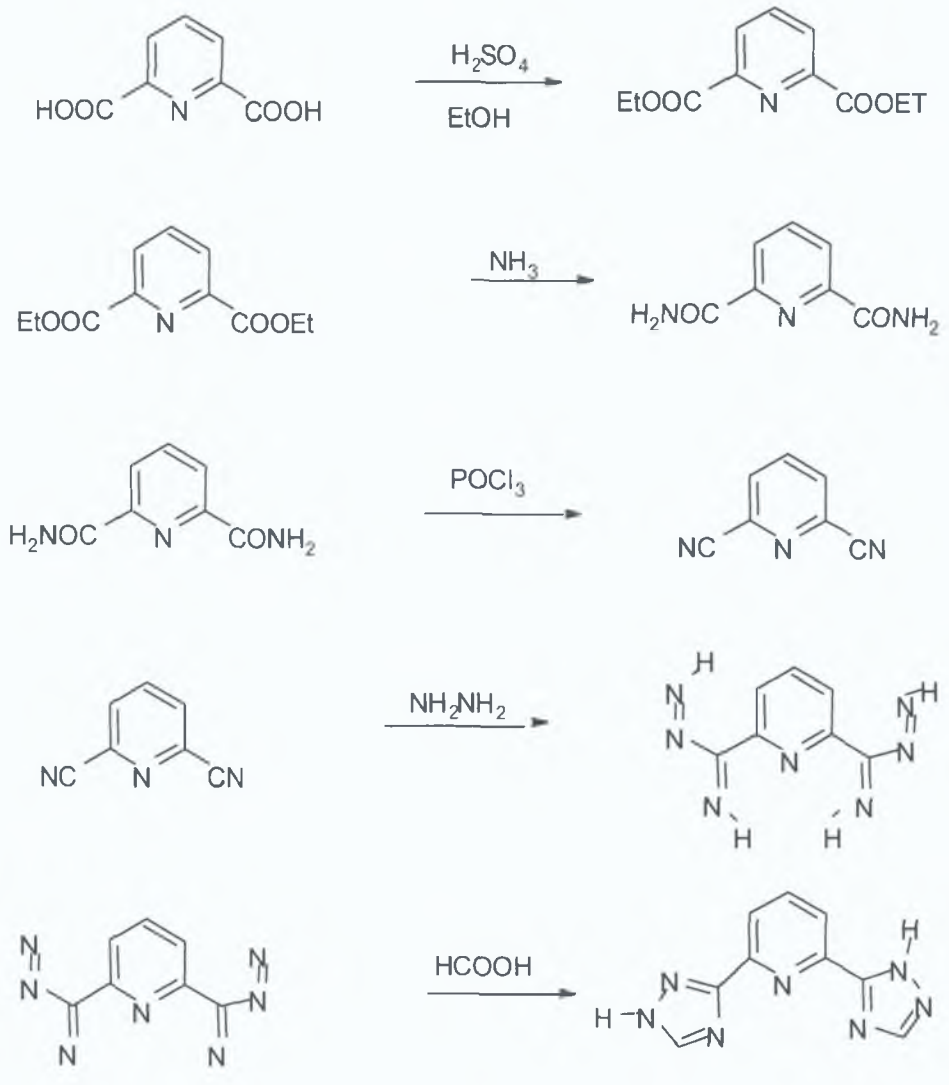

Figure 3.8: Synthesis of the [2,6-bis-([1,2,4]triazol-3-yl)pyridine] (H_2L1)

As shown in Figure 3.8, the preparation of [2,6-bis-([1,2,4]triazol-3-yl)pyridine] involved five steps:

1) Synthesis of pyridine-2,6-dicarboxylic acid diethyl ester

First step involves the reaction between pyridine-2,6-dicarboxylic acid and concentrate H_2SO_4 in ethanol solution. Firstly, the mixture was left to react for 10 hours, but TLC check confirmed the presence of starting material beside the product. The mixture was heated at reflux overnight and the product was finally isolated after neutralisation using a basic solution and extracted with CH_2Cl_2. After evaporation of the solvent, a pale yellow oil was obtained. The oil which solidified on standing was used without any other purification. The reaction afforded 81% of yield.

2) Synthesis of pyridine-2,6-dicarboxy diamide

In the second step reaction, NH_3 was added slowly to the pyridine-2, 6-dicarboxylic acid diethyl ester and dissolved in methanol. The solution was carefully cooled using an ice bath. After 30-35 minutes, the product precipitated. The mixture was stirred overnight at room temperature. The solid was then filtered and washed with small amount of cold methanol. The final yield was 72%.

3) Synthesis of pyridine-2,6-dicarbonitrile

Third step required strong conditions and proved to be somewhat problematic. The major problem encountered involved the solubility of the starting material. A range of different solvents have been previously and DMF was found to be the favourite. To pyridine-2,6-dicarboxy diamide was added slowly $POCl_3$, using carefully an ice bath for cooling the solution. The yellow solution was stirred at room temperature for 3 hours, CH_2Cl_2 and water were added and the organic layer was then collected and washed with more water. To help the precipitation of the desired product, a small amount of ice was added to the solution. The product obtained in a 61% of yield, was washed with cold water and dried very well for next step.

4) Synthesis of pyridine-2,6 diimidrazone

To a solution of pyridine-2,6-dicarbonitrile and EtOH, hydrazine monohydrate was added. After 1 hour, a precipitation occurred. The resulting solution was then warmed at 60°C and stirred for another hour to help the precipitation of the product. A big amount of yellow pale product was collected by filtration and washed with a small portion of cold MeOH and dried. The yield was 75%.

Step 5 Synthesis of 2,6-bis-([1,2,4]triazol-3-yl)pyridine (H_2L1)

Particular attention was required for the last step of the reaction. Formic acid was carefully added to pyridine-2,6 diimidrazone at 0 °C. The solution was stirrer for 3 hours. The acid was then removed under vaccum and the resulting oil, was dissolved using 1,2-ethandiol and heated under reflux for 1 hour (no other solvents could be used to dissolve the oil). The solution was cooled, mixed with a small amount of ice and left overnight in the fridge. A big amount of product was collected, washed with diethyl ether and used without any further purification. The product was obtained in a 56% of yield.

The same procedure was followed for the preparation of [2,6-bis-(5-phenyl-[1,2,4]triazol-3-yl)pyridine] (H_2L2) (Figure 3.9).

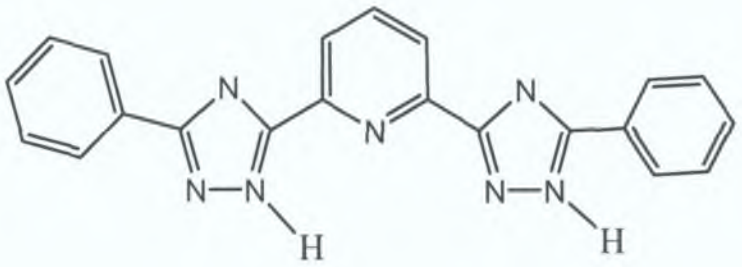

Figure 3.9: Synthesis of [2,6-bis-(5-phenyl-[1,2,4]triazol-3-yl)pyridine]

A similar way followed for the preparation of (H_2L1) was used. For the preparation of (H_2L2) five are the steps involved:

1) Synthesis of pyridine-2,6-dicarboxylic acid diethyl ester
2) Synthesis of pyridine-2,6-dicarboxy diamide
3) Synthesis of pyridine-2,6-dicarbonitrile
4) Synthesis of pyridine-2,6 diimidrazone

1) Synthesis of pyridine-2,6-dicarboxylic acid diethyl ester

First step involves the reaction between pyridine-2,6-dicarboxylic acid and concentrate H_2SO_4 in ethanol solution. The mixture was heated at reflux overnight and the product was isolated after neutralisation using a basic solution and extracted with CH_2Cl_2. A yellow oil was obtained. The oil which solidified on standing was used without any other purification. The reaction afforded 83% of yield.

2) Synthesis of pyridine-2,6-dicarboxy diamide

NH_3 was added slowly to the pyridine-2,6-dicarboxy acid diethyl ester and dissolved in methanol. The solution was carefully cooled using an ice bath. After 40 minutes, the product precipitated. The mixture was stirred overnight at room temperature. The solid was then filtered and washed with small amount of cold methanol. The final yield was 75%.

3) Synthesis of pyridine-2,6-dicarbonitrile

Third step proved to be somewhat problematic. The major problem encountered involved the solubility of the starting material. A range of different solvents have been previously and DMF was found to be the favourite. To pyridine-2,6-dicarboxy diamide was added slowly $POCl_3$, using carefully an ice bath for cooling the solution. The solution was stirred at room temperature for 3 hours, CH_2Cl_2 and water were added and the organic layer was then collected and washed with more water. To help the precipitation of the desired product, a small amount of ice was added to the solution. The product obtained in a 64% of yield, was washed with cold water and dried.

4) Synthesis of pyridine-2,6 diimidrazone

To a solution of pyridine-2,6-dicarbonitrile and EtOH, hydrazine monohydrate was added. After 1 hour a precipitation occurred. The solution was then warmed at 60°C and stirred for another hour to help the precipitation of the product. A yellow pale product was collected by filtration and washed with a small portion of cold MeOH and dried. The yield was 79%.

Step 5 Synthesis of [2,6-bis-(5-phenyl-[1,2,4]triazol-3-yl)pyridine] (H_2L2)

The pyridine-2,6 diimidrazone obtained at the last step, has been stirrer overnight in THF with triethylamine and EtOH, then heated at reflux for 2 hours in 1,2-ethandiol and left in the fridge overnight to help the precipitation of the product. A big amount of yellow precipitate was filtered and washed with diethyl ether and was used without any further purification. The yield was 74%.

3.2.4 Synthesis of [2,6-bis-([1,2,3,4]tetrazol-5-yl)pyridine (H_2L3)]

The tridentate ligand [2,6-bis-([1,2,3,4]tetrazol-5-yl)pyridine] (H_2L3), (Figure 3.10) was synthesised according to the literature for similar ligands[17], using little modifications.

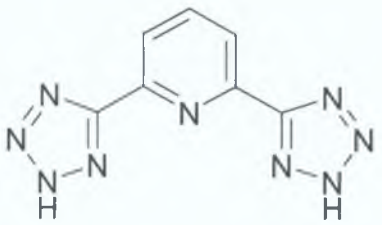

Figure 3.10: Structure of 2,6-bis-([1,2,3,4]tetrazol-5-yl)pyridine (H_2L3)

The ligand (H_2L3), was prepared by reacting 2,6 pyridine dicarbonitrile, sodium azide, NH_4Cl and LiCl (Figure 3.11). Special attention was paid to the reaction conditions; using DMF a solvent, the reaction mixture was carefully stirred under nitrogen at temperature maintained between 100° and 120°, for 10 hours. After evaporation of the solvent, a solid precipitated. It was re dissolved in water. Drop wise addition of HCl 1M afforded a white product was then collected, recrystallised from a solution of water and EtOH (1/1). During the acidification volatile NH_3 could be formed; to overcome this problem, the flask was carefully connected to a bubbler with a concentrate NaOH solution. The product was obtained with 70% of yield.

The (H_2L3) ligand contains a pyridine ring which is a relatively good π acceptor and two tetrazolate moieties which are strong σ donors. The coordination to ruthenium complexes is expected to be tridentate, in a pseudo-octahedral coordination.

Figure 3.11: Synthetic procedure for [2,6-bis-([1,2,3,4]tetrazol-5-yl)pyridine] (H_2L3)

3.3 Synthesis of Ru(II) terpyridine complexes

Several synthetic methods for the synthesis of metal terpyridine complexes have been investigated in this thesis. The procedures used for the ruthenium (II) complexes synthesised are listed in Table 3.3.

complex	solvent	precursor	Yield
$[Ru(py\text{-}tpy)_2][PF_6]_2$	Method (a) : Ethylene glycol	$RuCl_3\ H_2O$	33%
	Method (b) : $AgBF_4$, dry acetone, DMF	$[H(Ru(py\text{-}tpy)Cl_3)][PF_6]$	29%
$[Ru(tpy\text{-}ph\text{-}Br)(L3)][H_2O]$	Ethylene glycol, NaOH, N-ethylmorpholine	$[Ru(tpy\text{-}ph\text{-}Br)Cl_3]$	35%
$[Ru(tpy)(tpy\text{-}ph\text{-}Br)][PF_6]_2$	$AgBF_4$, dry acetone, DMF	$[Ru(tpy)Cl_3]$	41%
$[Ru(py\text{-}tpy)(tpy\text{-}ph\text{-}Br)][PF_6]_2$	Method (a) : $AgBF_4$, dry acetone, DMF	$[Ru(tpy\text{-}ph\text{-}Br)Cl_3]$	23%
	Method (b) : $AgBF_4$, dry acetone, DMF	$[H(Ru(py\text{-}tpy)Cl_3)][PF_6]$	67%
$[Ru[2,6\text{-}(2,3\text{-}ph\text{-}4\text{-}CH_3\text{-}pyrazol)py](tpy)[PF_6]_2$	H_2O, NaOH, N-ethylmorpholine	$[Ru(tpy)Cl_3]$	40%

Table 3.3: Reaction conditions for synthesis of ruthenium (II) complexes

For the synthesis of Ru(II) complexes the precursor [Ru(tpy-R)Cl_3] was prepared as described in Figure 3.12.

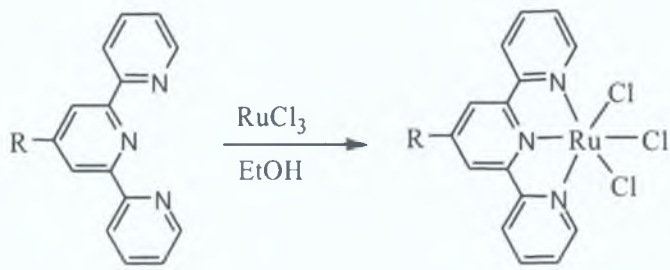

Figure 3.12: Synthetic reaction for the preparation of [Ru(tpy-R)Cl_3], where R = H, pyridine, phenyl-br

The transition metal chloride [$RuCl_3$ $2H_2O$] reacts with the corresponding terpyridine ligand in approximately stoichiometric proportions. The synthesis was performed in EtOH solution. The terpyridine metal trichloride complexes are poorly soluble and can be easily isolated by filtration. The [Ru(tpy-R)Cl_3] intermediate is then reacted, under reductive conditions, with the second ligand to yield the appropriate[Ru(tpy-R)(R')]$^{n+}$ complex [18]. Two different synthetic approaches were followed for the synthesis of Ru (II) terpyridine complexes, as shown in Figure 3.13 and 3.14 respectively.

Method (a) for synthesis of Ru (II) complexes

Method (a) described in Figure 3.13 consists of the complexation of a terpyridine ligands with a [Ru(tpy-R)Cl_3]. The terpyridine metal trichloride is suspended with the second ligand in a solution containing N-ethylmorpholine as reducing agent.

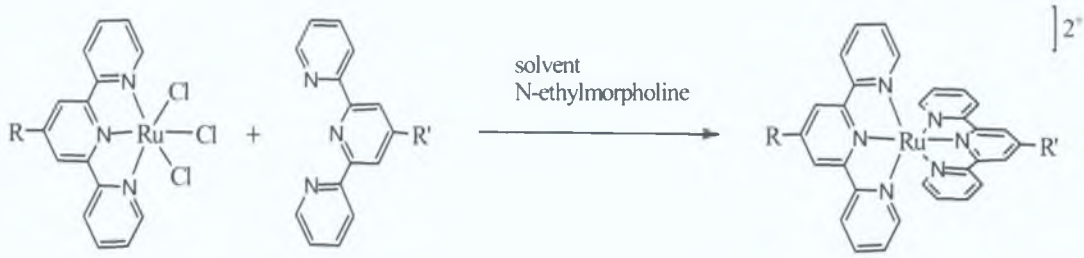

Figure 3.13: Method (a) for synthetic strategy towards symmetric terpyridine complexes; R = H, pyridine, phenyl-Br

Ethylene glycol or water was used as solvents for carrying reactions with method (a); it was the favourite method for the synthesis of ruthenium symmetrical terpyridine complexes. As described in Section 3.3.1, the synthesis of $[Ru(py\text{-}tpy)_2][PF_6]_2$ afforded 33% of yield, using method (a), whereas same synthesis carried out with method (b) afforded only 29% of yield). Method (a) was also used for the synthesis of [Ru(tpy-ph-Br)(2,6-bis-([1,2,3,4]tetrazol-5-yl)pyridine)(H_2O)] and $[Ru(tpy)(2,6\text{-}(2,3\text{-ph-4-}CH_3\text{-pyrazol})py][PF_6]_2$. Because of the poor solubility of the two ligands, [2,6-bis-([1,2,3,4]tetrazol-5-yl)pyridine] and $[2,6\text{-}(2,3\text{-ph-4-}CH_3\text{-pyrazol})py]$, it was the favourite synthetic method for these complexes.

Method (b) for synthesis of Ru (II) complexes

In method (b) (see Figure 3.14), silver tetrafluoroborate is used as a chloride abstractor.

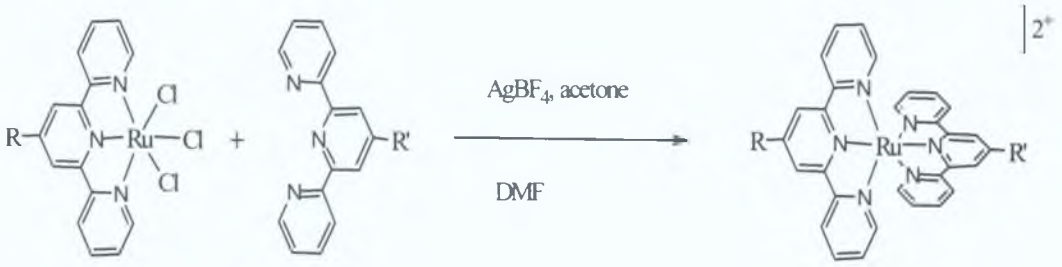

Figure 3.14: Method (b) for synthetic strategy towards asymmetric terpyridine complexes

In this first step, the three chloride bonded to the metal centre, are substituted by three acetone groups [19]. The vacant coordination sites are now occupied by the weakly binding solvent molecules, thereby activating the ruthenium (II) complex. Unlike terpyridine ruthenium (II) trichloride that is reacted in suspension, the activated acetone species is soluble. The formed silver chloride was filtered off by vacuum filtration and than the intermediate triacetate was reacted in DMF without isolation with the second terpyridine which leads to the desired bis (terpyridine) ruthenium (II) complex.

3.3.1 Synthesis of $[Ru(py\text{-}tpy)_2][PF_6]_2$

The most efficient method used for synthesising $[Ru(py\text{-}tpy)_2][PF_6]_2$, is method (a) shown in Figure 3.15.

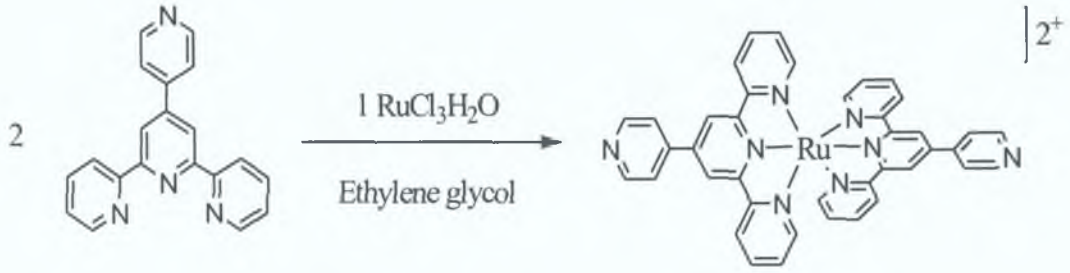

Figure 3.15: Synthetic reaction of $[Ru(py\text{-}tpy)]_2[PF_6]_2$

This scheme reaction is normally used for the synthesis of symmetric terpyridine complexes[20][21]. One equivalent of $[(RuCl_3)2H_2O]$ and 2 equivalents of (py-tpy) ligand were heated at reflux for 6 hours in ethylene glycol. The yield reported for the reaction is 33%. Method (b) has been also used for the synthesis of $[Ru(py\text{-}tpy)_2][PF_6]_2$, reacting $[Ru(py\text{-}tpy)Cl_3][PF_6]$ and $AgBF_4$ in dry acetone and consequently by adding the second (py-tpy) ligand the product was afforded. The product was recrystallised from acetonitrile. This method did not improve the yield of the reaction, which was 29%.

3.3.2 Synthesis of $[Ru(tpy\text{-}ph\text{-}Br)(L3)(H_2O)]$

Method (a) was the method used for the synthesis of the new complex $[Ru(tpy\text{-}ph\text{-}Br)(L3)(H_2O)]$. Starting material $[Ru(tpy\text{-}ph\text{-}Br)Cl_3]$ was synthesised as described in Figure 3.13, by heating at reflux for two hours, $[(RuCl_3)\ 2H_2O]$ and the ligand 4'(4-bromo-phenyl) 2,2'; 6',2" - terpyridine in a stoichiometric proportions (1:1), in ethanol solution. This complex was then heated at reflux with the ligand (H_2L3) in ethylene glycol and precipitated by adding a small amount of water. The synthesis of the complex $[Ru(tpy\text{-}ph\text{-}Br)(L3)(H_2O)]$ proved to be problematic because of the poor solubility of the (H_2L3) ligand. Several solvents were used to carry out the reaction; finally the reaction succeeds using a basified solution of ethylene glycol containing few drops of N-ethylmorpholine.

The pure product was obtained after purification by silica column, using a mixture of acetonitrile and water (3:1) as eluent.

3.3.3 Synthesis of $[Ru(tpy)(tpy\text{-}ph\text{-}Br)][PF_6]_2$

Scheme (b) described in Figure 3.14 was used for the synthesis of $[Ru(tpy)(tpy\text{-}ph\text{-}Br)][PF_6]_2$. $[Ru(tpy)Cl_3]$ was firstly suspended in acetone in presence of $AgBF_4$. The resulting ruthenium terpyridine triacetate was heated at reflux, under argon for four hours with the ligand (tpy-ph-Br). Adding a concentrated aqueous solution of ammonium hexafluorophosphate easily precipitated the desired product. The product was filter and dry with diethyl ether. Yield is around 40%.

3.3.4 Synthesis of $[Ru(py\text{-}tpy)(tpy\text{-}ph\text{-}Br)][PF_6]_2$

Following method (b), two different approaches were investigated for the synthesis of $[Ru(py)(tpy\text{-}ph\text{-}Br)][PF_6]_2$ (Figure 3.16 and 3.17), starting from either $[Ru(py\text{-}tpy)Cl_3]$ or $[Ru(tpy\text{-}ph\text{-}Br)Cl_3]$. Both complexes were suspended in acetone in presence of $AgBF_4$. The desired products were purified by column chromatography, using acetonitrile/H_2O (8:2) and KNO_3 (0.5%) as eluent. Starting from the $[Ru(tpy\text{-}ph\text{-}Br)Cl_3]$ instead of $H[Ru(py\text{-}tpy)Cl_3](PF_6)$, low yield was obtained, 23%.

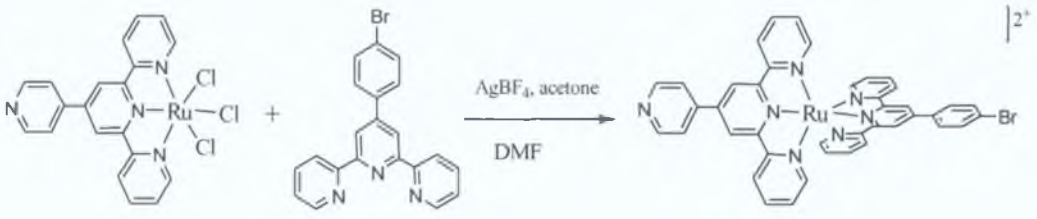

Figure 3.16: Synthesis of $[Ru(py\text{-}tpy)(tpy\text{-}ph\text{-}Br)][PF_6]_2$ complex

Alternatively, ruthenium complex $[Ru(py\text{-}tpy)Cl_3]$ was reacted with $AgBF_6$ in acetone and subsequently refluxed in DMF with the ligand (tpy-ph-Br) (molar ratio 1:1).

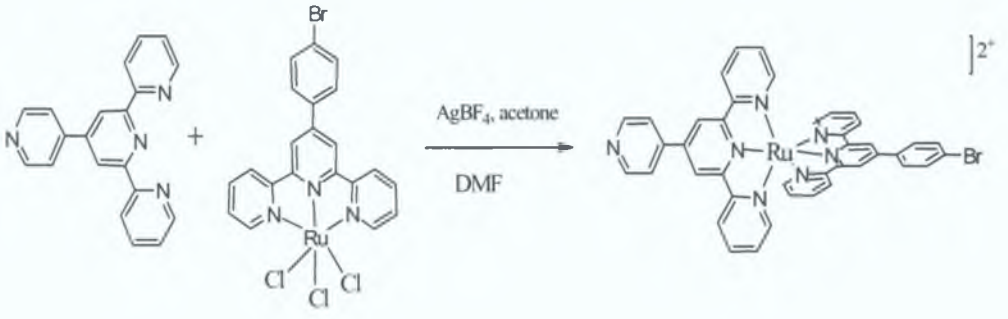

Figure 3.17: Synthesis of [Ru(py-tpy)(tpy-ph-Br)][PF_6]$_2$ complex

Starting material [Ru(py-tpy)Cl_3] is precipitated in a protonated form, as PF_6 salt: H[Ru(py-tpy)Cl_3](PF_6). The product was precipitated by adding a concentrated aqueous solution of ammonium hexafluorophosphate and purified by silica column using acetonitrile/H_2O (8:2) and KNO_3 (0.5%) as eluent. The product was obtained in a 67% of yield.

3.3.5 Synthesis of [Ru(2,6-(2,3-ph-4-CH_3-pyrazol)py](tpy)[PF_6]$_2$

Method (a) was also used for the synthesis of [Ru(2,6-(2,3-ph-4-CH_3-pyrazol)py](tpy)[PF_6]$_2$. The ideal conditions for this synthesis are obtained using a basic aqueous solution in presence of N-ethylmorpholine as reducing agent. The precursor [Ru(tpy)Cl_3] was reacted with the ligand [2,6-(2,3-ph-4-CH_3-pyrazol)py] and the solution was heated at reflux for 4 hours and acidified using HCl (2M). By addition of a concentrated aqueous solution of ammonium hexafluorophosphate, the complex was obtained, after recrystallisation from EtOH and afforded 40% of yield.

3.4 ^{1}H-NMR of Ru(II) terpyridine complex

All the ruthenium (II) complexes synthesised in this thesis have been characterised by ^{1}H-NMR spectroscopy. The ^{1}H-NMR spectra of the complexes were assigned by comparison with spectra of the free ligands and of the prototype $[Ru(tpy)_2]^{2+}$ and are collected in Appendix 1.

3.4.1 ^{1}H-NMR of $[Ru(tpy)_2]^{2+}$

In this Section, the ^{1}H-NMR of the present compound $[Ru(tpy)_2]^{2+}$ will be discussed. The proton numbering of the Ru(II) terpyridine prototype complex is shown in Figure 3.18.

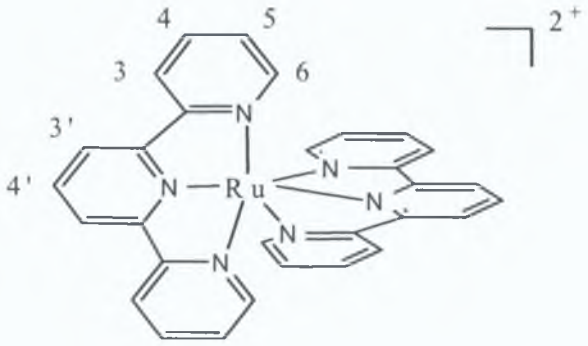

Figure 3.18: Structure of $[Ru(tpy)_2]^{2+}$

and the spectrum obtained for $[Ru(tpy)_2][PF_6]_2$ is shown in Figure 3.19.

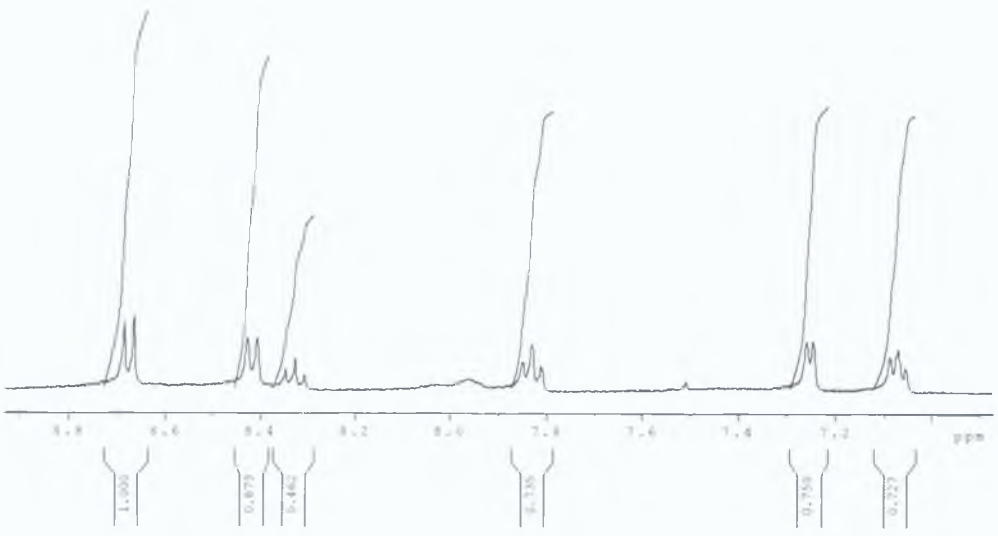

Figure 3.19: ^{1}H-NMR of $[Ru(tpy)_2][PF_6]_2$ in CD_3CN

In general in Ru (II) terpyridine complexes, the lowest field resonance is assigned to $H^{3'}$, followed by the signals of H^3, $H^{4'}$, H^4 and finally, H^6 and H^5.

In Table 3.4, ^{1}H-NMR spectroscopic data for terpyridine ligand and $[Ru(tpy)_2]^{2+}$, are compared.

ppm	H^3 (d)	H^4 (dd)	H^5 (dd)	H^6 (d)	$H^{3'}$ (d)	$H^{4'}$ (dd)
(tpy)	8.70	8.00	7.50	8.60	8.55	8.10
$[Ru(tpy)_2]^{2+}$	8.43	7.83	7.18	7.28	8.70	8.34

Table 3.4: ^{1}H-NMR data for CD_3CN of terpyridine and $[Ru(tpy)_2]^{2+}$

In the free ligand, H^3 and H^6 appear as doublets at 8.60 ppm (H^6) and 8.70 ppm (H^3); whereas, in the spectrum of the complex, the same doublets are found at 7.28 ppm and 8.43 ppm, respectively. The upfield shift of H^6 with respect to H^3 is explained by the fact that it lies in the shielding region above a pyridine ring of the other ligand. The two doublet of doublets that appear in the spectrum of the free ligand at 7.50 ppm and 8.00 ppm, H^5 and H^4 respectively, shift to 7.18 ppm H^5 and at 7.83 ppm H^4 in the complex; whereas $H^{4'}$ appears as doublet of doublets at 8.34 ppm, and H^3 as a doublet at 8.43 ppm. In comparison of the spectrum of the ligand, they shift down field (in the terpyridine spectrum, $H^{4'}$ is at 8.10 ppm and H^3 is at 8.70 ppm). The shift of the two protons is a consequence of steric interaction between the two terpyridine rings in the complex. The doublet of $H^{3'}$ is identified at the lowest field, with a shift, from 8.55 ppm in the free ligand, to 8.70 ppm in the complex; this shift is evidence for steric interaction between the two pyridine rings. In general, the three protons H^6, $H^{3'}$ and $H^{4'}$ are the terpyridine protons most sensitive to the presence of a new ligand in the complex. In particular, the $H^{3'}$ and $H^{4'}$ shifts are an evidence of a strong steric interaction between the two pyridine rings lying on the C_2 axes of symmetry of the complex.

3.4.2 ^{1}H-NMR spectra for ruthenium complexes prepared

The ^{1}H-NMR spectra for the ruthenium complexes prepared in this thesis are shown in Appendix I. The structure and the numbering of the protons present in $[Ru(py\text{-}tpy)_2][PF_6]_2$ are shown in Figure 3.20.

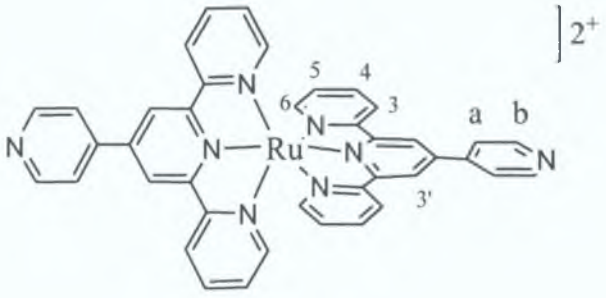

Figure 3.20: Structure of $[Ru(py\text{-}tpy)_2][PF_6]_2$

and signals assigned to the $[Ru(py\text{-}tpy)_2][PF_6]_2$ complex are reported in Table 3.5.

ppm	H^3	H^4	H^5	H^6	$H^{3'}$	H^a	H^b
(py-tpy)	8.70	7.85	7.33	8.68	8.72	7.78	8.62
$[Ru(py\text{-}tpy)_2]^{2+}$	8.68	8.00	7.23	7.43	9.10	8.18	8.98

Table 3.5: ^{1}H-NMR data in CD_3CN (py-tpy) and $[Ru(py\text{-}tpy)_2][PF_6]_2$

The spectrum of the complex (Figure 5, Appendix I) shows well-resolved signals in the aromatic region between 7.23 and 9.10 ppm. The $H^{3'}$ proton is observed at 9.10 ppm, as a singlet. Two doublets of H^a and H^b appear respectively at 8.18 and 8.98 ppm. The shift to low field of the two protons H^a and H^b, is probably due to the influence of the pyridine ring of the opposite (py-tpy) group lying on the C_2 axes of symmetry of the complex. The doublet at 8.68 ppm is the signal of H^3, whereas the doublet at upfield, 7.43 ppm, is assigned to H^6. The two doublets - of - doublets at 7.53 ppm and 7.85 ppm, for H^5 and H^4 respectively in the free ligand, have shifted to 7.23 ppm (H^5) and 8.00 ppm (H^4) in the complex.

The structure and the numbering of protons in $[Ru(tpy)(tpy\text{-}ph\text{-}Br)][PF_6]_2$ are shown in Figure 3.21.

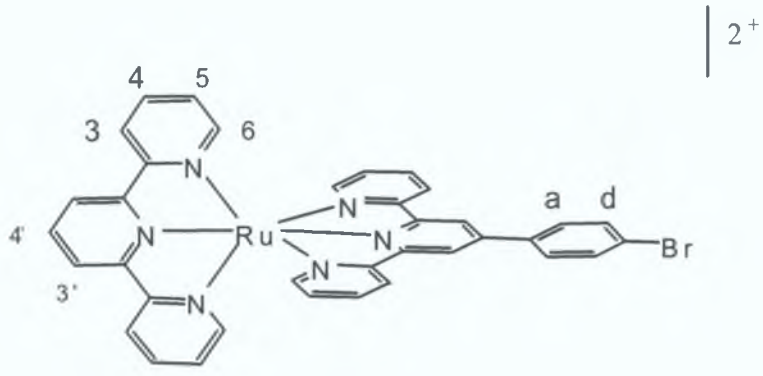

Figure 3.21: structure of [Ru(tpy)(tpy-ph-Br)][PF_6]$_2$

The ^{1}H-NMR signals assigned to [Ru(tpy)(tpy-ph-Br)][PF_6]$_2$ complex are reported in Table 3.6.

ppm	H^3	H^4	H^5	H^6	$H^{3'}$	$H^{4'}$	H^a	H^b
(tpy)	8.70	8.00	7.50	8.60	8.55	8.10		
(tpy-ph-Br)	8.66	7.82	7.30	8.59	8.63		7.57	7.72
[Ru(tpy)(tpy-ph-Br)]$^{2+}$								
(tpy)	7.90/8	7.20	7.40	7.48	7.90	8.42		
(tpy-ph-Br)	8.69	7.90	7.20	8.55	9.10		8.18	8.81

Table 3.6: ^{1}H-NMR data in CD_3CN, (tpy), (tpy-ph-Br) and [Ru(tpy)(tpy-ph-Br)][PF_6]$_2$

Spectrum of the complex [Ru(tpy)(tpy-ph-Br)][PF_6]$_2$ (Figure 6, Appendix I) shows

$H^{3'}$ of (tpy-ph-Br) as doublet at the lowest field, with a shift, from 8.63 ppm in the free ligand, to 9.10 ppm in the complex. Different behaviour was observed for the same proton on the terpyridine ligand $H^{3'}$ (see Figure 3.21); it shifted from 8.55 in the free ligand to 8.00 ppm in the complex. Protons H^d and H^a are easily recognisable by the doublets of same splitting pattern that are of equal intensity; signals are found at 8.18 ppm (H^a) and 8.81 ppm (H^d). In the spectrum of (tpy-ph-Br), proton H^6 and H^3, appear as doublets at 8.59 (H^6) and 8.66 (H^3); whereas in the spectrum of the complex, the same doublets appear at 8.55 ppm and 8.69 ppm, respectively. The position of the proton H^6, lies above a pyridine ring of the (tpy-

ph-Br), explains why it shifted upfield, with respect to H^3. They appear at 8.60 ppm (H^6) and 8.70 ppm (H^3) in the ligand and are shifted to 7.48 and 7.90 ppm respectively. The two triplets of H^5 and H^4 that appear in the spectrum of free (tpy-ph-Br), at 7.30 ppm and 7.82 ppm have been pushed upfield to 7.20 ppm and at 7.90-8.00 ppm in the complex. Finally, the proton H^4 shifted to low field from 8.10 ppm to 8.42 ppm when the terpyridine is bound to ruthenium; this is explained by the fact that proton $H^{4'}$ is sensitive to the presence of a new ligand; because of a steric interaction between the two pyridine central rings lying on the C_2 axes of symmetry of the complex.

The structure and the numbering of protons in [Ru(py-tpy)(tpy-ph-Br)][PF_6]$_2$ are shown in Figure 3.22. The ^{1}H-NMR spectra of both free ligand and complex were recorded in $CDCl_3$.

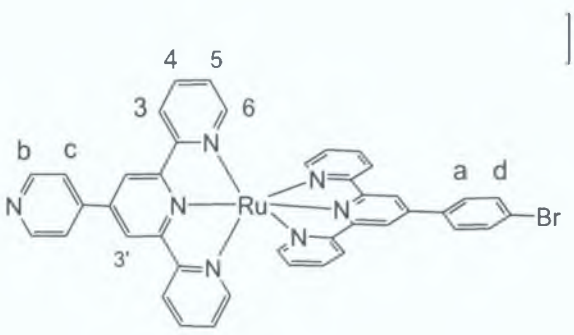

Figure 3.22: structure of [Ru(py-tpy)(tpy-ph-Br)][PF_6]$_2$

whereas the signals assignments are given in Table 3.7.

ppm	H^3	H^4	H^5	H^6	$H^{3'}$	H^a	H^d	H^c	H^b
(tpy-ph-Br)	8.66	7.82	7.30	8.59	8.63	7.57	7.72		
(py-tpy)	8.70	7.85	7.33	8.68	8.72	7.78	8.62		
[Ru(tpy-ph-Br)(py-tpy)]^{2}									
(tpy-ph-Br)	7.90	7.90	7.90	8.08	8.90	7.55	7.62		
(py-tpy)	8.08	7.90	7.15	8.58	8.98			7.31	7.37

Table 3.7: ^{1}H-NMR data in $CDCl_3$, (tpy-ph-Br), (py-tpy) and [Ru(tpy-ph-Br)(py-tpy)][PF_6]$_2$

Spectrum of [Ru(tpy-ph-Br)(py-tpy)][PF_6]$_2$ (Figure 7, Appendix I) shows doublet lowest field 8.98 ppm assigned to $H^{3'}$ of the (py-tpy) ligand, whereas this proton

appears at 8.90 ppm for the free ligand. For the complex singlet a shift to low field is observed comparing with the signals of the free ligands. H^6 protons are the most sensitive to the presence of the other ligand. In the complex these peaks appear at 8.08 ppm for (tpy-ph-Br) and 8.58 ppm for (py-tpy). Doublet signals are characteristic for the protons H^c, H^a, H^b and H^d between 7.31 ppm and 7.62 ppm. Proton H^c is pushed further upfield by the electron withdrawing nature of the nitrogen on the pendant pyridyl group. Proton H^d, close to the bromine, shifts to low field compare to the other proton H^a, on the same ring. A doublet - of - doublets at 7.90 ppm is observed for H^4 protons and at 7.90-7.15 ppm for H^5 protons. Protons H^3 are identified as doublet signals in the low field region at 8.08 ppm H^3 of (py-tpy) and at 7.90 ppm, H^3 of (tpy-ph-Br).

The structure and the numbering of protons in [Ru(tpy-ph-Br)(L3)(H_2O)] are shown in Figure 3.23 The ^{1}H-NMR spectrum was recorded in CD_3CN (Figure 8, Appendix I).

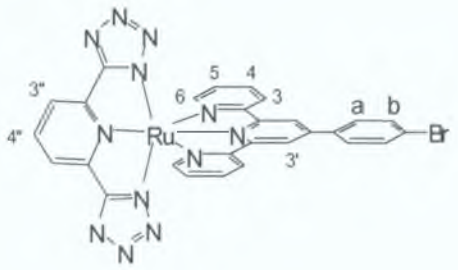

Figure 3.23: structure of [Ru(tpy-ph-Br)(L3)(H_2O)]

The ^{1}H-NMR signals obtained for [Ru(tpy-ph-Br)(L3)(H_2O)] complex are listed in Table 3.8.

ppm	H^3	H^4	H^5	H^6	$H^{3'}$	H^a	H^b	$H^{3''}$	$H^{4''}$
(tpy-ph-Br)	8.66	7.82	7.30	8.59	8.63	7.57	7.72		
(H_2L3)								7.90	7.10
[Ru(tpy-ph-Br)(L3)]:									
(tpy-ph-Br)	8.70	8.15	7.28	7.53	9.55	8.48	9.18		
(H_2L3)								8.70	8.70

Table 3.8: ^{1}H-NMR data in CD_3CN, (tpy-ph-Br) and [Ru(tpy-ph-Br)(L3)(H_2O)]

The lowest field resonance observed for the complex is $H^{3'}$ of the (tpy-ph-Br) ligand; while H3' appears as a singlet at 9.55 ppm, followed by H^b, H^3, H^a, H^4, H^6 and H^5. The shift of $H^{3'}$ (in the free ligand the signal is at 8.63 ppm) is related to the interaction between the central ring of the (tpy-ph-Br) and the pyridyl rings of the $(L3)^{2-}$ ligand. As noted before, protons H^b and H^a are easily recognisable by the doublets of similar splitting pattern; signals appear at 8.48 ppm (H^a) and 9.18 ppm (H^b). A doublet of H^3 appears at 8.70 ppm, whereas H^6, is a doublet found upfield, at 7.53 ppm. H^6 is that it lies in the shielding region above the tetrazolate ring of the (tpy-ph-Br) ligand. Protons H^5 and H^4 appear as triplets at 7.28 and 8.15 ppm, respectively. H^5 shifts to upfield compare with the other protons of the ring, because is felt less the presence of the nitrogen group. Finally, protons $H^{3'''}$, $H^{4'''}$ of the pyridine ring of the tetrazole ligand, appear at 8.70 ppm. In the spectrum of free ligand these protons are found at 8.30 and 8.40 ppm.

The structure and the numbering of protons in [Ru[2,6-(2,3-ph-4-CH_3-pyrazol)py](tpy)$[PF_6]_2$ are shown in Figure 3.24.

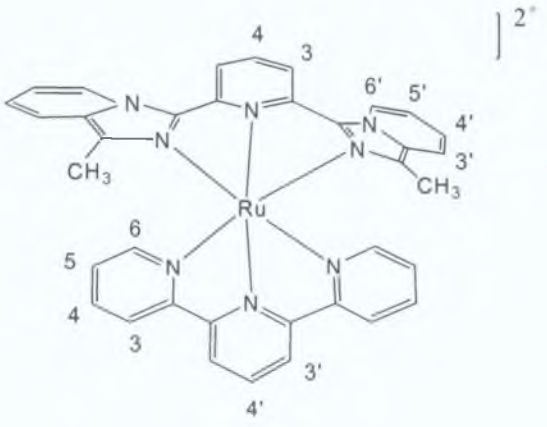

Figure 3.24: structure of [Ru[2,6-(2,3-ph-4-CH_3-pyrazol)py](tpy)$[PF_6]_2$

The ^{1}H-NMR signals assigned to [Ru[2,6-(2,3-ph-4-CH_3-pyrazol)py](tpy)$[PF_6]_2$ complex are reported in Table 3.9; whereas the spectrum is shown in Figure 9, Appendix I.

ppm	H^3	H^4	H^5	H^6	$H^{3'}$	$H^{4'}$	$H^{5'}$	$H^{6'}$	CH_3
(tpy)	8.70	8.00	7.50	8.60	8.55	8.10			
[2,6-(2,3-ph-4-CH_3-pyrazol)py]	8.18	8.10			7.90	7.10	7.00	9.43	2.8
Complex:									
(tpy)	9.10	8.78	7.28	7.45	8.83	8.53			
[2,6-(2,3-ph-4-CH_3-pyrazol)py]	8.18	8.10			7.90	7.10	7.00	9.43	2.8

Table 3.9: ^{1}H-NMR data in DMSO of tpy, [2,6-(2,3-ph-4-CH_3-pyrazol)py] ligand and the complex [Ru[2,6-(2,3-ph-4-CH_3-pyrazol)py](tpy)[PF_6]$_2$

The spectrum of the complex shows well-resolved signals in the aromatic region between 7 and 9 ppm. Four of them correspond to the terminal pyridine ring of the terpyridine ligand: H^3, H^4, H^6, and H^5, as already described for $[Ru(tpy)_2][PF_6]_2$. The aromatic signals of the pyrazole ligand are clearly observed between 7.00 and 9.45 ppm. Protons $H^{6'}$, H^3 and $H^{3'}$ are easily identified as doublets at 9.43, 8.18 and 7.90 ppm. The three doublets of doublets appear at 8.10 ppm (H^4), 7.10 ppm ($H^{4'}$) and 7.00 ppm ($H^{5'}$). In comparison with the spectrum of the free ligand, these signals do not show significant shifts.

In Table 3.10, the resonances for the terpyridine ligand and for the terpyridine ligand in the ruthenium complexes investigated are shown. On passing from the free terpyridine ligand to the (tpy) complexes, some significant changes in the ^{1}H-NMR resonances have been observed. In particular, for all three complexes, signals of H^6, $H^{3'}$ and $H^{4'}$ showed a shift to low field comparing with the terpyridine ligand; as expected these protons are the most sensitive to the presence of the second terpyridine system (steric interactions between the two pyridine rings lying on the C_2 axes of the symmetry of the complex). Whereas, opposite behaviour has been observed for H^3, H^4 and H^5 in $[Ru(tpy)_2]^{2+}$ and $[Ru(tpy)(tpy\text{-}ph\text{-}Br)]^{2+}$ complexes. The signals of these protons are shifted upfield compare with the signals of the free ligand.

By observing the geometrical structure of the complexes, it is clear that these protons do not feel strongly the presence of the pyridine rings of the second ligand. Some changes have been noticed for the protons H^3, H^4 in the complex $[Ru(tpy)(2,6\text{-}(2,3\text{-ph-4-}CH_3\text{-pyrazol})py]^{2+}$ which are pushed downfield. It may be attribuited to the fact that they are most sensitive to the changes occurring in the configuration of the no - coordinated pyridine ring upon adoption of the ligand [(2,6-(2,3-ph-4-CH_3-pyrazol)py].

ppm	H^3	H^4	H^5	H^6	$H^{3'}$	$H^{4'}$
(Tpy) *free ligand*	8.70	8.00	7.50	8.60	8.55	8.10
(Tpy) *in* $[Ru(tpy)_2]^{2+}$	8.43	7.83	7.18	7.28	8.70	8.34
(Tpy) *in* $[Ru(tpy)(tpy\text{-}ph\text{-}Br)]^{2+}$	7.90/8	7.20	7.40	7.48	7.90	8.42
(Tpy) *in* $[Ru(tpy)(2,6\text{-}(2,3\text{-}ph\text{-}CH_3\text{-}pyrazol)py]^{2+}$	9.10	8.78	7.28	7.45	8.83	8.53

Table 3.10: ^{1}H-NMR data observed for the terpyridine ligand in the ruthenium (II) complexes

In Table 3.11, the resonances for the (py-tpy) ligand and for the terpyridine ligand in the ruthenium complexes investigated are shown.

By comparing the resonances for the free (py-tpy) ligand and this of the ligand in the ruthenium complexes, no unexpected changes have been noticed. In particular, similar shift have been observed for protons H^3, H^4 and H^5 (less sensitive to the presence of the second ligand) in all the complexes; whereas different behaviour has been noted for H^6, $H^{3'}$, H^a and H^b, very sensitive to the pyridine rings. In particular, after introduction of the (tpy-ph-Br) ligand, the protons $H^{3'}$ shifts upfield compare with the free ligand resonance and it is strongly shifted in the same direction after the introduction of (py-tpy) (influence of the terpyridine

system and pyridine group in the new (py-tpy) group). Same bahaviour has been noticed for H^a and H^b in $[Ru(py\text{-}tpy)_2]^{2+}$ complex. However, the presence of (tpyphBr) did not influence the shift of the (py-tpy) unit: protons H^6, H^a and H^b shift to lowest field compare with the previous complex. It has been suggested that the steric interaction between the two units, (py-tpy) and (tpy-ph-Br) is not so strong such as this observed between the two (py-tpy) groups (interaction which involves the two pyridine rings lying on the C_2 axes of symmetry of the complex).

ppm	H^3	H^4	H^5	H^6	$H^{3'}$	H^a	H^b
(Py-tpy) *free ligand*	8.70	7.85	7.33	8.68	8.72	7.78	8.62
(Py-tpy) *in* $[Ru(py\text{-}tpy)_2]^{2+}$	8.68	8.00	7.23	7.43	9.10	8.18	8.98
(Py-tpy) *in[Ru(tpy-ph-Br)(tpy)]*$^{2+}$	8.08	7.90	7.15	8.58	8.98	7.31	7.37

Table 3.11: ^{1}H-NMR data observed for the (py - tpy) ligand in the ruthenium (II) complexes

3.5 Synthesis of Os (II) tpy complexes

The synthetic approach used for Os(II) terpyridine complexes is a modification of the procedure described in the literature[22].

Compared to the ruthenium coordination sphere, which is considered reasonably labile, the substitution of ligands within the coordination sphere of osmium is notoriously difficult and requires more extreme conditions. The reaction conditions investigated for the preparation of osmium (II) terpyridine complexes are shown in Table 3.12.

complex	Solvent	precursor	yield
$[Os(py\text{-}tpy)_2][PF_6]_2$	Ethylene glycol, N-ethylmorpholine	$[(NH_4)_2OsCl_6]$	24%
$[Os(tpy)(tpy\text{-}ph\text{-}Br)][PF_6]_2$	Ethylene glycol, NaOH,N-ethylmorpholine	$[Os(tpy)Cl_3]$	22%
$[Os(py\text{-}tpy)(tpy\text{-}ph\text{-}Br)][PF_6]_2$	Ethylene glycol, NaOH,N-ethylmorpholine	$[Os(tpy\text{-}ph\text{-}Br)Cl_3]$	32%
$[Os(tpy)(L1)][PF_6]_2$	Ethylene glycol, NaOH,N-ethylmorpholine	$[Os(tpy)Cl_3]$	isomers
$[Os(tpy)(L2)][PF_6]_2$	Ethylene glycol, NaOH,N-ethylmorpholine	$[Os(tpy)Cl_3]$	isomers
$[Os(tpy)(L3)(H_2O)]$	Ethylene glycol, NaOH,N-ethylmorpholine	$[Os(tpy)Cl_3]$	75%
$[Os[2,6\text{-}(2,3\text{-}ph\text{-}4\text{-}CH_3\text{-}pyrazol)py](tpy)[PF_6]_2$	Ethylene glycol, NaOH,N-ethylmorpholine	$[Os(tpy)Cl_3]$	58%

Table 3.12: Reaction conditions for synthesis of osmium (II) complexes

Two different synthetic pathways were followed for the synthesis of Os(II) terpyridine complexes:

1 - Method (a) for the synthesis of heteroleptic terpyridine complexes (Figure 3.25).

2 - Method (b) for the synthesis of homoleptic terpyridine complexes (Figure 3.26).

For the heteroleptic complexes, the precursor compound $[Os(tpy\text{-}R)Cl_3]$ was prepared heating at reflux, under nitrogen, 1 equivalent of $[(NH_4)_2OsCl_6]$ and 1 equivalent of (tpy-R) in DMF (see Figure 3.25).

The reaction was carried out in 4 hours, when R = H and 6 hours, when R = (pyridine) group or (phenyl-Br). After filtration of the formed ammonium chloride, ethyl ether was added to the solution and a fine green precipitate crashed out.

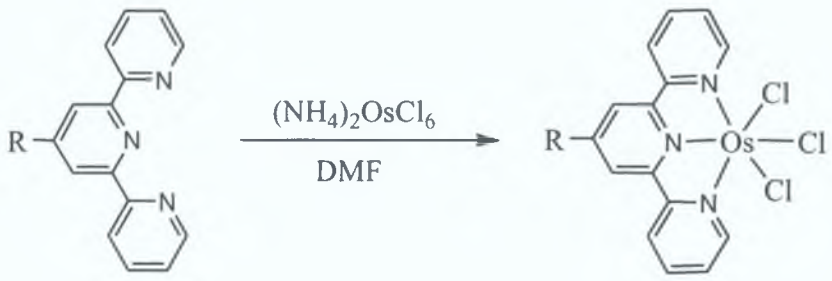

Figure 3.25: Synthesis of starting material [Os(tpy-R)Cl_3]; R = -H, - pyridine, - phenyl-br

Unfortunately, because of the paramagnetic properties of these compounds, it was not possible to purify and characterise these compounds by ^{1}H-NMR. To confirm the formation of these starting materials, they have been reacted with terpyridine ligand and the complexes resulted have been fully characterised by ^{1}H-NMR., after purification by column chromatography. The yield of the reaction is typically between 60% and 70%. The product was used without any other purification.

Method (a) for synthesis of heteroleptic Os(II) complexes

The trichloride osmium complex obtained from the first step of the reaction, is reacted with the second tridentate ligand R' (see Figure 3.26)

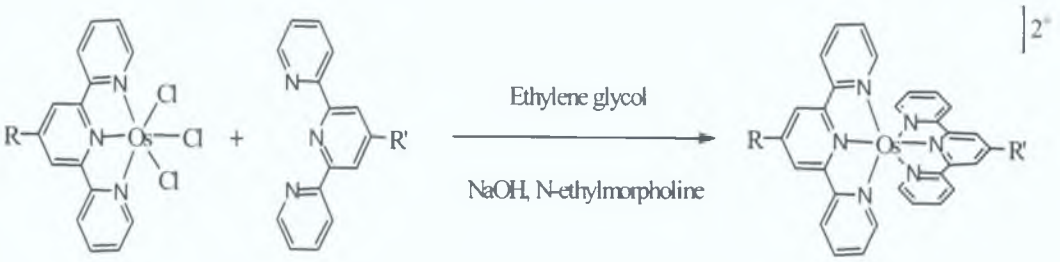

Figure 3.26: Method (a) for synthetic strategy towards heteroleptic osmium terpyridine complexes

The reaction was carried out in ethylene glycol, containing a slight molar excess of NaOH and few drops of N-ethylmorpholine. By adding a saturated solution of aqueous ammonium hexafluorophosphate, [Os(tpy-R)(tpy-R')] complex precipitated.

Method (a) was used for the synthesis of $[Os(tpy\text{-}ph\text{-}Br)(tpy)][PF_6]_2$, $[Os(py\text{-}tpy)(tpy\text{-}ph\text{-}Br)][PF_6]_2$, $[Os(tpy)[2,6\text{-}(2,3\text{-}ph\text{-}4\text{-}CH_3\text{-}pyrazol)py][PF_6]_2$.

Method (b) for synthesis of homoleptic Os(II) complexes

For the synthesis of osmium symmetric terpyridine complexes, as Os(II) $(tpy\text{-}R)_2(PF_6)_2$, (where R = H, (py-tpy)) salt $[(NH_4)_2OsCl_6]$ was used as stating material. It was reacted with 2 equivalents of (tpy-R) ligand in ethylene glycol, in presence of N-ethylmorpholine as reducing agent. The product was precipitated by adding NH_4PF_6 (see Figure 3.27). Method (b) was followed for the preparation of $[Os(tpy)_2[PF_6]_2$ and $[Os(py\text{-}tpy)_2][PF_6]_2$.

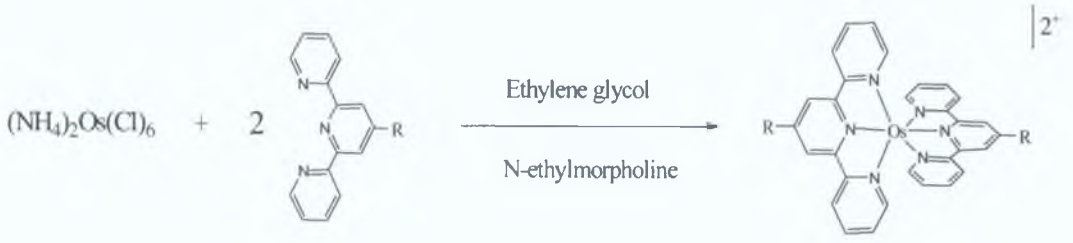

Figure 3.27: Synthetic strategy towards symmetric osmium terpyridine complexes; R = H or pyridine

3.5.1 Synthesis of $[Os(py\text{-}tpy)_2][PF_6]_2$

The reaction scheme described in Figure 3.27 was used for the synthesis of $[Os(py\text{-}tpy)_2][PF_6]_2$ complex. 2 equivalents of (py-tpy) react with $[(NH_4)_2OsCl_6]$, in ethylene glycol. By adding a saturated solution of aqueous ammonium hexafluorophosphate, a dark brown product precipitated. Recrystallisation from acetonitrile afforded the pure product with a 24% of yield. Method (a) has been also used for the synthesis of $[Os(py\text{-}tpy)_2][PF_6]_2$. $[Os(py\text{-}tpy)Cl_3]$ and (py-tpy) ligand were reacted in ratio (1:1), in ethylene glycol solution.

3.5.2 Synthesis of $[Os(tpy)(tpy\text{-}ph\text{-}Br)][PF_6]_2$

The reaction conditions described in Figure 3.26, were used for the synthesis of $[Os(tpy)(tpy\text{-}ph\text{-}Br)][PF_6]_2$. $[Os(tpy)Cl_3]$ and 1 equivalent of (tpy-ph-Br) were dissolved in ethylene glycol, containing few drops of N-ethylmorpholine. The

reaction mixture was heated at reflux under nitrogen. After 4 hours, an aqueous solution of NH_4PF_6 was added and a dark brown product precipitated. It was collected by vacuum filtration and purified with silica column using acetonitrile/H_2O (8:2) and KNO_3 (0.5%) as eluent. The desired complex afforded a 22% of yield.

3.5.3 Synthesis of [Os(py-tpy)(tpy-ph-Br)][PF_6]$_2$

The reaction conditions described in Figure 3.26, were used for the synthesis of [Os(py-tpy)(tpy-ph-Br)][PF_6]$_2$ complex. [Os(py-tpy)Cl_3] was used as starting material. As observed for [Os(tpy)Cl_3], [Os(py-tpy)Cl_3] showed poor solubility. It was dissolved in ethylene glycol in presence of N-ethylmorpholine as reducing agent. The reaction was heated at reflux for 8 hours, under nitrogen. The brown product was precipitated by adding a saturated solution of aqueous ammonium hexafluorophosphate. The synthetic procedure after purification by chromatography column produced an overall yield of 32%. As observed for the previous reaction, mixture of acetonitrile/H_2O (8:2) and KNO_3 (0.5%) has been used with success as eluent for the purification of the compound.

3.5.4 Synthesis [Os(tpy)(L3)(H_2O)]

Method (a) was used for the synthesis of [Os(tpy)(L3)(H_2O)]. In the course of the preparation, a number of different solvents were screened, but because of the poor solubility of [Os(tpy)Cl_3] and of the ligand, ethylene glycol, containing a slight molar excess of NaOH was found to be the favourite. N-ethylmorpholine was used as reducing agent. [Os(tpy)Cl_3] was reacted with the ligand in a stoichiometric proportions (1:1). By adding water, the product was precipitated. Purification by column chromatography on silica, using acetonitrile/H_2O (8:2) and KNO_3 (0.5%) as eluent, produced the pure desired product, with a 75% of yield.

3.5.5 Synthesis of [Os(2,6-(2,3-ph-4-CH_3-pyrazol)py](tpy)[PF_6]$_2$

Method (a) was followed for the preparation of [Os(2,6-(2,3-ph-4-CH_3-pyrazol)py](tpy)[PF_6]$_2$. [Os(tpy)Cl_3] and the pyrazole ligand (ratio 1:1), were reacted in a stoichiometric proportions. The solution was first heated in ethylene

glycol for 20 minutes, under vigorous stirrer, to complete the dissolution of the ligand and then was followed by adding of [Os(tpy)Cl_3]. The solution was further heated at under nitrogen. The product was acidified and precipitated by adding a saturated solution of aqueous ammonium hexafluorophosphate finally purified by column chromatography using acetonitrile/H_2O (8:2) and KNO_3 (0.5%).. The yield for this reaction is 58%.

Attempted synthesis of [Os(tpy)(L2)]

In this work, synthesis of the corresponding osmium (II) complex [Os(tpy)L2] was attempted. The formation of two isomers (see Figure 3.28) has been confirmed by ^{1}H-NMR spectroscopy, but no separation of the two species has been obtained.

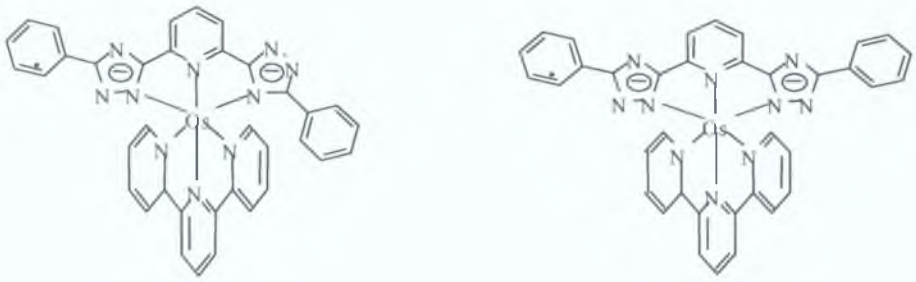

Figure 3.28: Structures of the two isomers obtained reacting [Os(tpy)Cl_3] and (H_2L2)

The synthesis of [Os(tpy)(L1)] was attempted in the course of these studies. The ^{1}H-NMR showed the presence of the three isomers described in Figure 3.29. Unfortunately, the three species has not been separated.

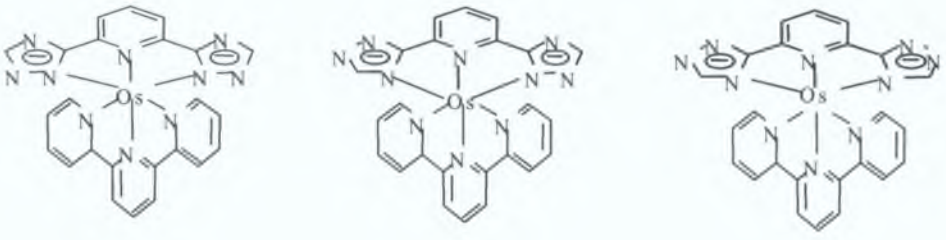

Figure 3.29: Structures of the three isomers resulting from the reaction between [Os(tpy)Cl_3] and the ligand (H_2L1)

3.6 ^{1}H-NMR of Os(II) terpyridine complex

The osmium (II) complexes synthesised in this thesis have been characterised by ^{1}H-NMR spectroscopy. The ^{1}H-NMR spectra of the complexes were assigned by comparison with spectra of the free ligands and of the prototype $[Os(tpy)_2]^{2+}$ and are collected in Appendix 1.

3.6.1 ^{1}H-NMR of $[Os(tpy)_2]^{2+}$

In this Section, first the ^{1}H-NMR spectrum of the $[Os(tpy)_2]^{2+}$will be discussed. The proton numbering of $[Os(tpy)_2][PF_6]_2$ is shown in Figure 3.30.

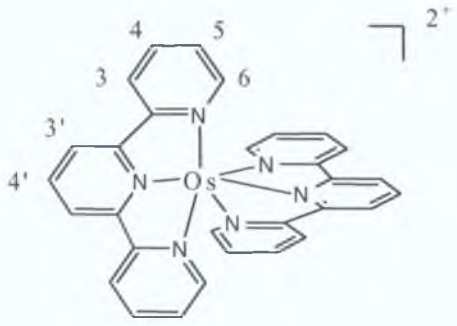

Figure 3.30: Structure of $[Os(tpy)_2][PF_6]_2$

The ^{1}H-NMR signals obtained for $[Os(tpy)_2][PF_6]_2$ complex are shown in Figure 3.31.

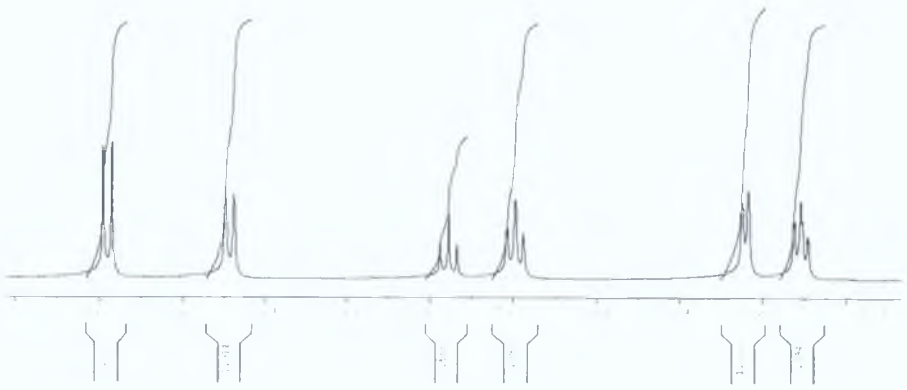

Figure 3.31: ^{1}H-NMR of $[Os(tpy)_2][PF_6]_2$ in CD_3CN

As for ruthenium complexes, in Os(II) terpyridine complexes, the lowest field resonance is assigned to $H^{3'}$, followed by the signals of H^3, $H^{4'}$, H^4 and finally, H^6 and H^5. In Table 3.13, the ^{1}H-NMR spectroscopic data of terpyridine and $[Os(tpy)_2]^{2+}$ are compared.

ppm	**H^3**	**H^4**	**H^5**	**H^6**	**$H^{3'}$**	**$H^{4'}$**
	(d)	**(dd)**	**(dd)**	**(d)**	**(d)**	**(dd)**
(tpy)	8.70	8.00	7.50	8.60	8.55	8.10
$[Os(tpy)_2]^{2+}$	8.50	7.81	7.10	7.23	8.80	7.95

Table 3.13: ^{1}H-NMR data for CD_3CN solutions of terpyridine and $[Os(tpy)_2]^{2+}$.

In the free ligand, proton H^6 and H^3, appear as doublets at 8.60 ppm and 8.70 ppm respectively; whereas in the complex, the same doublets appear respectively at 7.23 ppm and 8.50 ppm,. The upfield shifting of H^6 with respect to H^3 is explained by the fact that it lies in the shielding region above a pyridine ring of the other ligand. The two doublet – of- doublets at 7.50 ppm and 8.00 ppm, respectively H^5 and H^4, have in the complex shifted to 7.10 ppm (H^5) and 7.81 ppm (H^4). The proton $H^{4'}$ in the complex appears as a doublet of doublets at 7.95 ppm, whereas the signal of H^3, is a doublet at 8.50 ppm. In comparison of the spectrum of the ligand, they shift at down field (see table 3.13).

The two protons shifts are a consequence of a steric interaction between the two terpyridine rings. As in the ruthenium complexes, the three protons H^6, $H^{3'}$ and $H^{4'}$ are more sensitive to the presence of a new ligand. In particular, the $H^{3'}$ and $H^{4'}$ shifts are an evidence of a steric interaction between the two pyridine rings. The $H^{3'}$ is shifted from 8.55 ppm in the free ligand, to 8.80 ppm in the complex.

3.6.2 ^{1}H-NMR spectra for osmium complexes prepared

The structure and the numbering of the protons present in [Os(py-tpy)$_2$][PF$_6$]$_2$ are shown in Figure 3.32 (Figure 11, Appendix I).

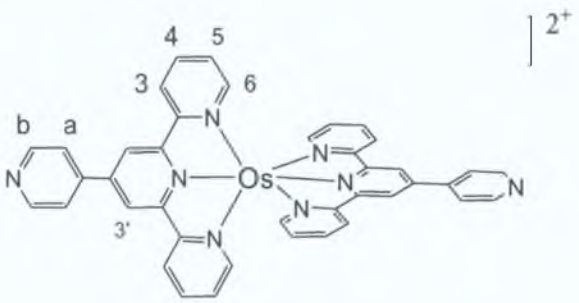

Figure 3.32: structure of [Os(py-tpy)$_2$][PF$_6$]$_2$

^{1}H-NMR resonances are reported in Table 3.14.

ppm	H^3	H^4	H^5	H^6	$H^{3'}$	H^a	H^b
(py-tpy)	8.70	7.85	7.33	8.68	8.72	7.78	8.62
$[Os(py\text{-}tpy)_2]^{2+}$	8.59	7.76	7.05	7.23	9.10	8.05	8.88

Table 3.14: ^{1}H-NMR data in CD_3CN, (py-tpy) and [Os(py-tpy)$_2$][PF$_6$]$_2$

In the free ligand, H^3 and H^6, appear as doublets at 8.68 ppm (H^6) and 8.70 ppm (H^3); whereas in the complex, these two doublets are at 7.23 ppm and 8.59 ppm respectively. The upfield shift of H^6 with respect to H^3 is explained by the fact that it lies in the shielding region above a pyridine ring of the other ligand. The two doublet of doublets that appear in the spectrum of free ligand at 7.33 and 7.85 ppm, (respectively H^5 and H^4), in the complex have shifted to7.05 ppm and 7.76 ppm. $H^{3'}$ and H^6 are more sensitive to the presence of a new ligand in the complex. In particular, the shift of $H^{3'}$ is evidence for steric interaction between the two pyridine rings; the signal of $H^{3'}$, shifted from 8.72 ppm to 9.10 ppm in the complex. The two H^a and H^b doublets are found at 8.05 and 8.88 ppm respectively. In comparison with the spectrum of the free ligand, these signals do not show significant shifts.

The structure and the numbering of the protons present in [Os(tpy)(tpy-ph-Br)][PF_6]$_2$ are shown in Figure 3.33.

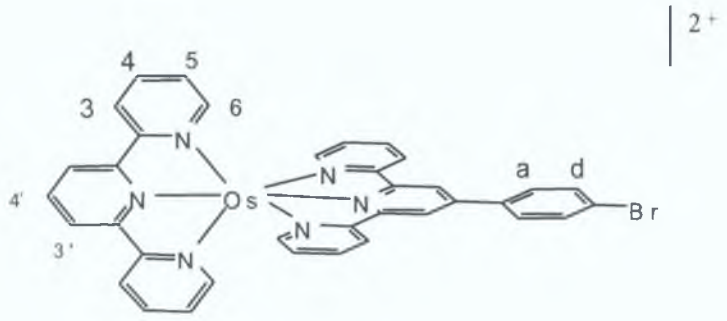

Figure 3.33: structure of [Os(tpy)(tpy-ph-Br)][PF_6]$_2$

The ^{1}H-NMR signals assigned to [Os(tpy)(tpy-ph-Br)][PF_6]$_2$ complex are reported in Table 3.15.

ppm	H^3	H^4	H^5	H^6	$H^{3'}$	$H^{4'}$	H^a	H^d
(tpy)	8.70	8.00	7.50	8.60	8.55	8.10		
(tpy-ph-Br)	8.66	7.82	7.30	8.59	8.63		7.57	7.72
[Os(tpy)(tpy-ph-Br)]$^{2+}$:								
(tpy)	7.43	7.43	7.63	7.63	7.63	7.43		
(tpy-ph-Br)	8.60	7.85	7.43	8.70	8.66		7.58	7.52

Table 3.15: ^{1}H-NMR data in $CDCl_3$*, (tpy), (tpy-ph-Br) and [Os(tpy)(tpy-ph-Br)][PF_6]$_2$*

The $H^{3'}$ doublet of (tpy-ph-Br) is shifted only slightly to low field, from 8.63 ppm in the free ligand, to 8.66 ppm in the complex; this shift is an evidence for steric interaction between the two pyridine rings. Different behaviour is observed for the terpyridine proton $H^{3'}$ (see Figure 3.30); this is shifted from 8.55 ppm to 7.63 ppm in the complex. The protons H^d and H^a doublets are found at 7.52 ppm (H^a) and 7.58 ppm (H^d). In comparison with the spectrum of the free ligand, these signals don't show significant shifts. Proton H^6 and H^3, appear in the spectrum of (tpy-ph-Br), as doublets at 8.59 ppm (H^6) and 8.66 pm (H^3); whereas in the spectrum of

the complex, the same doublets are at 8.70 ppm and 8.60 ppm, respectively. Protons H^6 and H^3, appear as doublet at 8.60 ppm (H^6) and 8.70 ppm (H^3) in the free ligand, they shifted at 7.63 and 7.43 ppm in the complex. The two doublet of doublets of H^5 and H^4 found in the free ligand at 7.30 ppm and 7.82 ppm respectively, are more upfield at 7.43 ppm and at 7.85 ppm respectively in the complex.

The structure and the numbering of the protons present in [Os(py-tpy)(tpy-ph-Br)][PF_6]$_2$ are shown in Figure 3.34.

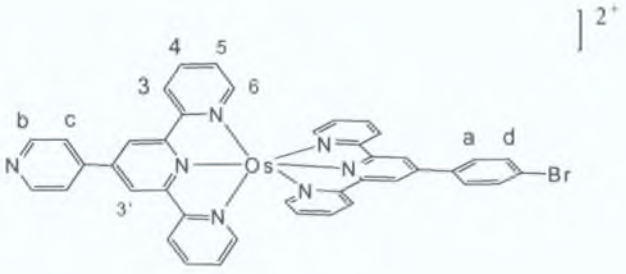

Figure 3.34: structure of [Os(py-tpy)(tpy-ph-Br)][PF_6]$_2$

^{1}H-NMR resonances are reported in Table 3.16.

ppm	H^3	H^4	H^5	H^6	$H^{3'}$	H^a	H^d	H^c	H^b
(tpy-ph-Br)	8.66	7.82	7.30	8.59	8.63	7.57	7.72		
(py-tpy)	8.70	7.85	7.33	8.68	8.72	7.78	8.62		
[Os(tpy-ph-Br)(py-tpy)]$^{2+}$:	8.50	7.90	7.90	7.88	8.50	7.55	7.52		
(tpy-ph-Br)	7.88	7.90	7.40	8.58	8.65			7.62	7.40
(py-tpy)									

Table 3.16: ^{1}H-NMR data in CD_3CN, (tpy-ph-Br), (py-tpy) and [Os(tpy-ph-Br)(py-tpy])[PF_6]$_2$

Comparing the spectra of the two free ligands and the spectrum of the complex (Figure 13, Appendix I) it is observed that the three protons of (tpy-ph-Br), H^6, $H^{3'}$ and H^3 shift from 8.59, 8.63 and 8.66 ppm to 7.88, 8.50, 8.50 ppm in the complex. The same behaviour is observed for the H^6, $H^{3'}$ and H^3 of the (py-tpy) ligand, with shift from 8.68, 8.72 and 8.70 ppm to 8.58, 8.65 and 7.88 ppm

respectively. Protons H^c, H^a, H^b and H^d between 7.40 ppm and 7.62 ppm, appear as doublets. Proton H^c is pushed further upfield by the electron withdrawing nature of the nitrogen on the pendant pyridyl group. Proton H^d, close to the bromine, shift to low field compared to the other proton H^a, on the same ring. As in the spectra of the free ligands, doublet – of -doublets at 7.90 ppm are observed for H^4 and at 7.90-7.40 ppm for the H^5 protons. H^3 protons doublet are found at 7.88 ppm for H^3 of (py-tpy) and at 8.50 ppm, for H^3 of (tpy-ph-Br). $H^{3''}$ of the (py-tpy) appears as singlet at 8.65 ppm, whereas $H^{3'}$ of (tpy-ph-Br) appears as singlet at 8.50 ppm; these shifts are an evidence of a steric interaction between the two pyridine rings involved in the new symmetry of the complex.

The structure and the numbering of the protons present in [Os(tpy)(L3)(H_2O)] are shown in Figure 3.35 (Figure 14, Appendix I).The ^{1}H-NMR spectrum was recorded in d^6-DMSO; H_2L3: [2,6-bis-([1,2,3,4]tetrazol-5-yl)pyridine].

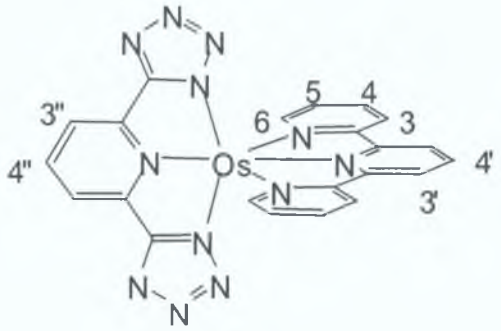

Figure 3.35: structure of [Os(tpy)(L3)(H_2O)]

The ^{1}H-NMR signals assigned are reported in Table 3.17.

ppm	H^3	H^4	H^5	H^6	$H^{3'}$	$H^{4'}$	$H^{3''}$	$H^{4''}$
(tpy)	8.70	8.00	7.50	8.60	8.55	8.10		
(H_2L3)					7.90	7.10		
[Os(tpy)(L3)]:								
(tpy)	8.70	7.78	7.18	7.28	8.95	7.78		
(H_2L3)							8.43	7.90

Table 3.17: ^{1}H-NMR data in d^3-DMSO solutions of tpy, (H_2L3) where ligand (L3) = (2,6-bis-([1,2,3,4]tetrazol-5-yl)pyridine and [Os(tpy)(L3)(H_2O)]

In the spectrum of the complex, the lowest field resonance is assigned to $H^{3'}$; the signal from 8.55 ppm, shifted to 8.95 ppm in the complex; this shift is an evidence of the interaction of the two pyridine rings. Same shift is observed for the protons $H^{3''}$ and $H^{4''}$ that shifted respectively from 7.90 to 8.43 ppm and from 7.10 to 7.90 in the complex and for the proton $H^{4'}$, that shifted from 8.10 to 7.78 ppm in the complex. Protons H^3 appears as a doublet at 8.70 ppm, whereas H^4, H^6 and H^5 appear as triplet respectively at 7.78, 7.28 and 7.18 ppm. This shift to upfield is justified by the presence of the (H_2L3) ligand, with a pyridine central ring that influences the signal of the close protons.

The structure and the numbering of the protons present in [Os[2,6-(2,3-ph-4-CH_3-pyrazol)py](tpy)[PF_6]$_2$ are shown in Figure 3.36. The ^{1}H-NMR spectrum was recorded in d^6-DMSO (Figure 15, Appendix I).

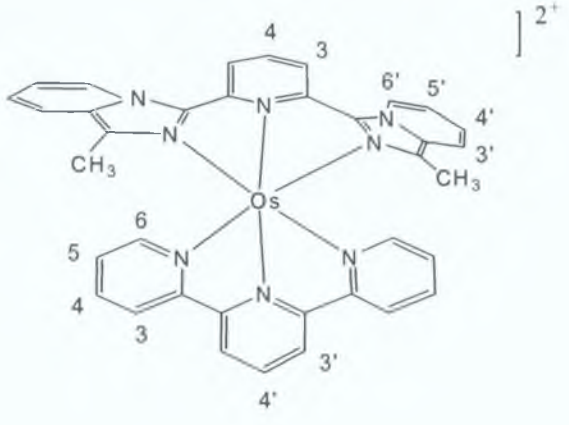

Figure 3.36: structure of [Os[2,6-(2,3-ph-4-CH_3-pyrazol)py](tpy)[PF_6]$_2$

The ^{1}H-NMR signals assigned to [Os[2,6-(2,3-ph-4-CH_3-pyrazol)py](tpy)[PF_6]$_2$ complex are reported in Table 3.18.

ppm	H^3	H^4	H^5	H^6	$H^{3'}$	$H^{4'}$	$H^{5'}$	$H^{6'}$
(tpy)	8.70	8.00	7.50	8.60	8.55	8.10		
[2,6-(2,3-ph-4-CH_3-pyrazol)py]	8.18	8.10			7.90	7.10	7.00	9.43
Complex:								
(tpy)	9.38	8.88	7.10	7.88	9.18	8.80		
[2,6-(2,3-ph-4-CH_3-pyrazol)py]	8.20	8.20			8.00	6.98	7.00	9.55

Table 3.18: ^{1}H-NMR data in DMSO of tpy, ligand and [Os[2,6-(2,3-ph-4-CH_3-pyrazol)py](tpy)[PF_6]$_2$

The spectrum of the complex shows well-resolved signals in the aromatic region between 7 and 9 ppm. Protons of the terpyridine ligand, H^3, H^4 and $H^{4'}$ appear respectively as doublet and two triplet at 9.38, 8.88 and 8.80 ppm respectively; they shift to low field compared to the signals recorded in the free terpyridine spectrum., as expected from the presence of the other terpyridine ring of ligand. Opposite behaviour for the protons H^6 and H^5 that have been pushed upfield, H^6 shifted to 7.88 ppm and H^5 to 7.10 ppm in the complex spectrum. The two remaining protons of the tpy central pyridine ring, $H^{3'}$ and $H^{4'}$ are pushed down field. The shift is probably related to the interaction between the central pyridine ring and the metal. The aromatic signals of the pyrazole ligand, $H^{6'}$, H^3 and $H^{3'}$ are easily identified as doublets at 9.55, 8.20 and 8.00 ppm respectively. Three doublet - of - doublets appear at 8.20 ppm (H^4), 6.98 ppm ($H^{4'}$) and 7.00 ppm ($H^{5'}$). In comparison with the spectrum of the free ligand, these signals do not show more significant shifts, they are not sensitive to the different coordination of the ligand and to the possible interaction with the rings of the (tpy) group.

Table 3.19 shows resonances of terpyridine ligand in a range of osmium complexes. All data have been collected and compared with the signal of the free terpyridine group. No relevant changes have been noticed by comparing the signals of the free terpyridine ligand and these of the terpyridine group in the bis terpyridine complex. In particular, as shown in Table 3.19, all the protons in the

complex are shifted upfield, except for $H^{3'}$, (8.55 ppm in the free ligand and 8.80 ppm in the complex).

ppm	H^3	H^4	H^5	H^6	$H^{3'}$	$H^{4'}$
(Tpy) *free ligand*	8.70	8.00	7.50	8.60	8.55	8.10
(Tpy) *in* $[Os(tpy)_2]^{2+}$	8.50	7.81	7.10	7.23	8.80	7.95
(Tpy) *in* $[Os(tpy)(tpy\text{-}ph\text{-}Br)]^{2+}$	7.43	7.43	7.63	7.63	7.63	7.43
(Tpy) *in [Os(tpy)(L3)]*	8.70	7.78	7.18	7.28	8.95	7.78
(Tpy) *in* $[Os(tpy)(2,6\text{-}(2,3\text{-}ph\text{-}4\text{-}CH_3\text{-}pyrazol)py]^{2+}$	9.38	8.88	7.10	7.88	9.18	8.80

Table 3.19: ^{1}H-NMR data observed for the terpyridine ligand in the Os(II) complexes; ligand L3 = [2,6-bis-([1,2,3,4]tetrazol-5-yl)pyridine]

Similar behaviour was already observed for the analogous ruthenium complex as shown in Section 3.4.2. Interesting shifts in terpyridine protons have been noticed by introducing the tetrazole ligand (H_2L3). By comparing the resonance of $H^{3'}$ in the free terpyridine with that observed in the complex, a downfield shift from 8.55 ppm to 8.95 ppm was observed, whereas all the other protons showed upfield shifting compare to the free terpyridine. This may be explained by the fact that these protons lie in the shielding region above the tetrazolate ring of the ligand. Electronic changes occurred when the (H_2L3) is coordinated to the metal centre (transfer of electron density from the negatively charged tetrazole to the metal). The resonances for terpyridine protons $H^{3'}$ and $H^{4'}$ in the complex $[Os(tpy)(2,6\text{-}(2,3\text{-ph-4-}CH_3\text{-pyrazol})py]^{2+}$, (as already shown in Table 3.10 for analoguos ruthenium complex), showed a very large down shift. This shift may be related in part to Van der Waals interaction deshielding by H^3 and in part it may be attributed to the metal interaction with the central pyridine ring which is greater than that with the terminal rings.

As already shown for ruthenium complexes, the resonances of (py-tpy) ligands for the osmium complexes investigated are also shown in Table 3.20. By comparing the resonances for the free (py-tpy) ligand and for the ligand in the osmium (II) complexes investigated, no unexpected changes have been noticed. In particular similar bahaviuor observed for ruthenium complexes has been noticed for osmium complexes. By comparing the resonances of free (py-tpy) and that of (py-tpy) in the complex $[Os(py\text{-}tpy)_2]^{2+}$, no evident shift have been noticed for protons H^3, H^4 and H^5, as shown for $[Ru(py\text{-}tpy)_2]^{2+}$. Whereas strong downfield shift has been observed for protons $H^{3'}$, H^a and H^b. In particular, $H^{3'}$ which was at 8.72 ppm in the free ligand, it appears at 9.19 ppm in $[Os(py\text{-}tpy)_2]^{2+}$. This shift is an evidence of a strong interaction between the two pyridine rings lying on the C_2 axes of symmetry of the complex. Protons H^a, H^b show same shift (downfield), which resultes less stronger than that of protons above described. Possible factor involved in this shift may be a purely electronic change on the no- coordinated pyridyl ring. Finally, no significant different have been observed between resonances of the free (py-tpy) and these of (py-tpy) in the complex [Os(tpy-ph-Br)(py-tpy)]$^{2+}$. All the protons are shifted upfield as already shown for [Ru(tpy-ph-Br)(py-tpy)]$^{2+}$. It is clear that these protons do not feel strongly the presence of the pyridine rings of the second ligand. Same shift up field shown for H^3 in [Ru(tpy-ph-Br)(py-tpy)]$^{2+}$ complex has been observed for that of osmium complex [Os(tpy-ph-Br)(py-tpy)]$^{2+}$ (7.88 ppm) whereas in the free ligand appears at 8.70 ppm.

ppm	H^3	H^4	H^5	H^6	$H^{3'}$	$H^{4'}$
(Py-tpy) *free ligand*	8.70	7.85	7.33	8.68	8.72	7.78
(Py-tpy) *in* $[Os(pytpy)_2]^{2+}$	8.50	7.81	7.10	7.23	8.80	7.95
(Py-tpy) *in [Os(py-tpy)(tpy-ph-Br)]*$^{2+}$	7.88	7.90	7.40	8.58	8.65	7.55

Table 3.19: ^{1}H-NMR data observed for the terpyridine ligand in the osmium(II) complexes; ligand L3 = [2,6-bis-([1,2,3,4]tetrazol-5-yl)pyridine]

3.7 Conclusion

Starting from the concept that terpyridine metal complexes can act as anchoring points on surfaces and on nanoparticles, a number of functionalised terpyridine compounds have been synthesised.

All synthesis and ^{1}H-NMR data recorded for ligands, ruthenium and osmium complexes are described in this Chapter. The purity of all compounds and their identity (for the new species) were checked by elemental analysis, ^{1}H-NMR, mass spectrometry as described in Chapter 2.

Three ligands have been mainly used for these synthesis: 4'(pyrid-4-yl) 2,2'; 6', 2" - terpyridine (py-tpy), 4'(4-bromo-phenyl) 2,2'; 6', 2" - terpyridine (tpy-ph-Br) and 2,6-bis-([1,2,3,4]tetrazol-5-yl)pyridine (H_2L3). Because pyridine groups are considered a quite promising functional species to be incorporated in a monolayer, two new species have been prepared and characterised [Ru(py-tpy)(tpy-ph-Br)][PF_6]$_2$ and [Os(py-tpy)(tpy-ph-Br)][PF_6]$_2$. The complexes [Ru(py-tpy)$_2$][PF_6]$_2$ and [Os(py-tpy)$_2$][PF_6]$_2$ are also been prepared, characterised and compared with the precursor species.

The ligand (tpy-ph-Br) and its relative compounds have been prepared as a precursor for the introduction of the thiol group, which is an ideal functional group for connecting linkers to solid component. Chapter 5 describes all the Suzuki coupling reaction investigated for the preparation of terpyridine thiol substituted compounds. However, the bromide terpyridine ligand has been used for the preparation of a new class of ruthenium and osmium complexes, as [M(tpy)(tpy-ph-Br)][PF_6]$_2$ and [Ru(tpy-ph-Br)(L3)(H_2O)].

Table 3.3 and 3.10 describes all the reaction conditions for ruthenium and osmium complexes respectively.

The ^{1}H-NMR data are also discussed in this Chapter, whereas all the spectra are collected in Appendix I. The ^{1}H-NMR signals of the terpyridine group are described for the prototype [Ru(tpy)$_2$][PF_6]$_2$ in Table 3.4 and for [Os(tpy)$_2$][PF_6]$_2$ in Table 3.11. All the spectra recorded for the complexes synthesised in this thesis have been compared with the archetype spectra. Some relevant shifts have been observed for the terpyridine proton in complexes containing (py-tpy) ligand, whereas (tpy-ph-Br) ligand does not influence

significantly the peaks distribution in the spectrum. By introducing the [2,6-bis-([1,2,3,4]tetrazol-5-yl)pyridine], ligand (H_2L3), few differences have been noticed. The introduction of tetrazole molecule in a terpyridine complex shows a quite important shift in the terpyridyl protons; all these protons feel the influence of the tetrazolate central ring. This behaviour may depend on the different properties of the tetrazole group, stronger σ donor then terpyridine.

Finally, by comparing the ^{1}H-NMR spectra of ruthenium complexes with those of the osmium complexes, no relevant differences have been observed in the ^{1}H-NMR spectra. Whereas relevant differences between Ru(II) and Os(II) complexes have been observed in Chapter 4 by comparing emission, exited states and electrochemical properties.

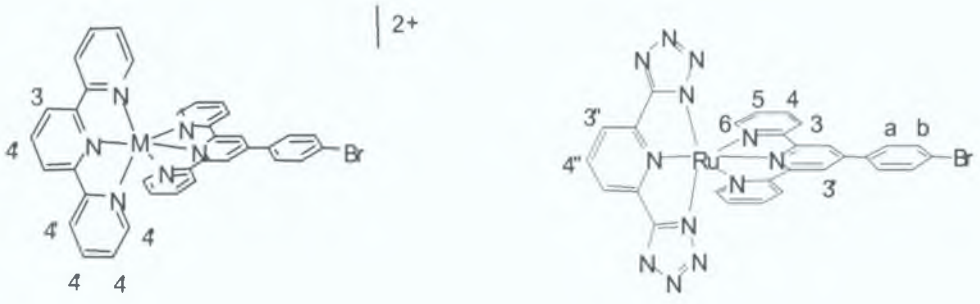

Figure 3.38: Structure of the [M(tpy)(tpy-ph-Br)][PF_6]$_2$ and [Ru(tpy-ph-Br)(L3)(H_2O)] complexes: M = Ru or Os

3.8 Bibliography

[1] Morgan, G. T., Burstall, F. H., J. Chem. Soc. *1932*, 20.

[2] Cargill Thompson, A.M.W., Coord Chem. Rev. *1997*, 160, 1.

[3] P Tsukruk, V., V. Adv. Mater. *1998*, 10, 253-257.

[4] Service, R.F., Science *2000*, 290, 1524-1525.

[5] Ward M.D., Chem. Soc. Rev. *1995*, 121.

[6] Sauvage, J.-P., Collin, J.-P., Chambron, J.-C. Guillerez, S., Coudret, C., Balzani, V., Barigelletti, F., De Cola, L., Flamigni, L., Chem. Rev. *1994*, 94, 993.

[7] Shih-Sheng Sun and Alistair J. Lees Coord. Chem. Rev., *2002* 230, 1-2, 170.

[8] Pickaert G., Ziessel, R., Tetrahedon Letters *1998*, 39,3497.

[6] Meyer, T.J., Prog.Inorg. Chem., *1983*, 30, 389.

[7] Balzani, V., Bolletta, F., Gandolfi, M.T., Maestri, M., Top. Curr. Chem., *1978*, 75, 1.

[8] Satin, N., J. Photochem., *1979*, 10, 19.

[9] Constable, E.C., Adv. Inorg. Chem. Radiochem., *1986*, 30, 69.

[10] Thummel, R.P., Jahng, Y., Inorg. Chem., *1986*, 25, 2527.

[11] Bessel, C.A., See, R.F., Jameson, D.L., Churchill, M.R., Takeuchi, K.J., J. Chem. Soc., Dalton Trans., *1992*, 3223.

[12] Craig, D.C., Scudder, M.L., McHale, W.A., Goodwin, H.A., Aust. J. Chem., *1998*, 51, 1131.

[13] Duati, M., Fanni, S., Vos, J.G, Inorg. Chem. Commun., *2000*, 3, 68.

[14] Krohnke, F., Synthesis, *1976*.

[15] Maestri, M., Armaroli, N., Balzani, V., Constable, E.C., Cargill Thompson, A..M.W., Inorg. Chem. 34, *1995*, 2759.

[16] (a) Hage.R, Ph. D. Thesis, *1991*, Leiden University. The Nederlands; (b) Duati, M., Tasca, S., Lynch, F., Bohlen, Holger, Vos, Han, Inorganic Chemistry, *2003*, 42, 8377.

[17] Sugiyarto, K. H., Craig, D. C., Rae, A. D.; Goodwin, H. A., Aust. J. Chem., *1993*, 46, 1269.

[18] Constable, E.C., Cargill Thompson, A.M.W., Tocher, D.A., Daniels, M.A.M., New. J. Chem., *1992*, 16, 855.

[19] (a) Adcock, P.A., Keene, F.R:, Smythe, R.S., Snow, M.R., Inorg. Chem., *1984*, 23, 2236; (b) Kober, E.M., Caspar, J.V., Sullivan, B.P., Meyer, T., J. Inorg. Chem., *1988*, 27, 4587.

[20] Young, R.C:, Nagle, J.K., Meyer, T.J., Whitten, D.G., J. Am. Chem. Soc., *1978*, 100, 4773.

[21] Beley, M., Collin, J.P., Louis, R., Metz, B., Sauvage, J.P., J. Am. Chem. Soc., *1991*, 113, 8521.

[22] Arana, C., Abruna, H.D., Inorg. Chem., *1993*, 32, 194.

Chapter 4

Characterisation of the Ru (II) and Os (II) Terpyridine Complexes: Study of Excited States and Electrochemical Properties

In this Chapter the absorption, emission and electrochemical characterisation of the functionalised terpyridine complexes, containing either ruthenium (II) or osmium (II) centres are reported.

The results obtained are compared with the archetype $[Ru(tpy)_2]^{2+}$ *and* $[Os(tpy)_2]^{2+}$ *complexes. Special attention is paid to their electrochemical and excited state properties.*

4.1 Introduction

A continuing theme in photochemistry is the use of metal to ligand charge transfer (MLCT) excited states as sensitiziers in a variety of photochemical and photophysical applications. One goal is to extend the list of available MLCT excited states by synthetic studies designed to take advantage of variations in the metal and ligands. The choice of Ru(II) polypyridine family is dictated by the fact that these complexes are particularly interesting as excited state reactants or products in electron transfer processes and as mediators of electron transfer reactions involving light.

Absorption and emission spectra reveal that a metal – ligand charge transfer takes place in terpyridine ruthenium complexes. As opposed to bypyridine complexes, where phosphorescence phenomena may be observed over a wide temperature range, no emission is detected at room temperature in the case of the parent compound $[Ru(tpy)_2]^{2+}$ due to non-radiative deactivation of the excited triplet metal to ligand charge transfer ^{3}MLCT state, via a triplet metal-centred ^{3}MC state to the ground state[1]. However, at low temperatures, this path becomes less efficient and therefore luminescence is observed[2][3][4].

The excited state lifetime of normal terpyridine complexes is accepted as being due to the small gap between the emitting ^{3}MLCT state and the deactivating ^{3}MC state. This is a limitation to the use of terpyridine compounds as molecular wires[5]. Efforts to improve the luminescence properties of these complexes is more usually directed at lowering of the energy of the emitting ^{3}MLCT state, for example, by substitution of the 4' positions of the ligand using electron donating or electron accepting substituents[5]. In contrast, another approach is to raise the energy of the ^{3}MC state state by manipulation of the metal based σ – antibonding orbital. Examples where terpyridines have been combined with tridentate such as bis(triazole)pyridine terpyridine analogues, have been reported[6]. Compared to $[Ru(tpy)_2]^{2+}$, the luminescence lifetime of these systems showed a 300 – fold increase and is explained by a rise of the energy of the ^{3}MC level. Furthermore, 5 - phenyl – bis(triazole) and bis(tetrazole)pyridines have been reported[5]. The

triazole rings are deprotonated in the complexes (6π – aromatic) and a reprotonation results in quenching of the emission.

Starting with the photochemical and electrochemical properties of the archetype $[Ru(tpy)_2]^{2+}$ and $[Os(tpy)_2]^{2+}$, all the data for the Ru(II) and Os(II) complexes investigated in this thesis, are reported in this Chapter. Absorption, emission and electrochemical measurements are described. Section 4.2.1 describes absorption and emission properties of $[Ru(tpy)_2]^{2+}$, whereas the electrochemical behaviour is reported in Section 4.4.2. Section 4.3.1 and 4.4.2 describe Uv/Vis. spectra and electrochemical properties of $[Os(tpy)_2]^{2+}$ respectively.

4.2 Results and Discussion

Absorption and emission spectra for all Ru(II) complexes are described in this Section. Absorption were obtained at room temperature in acetonitrile or in DMF. The emission spectra were recorded at 77 K, using a rigid matrix, Ethanol/Methanol mixture (4/1) and where possible at room temperature in acetonitrile.

The ε molar extinction coefficient for all the ruthenium terpyridine complexes synthesised, has been calculated and described in Appendix II.

4.2.1 Absorption spectroscopy: Ru (II) bis terpyridine complex

In this Section, the absorption spectra of the ruthenium terpyridine based complexes have been discussed. The absorption spectrum for the prototype $[Ru(tpy)_2][PF_6]_2$ is shown in Figure 4.1. In the UV region two very intense bands at 275 nm and 320 nm, have been assigned to the ligand-centred (^{1}LC) π–π* transitions. These are typical transitions of pyridine centre in transition metal complexes. The relatively intense and broad absorption band in the visible region, which is responsible for the deep red colour of the complex, is due to a spin-allowed d-π metal-to-ligand charge transfer (MLCT) transitions[3] and appears clearly at 474 nm. In the rigid matrix at 77 K, $[Ru(tpy)_2]^{2+}$ exhibits at 618 nm a strong long-lived luminescence characteristic of a triplet metal-to-ligand

charge transfer (^{3}MLCT) level. On increasing the temperature, the luminescence intensity of the complex decrease. At room temperature, $[Ru(tpy)_2]^{2+}$ is practically non - luminescent [3][4][7][8-11].

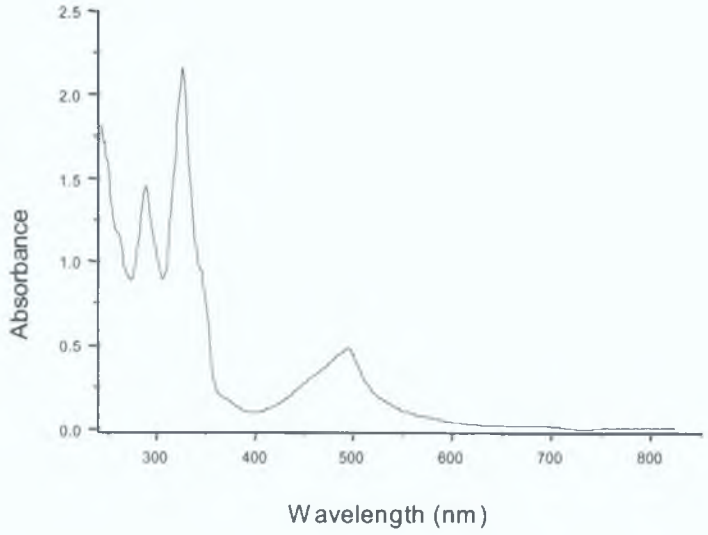

Figure 4.1: Absorption spectrum of $[Ru(tpy)_2]^{2+}$ in acetonitrile solution

4.2.2 Absorption spectra of Ru(II) terpyridine complexes

In this Section, the absorption spectra for ruthenium terpyridine based complexes have been discussed. All the spectra are shown in Figure 4.2 – Figure 4.6.

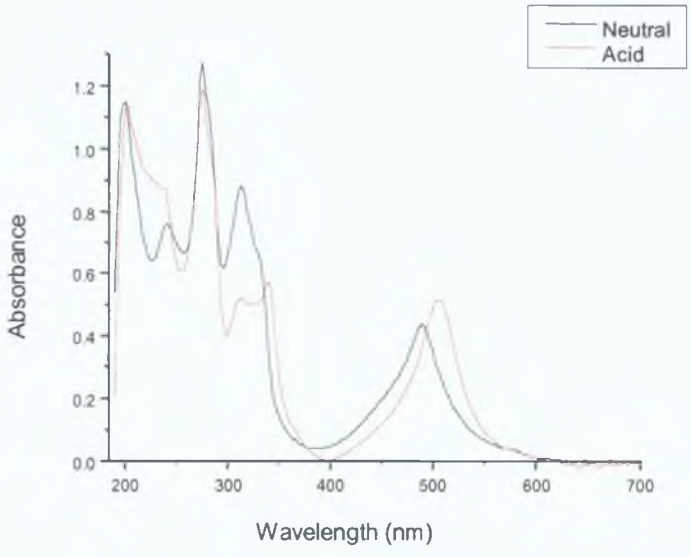

Figure 4.2: Absorption spectrum of $[Ru(py\text{-}tpy)_2][PF_6]_2$, in neutral and acidic solution, in acetonitrile; concentration of $[Ru(py\text{-}tpy)_2][PF_6]_2 = 5.97\ 10^{-5}$ M.

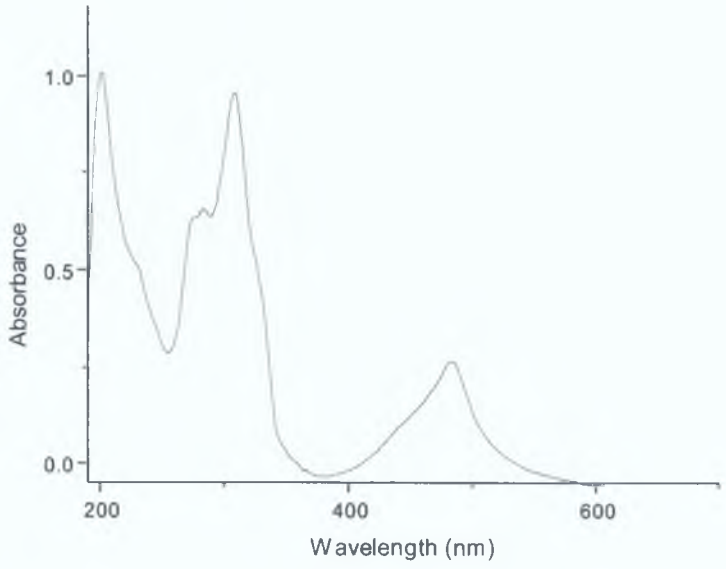

Figure 4.3: Absorption spectrum of [Ru(tpy)(tpy-ph-Br)][PF_6]$_2$ in acetonitrile; concentration of [Ru(tpy)(tpy-ph-Br)][PF_6]$_2$ = 4.65 10^{-5} M.

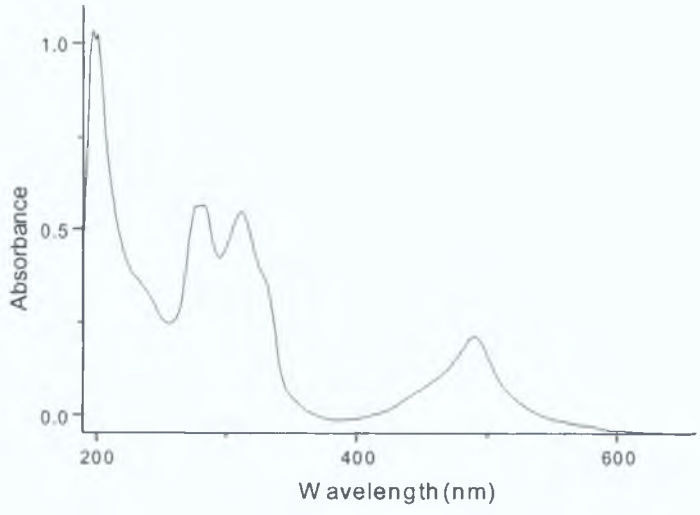

Figure 4.4: Absorption spectrum of [Ru(py-tpy)(tpy-ph-Br)][PF_6]$_2$ in acetonitrile; concentration of [Ru(py-tpy)(tpy-ph-Br)][PF_6]$_2$ = 4.12 10^{-5} M.

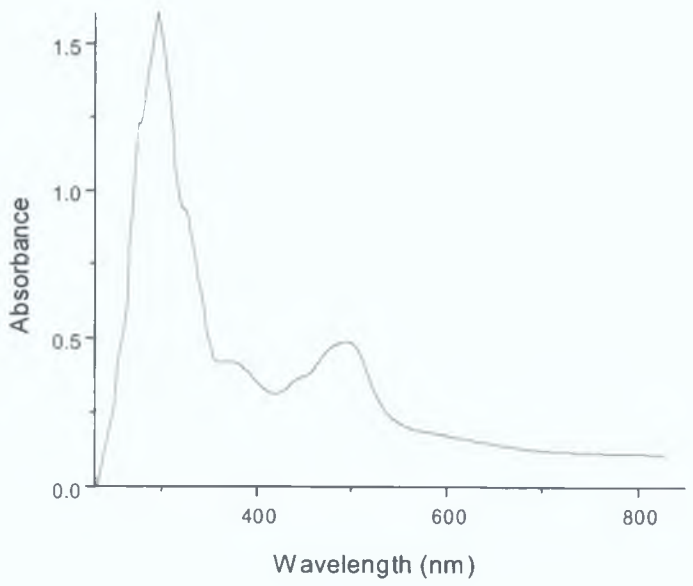

Figure 4.5: Absorption spectrum of [Ru(tpy-ph-Br)(L3)(H_2O)] in DMF; concentration of [Ru(tpy-ph-Br)(L3)(H_2O)] = 6.36 10^{-5} M.

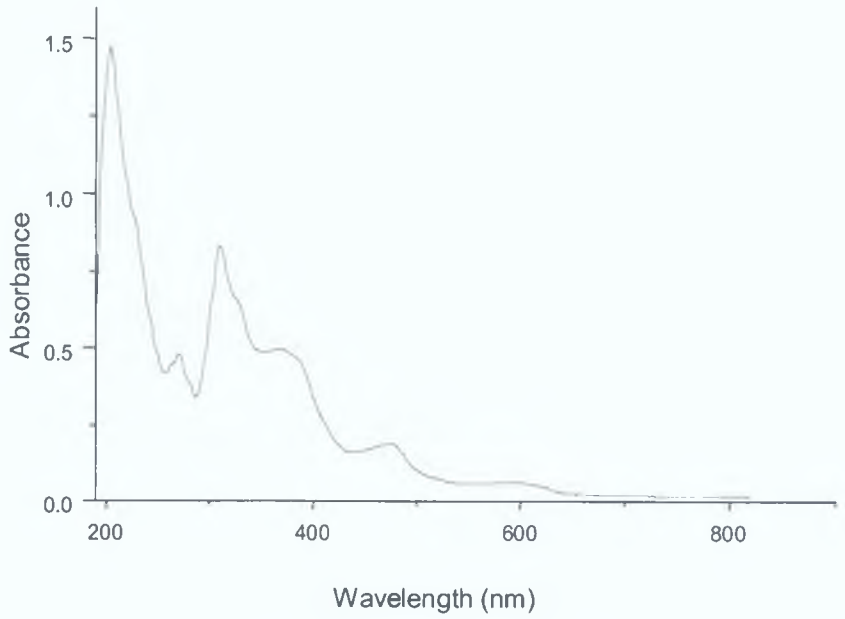

Figure 4.6: Absorption spectrum of [Ru(tpy)[2,6-(2,3-ph-4-CH_3-pyrazol)py)]$[PF_6]_2$ in acetonitrile; concentration of [Ru(tpy)[2,6-(2,3-ph-4-CH_3-pyrazol)py)]$[PF_6]_2$ = 2.56 10^{-5} M.

The absorption spectrum of $[Ru(py\text{-}tpy)_2][PF_6]_2$, in neutral and acidic solution is shown in Figure 4.2. The UV - Vis. absorption spectrum of the neutral complex $[Ru(py\text{-}tpy)_2][PF_6]_2$, has its most intense metal to ligand charge transfer band (MLCT), in the visible region, at 498 nm. This is a broad peak responsible for the colour of the complex (orange). The bands at higher energies, around 270 and 320 nm, are assigned to the intra ligand $\pi - \pi^*$ transition. The MLCT transition for the protonated species appears at 510 nm, slightly lower in energy then this observed for $[Ru(tpy)_2]^{2+}$. The band at 270 nm, is not significantly affected by protonation (after addition of 1 drop of trifluoracetic acid), whereas for the protonated species, the band at 320 nm, is observed at lower energy, 348 nm and the "shoulder" of this peak, is not pronounced as in the neutral species. The red shift may be explained by an increase in conjugation which causes a lowering of the π^* orbitals.

The absorption spectrum of $[Ru(tpy)(tpy\text{-}ph\text{-}Br)][PF_6]_2$ complex is shown in Figure 4.3. The $[Ru(tpy)(tpy\text{-}ph\text{-}Br)][PF_6]_2$ complex shows an intense peak at 490 nm, assigned to a metal-to-ligand charge transfer (MLCT). In the UV region, two other bands appear at 210 nm and 320 nm; they are attributed to the ligand based transitions, π_L - π_L^*. By comparing the absorption spectrum of the prototype $[Ru(tpy)_2]^{2+}$ and the spectrum of the $[Ru(tpy)(tpy\text{-}ph\text{-}Br)][PF_6]_2$ complex, a red shift of the (MLCT) band is observed (474 nm for $[Ru(tpy)_2]^{2+}$ and 490 nm for $[Ru(tpy)(tpy\text{-}ph\text{-}Br)][PF_6]_2$).

Figure 4.4 shows the absorption spectrum of $[Ru(py\text{-}tpy)(tpy\text{-}ph\text{-}Br)][PF_6]_2$. The lowest energy absorption band observed in the visible region at 495 nm, is assigned to a ^{1}MLCT transition. This band appears as a large and intense peak. In the UV region, two intense bands at 298 nm and 330 nm, have been assigned to the ligand centred $\pi - \pi^*$ transitions. A comparison with the absorption spectrum of $[Ru(tpy)(tpy\text{-}ph\text{-}Br)][PF_6]_2$ complex (see Figure 4.3), shows that by changing a terpyridine group with a (py-tpy) ligand, the λ_{max} of the MLCT transition, shifts to lower energy, but the difference between the two values is quite small: 490 nm for $[Ru(tpy)(tpy\text{-}ph\text{-}Br)][PF_6]_2$ and 495 nm for $[Ru(py\text{-}tpy)(tpy\text{-}ph\text{-}Br)][PF_6]_2$.

The absorption spectrum of [Ru(tpy-ph-Br)(L3)(H_2O)] is shown in Figure 4.5. The tetrazole ligand contains a central pyridine ring that is a good π - acceptor and two tetrazole moieties that are strong σ donators. Therefore, in coordination compounds, (H_2L3) ligand is a better σ donor and a poorer π acceptor then terpyridine. This causes a shift of the MLCT transition to lower energy. By observing wavelengths of the lowest energy absorption maximum of ruthenium complexes (Table 4.1), it is noted that [Ru(tpy-ph-Br)(L3)(H_2O)] shows the MLCT band to lower energy compare with the (Ru-tpy) prototype (absorption maximum value of [Ru(tpy-ph-Br)(L3)(H_2O)] is 485 nm, whereas for is 474 nm). This behaviour may be explained by the fact that the substitution of a tpy group with the $(L3)^{2-}$ ligand, causes an increase in the electronic charge on the ruthenium centre with a consequent red shift of the MLCT absorption band. Finally, an intense absorption band at higher energy, 285 nm, is assigned at $\pi - \pi^*$ transitions associated with the aromatic rings of the tetrazole ligand. A weak shoulder band is observed at 375 nm and may be assigned to intra ligand $\pi - \pi^*$ transition.

The absorption spectrum of [Ru(tpy)[2,6-(2,3-ph-4-CH_3-pyrazol)py][PF_6]$_2$ complex is shown in Figure 4.6. The absorption spectrum of the [Ru(tpy)[2,6-(2,3-ph-4-CH_3-pyrazol)py][PF_6]$_2$ complex in acetonitrile, exhibits its lowest energy band at 486 nm, which is (^{1}MLCT) in nature. Two intense bands appear at 310 nm, and at 210 nm which have been assigned to $\pi - \pi^*$ transitions associated with the terpyridine rings and to the central pyridine of the ligand [2,6-(2,3 phenyl-4-methyl pyrazol)pyridine]. The complex exhibits also a weak shoulder at 360 nm which may also be the $\pi - \pi^*$ in nature. By changing a terpyridine group with the tridentate ligand [2,6-(2,3 phenyl-4-methyl pyrazol)pyridine], no significant differences are observed in the visible region. The band for $[Ru(tpy)_2]^{2+}$ appeared at 474 nm whereas 486 nm is the value observed for the complex [Ru(tpy)[2,6-(2,3-ph-4-CH_3-pyrazol)py][PF_6]$_2$.

4.2.3 Emission spectroscopy: Ru (II) bis terpyridine complex

In the last Section, the absorption spectra of the Ru(II) tpy complexes have been discussed. It is generally accepted that while the lowest energy absorption is ^{1}MLCT in nature that the emission is originating from the ^{3}MLCT state.

In this Section, these emitting properties of the ruthenium terpyridine based complexes will be cleared. The emission spectrum for the prototype $[Ru(tpy)_2][PF_6]_2$ in EtOH/MeOH (4/1) at 77 K, is shown in Figure 4.7.

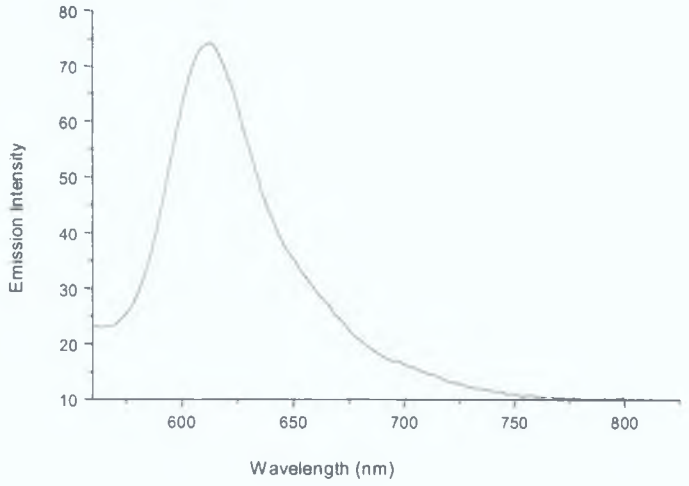

Figure 4.7: Emission spectrum of $[Ru(tpy)_2]^{2+}$ at 77 K, in Ethanol/Methanol mixture (4/1)

The anomalously weak emission of $[Ru(tpy)_2]^{2+}$ at room temperature compared with the strong emission of most ruthenium (II) polypyridine complexes was first attributed to the equilibration of the ^{3}MLCT state with high-spin d-d (metal centred MC) states [12][14].

Meyer and co-workers[15] have suggested that the unfavourable bite angles associated with the terpyridine ligand result in a relatively weak ligand field in $[Ru(tpy)_2]^{2+}$ such that low-lying MC states are available to quench the luminescence ^{3}MLCT state (see discussion[16-19] in Section 3.1).

Ligand substituents cause considerable variations in the absorption and luminescence properties of ruthenium terpyridine complexes and most importantly, in the emission lifetime. A substituent effect on the energy of the

absorption and emission bands results from a combined perturbation of the LUMO (ligand π*) and HOMO (metal t_{2g}, in octahedral symmetry) orbitals.

The effect on the luminescence quantum yield is likely to be attributed to the above perturbations, as well as to the substituent effect on the ligand field strength. As already mentioned in the introduction of this Chapter, investigations of Ru (II) terpyridine complexes with substituents in the 4' position of 2, 2'': 6', 2'' - terpyridine, have shown that electron donating or electron - accepting substituents are effective in changing groups in the luminescence properties[5]. When the substituents are electron accepting groups, the π* ligand-centred orbital is stabilized the with respect to the π (t_{2g}) metal-centred orbital and the metal (in the excited state) does not receive any charge compensation from the tpy-A ligand in the electronic transition. When the substituents are electron-donating groups, the π* ligand-centred orbital is destabilised with respect to the π (t_{2g}) metal-centred orbital in the ground state complex, but in the MLCT excited state the π (t_{2g}) metal orbital is strongly destabilized because of the presence of the (tpy-D) ligand not involved in the MLCT transition.

All the ruthenium terpyridine compounds exhibit a strong emission at low temperature (in some cases room temperature emission is also observed). Electronic absorption and emission data for the ruthenium complexes investigated are summarised in Table 4.1. The emission lifetime of the excited state obtained for ruthenium complexes are also shown in Table 4.1.

Complex	Absorption λ, nm	*Emission (298K)* λ, nm	τ^b, ns	*Emission (77K)*[c] λ, nm
$[Ru(tpy)_2][PF_6]_2$	474	-	0.25	618
$[Ru(py\text{-}tpy)_2][PF_6]_2$	498	-	-	670
$[Ru(tpy)(tpy\text{-}ph\text{-}Br)][PF_6]_2$	490	631	-	626
$[Ru(py\text{-}tpy)(tpy\text{-}ph\text{-}Br)][PF_6]_2$	495	-	-	636
$[Ru(tpy\text{-}ph\text{-}Br)(L3)(H_2O)]$	485[a]	628	42	624
$[Ru(tpy)[2,6\text{-}(2,3\text{-}ph\text{-}4\text{-}CH_3\text{-}pyrazol)py][PF_6]_2$	486	-	-	602

Table 4.1: Absorption and luminescence data for ruthenium terpyridine complexes at room temperature in acetonitrile solution; (a) room temperature in DMF solution; (b): Luminescence emission lifetime in deaerated acetonitrile; (c) Luminescence emission in Ethanol/Methanol (4/1)

4.2.4 Emission spectra of Ru(II) terpyridine complexes

The emission spectra for ruthenium terpyridine based complexes have been discussed in this Section. All the spectra are shown in Figure 4.8 – Figure 4.12.

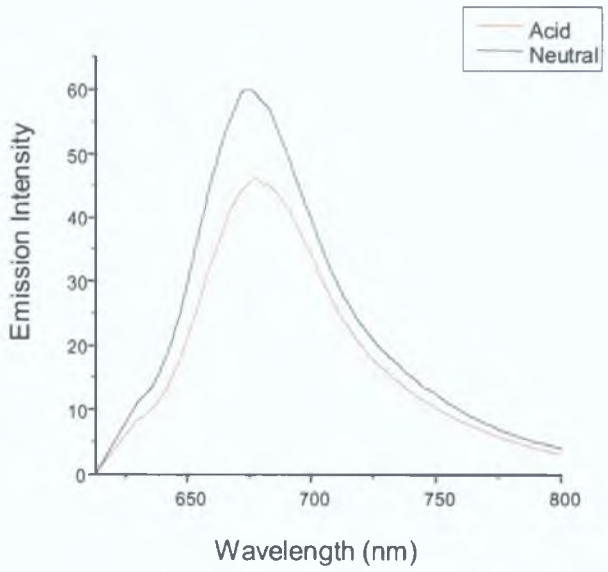

Figure 4.8: Emission spectrum of $[Ru(py\text{-}tpy)_2][PF_6]_2$, in neutral and acid solution at 77 K, in Ethanol/Methanol mixture (4/1)

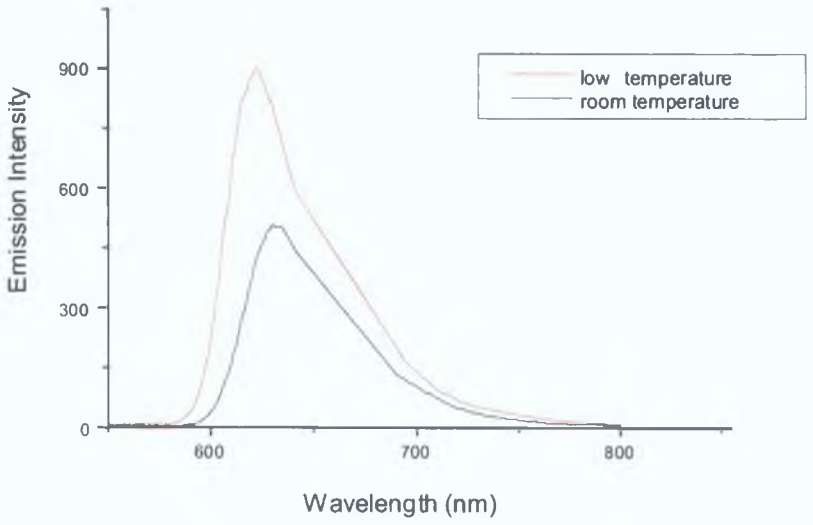

Figure 4.9: Emission spectrum of [Ru(tpy)(tpy-ph-Br)][PF_6]$_2$, at 77 K, in Ethanol/Methanol mixture (4/1)

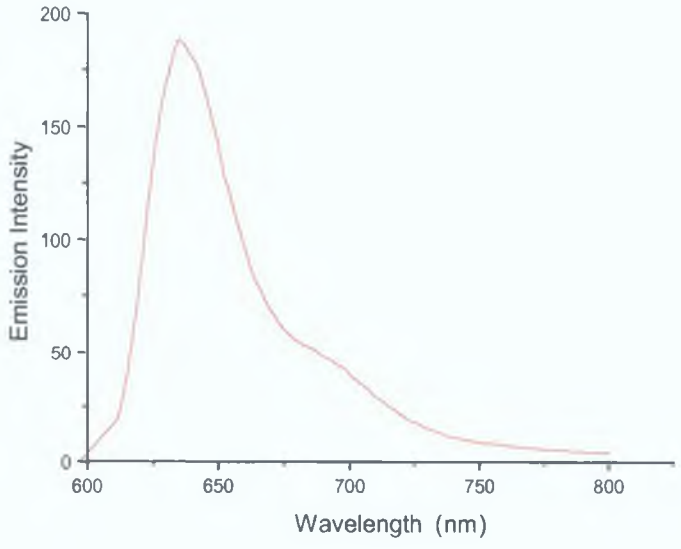

Figure 4.10: Emission spectrum of [Ru(py-tpy)(tpy-ph-Br)][PF_6]$_2$, in acetonitrile at 77 K, in Ethanol/Methanol mixture (4/1)

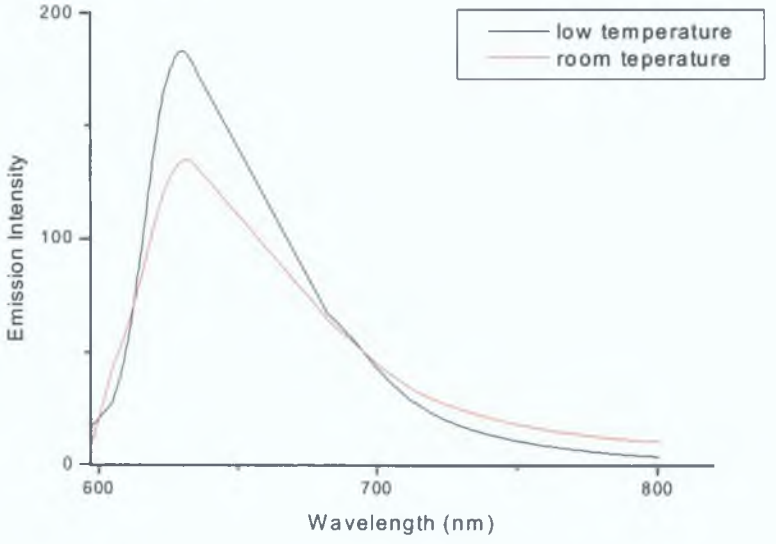

Figure 4.11: Emission spectrum of [Ru(tpy-ph-Br)(L3)(H_2O)] in DMF at room temperature and at 77 K, in Ethanol/Methanol mixture (4/1)

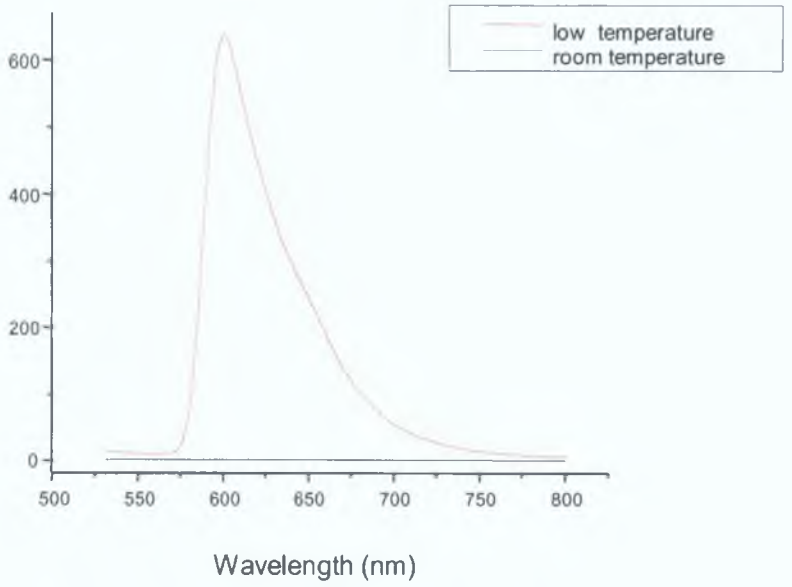

Figure 4.12: Emission spectrum of[Ru(tpy)[2,6-(2,3-ph-4-CH_3-pyrazol)py][PF_6]$_2$in acetonitrile at room temperature and at 77 K, in Ethanol/Methanol mixture (4/1)

Figure 4.8 shows the emission spectrum of $[Ru(py\text{-}tpy)_2][PF_6]_2$ in EtOH/MeOH (4/1) mixture at 77 K, in neutral and acidic solution. On cooling to 77 K, a phenomenon defined by Wrighton and co-workers[20] as "rigid chromism" can be observed. At low temperature, the solvent dipoles are immobile on the time scale of the excited state and consequently they can not respond to the change in electronic configuration between the ground and excited state.

Emission spectrum at low temperature for the neutral complex $[Ru(py\text{-}tpy)_2][PF_6]_2$ shows a band at 670 nm. After addition of 1 drop of trifluoracetic acid, the emission of the complex shifted to lower energy and increased in intensity; a red shift at 680 nm for the protonated species. $[Ru(py\text{-}tpy)_2][PF_6]_2$ complex does not show luminescence at room temperature. This is attributed to the existence of metal-centred (MC), states lying in close proximity to the MLCT states.

Figure 4.9 shows the emission spectrum of $[Ru(tpy)(tpy\text{-}ph\text{-}Br)][PF_6]_2$ complex in acetonitrile, at room temperature and in EtOH/MeOH (4/1) at 77 K. According to Maestri[21], Ru (II) complexes of 4'-phenyl substituted terpyridine exhibited much more efficient luminescence than the corresponding terpyridine complexes as observed by comparing the emission of $[Ru(tpy)_2]^{2+}$, λ = 618 nm and $[Ru(tpy)(tpy\text{-}ph\text{-}Br)][PF_6]_2$, with λ = 626 nm, at low temperature. The presence of the phenyl group increases the emission of the ruthenium terpyridine complex, at low temperature, but also at room temperature. Whereas $[Ru(tpy)_2]^{2+}$ is practically non - luminescent at room temperature, the $[Ru(tpy)(tpy\text{-}ph\text{-}Br)][PF_6]_2$, shows a quite intense band at 631 nm (see Figure 4.9). However, by adding a withdrawing group such as a bromide in 4'-phenyl position, a very small effect on the emission wavelength was observed.

Figure 4.10 shows the emission spectrum of $[Ru(py\text{-}tpy)(tpy\text{-}ph\text{-}Br)][PF_6]_2$ in EtOH/MeOH (4/1) at 77 K. As observed before for the $[Ru(tpy)_2][PF_6]_2$ complex, $[Ru(py\text{-}tpy)(tpy\text{-}ph\text{-}Br)][PF_6]_2$ complex, is practically non - luminescent at room temperature. However, in rigid matrix at 77 K, the complex exhibits a strong luminescence band characteristic of a MLCT based emission at 636 nm.

On changing a terpyridine with a py-terpyridine group, from [Ru(tpy)(tpy-ph-Br)][PF_6]$_2$ to [Ru(py-tpy)(tpy-ph-Br)][PF_6]$_2$, the emission spectrum shows a red shift. λ_{max} is 626 nm for [Ru(tpy)(tpy-ph-Br)][PF_6]$_2$ (see Figure 4.9) whereas for the [Ru(py-tpy)(tpy-ph-Br)][PF_6]$_2$ complex is 636 nm.

Figure 4.11 shows the emission spectrum of [Ru(L3)(tpy-ph-Br)(H_2O)] in DMF at room temperature and in EtOH/MeOH (4/1) at 77 K. The complex [Ru(tpy-ph-Br)(L3)(H_2O)], shows quite intense emission at room temperature, with a λ = 628 nm. The emission spectrum of [Ru(tpy-ph-Br)(L3)(H_2O)], at low temperature, shows an intense band at 624 nm. The substitution of terpyridine group with a tetrazole ligand greatly increases the luminescence intensity at room temperature. In coordination compounds, the deprotonated ligand $(L3)^{2-}$ ligand is a better σ donor and a poorer π acceptor than terpyridine, with the emission spectrum of [Ru(tpy-ph-Br)(L3)(H_2O)], showing a red shifted metal to ligand charge transfer band (λ = 628 nm of the complex respect to the prototype terpyridine complex, where λ was 618 nm). The decrease in energy of the ^{3}MLCT state, reflected by the red shifted emission in comparison with the emission of $[Ru(tpy)_2]^{2+}$ is due to the destabilisation of the t_{2g} metal orbital by the negative charges present on the ligand. This effect can be understood by considering the removal of one electron from the metal results in the formation of Ru(III) which withdraws electronic charge from the negative charged $(L3)^{2-}$ ligand destabilising the t_{2g} metal orbitals, similar results are obtained from the electrochemistry. The protonation of one or both tetrazole rings results in a total quenching of the emission. The origin of the quenching of the luminescence of the protonated complexes is not clear. In studies of the effects of protonation on the excited-state behaviour of $[(bpy)_2Ru(CN)_2]$, Scandola and co-worker postulated that protonation of the complex results in a decrease in the ^{3}MLCT-^{3}MC gap and a subsequent increase in the non-radiative relaxation rate. Those changes, which occur upon protonation, should serve to decrease the energy gap between the ^{3}MLCT and ^{3}MC states. The ^{3}MLCT transition results from a (Ru – tpy) transition, while the ^{3}MC state has its origin as a $Ru(t_{2g})$ –$Ru(e_g)$ transition.

Protonation of the complex results in a stabilisation of the ground state since (H_2L3) is a weaker σ-donating ligand than $(L3)^{2-}$ and, assuming an averaged ligand field environment for both species, the $Ru(t_{2g})$ –$Ru(e_g)$ energy should be larger for the deprotonated species. Thus both changes in metal-ligand interaction which occurs upon protonation should serve to decrease the energy gap between the ^{3}MLCT and ^{3}MC states. Finally the introduction of the ligand (H_2L3) causes an increase in the lifetime of the ^{3}MLCT excited state, as shown in Table 4.1, 0.25 ns was found for $[Ru(tpy)_2][PF_6]_2$, whereas 42 ns is the lifetime obtained for [Ru(tpy-ph-Br)(L3)(H_2O)].

Figure 4.12 shows the emission spectrum of [Ru(tpy)[2,6-(2,3-ph-4-CH_3-pyrazol)py][PF_6]$_2$ complex in acetonitrile, at room temperature and in EtOH/MeOH (4/1) at 77 K. The complex shows weak luminescence at room temperature, as already observed for the prototype $[Ru(tpy)_2][PF_6]_2$. Emission spectrum of [Ru(tpy)[2,6-(2,3-ph-4-CH_3-pyrazol)py][PF_6]$_2$ at low temperature, shows a band at 602 nm resulting in a low intensity emission from the MLCT transition of low energy. It has been observed that the ^{3}MLCT state for the complex [Ru(tpy)[2,6-(2,3-ph-4-CH_3-pyrazol)py][PF_6]$_2$, moves to higher energies compared to the same state observed for $[Ru(tpy)_2][PF_6]_2$ (see Figure 4.7). This effect is shown with a red shifted emission from 618 nm λ_{em} of $[Ru(tpy)_2][PF_6]_2$ to 602 nm λ_{em} of [Ru(tpy)[2,6-(2,3-ph-4-CH_3-pyrazol)py][PF_6]$_2$. This complex shows a quite intense band at 77 K.

4.3 Absorption and emission spectroscopy: Os (II) terpyridine complexes

One disadvantage of ruthenium terpyridine complexes is clearly that they are characterised by relatively low-lying dd states[22][23]. These states can lead to excited states[20-24]. In work by Creutz[11] and Sauvage[12] the photophysical properties of the excited states of a series of polypyridine complexes of Os(II) were investigated. Three important feature of osmium chemistry are:

- The oxidation potentials of osmium (II) compounds are generally lower than those of the analogues ruthenium (II) complexes.
- Due to the lower oxidation potentials for osmium (II) complexes, the energies of the luminescent ^{3}MLCT states are lower than those of the analogous ruthenium complexes.
- The metal-ligand interaction is stronger for osmium than for ruthenium this leads to a larger ligand field splitting.

Another major difference between osmium and ruthenium is spin-orbit coupling, which is much larger for third-row transition elements than second-row metals. This result in mixing of the singlet and triplet states and formally forbidden transitions will often be observed. For example, the ($d\pi$-π) ^{3}MLCT absorption band is very weak for ruthenium polypyridyl complexes, but quite intense for the corresponding osmium complexes.

Absorption and emission spectra for the complex $[Os(tpy)_2][PF_6]_2$ are described in this Section. The absorption and emission measurements were recorded at room temperature in acetonitrile. The data obtained are given in Table 4.2.

Since a very little material was available, I was not able to obtain accurate extinction coefficient for Os(II) terpyridine complexes.

4.3.1 Absorption spectroscopy: Os (II) bis terpyridine complex

In this Section, the absorption spectra of the osmium terpyridine based complexes have been discussed. The absorption spectrum for the prototype $[Os(tpy)_2][PF_6]_2$ is shown in Figure 4.13.

In the UV region two very intense bands at 260 nm and 306 nm, may be assigned to the ligand-centred π–π* transitions. Two MLCT transition bands are observed in the visible region; at 477 nm appears the ^{1}MLCT transition and at 657 nm an additional tail with a weak absorption, due to ^{3}MLCT transition, corresponding to direct, spin-forbidden population of Os-L charge transfer (CT) triplet excited state[12][24]. Os(II) is easier to oxidise than Ru(II), however the absorption

maximum of the spin-allowed MLCT band in the visible region for $[Os(tpy)_2]^{2+}$ lies at the same wavelength as that of $[Ru(tpy)_2]^{2+}$ (λ_{em} = 477 nm for $[Os(tpy)_2]^{2+}$ and λ_{em} = 476 nm for $[Ru(tpy)_2]^{2+}$. This could be due to a more covalent character of the metal-ligand interaction in the osmium complex.

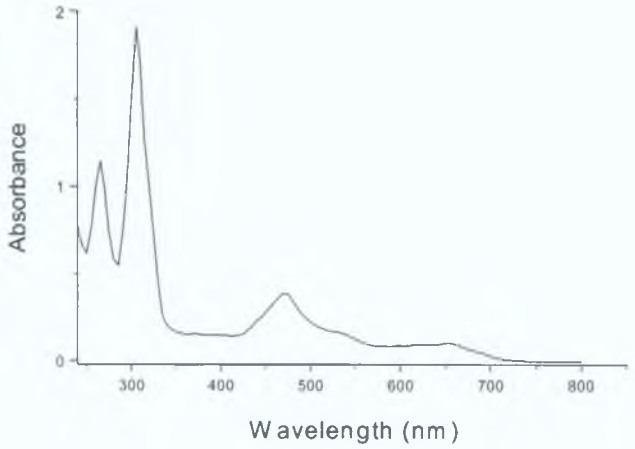

Figure 4.13: Absorption spectrum of $[Os(tpy)_2]^{2+}$ in acetonitrile

4.3.2 Absorption spectra of Os(II) terpyridine complexes

In this Section, the absorption spectra for osmium terpyridine based complexes have been discussed. All the spectra are shown in Figure 4.14 – Figure 4.18.

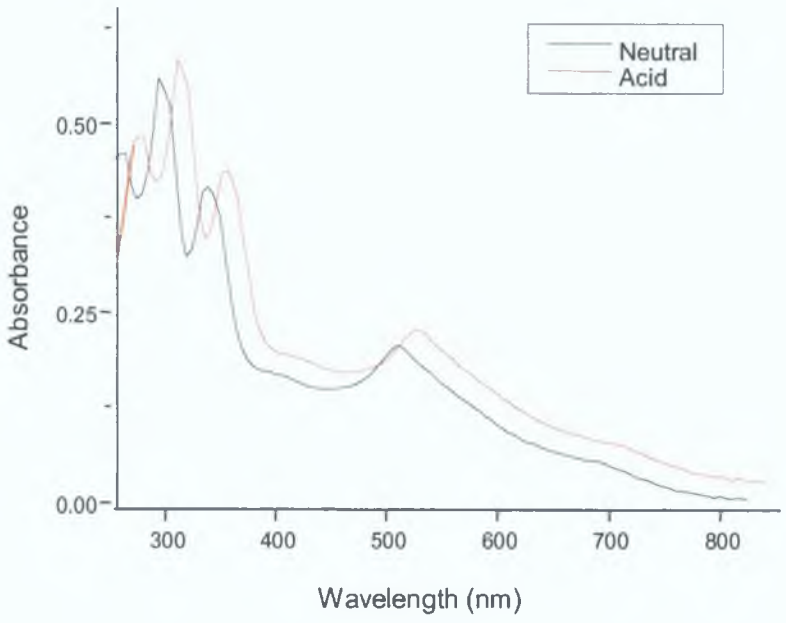

Figure 4.14: Absorption spectrum of $[Os(py\text{-}tpy)_2][PF_6]_2$ in acetonitrile

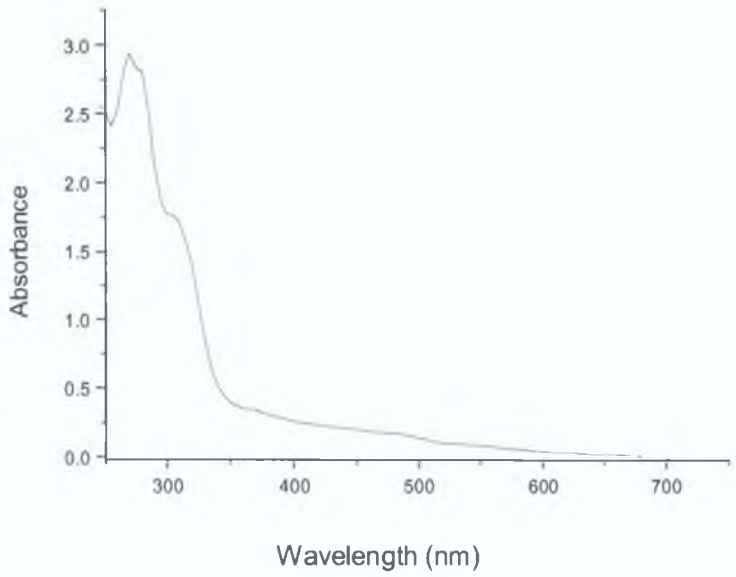

Figure 4.15: Absorption spectrum of $[Os(tpy)(tpy\text{-}ph\text{-}Br)][PF_6]_2$ in acetonitrile

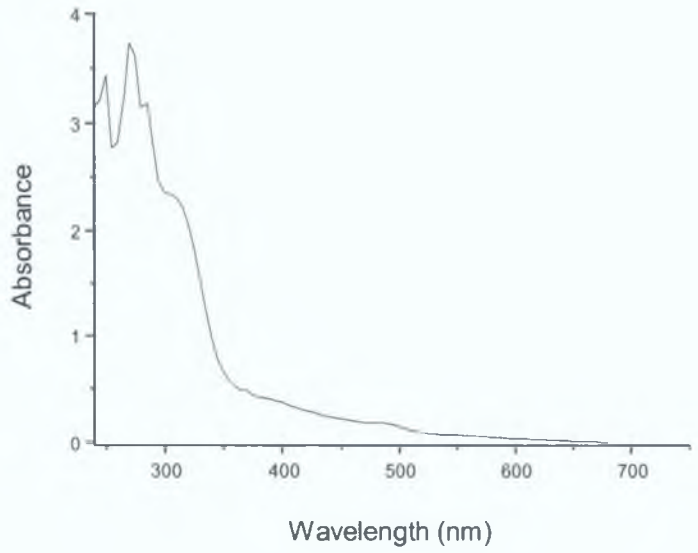

Figure 4.16: Absorption spectrum of $[Os(py\text{-}tpy)(tpy\text{-}ph\text{-}Br)][PF_6]_2$ in acetonitrile

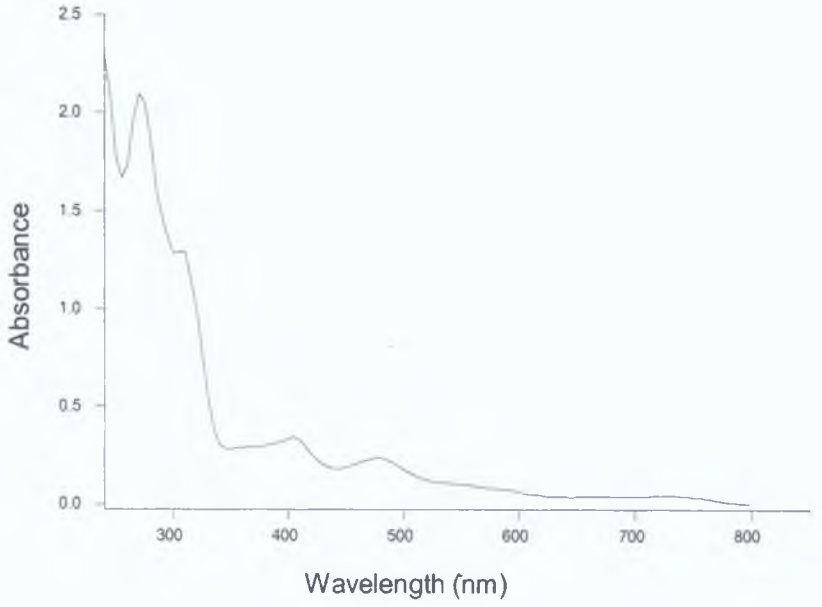

Figure 4.17: Absorption spectrum of [Os(tpy)(L3)(H_2O)] in acetonitrile

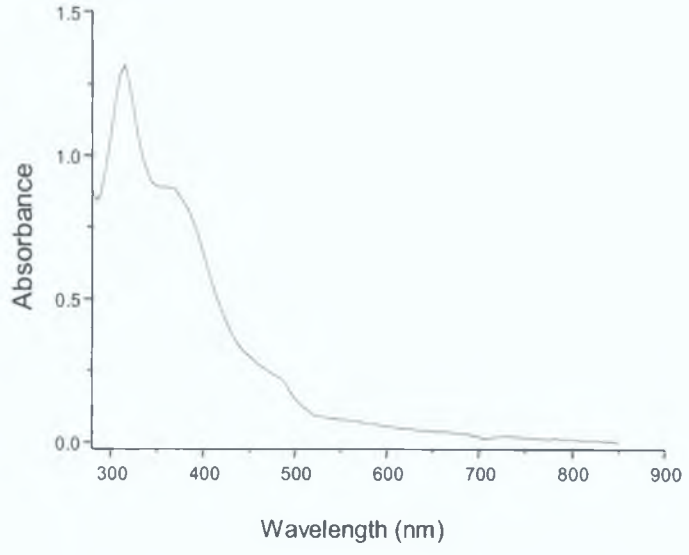

Figure 4.18: Absorption spectrum of [Os(tpy)[2,6-(2,3-ph-4-CH_3-pyrazol)py][PF_6]$_2$ in acetonitrile

The absorption spectrum of $[Os(py\text{-}tpy)_2][PF_6]_2$, in neutral and acidic solution, at room temperature is shown in Figure 4.14. The absorption spectrum of $[Os(py\text{-}tpy)_2][PF_6]_2$ in acetonitrile, shows the metal to ligand charge transfer band

(MLCT), in the visible region, at 502 nm, which appears as a broad peak. The bands at higher energies, around 290 nm and 340 nm, are assigned to the intra ligand $\pi - \pi^*$ transition. Spectrum of the protonated complex has been observed after addition of 1 drop of trifluoracetic acid. The MLCT transition for the protonated species appears at lower energies, 530 nm. After protonation, the band at 290 nm shifts at 320 nm and the band at 340 nm, is observed at lower energy, 355 nm.

The absorption spectrum of $[Os(tpy)(tpy\text{-}ph\text{-}Br)][PF_6]_2$ complex is shown in Figure 4.15. $[Os(tpy)(tpy\text{-}ph\text{-}Br)][PF_6]_2$ complex shows in the UV region, two bands at 280 nm and 320 nm; which have been attributed to the ligand based transitions, $\pi_L - \pi_L^*$. A weak band at 488 nm, has been assigned as the metal-to-ligand charge transfer band (MLCT). This absorption maximum of the spin-allowed MLCT band observed for $[Os(tpy)(tpy\text{-}ph\text{-}Br)][PF_6]_2$ is blue shifted compared to the analogous ruthenium complex $[Ru(tpy)(tpy\text{-}ph\text{-}Br)][PF_6]_2$ the wavelengths values are 498 nm for $[Ru(tpy)(tpy\text{-}ph\text{-}Br)][PF_6]_2$ and $\lambda = 488$ nm for $[Os(tpy)_2]^{2+}$.

The absorption spectrum of $[Os(py\text{-}tpy)(tpy\text{-}ph\text{-}Br)][PF_6]_2$ complex is shown in Figure 4.16. The lowest energy absorption band observed in the visible region at 498 nm, is assigned to the d-π metal – to – ligand charge transfer (MLCT) transitions. In the UV region, two intense bands at 298 nm and 322 nm, can be assigned to the ligand centred $\pi - \pi^*$ transitions. A comparison with the absorption spectrum of $[Os(tpy)(tpy\text{-}ph\text{-}Br)][PF_6]_2$ complex (see Figure 4.16), shows that by changing a terpyridine group with a (py-tpy) ligand, the λ_{max} of the MLCT transition, shifts to lower energy, but the difference between the two values of λ is quite small: 488 nm for $[Os(tpy)(tpy\text{-}ph\text{-}Br)][PF_6]_2$ and 498 nm for $[Os(py\text{-}tpy)(tpy\text{-}ph\text{-}Br)][PF_6]_2$.

The absorption spectrum of $[Os(tpy)(L3)(H_2O)]$ complex is shown in Figure 4.17. As obtained for $[Ru(tpy\text{-}ph\text{-}Br)(L3)(H_2O)]$, tetrazole ligand contains a central pyridine ring that is a good π - acceptor and two tetrazolate moieties that are strong σ donators, but in coordination compounds, the deprotonated $(L3)^{2-}$ ligand is a better σ donor and a poorer π acceptor then terpyridine. This causes a

shift of the MLCT transition to higher energy. The MLCT band for the $[Os(tpy)(tpy\text{-}ph\text{-}Br)][PF_6]_2$ complex appeared at 488 nm (see Figure 4.15), whereas of the replacement of the terpyridine with $(L3)^{2-}$ ligand, shows the same transition, at 478 nm. An intense absorption band at higher energy, 295 nm, is assigned at $\pi - \pi^*$ transitions associated with the aromatic rings of the tetrazole ligand. A weak shoulder band at 320 nm and a band at 380 nm may be assigned to intra ligand $\pi - \pi^*$ transition.

The absorption spectrum of $[Os(tpy)[2,6\text{-}(2,3\text{-}ph\text{-}4\text{-}CH_3\text{-}pyrazol)py][PF_6]_2$ complex is shown in Figure 4.18. The absorption spectrum of the $[Os(tpy)[2,6\text{-}(2,3\text{-}ph\text{-}4\text{-}CH_3\text{-}pyrazol)py][PF_6]_2$ complex shows the metal to ligand charge transfer band (MLCT), at 490 nm, in the visible region; this is a relatively weak band, whereas in the corresponding ruthenium complex, $[Ru(tpy)[2,6\text{-}(2,3\text{-}ph\text{-}4\text{-}CH_3\text{-}pyrazol)py][PF_6]_2$ the MLCT transition showed an intense band at 486 nm (see Figure 4.6). The intense band at 325 nm may be assigned to $\pi - \pi^*$ transitions associated with the terpyridyl rings and to the central pyridine of the ligand. The complex exhibits also an intense shoulder at 352 nm, this may be assigned to the $\pi - \pi^*$ transition. By changing a terpyridine group with the tridentate ligand [2,6-(2,3 phenyl-4-methyl pyrazol) pyridine], significant differences are observed in the visible region for the metal-to-ligand charge-transfer. The band for $[Os(tpy)_2]^{2+}$ appeared at 477 nm whereas 490 nm is the value observed for the complex $[Os(tpy)[2,6\text{-}(2,3\text{-}ph\text{-}4\text{-}CH_3\text{-}pyrazol)py][PF_6]_2$. Same behaviour difference has been observed for ruthenium complexes, where the difference in the λ for $[Ru(tpy)_2]^{2+}$ and $[Ru\ (tpy)[2,6\text{-}(2,3\text{-}ph\text{-}4\text{-}CH_3\text{-}pyrazol)py][PF_6]_2$ was only 12 nm.

4.3.3 Emission spectroscopy: Os (II) bis terpyridine complex

In the last Section, the absorption spectra of the Os(II) terpy complexes have been discussed. It is generally accepted that while the lowest energy absorption is ^{1}MLCT in nature that the emission is originating from the ^{3}MLCT state.

In this Section, these emitting properties of the ruthenium terpyridine based complexes will be cleared. The emisson spectrum for the prototype $[Os(tpy)_2][PF_6]_2$ in EtOH/MeOH (4/1) at 77 K, is shown in Figure 4.19.

In going from $[Ru(tpy)_2]^{2+}$ to $[Os(tpy)_2]^{2+}$, some differences may be noticed. $[Ru(tpy)_2]^{2+}$ does not emit at room temperature, $[Os(tpy)_2]^{2+}$ exhibits an intense luminescence at this temperature, with λ_{max} = 712 nm. At 77 K, the luminescence band of $[Os(tpy)_2]^{2+}$ is considerably red shifted compared to the spectrum of $[Ru(tpy)_2]^{2+}$ complex, with a maximum at 689 nm (see Figure 4.19). This indicates that in the osmium complex the short-lived ^{3}MC levels cannot be populated at room temperature. In $[Os(tpy)_2]^{2+}$ in fact, the ^{3}MLCT / ^{3}MC energy gap is much higher than in the analogous ruthenium complex.

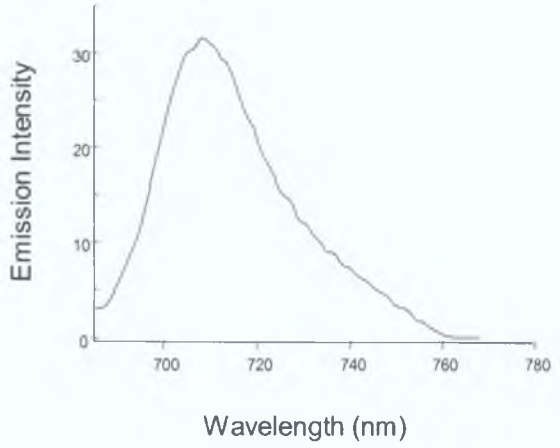

Figure 4.19: Emission spectrum of $[Os(tpy)_2]^{2+}$ in acetonitrile at room temperature

Electronic absorption and emission data of all the osmium complexes investigated are summarised in Table 4.2.

Complex	Absorption	*Emission (298K)*	
	λ, nm	λ, nm	τ^b,ns
$[Os(tpy)_2][PF_6]_2$	477, 657	712	$<40^{(c)}$
$[Os(py\text{-}tpy)_2][PF_6]_2$	502	748	162
$[Os(tpy)(tpy\text{-}ph\text{-}Br)]\ [PF_6]_2$	488	714	144
$[Os(py\text{-}tpy)(tpy\text{-}ph\text{-}Br)][PF_6]_2$	498	746	-
$[Os(tpy)(L3)(H_2O)]$	478	717	64
$[Os(tpy)[2,6\text{-}(2,3\text{-}ph\text{-}4\text{-}CH_3\text{-}$ pyrazol)py$][PF_6]_2$	490	718	55

Table 4.2: Absorption and luminescence data for osmium terpyridine complexes in acetonitrile; (b): Luminescence emission lifetime in deaerated acetonitrile, (c): Luminescence emission lifetime in air saturated acetonitrile

4.3.4 Emission spectra of Os(II) terpyridine complexes

The emission spectra for osmium terpyridine based complexes are discussed in this Section. All the spectra show in Figure 4.20 – Figure 4.24 are recorded at room temperature.

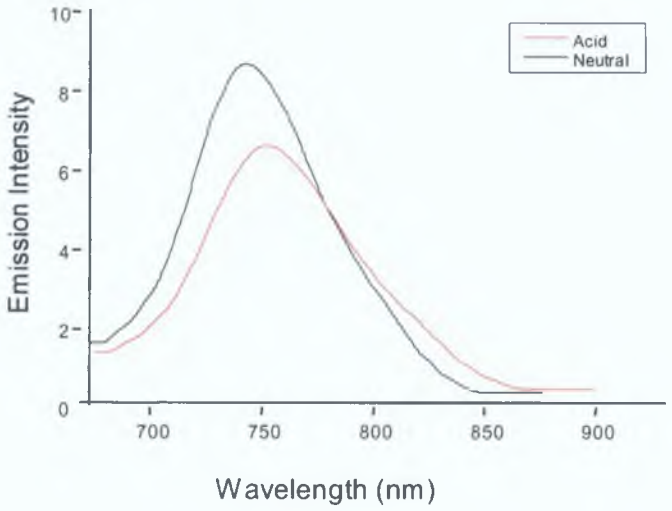

Figure 4.20: Emission spectrum of $[Os(py\text{-}tpy)_2[PF_6]_2$ in neutral and acid solution of acetonitrile at room temperature

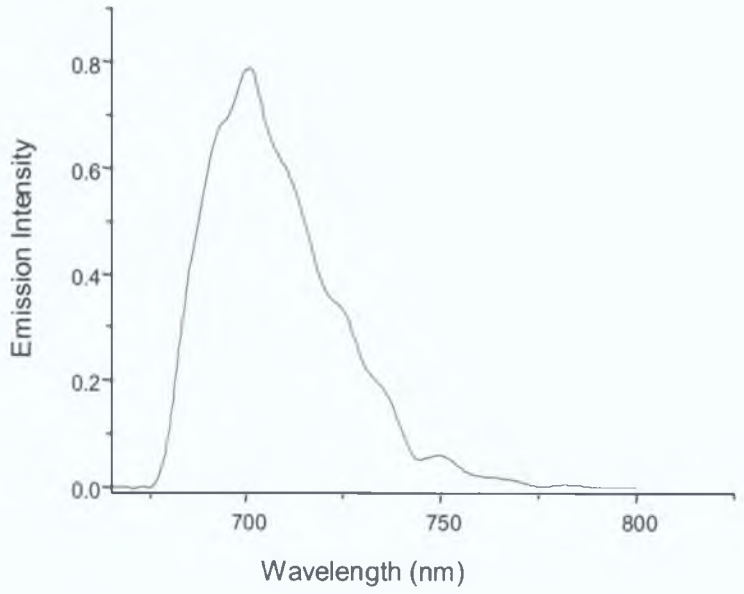

Figure 4.21: Emission spectrum of [Os(tpy)(tpy-ph-Br)][PF_6]$_2$ in acetonitrile at room temperature

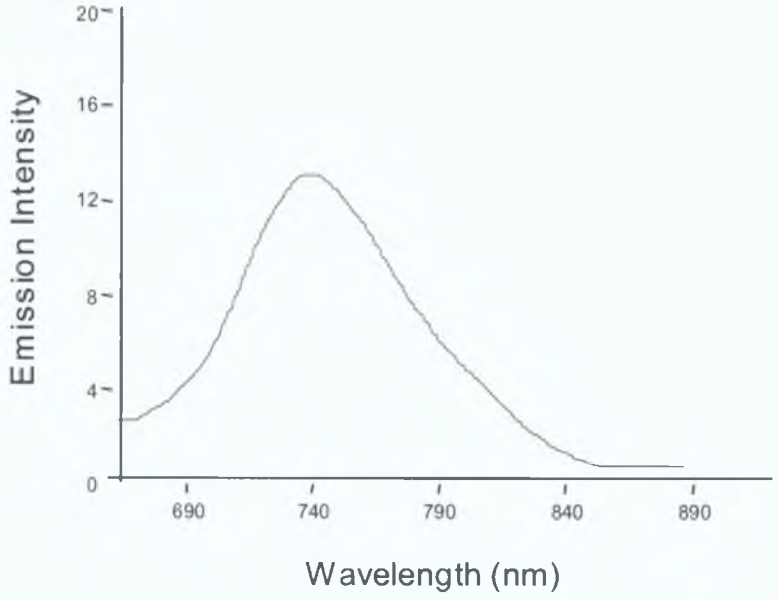

Figure 4.22: Emission spectrum of [Os(py-tpy)(tpy-ph-Br)][PF_6]$_2$ in acetonitrile at room temperature

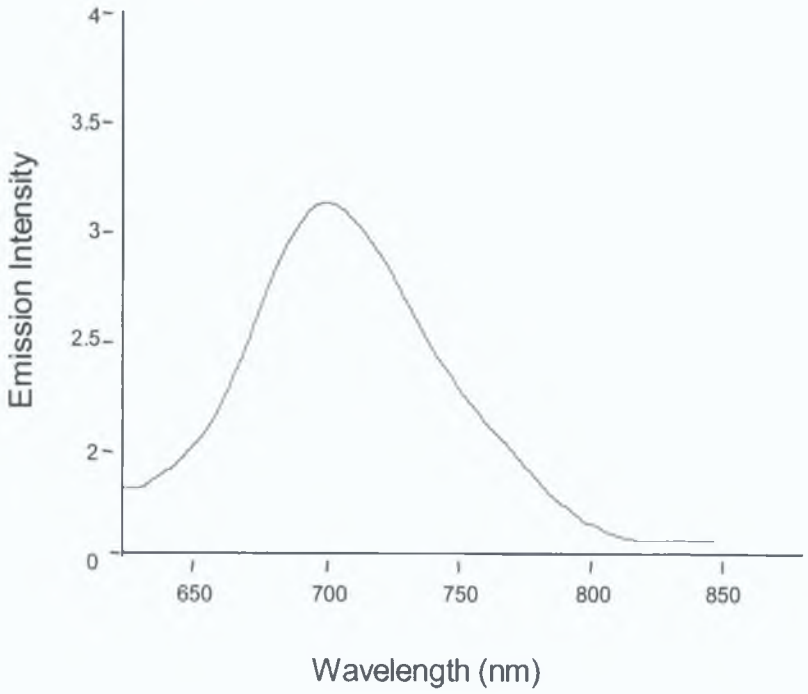

Figure 4.23: Emission spectrum of [Os(tpy)(L3)(H_2O)], in acetonitrile at room temperature

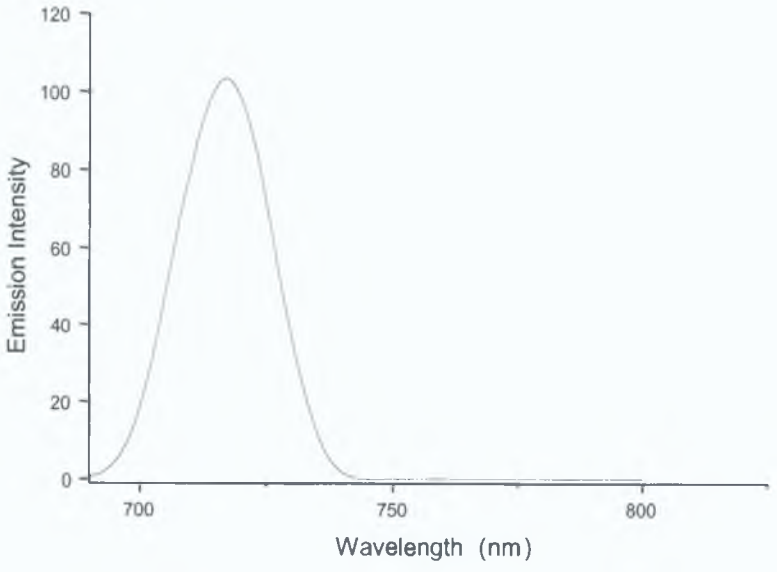

Figure 4.24: Emission spectrum of [Os(tpy)[2,6-(2,3-ph-4-CH_3-pyrazol)py)][PF_6]$_2$, in acetonitrile at room temperature

Figure 4.20 shows the room temperature emission spectrum of $[Os(py\text{-}tpy)_2][PF_6]_2$ complex in neutral and acidic acetonitrile solution. The emission spectrum for the neutral complex $[Os(py\text{-}tpy)_2][PF_6]_2$ shows a band at 748 nm. Two (py-tpy) ligands may be protonated by acid, resulting in it being observed in the emission spectrum. After addition of trifluoracetic acid (1 drop), the emission of the complex shifted to lower energy and increased in intensity; a red shift at 751 nm for the protonated species.

Figure 4.21 shows the emission spectrum of $[Os(tpy)(tpy\text{-}ph\text{-}Br)][PF_6]_2$ in acetonitrile. As observed for the equivalent ruthenium compound $[Ru(tpy)(tpy\text{-}ph\text{-}Br)][PF_6]_2$ (see Figure 4.9), the osmium complex $[Os(tpy)(tpy\text{-}ph\text{-}Br)][PF_6]_2$, shows an intense band characteristic of a MLCT transitionat 714 nm. The substitution of a terpyridine with a 4'-phenyl - terpyridine ligand exhibits a more efficient luminescence that may be observed by comparing the emission of $[Os(tpy)_2]^{2+}$, λ = 712 nm (see Figure 4.19) with the emission of $[Os(tpy)(tpy\text{-}ph\text{-}Br)][PF_6]_2$, with λ = 7.14 nm. Finally the presence of the bromide atom in position 4' of the phenyl group does not show a considerable effect on the fluorescence wavelength as already observed for the ruthenium complex.

In Figure 4.22 the emission spectrum of $[Os(py\text{-}tpy)(tpy\text{-}ph\text{-}Br)][PF_6]_2$ in acetonitrile at room temperature is shown. $[Os(py\text{-}tpy)(tpy\text{-}ph\text{-}Br)][PF_6]_2$ shows a strong luminescence band characteristic of a MLCT transition at 746 nm. On passing from $[Os(tpy)(tpy\text{-}ph\text{-}Br)][PF_6]_2$ to $[Os(py\text{-}tpy)(tpy\text{-}ph\text{-}Br)][PF_6]_2$ complex, λ_{max} is red shift from 714 nm to 746 nm.

Figure 4.23 shows the emission spectrum of $[Os(tpy)(L3)(H_2O)]$ in acetonitrile at room temperature. $[Os(tpy)(L3)(H_2O)]$, shows emission at room temperature, with a λ = 717 nm (see Figure 4.23). In coordination compounds, (H_2L3) ligand is a better σ donor and a poorer π acceptor than terpyridine; the emission spectrum show a red shift of the metal to ligand charge transfer band, with respect to the analogous (tpy) complex, with λ = 712 nm. As shown in Table 4.2, the luminescence emission lifetime of the complex $[Os(tpy)(L3)(H_2O)]$, is 64 ns, whereas the ^{3}MLCT state of $[Os(tpy)(tpy\text{-}ph\text{-}Br)][PF_6]_2$ and $[Os(py\text{-}tpy)_2][PF_6]_2$ complexes are long lived, 144 ns and 162 ns respectively.

The introduction of the ligand $(L3)^{2-}$ to the osmium metal centre causes an increase in the lifetime of the ^{3}MLCT excited state compared to the prototype bis-terpyridine. Opposite behaviour is observed for the corresponding ruthenium complexes. In comparison with $[Os(py\text{-}tpy)_2][PF_6]_2$, the complex $[Os(tpy)(L3)(H_2O)]$, shows a decrease in the energy of the ^{3}MLCT state with emission maxima red shifted. The short lifetime of the excited state is due to the small gap between the emitting state and the upper lying ^{3}MC state.

$[Os(tpy)[2,6\text{-}(2,3\text{-ph-}4\text{-}CH_3\text{-pyrazol})py][PF_6]_2$ emits at room temperature (see Figure 4.24), whereas the corresponding ruthenium compound did not show any emission at room temperature (see Figure 4.12). The emission spectrum of $[Os(tpy)[2,6\text{-}(2,3\text{-ph-}4\text{-}CH_3\text{-pyrazol})py][PF_6]_2$, shows a band at 718 nm related to emission from the ^{3}MLCT transition with a lifetime of 55 ns. By comparing $[Os(tpy)_2][PF_6]_2$ and $[Os(tpy)[2,6\text{-}(2,3\text{-ph-}4\text{-}CH_3\text{-pyrazol})py][PF_6]_2$, it is observed that the ^{3}MLCT state for $[Os(tpy)[2,6\text{-}(2,3\text{-ph-}4\text{-}CH_3\text{-pyrazol})py][PF_6]_2$, moves to higher energy. This effect is shown with a red shifted emission: λ = 712 nm for $[Os(tpy)_2][PF_6]_2$ and λ = 718 nm for $[Os(tpy)[2,6\text{-}(2,3\text{-ph-}4\text{-}CH_3\text{-pyrazol})py][PF_6]_2$.

4.4. Electrochemical investigation of metal (II) terpyridine complexes

Polypyridyl Ru(II) and Os(II) complexes exhibit in general one metal-based oxidation at positive potentials corresponding to the M(II/III) couple. In the negative potential region, the redox processes observed are sequential ligand-based reduction. The redox potentials of all the ruthenium and osmium complexes synthesised in this thesis have been determined by cyclic voltammetry in acetonitrile solution with $TBABF_4$ (0.1 M) as supporting electrolyte, vs ferrocene-ferrocenium. The oxidation and reduction potentials of the complexes are given in Table 4.3.

4.4.1 Ruthenium (II) and Osmium (II) bis terpyridine complexes

The cyclic voltammogram as shown in Figure 4.25 for the oxidation of $[Ru(tpy)_2]^{2+}$ exhibits a reversible, one-electron redox process at +1.23 V, corresponding to the Ru(II/III) couple.

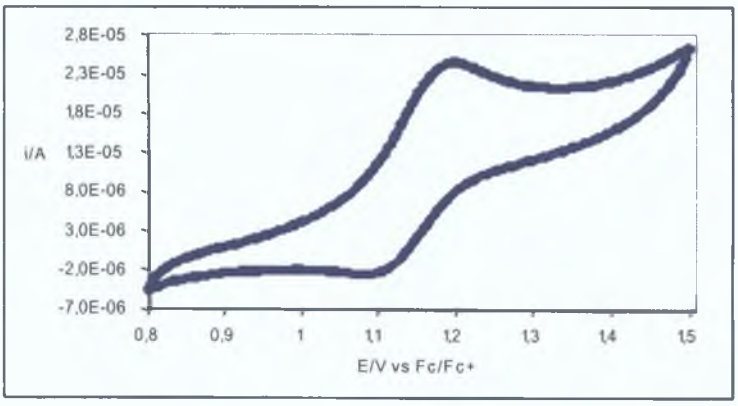

Figure 4.25: Cyclic voltammogram of $[Ru(tpy)_2]^{2+}$, at a Pt-disk electrode in 0.1 M $TBABF_4$/acetonitrile solution

As observed for the ruthenium complex, $[Os(tpy)_2]^{2+}$ (see Figure 4.26) exhibits the same redox process for the Os(II/III) couple at + 0.73 V, but at more positive potential as expected due to the more covalent character of Os(II). The same behaviour is observed for all other osmium complexes.

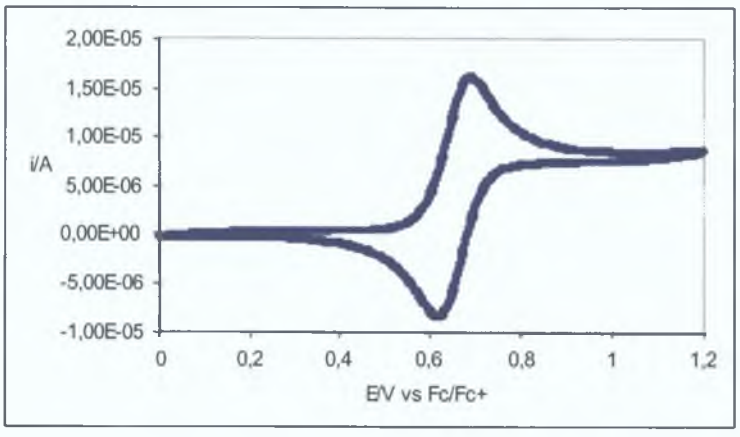

Fig. 4.26: Cyclic voltammogram oxidation of $[Os(tpy)_2]^{2+}$, at a Pt-disk electrode in 0.1 M $TBABF_4$/acetonitrile solution

The electrochemistry of $[Ru(tpy)_2]^{2+}$, at negative potentials, is characterised by the appearance of two reduction peaks which are assigned to reduction of the terpyridine ligands, at - 1.25 V and at - 1.51 V (see figure 4.27).

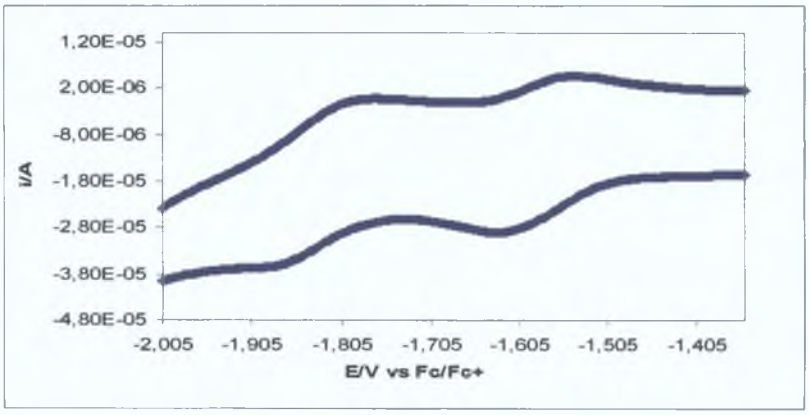

Figure 4.27: Cyclic voltammogram reduction of $[Ru(tpy)_2]^{2+}$, at a Pt-disk electrode in 0.1 M $TBABF_4$/acetonitrile solution

Figure 4.28 shows the cyclic voltammogram reduction in the negative potential region for $[Os(tpy)_2]^{2+}$. The sequential ligand-based reduction is characterised by the appearance of two reversible peaks at - 1.47 V and - 1.76 V due to the terpyridine ligands. When comparing ruthenium and osmium bis terpyridine it has clear that the terpyridine ligands are reduced at similar potentials, slightly more negative in the osmium complex.

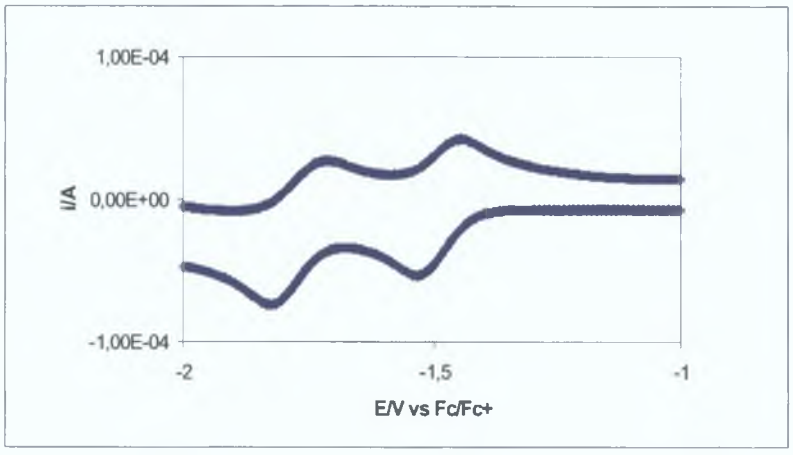

Figure 4.28: Cyclic voltammogram reduction of $[Os(tpy)_2]^{2+}$, at a Pt-disk electrode in 0.1 M $TBABF_4$/acetonitrile solution

The cyclic voltammetric data for all ruthenium and osmium complexes investigated in this thesis are presented in Table 4.3.

complex	E° (V vs Ag/Ag^+)*		
$[Ru(tpy)_2][PF_6]_2$	+1.23	-1.25	-1.51
$[Ru(py\text{-}tpy)_2][PF_6]_2$	+1.07	-1.44	-1.68
$[Ru(tpy)(tpy\text{-}ph\text{-}Br)][PF_6]_2$	+1.06	-1.44	-1.69
$[Ru(py\text{-}tpy)(tpy\text{-}ph\text{-}Br)][PF_6]_2$	+1.04	-1.52	-1.80
$[Ru(tpy\text{-}ph\text{-}Br)(L3)(H_2O)]$	+1.02	-1.21	
[Ru(tpy)[2,6-(2,3-ph-4-CH_3-pyrazol)py][PF_6]$_2$	+1.03	-1.57	-1.79
$[Os(tpy)_2][PF_6]_2$	+0.73	-1.47	-1.76
$[Os(py\text{-}tpy)_2][PF_6]_2$	+0.67	-1.43	-1.70
$[Os(tpy)(tpy\text{-}ph\text{-}Br)][PF_6]_2$	+0.65	-1.44	-1.75
$[Os(py\text{-}tpy)(tpy\text{-}ph\text{-}Br)][PF_6]_2$	+0.63	-1.53	-1.87
$[Os(tpy)(L3)(H_2O)]$	+0.40	-1.33	-1.75
[Os(tpy)[2,6-(2,3-ph-4-CH_3-pyrazol)py][PF_6]$_2$	+0.48	-1.65	

Table 4.3: Formal potentials for ruthenium and osmium terpyridine complexes at a platinum electrode in a 0.1M acetonitrile solution of $TBABF_4$. (*) = calibrated versus Ferrocene/Ferrocenium.

Examples of cyclic voltammograms of ruthenium and osmium complexes investigated are reported in Figures 4.29 - 4.32.

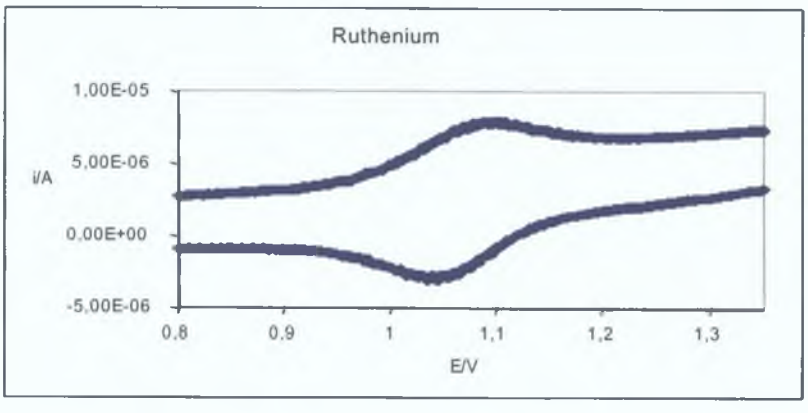

Figure 4.29: Cyclic voltammogram oxidation of $[Ru(py\text{-}tpy)(tpy\text{-}ph\text{-}Br)]^{2+}$, at a Pt-disk electrode in 0.1 M $TBABF_4$/acetonitrile solution

The corresponding cyclic voltammogram at negative potentials, for the complex [Os(L3)(tpy)(H_2O)] is shown in Figure 4.30.

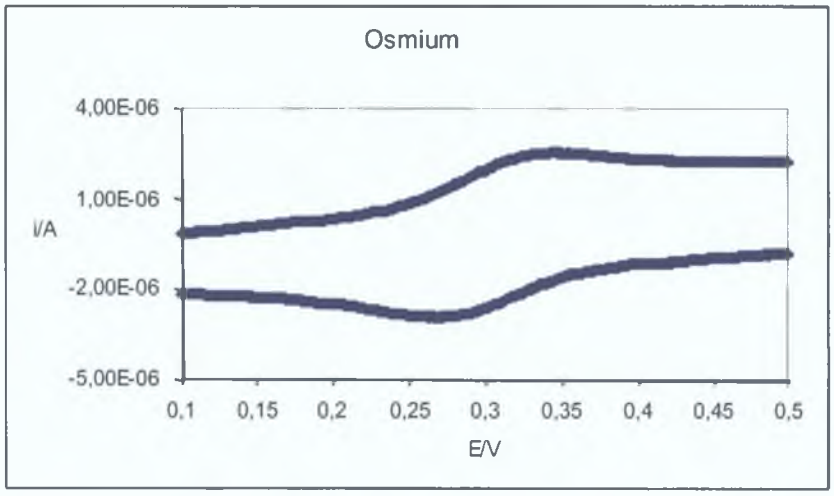

Figure 4.30: Cyclic voltammogram oxidation of [Os(tpy)(L3)(H_2O)] at a Pt-disk electrode in 0.1 M $TBABF_4$/acetonitrile solution

Figure 4.31 shows an example of the sequential ligand-based reduction for [Ru(py-tpy)(tpy-ph-Br)][PF_6]$_2$.

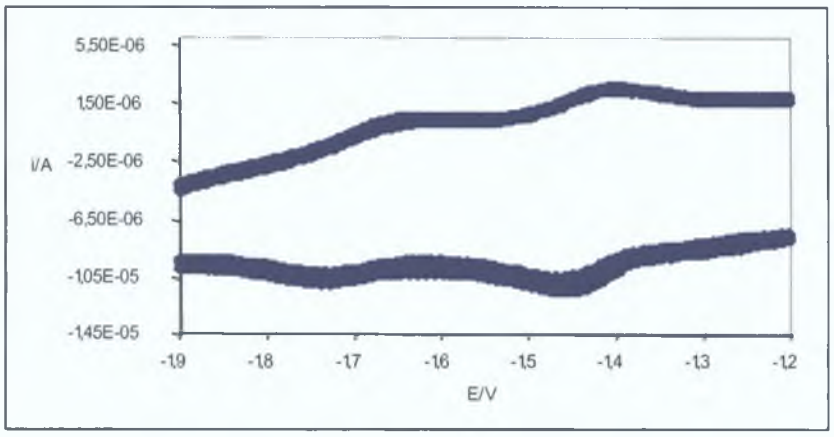

Figure 4.31: Cyclic voltammogram reduction of [Ru(py-tpy)(tpy-ph-Br)[PF_6]$_2$ at a Pt-disk electrode in 0.1 M $TBABF_4$/acetonitrile solution

Figure 4.32, shows the cyclic voltammogam of the osmium complex with (tpy-ph-Br) as ligand.

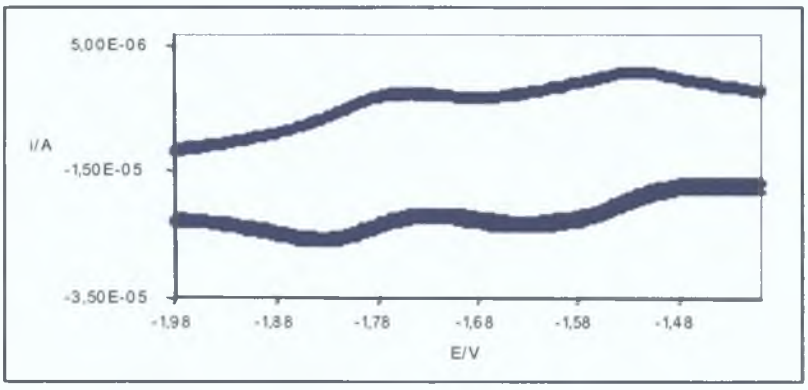

Figure 4.32: Cyclic voltammogram reduction of [Os(py-tpy)(tpy-ph-Br)[PF_6]$_2$ at a Pt-disk electrode in 0.1 M $TBABF_4$/acetonitrile solution

4.4.2 [Ru(py-tpy)$_2$][PF_6]$_2$ and [Os(py-tpy)$_2$][PF_6]$_2$ complexes

[Ru(py-tpy)$_2$][PF_6]$_2$ complex exhibits one metal-based oxidation at positive potential, +1.07 V, corresponding to the Ru(II/III) couple. In the negative potential region, two pyridine terpyridine ligands based reductions are observed show at – 1.47 V and at – 1.76 V.

The corresponding osmium complex, [Os(py-tpy)$_2$][PF_6]$_2$ shows a reversible, one electron oxidation at + 0.67 V corresponding to the Os(II/III) couple. As expected, the oxidation of the osmium complex is observed at less positive value than the corresponding oxidation for the analogous ruthenium compound; Os(II) complexes are easier to oxidise than Ru(II). [Os(py-tpy)$_2$][PF_6]$_2$ shows two one electron ligand based reductions at –1.43 V and – 1.70 V, both of which values are relatively close to those obtained for the analogous ruthenium complex. These potentials are insensitive to the nature of the metal which confirms they are ligand based. Furthermore, the difference in potentials between [Os(py-tpy)$_2$][PF_6]$_2$ and the analogous ruthenium complex is typical of these metals complexes which have the same coordination.

4.4.3 Redox process of mixed ligand complexes

[Ru(tpy)(tpy-ph-Br)][PF_6]$_2$ and [Os(tpy)(tpy-ph-Br)][PF_6]$_2$ complexes

[Ru(tpy)(tpy-ph-Br)][PF_6]$_2$ complex exhibits one metal-based oxidation at +1.06 V corresponding to the Ru(II/III) couple. In the negative potential region, the two terpyridine ligands show one reduction in acetonitrile solution at – 1.44 V and one at – 1.69 V. The two sequential ligand-based reductions are shifted to less negative potentials compared with the $[Ru(tpy)_2]^{2+}$. The analogous osmium complex, [Os(tpy)(tpy-ph-Br)][PF_6]$_2$, also has one reversible, one electron oxidation at + 0.65 V corresponding to the Os(II/III) couple.

[Os(tpy)(tpy-ph-Br)][PF_6]$_2$ shows two one reversible electron ligand based reductions at –1.43 V and – 1.70 V, values quite close to those obtained for the analogous ruthenium complex. The first reduction at –1.43 V has been assigned to the terpyridine ligand whereby comparing the potential of [Os(tpy)(tpy-ph-Br)][PF_6]$_2$ and the potentials of the [Os(py-tpy)(tpy-ph-Br)][PF_6]$_2$ it was possible to assigne the second reduction at –1.75 V to the (tpy-ph-Br) ligand.

[Ru(py-tpy)(tpy-ph-Br)][PF_6]$_2$ and [Os(py-tpy)(tpy-ph-Br)][PF_6]$_2$ complexes

The cyclic voltammogram of [Ru(py-tpy)(tpy-ph-Br)][PF_6]$_2$ in acetonitrile solution exhibits a reversible, one-electron oxidation at + 1.04 V, corresponding to a Ru(II/III) couple (see Figure 4.31). By introducing (tpy-ph-Br) instead of a (py-tpy) ligand, only a slight difference has been observed on the oxidation values (0.03 V). Two reversible reductions at negative potentials are observed for [Ru(py-tpy)(tpy-ph-Br)][PF_6]$_2$, at - 1.52 V and - 1.80 V and are assigned to the two ligands reductions. By comparing these results with those of the [Ru(py-tpy)$_2$][PF_6]$_2$, it is possible assigned the reduction at 1.52 V to the (py-tpy) ligand and the second reduction at 1.80 V to the (tpy-ph-Br).

For [Os(py-tpy)(tpy-ph-Br)][PF_6]$_2$ at + 0.63 V the Os(II/III) couple is observed. This potential oxidation and the potential observed for the [Os(py-

$tpy)_2][PF_6]_2$ (0.67 V), are very similar. The first reduction potential for [Os(py-tpy)(tpy-ph-Br)][PF_6]$_2$, is observed at – 1.53 V and has been assigned to the (py-tpy) ligand after comparison with the $[Os(py\text{-}tpy)_2][PF_6]_2$ complex, that shows similar reduction potential at –1.43 V. The second reduction of [Os(py-tpy)(tpy-ph-Br)][PF_6]$_2$, at – 1.87 V has been ascribed to the (tpy-ph-Br) ligand.

[Ru(tpy-ph-Br)(L3)(H_2O)] and [Os(tpy)(L_3)(H_2O)] complexes

For [Ru(tpy-ph-Br)(L3)(H_2O)] the Ru(II/III) couple is observed at + 1.02 V. In the negative potential region, one reduction potential is observed at – 1.21 V. The similar osmium complex, [Os(tpy)(L3)(H_2O)] also shows one reversible, one electron oxidation at + 0.40 V corresponding to the Os(II/III) couple.

[Os(tpy)(L3)(H_2O)] shows two one electron ligand based reduction at – 1.33 V, value relatively close to that obtained for the analogous ruthenium complex. By changing a terpyridine group with the tetrazole ligand, a slight differences in the reduction potentials have been observed, whereas the oxidation for [Os(tpy)(L3)(H_2O)] is significantly less positive than the corresponding $[Os(tpy)_2][PF_6]_2$ (by 330mV).

[Ru(tpy)[2,6-(2,3-ph-4-CH_3-pyrazol)py][PF_6]$_2$ and [Os(tpy)[2,6-(2,3-ph-4-CH_3-pyrazol)py][PF_6]$_2$ complexes

The cyclic voltammogram of [Ru(tpy)[2,6-(2,3-ph-4-CH_3-pyrazol)py][PF_6]$_2$ exhibits a reversible oxidation at + 1.03 V, corresponding to a Ru(II/III) couple. By introducing ligand [2,6-(2,3 phenyl-4-methyl pyrazol) pyridine] instead of a tpy ligand, less positive oxidation potential has been observed: + 1.03 V for [Ru(tpy)[2,6-(2,3-ph-4-CH_3-pyrazol)py][PF_6]$_2$ and +1.23 V for $[Ru(tpy)_2]^{2+}$. Two reversible reductions at negative potentials are observed for the complex [Ru(tpy)[2,6-(2,3-ph-4-CH_3-pyrazol)py][PF_6]$_2$ at - 1.57 V and - 1.79 V and are assigned to the two ligands reductions. In particular, by comparing these results with those of the $[Ru(tpy)_2][PF_6]_2$ complex, it is possible to assign the reduction at -1.57 V to the (tpy) ligand and the second reduction at -1.79 V to the ligand [2,6-(2,3 phenyl-4-methyl pyrazol) pyridine].

The analogous osmium complex, [Os(tpy)[2,6-(2,3-ph-4-CH_3-pyrazol)py][PF_6]$_2$ also shows one reversible, one redox process at + 0.48 V corresponding to the Os(II/III). The first reduction potential for [Os(tpy)[2,6-(2,3-ph-4-CH_3-pyrazol)py][PF_6]$_2$, is observed at – 1.65 V whereas the second reductive process expected is poorly resolved. The oxidation of the osmium complex is observed to a less positive value than the corresponding oxidation for the analogues ruthenium species: + 0.40 V and +1.08 V respectively.

4.5 Comparison between the spectroscopic and electrochemical properties

It has been noted that a correlation exists between the electrochemical measure of the HOMO-LUMO energy gap and the spectroscopic measure of the gap if both processes involve the same orbitals[25-26]. A plot of $\Delta E_{1/2} = [(E_{1/2}(M^{II/III}) - (E_{1/2}(M^{II/I})]$ versus E^{abs} for this entire series of terpyridine complexes was generated. A linear correlation between spectroscopic and electrochemical data has been found for ruthenium and osmium complexes investigated in this thesis. Lever and Dodsworth have discussed in detail the factors that influence the fit of this type of data to a straight line[27]. The scatter observed result from a variation in the inner and outer sphere reorganizational energy trough this series of complexes or configuration interaction. This slope may change if a larger series of complexes is prepared with more widely varied energy of the absorption band. Lever and Dodsworth indicate in their paper that a non-unity value for the slope of this plot would indicate that the factor influencing the inequivalence of E_{op} and $\Delta E_{1/2}$ have a functional dependence upon the electrochemical potential:

$$E_{op} = \Delta E\,(redox) + Q + \Delta\,\Delta Gs + \Delta(sol) + \chi_o + \chi_i \qquad [1]$$

where Q = free energy of transfer of an electron from the reduced to the oxidised species in the gap phase; $\Delta\,\Delta Gs = 2\,\Delta\,Gs - \Delta Gs^{+} - \Delta\,Gs^{-}$; $\Delta(sol) = \Delta Gg^{*} - \Delta\,Gg$ χ_o = outer sphere reorganisation energy and χ_i = inner sphere reorganisational energy[27].

Table 4.4 shows the absorption spectrocsopic data and electrochemical potentials of a series of ruthenium tpy complexes. The spectroscopic values presented in Table 4.4 are the λ_{abs} for the lowest energy ^{1}MLCT band.

Complex	λ_{abs}, nm	E^0 (V vs SCI) [(b)]	ΔE^0, V
[Ru(tpy-ph-Br)(L3)(H_2O)]	485[a]	+1.02 -1.21	2.33
[Ru(tpy)(tpy-ph-Br)][PF_6]$_2$	490	+1.06 -1.44 -1.68	2.50
[Ru(tpy)[2,6-(2,3-ph-4-CH_3-pyrazol)py][PF_6]$_2$	486	+1.03 -1.57 -1.79	2.60
[Ru(py-tpy)(tpy-ph-Br)][PF_6]$_2$	495	+1.04 -1.52 -1.80	2.56
[Ru(py-tpy)$_2$][PF_6]$_2$	498	+1.07 -1.44 -1.68	3.12

Table 4.4: Absorption and electrochemical potentials data for ruthenium terpyridine complexes, recorded in acetonitrile solution; (a) = DMF solution; (b) = a platinum electrode in a 0.1M acetonitrile solution of $TBABF_4$.

The ε molar extinction coefficient has been calculated and described for all the ruthenium terpyridine complexes, in Appendix II.

Table 4.5 shows the absorption spectrocsopic data and electrochemical potentials of a series of osmium tpy complexes.

Complex	λ_{abs}, nm	E^0 (V vs Ag/Ag^+)* [(b)]	ΔE^0, V
[Os(tpy)(L3)(H_2O)]	478[a]	+0.40 -1.33 -1.75	1.73
[Os(tpy)(tpy-ph-Br)][PF_6]$_2$	488	+0.65 -1.44 -1.75	2.09
[Os(tpy)[2,6-(2,3-ph-4-CH_3-pyrazol)py][PF_6]$_2$	490	+0.48 -1.65	2.13
[Os(py-tpy)(tpy-ph-Br)][PF_6]$_2$	498	+0.63 -1.53 -1.87	2.16
[Os(py-tpy)$_2$][PF_6]$_2$	502	+0.73 -1.47 -1.76	2.49

Table 4.5: Absorption and electrochemical potentials data for ruthenium terpyridine complexes, recorded in acetonitrile solution; (a) = DMF solution; (b) = a platinum electrode in a 0.1M acetonitrile solution of $TBABF_4$.

A fit of the data shown in Table 4.4 and Table 4.5 resulted in a straight line as shown in Figure 4.33 for ruthenium complexes and Figure 4.34 for osmium complexes.

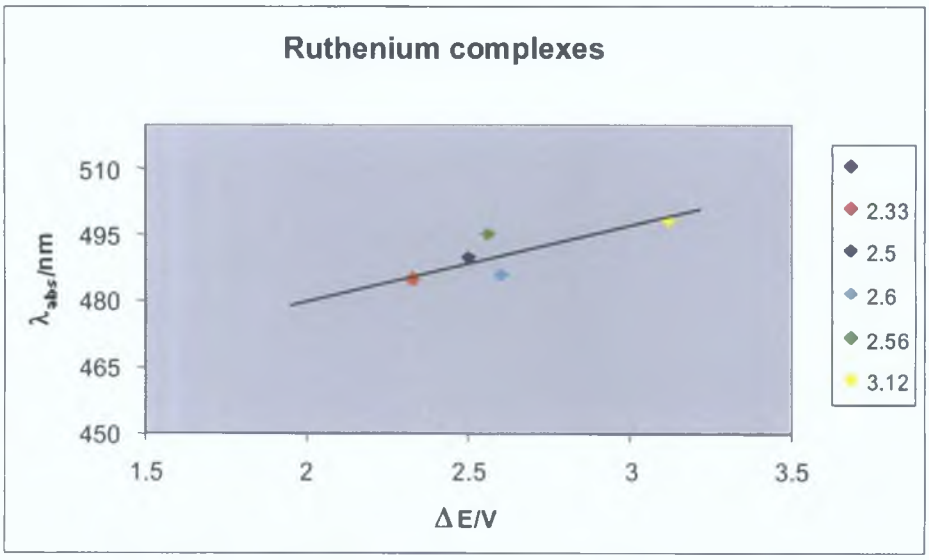

Figure 4.33: Plot of $\Delta E_{1/2}$ in V versus λ_{abs} in nm for M(dπ) ---> ligand (π) transition for ruthenium tpy complexes*

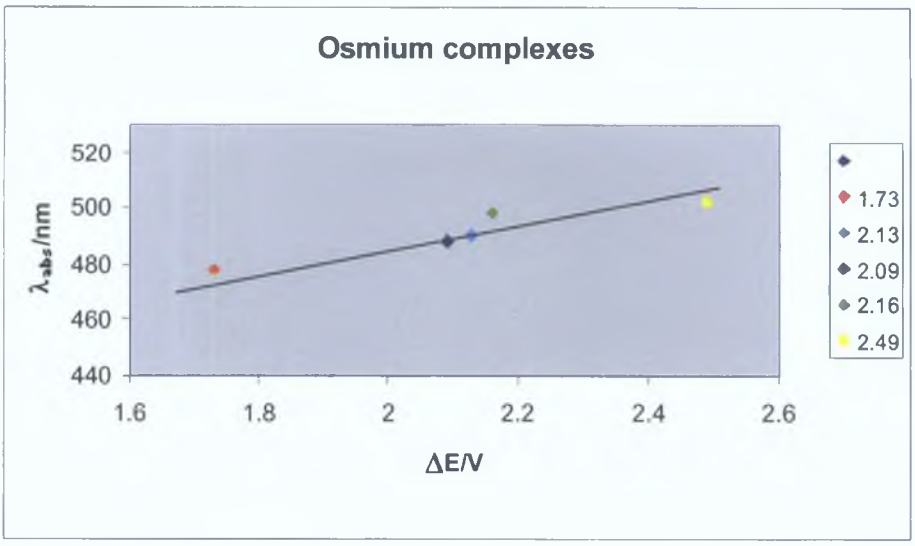

Figure 4.34: Plot of $\Delta E_{1/2}$ in V versus λ_{abs} in nm for M(dπ) ---> ligand (π) transition for osmium tpy complexes*

As already shown in Section 4.4, all these types of metal complexes are characterised by a metal - based oxidations. In particular, they possess a Ru (II / III) reversible oxidation. As expected, the $\Delta E_{1/2}$ of [Ru(tpy-ph-Br)(L3)(H_2O)], (where ligand L3 = 2,6-bis-([1,2,3,4]tetrazol-5-yl)pyridine), is lower than that of all the other ruthenium terpyridine complexes; which indicates that in coordination compounds, $(L3)^{2-}$ ligand is a stronger σ – donor and poor π – acceptor than terpyridine. Replacement of one terpyridine with $(L3)^{2-}$ ligand causes an increase in the electronic charge on the metal with a consequent red shift of the MLCT absorption (tpy based) (474 nm for the prototype and 485 nm for [Ru(tpy-ph-Br)(L3)(H_2O)]). By plotting $\Delta E_{1/2}$ versus λ_{abs}, complexes [Ru(tpy)(tpy-ph-Br)][PF_6]$_2$, [Ru(py-tpy)(tpy-ph-Br)][PF_6]$_2$ and [Ru(py-tpy)$_2$][PF_6]$_2$, show a linear correlation. For [Ru(tpy)(tpy-ph-Br)][PF_6]$_2$, $\Delta E_{1/2}$ is 2.50 V whereas 2.56 V and 3.12 are the values for [Ru(py-tpy)(tpy-ph-Br)][PF_6]$_2$ and [Ru(py-tpy)$_2$][PF_6]$_2$. In particular, by changing a terpyridine group with a (py-tpy) ligand, the absorbance wavelength increases and so does the $\Delta E_{1/2}$ potential. This red shift may be explained by an increase in conjugation due to the lowering of the π* orbital. Different behaviour has been observed for [Ru(tpy)[2,6-(2,3-ph-4-CH_3-pyrazol)py][PF_6]$_2$ which shows high energy and also high $\Delta E_{1/2}$., contradictory result compare with the other complexes. Some problems have been found during the electrochemical measurements of the complex, due especially to reductive processes poorly resolved. The anomalous behaviour of the complex has been attributed to this experimental factor.

Also Os(II) complexes all exhibit absorption bands in the visible region, assignable as *M(dπ) ---> ligand (π*)*. MLCT transitions. The assignment is verified by noting that absorption energy maxima increase linearly with $\Delta E_{1/2}$., as shown in Figure 4.34. The osmium and ruthenium complexes incorporating the same ligands have very similar spectroscopic characterisations despite very different electrochemical properties, for example, osmium metal oxidations that occur at much less positive potentials. This explain why the $\Delta E_{1/2}$ observed for

osmium complexes appeared in a range between 1.73 and 2.49 V, whereas for ruthenium complexes the values were more positive, between 2.33 and 3.12 V. As already observed for ruthenium complexes (Figure 4.33), [Os(tpy)(L3)(H_2O)], (L3 = 2,6-bis-([1,2,3,4]tetrazol-5-yl)pyridine), is the complex with the less positive $\Delta E_{1/2}$ (1.73 V). As expected, the ligand (L3), better σ – donor as terpyridine, increase the electronic charge on the metal centre; a consequent red shift of the MLCT was observed. By changing tetrazolate ligand with a terpyridine system, either wavelength absorption or $\Delta E_{1/2}$ increases. In particular, on passing from [Os(tpy)(tpy-ph-Br)][PF_6]$_2$, to [Os(tpy)[2,6-(2,3-ph-4-CH_3-pyrazol)py][PF_6]$_2$, [Os(py-tpy)(tpy-ph-Br)][PF_6]$_2$ and [Os(py-tpy)$_2$][PF_6]$_2$, it becomes easier to oxidise the metal centre. However small differences have been observed for the $\Delta E_{1/2}$ values of the three complexes: [Os(tpy)(tpy-ph-Br)][PF_6]$_2$, to [Os(tpy)[2,6-(2,3-ph-4-CH_3-pyrazol)py][PF_6]$_2$, [Os(py-tpy)(tpy-ph-Br)][PF_6]$_2$, 2.09 V, 2.13 V, 2.16 V respectively. Compared with the other complexes, [Os(py-tpy)$_2$][PF_6]$_2$, shows a more positive $\Delta E_{1/2}$ = 2.49 V, as already discussed for the analogous ruthenium complex (where $\Delta E_{1/2}$ = 3.12 V). This effect may be attributed to the presence of two py-tpy groups which reduce the electron density on the metal centre, with consequent red shift in the absorption band.

4.6 Conclusion

In this Chapter, characterisations by UV/Vis, emission spectroscopy and electrochemistry of all the ruthenium (II) and osmium (II) complexes investigated in this work are described. All the complexes show intense absorption bands in the visible part of the spectrum.

For ruthenium complexes the MLCT bands have been observed between 474 nm and 498 nm. Complex [Ru(tpy-ph-Br)(L3)(H_2O)] shows the most intense red shift at 485 nm, whereas [Ru(py-tpy)$_2$][PF_6]$_2$ is blue shifted to lower energy (498 nm).

For osmium complexes the MLCT bands appear in a range between 478 and 502 nm. As already observed for the ruthenium complexes, the band at higher energy is assigned to the complex with a tetrazole as substituent,

[Os(tpy)(L3)(H_2O)], because the tatrazolate ligand donates electron density to the metal centre, thus lowering the gap between the HOMO and LUMO causing a red shift in the absorption spectrum.

For the ruthenium complex $[Ru(py\text{-}tpy)_2]^{2+}$, the λ = 498 nm and for the analogous osmium compound λ = 502 nm. With the (tpy-ph br) ligand, the terpyridine complexes show a blue shift in the MLCT band, as clearly observed by comparing λ of $[Ru(tpy)_2]^{2+}$, 474 nm and λ of the complexes [Ru(py-tpy)(tpy-ph-Br)][PF_6]$_2$ and [Ru(tpy)(tpy-ph-Br)] [PF_6]$_2$ respectively 495 nm and 490 nm. Similar behaviour is observed for the osmium complexes: λ = 498 nm for [Os(py-tpy)(tpy-ph-Br)][PF_6]$_2$ and λ = 488 nm for [Os(tpy)(tpy-ph-Br)][PF_6]$_2$. This behaviour may be explained considering the electronic nature of the ligands.

Ligands may be grouped into one of two classes: σ-donors or π-acceptors. σ-donors increase electron density on the metal centre whereas π-acceptors reduce the electron density. As shown before, tetrazolate ligand is a good σ-donor and gives electron density to the metal centre (consequence red shift in the MLCT band) and vice versa, ligands such as (tpy-ph-Br) and (py-tpy) increase the electron withdrawing nature of the ligand and reduce the electron density on the metal. The λ emission of the ruthenium complexes are presented in Table 4.1, whereas the data for osmium complexes investigated are described in Table 4.2. The emission spectra for the osmium complexes have been recorded in acetonitrile at room temperature whereas the spectra of ruthenium complexes, weak emitters at room temperature, have been measured in rigid matrix in a mixture EtOH / MeOH (4/1) at 77 K. As described in Table 4.2, all the ruthenium complexes investigated are practically non - emitters at room temperature except for two complexes [Ru(tpy)(tpy-ph-Br)][PF_6]$_2$ and [Ru(tpy-ph-Br)(L3)(H_2O)] that showed a quite weak emission with λ_{max} = 631 nm and 630 nm respectively. On decreasing the temperature at 77 K, in rigid matrix (EtOH/MeOH mixture 4/1), all the complexes show an intense emission. In particular, the wavelengths are obtained are in the range between 602 nm and 670 nm. As observed for the absorption, [Ru(py-tpy)(tpy-ph-Br)][PF_6]$_2$, [Ru(py-tpy)$_2$][PF_6]$_2$ and [Ru(tpy)(tpy-ph-Br)] [PF_6]$_2$ show a similar behaviour with respect to the prototype $[Ru(tpy)_2]^{2+}$. The substituent effect of these ligands on the energy of the emission bands, results

in a red shift of the λ_{max}, from 618 nm for $[Ru(tpy)_2]^{2+}$ to 636 nm for [Ru(py-tpy)(tpy-ph-Br)][PF_6]$_2$, 670 nm for [Ru(tpy-ph-Br)(L3)(H_2O)] and 626 nm for [Ru(tpy)(tpy-ph-Br)][PF_6]. Electron-withdrawing substituents increase the luminescence intensity of the complexes.

Osmium (II) compounds show a different behaviour than ruthenium complexes. Osmium compounds are strongly luminescence at room temperature in fluid solution. This may be explained by the fact that the ligand-field strength is expected to increase on passing from metal ions in the first transition series to metals in the second and third transition series respectively. The nature of the metal centre is thus directly related to the separation of the MLCT and the d-d states. The emission maxima at room temperature, for the osmium complexes have been observed between 703 nm and 748 nm. As observed for the ruthenium compounds, [Os(py-tpy)$_2$][PF_6]$_2$ and [Os(py-tpy)(tpy-ph-Br)][PF_6]$_2$ complexes show a blue shift to 746 nm and 748 nm whereas the corresponding $[Os(tpy)_2]^{2+}$ appears at 712 nm. As expected, the complex containing tetrazolate substituent [Os(tpy)(L3)(H_2O)], show an intense red shifted emission to 698 nm.

As already mentioned in Section 4.1, rational strategies have been devised to increase the excited state lifetime of metal-tpy type complexes. Since one of the main origins of the short lifetime of the ^{3}MLCT excited state is the small energy gap between the emitting state and the upper lying 3MC state, increasing this energy gap is expected to be beneficial. In bis-tpy complexes, substitution of the 4' positions of the ligands has been used for this purpose. Investigations carried out on [Ru(X-tpy)(Y-tpy)] complexes[17][19] (where X and Y are substituents in the 4' position of the 2,2' 6',2" - terpyridine) have shown that electron- donating (D) or electron-accepting (A) substituents may cause changes in the luminescence and electrochemical properties. Electrochemical studies indicate:

- The electron accepting groups stabilise the LUMO π^* ligand orbitals more than the HOMO $\pi(t_{2g})$ metal orbitals.
- The electron-donor groups destabilise the HOMO $\pi(t_{2g})$ metal orbitals more than the LUMO π^* ligand orbitals.

Where luminescence properties are concerned, two general trends were found[18]:

- The energy of the emission maximum decreases regardless of the electron accepting and donating nature of the substituent.
- At high temperature, electron accepting substituents have the opposite effect.

These conclusions may be explained on the basis of the correlation between the electrochemical potentials and emission energies, the two processes involved in the electron transfer between the same molecular orbitals. It was concluded that when the substituents are electron acceptors, the π^* ligand centred orbital is more stabilised than the $\pi(t_{2g})$ metal centred orbital. When the substituents are electron donating groups, the MLCT excited state energy decreases as a consequence of the destabilisation of the metal centred $\pi(t_{2g})$ orbital. Heteroleptic complexes carrying an electron accepting and a electron donating group always show lower emission energies when compared with the parent homoleptic complexes because the π^* orbital of the A-tpy ligand is stabilised and the D-tpy destabilises the metal centred $\pi(t_{2g})$ orbitals. These effects may also explain why the room temperature luminescence quantum yield and lifetime increase upon replacing $H^{4'}$ with an electron accepting substituents and its decrease with electron-donating moieties. When the terpyridine are connected through their 4' position with π-delocalising[27-30] moieties, remarkable lifetime enhancements are observed. Again this can be rationalised in terms of stabilisation of the ^{3}MLCT upon delocalisation. However the concomitant decrease of the excited state distortion and, thus, of the Frank-Condon factors for radiationless decay probably add to the effects.

Finally, the cyclic voltammetric data for the complexes synthesised have been described in Table 4.3. In general all the monomeric complexes investigated, exhibited one metal-based oxidation at positive potentials corresponding to the M(II/III) couple. In the negative region, the redox processes observed were sequential ligand based reductions. The oxidation potentials for ruthenium complexes appear as one electron reversible process in a range between 1.02 V and 1.23 V. By adding (py-tpy) and (tpy-ph-Br) ligands instead of the terpyridine group, the oxidation potential shifted to less positive values compare to the prototype $[Os(tpy)_2]^{2+}$. The most positive potential was observed for [Ru(tpy-ph-

Br)(L3) (H_2O)], E = +1.02 V, followed by [Ru(py-tpy)(tpy-ph-Br)][PF_6]$_2$, with E = =1.04 V and [Ru(tpy)(tpy-ph-Br)][PF_6]$_2$ E = 1.06 V. Electron releasing substituents shift the reductive processes to more negative potentials, as observed for the ruthenium compounds. The redox potentials for the prototype $[Ru(tpy)_2]^{2+}$ appear at –1.25 V and –1.51 V, whereas all the ruthenium complexes show first redox potential between –1.31 V and – 1.57 V and the second redox potential between – 1.68 V and – 1.79 V. As shown in Table 4.4, the osmium complexes are oxidised at less positive potentials than the Ru(II) complexes, whereas the redox potentials did not show considerable differences. For the osmium compounds the oxidation potentials are observed in a range between + 0.40 V and + 0.73 V, whereas the one electron ligand based reductions are observed between – 1.33 V and - 1.55 V for the first redox process and – 1.70 V and – 1.87 V for the second redox process.

4.7 Bibliography

[1] Sauvage, J.P., Collin, J.P., Chambron, J.C.., Guillerez, S., Coudret, C., Balzani, V., Barigelletti, F., De Cola, L., Flamigni, L., Chem. Rev., *1994*, 94, 993.

[2] Islam, A., Ikeda, N., Nozaki, K., Okamoto, Y., Gholamkhass, B., Yoshimura, A., Ohno, T., Coord. Chem. Rev., *1998*, 171, 355.

[3] Stone, M.L., Crosby, G.A., Chem. Phys. Lett., *1981*, 79, 169.

[4] Klassen, D.M., Crosby, G.A., J. Chem. Phys., *1968*, 48, 1853.

[5] (a) Zeng, F., Zimmerman, S.C., Chem. Rev., *1997*, 97, 1681; (b) Constable, E.C., Housecroft, C.E., Neudburger, M., Schneider, A.G., Springler, B., Zehnder, M., Inorg. Chim. Acta, *2000*, 300, 49; (c) Johansson, O., Borgstrom, M., Lomoth, R., Palmblad, M., Bergquist, J., Hammarstrom, L., Sun. L., Akermark, B., Inorg. Chem., *2003*, 42, 2908; (d) Collin, J.P., Dietrich-Buchecker, C., Gavina, P., Jimenez-Molero, M.C., Sauvage, J.P., Acc. Chem. Res., *2001*, 34, 477.

[6] Duati, M., Tasca, S., Lynch, F., Bohlen, Holger, Vos, Han, Inorganic Chemistry, *2003*, 42, 8377.

[7] Lin. C.-I., Bottcher, W., Chou, M., Creutz, M., Sutin, N., J. Am. Chem. Soc., *1976*, 98, 6536.

[8] Young, R.C., Nagle, J.K., Meyer, T.J., Whitten, D.G., J. Am. Chem. Soc., *1978*, 100, 4773.

[9] Kirchoff, J.R., McMillin, D.R., Marnot, P.A., Sauvage, J.P., J. Am. Chem. Soc., *1985*, 107, 1138.

[10] Hacker, C.R., Gushurst, A.K.I., McMillin, D.R., Inorg. Chem., *1991*, 30, 538.

[11] Creutz, C., Chou, M., Netzel, T.L., Okumura, M., Sutin, N., J. Am. Chem. Soc., *1980*, 102, 1309.

[12] Collin, J.P., Guillerez, S., Sauvage, J.P., Barigelletti, F., Flamigni, L., De Cola, L., Balzani, V., Coordin. Chem.. Rev., *1991*, 111, 291.

[13] Fink, D.W., Ohnesorge, W.E., J. Am. Chem. Soc.,*1969*, 91, 4995.

[14] Lytle, F.E., Petrosky, L.M., Carlson, L.R., Anal. Chim. Acta, *1971*, 57, 239.

[15] Calvert, J.M., Casper, J.V., Binstead, R.A., Westmoreland, T.D., Meyer, T.J., J. Am. Chem. Soc., *1982*, 104, 6620.

[16] Bessel, C.A., See, R.F., Jameson, D.L., Churchill, M.R., Takeuchi, K.J. J. Chem. Soc., Dalton Trans., *1992*, 3223.

[17] Constable, E.C., Cargill Thompson, A.M.W., Tocher, D.A., Daniels, M.A.M., New. J. Chem., *1992*, 16, 855.

[18] Hecker, C.R., Fanwick, P.E., McMillin, D., Inorg. Chem., *1991*, 30, 659.

[20] Wrighton, M., Morse, L., J. Am. Chem. Soc., *1974*, 96, 996.

[21] Maestri, M., Armaroli, N., Balzani, V., Constable, E.C., Cargill Thompson, A.M., Inorg. Chem. 34, *1995*, 2759.

[22] (a) Van Houter, J., Watts, R.J., J. Am. Chem. Soc., *1976*, 98, 4853; (b) Van Houter, J., Watts, R.J., J. Inorg. Chem., *1978*, 17, 3381.

[23] Durham, B., Caspar, J.V., Nagle, J.K., Meyer, T.J., J. Am. Chem. Soc., *1982*, 104, 4803.

[24] (a) Caspar, J.V., Nagle, J.K., Meyer, T.J., J. Inorg. Chem., *1983*, 22, 2444; (b) Caspar, J.V., Nagle, J.K., Meyer, T.J., J. Am. Chem. Soc., *1983*, 105, 5583.

[25] Gleria, M., Minto, F., Baggiato, G., Bartolus, P., J. Chem. Soc., Chem. Commun., *1978*, 285.

[26] (a) Hoggard, P.E., Porter, G.B., J. Am. Chem. Soc., *1978*, 100, 1457; (b) Wallace, W.M., Hoggard, P.E., Inorg. Chem., *1980*, 19, 2141.

[27] Bignozzi, C.A., Schoonover, J. N., Scandola, F., Progr. Inorg. Chem., *1997*, 44, 1.

[27] (a) Kober, E.M., Sullivan, B.P., Dressick, W.J., Casper, J.V., Meyer, T.J., J. Am. Chem. Soc., 102, *1980*, 7385; (b) Kober, E.M., Marshall, J.L., Dressick, W.J., Sullivan, B.P., Casper, J.V., Meyer, T.J., Inorg. Chem., 24, *1985*, 2755.

[28] Johnson, S.R., Westmoreland, T.D., Caspar, J.V., Barqawi, K.R., Meyer, T.J., Inorg. Chem., 27, *1988*, 3195.

[29] Allen, G.H., Sullivan, B.P., Meyer, T.J., J. Chem. Soc. Chem. Commun., *1981*, 793.

[30] Sullivan, B.P., Calvert, J.M., Meyer, T.J., Inorg. Chem., 19, *1980*, 1404.

Chapter 5

Synthetic Methods for Metal Terpyridine Complexes with SH end group

Complexes, in which the metal centre is coordinated to terpyridinyl linkers containing a thiol end group, can absorb onto gold surface. Chapter 5 describes the synthetic methods investigated for the preparation of ruthenium and cobalt terpyridine complexes functionalised with a thiol group.

Special attention is paid to the conditions required for the Suzuki coupling reactions investigated. Synthesis and purification of both ligands and complexes required for the synthesis described in this Chapter are included in Chapter 2.

5.1 Introduction

One of the most important objectives in novel technology research is the need for decreasing the size of devices and components. Molecules and nanoparticles may in the future perform functions in electronic circuitry, presently performed by semiconductor components, because they are 100 times smaller than the smallest features that may be obtained using present semiconductor technology. Redox–active metal complexes are interesting for the investigation of fundamental aspects of charge transfer processes, for the development of optical materials, sensors and for technologically important applications. Self-assembled monolayer containing molecules with a functionalised tail-group, suitable for surface binding of particular functional groups or molecules, are of interest in fields, such as sensor applications and molecular electronics[1]. The aim of the SUSANA (Supramolecular Self-Assembly of Interfacial Nanostructures) project is to make junctions in which nanoparticles are linked to a metal contact or electrode, through molecular bridges, whose electron transfer barrier properties can be used as chemical switches. The goal of this Chapter is the investigation of synthetic methods of incorporating thiol functional groups to metal terpyridine complexes.

5.1.1 Self-assembled monolayers: thiol adsorption on gold surface

Self-assembly of organic monolayers was first noted in the 1950's when it was found that dilute solutions of long chain alcohols would spontaneously adsorb onto clean glass surfaces rendering them hydrophobic[1]. Long chain amines were also studied and shown to adsorb onto Pt surfaces[2]. However, these layers, based on simple physisorption were unstable and easily removed. More robust layers were obtained by the adsorption of fatty acids onto metal surfaces[3], the acids being deprotonated and binding quite strongly to the surface. The first types of strongly bound chemisorbed monolayers were those developed using siloxane chemistry[4], where a silicon surface is etched so as to clean and coat the surface with active silanol (Si-OH) groups.

These Si-OH surfaces were reacted with dilute solutions of long chain alkyl chlorosilanes (see Figure 5.1), to form siloxane attachments to the surface.

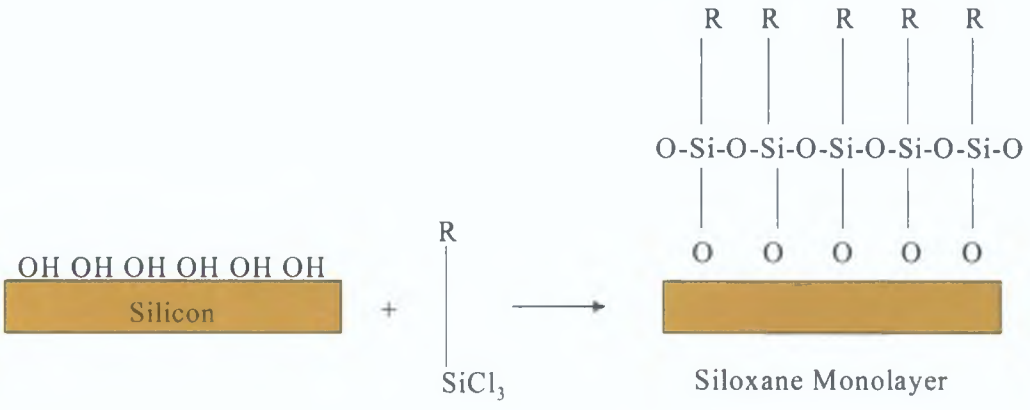

Figure 5.1: Deposition of a self-assembled polysiloxane monolayer

Reaction with water caused further hydrolysis and condensation of unreacted Si-Cl bonds, leading to the formation of a stable, polysiloxane structure and a robust monolayer. Unfortunately, silyl chlorides are very reactive, precluding the use of aqueous solutions and also meaning that only relatively inert substituents such as alkyl chains may be used. What is required is a simple functionality that binds strongly to an otherwise chemically inert surface, yet is relatively unreactive chemically so other active groups (-OH, - COOH, NH_2, etc.) may be incorporated within the molecules. Thiol compounds are known for their reactivity towards noble metals. Although there is a variety of substrates for deposition of thiols moieties gold is most commonly used (see Figure 5.2).

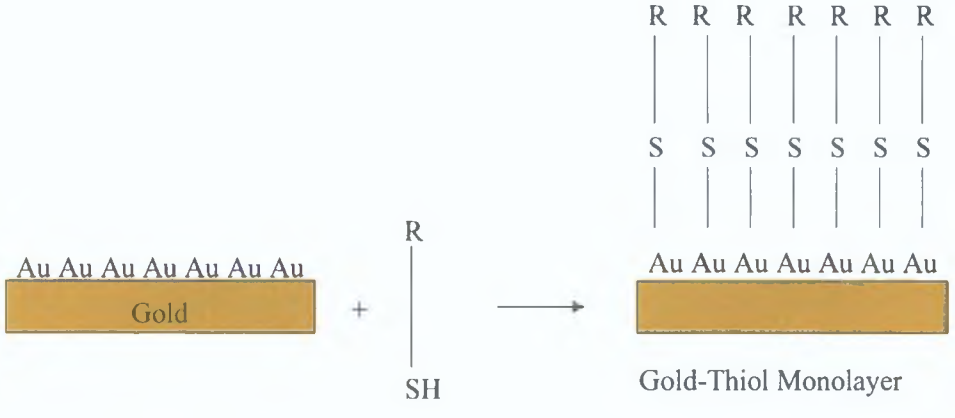

Figure 5.2: Deposition of a self-assembled gold-thiol monolayer

The gold – thiol interaction is based on binding between "soft" gold and sulphur atoms. Many other functional groups are relatively "hard" and do not interact strongly

with the gold surface. This means the use of di- or polyfunctional molecules is possible without any interference to the gold – sulphur-binding interaction. Also gold is relatively easy to clean, does not oxidise under standard laboratory conditions and any weakly physically adsorbed impurities are displaced by thiol species.

The best binding occurs between gold and thiol groups[5], but other species such as disulphides, thiones, thioesters, etc., have been used. Early studies looked at simple alkyl disulphides[6], and thiols[7], on gold. These form stable self – assembled monolayers, which are highly resistant to washing due to the strong chemisorption of the sulphur atoms. Initially, it was thought that there is a rapid reaction between a – SH group (for a thiol) and a gold atom with formation of an S – Au bond. After the fast adsorption of the thiols, the alkyl side chains then assemble to maximise the Van der Waal`s interactions between them[5].

The stability and thinness of these layers, plus the versatility of a gold substrate allowing the application of electrochemical methods, rapidly led to their investigation as possible sensing films. Between the chemical – sensing moieties, terpyridine may be easily attached to gold surfaces and used to detect various species. Besides being of interest themselves, the development of monolayers may be used also to assemble patterns of proteins, enzymes, virus and cells. Several reviews are available on this subject[8].

Bard and co-workers described self-assembled monolayers (SAMs) made of rigid thiols[9], however, these molecules exhibit a large cross – sectional area that results in sizeable mismatch with the size of many substituents. Studies of 4, 4`-dioctylbiphenyl, which spontaneously forms stable suspended liquid crystal films[10], were also carried out. The results suggest that 4`-substituted - 4- mercapto-biphenyl derivatives (see Figure 5.3) may form ordered SAMs on Au surfaces[11].

Beyond their rigidity, the advantage of these aromatic thiols is the conjugation between the adsorbing thiolate and the 4`-substituent. This conjugation affects the acidity of the thiol proton and hence, may make the thiolate a softer or a harder ligand[12].

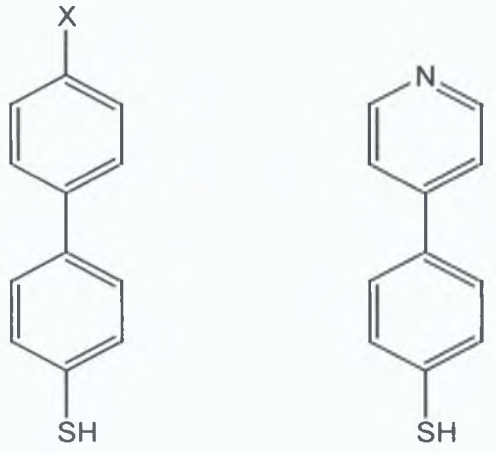

Figure 5.3: Examples of 4-Mercaptobiphenyls used in SAM on gold surface

Since the thiolate is an electron-donating group, an electron-attracting substituent will result in a significant molecular dipole moment. Dipolar interactions may alter absorption kinetics and the composition of mixed SAMs in equilibrium[13], as became apparent from recent studies.

Independently, Rubinstein and co-workers assembled thiophenol, 4-mercaptobiphenyl and 4-mercaptophenyl on gold and reported that the latter two formed reproducible SAMs that were substantially more stable than those from mercaptophenol, presumably due to greater intermolecular $\pi-\pi$ interactions[14].

Finally, Tao and co-workers applied cyclic voltammetry to study the structure of aromatic derivatives thiol monolayer on gold[15]. They showed that for phenyl substituted thiols, the stability of a monolayer formed on gold is dependent on the location of the benzene ring in the alkyl chain, as well as on the length of this chain.

There are several advantages to using the 4'-substituted-4-mercaptobyphenyl system. First is the fact that thiolates have been studied more than any other SAMs and many structural and physical properties are well understood[16].

A second advantage is the ability to alter the absorbing properties of the thiolate by using different substituents at the 4'-position of the biphenyl moiety. Among the linkers suitable for SAM preparation, alkenethiols and substituted alkanethiols have been widely studied while thioaromatic molecules have been less investigated[17].

Importantly conjugated aromatic groups provide better electronic conduction properties not only between the functional group (tail group) and the substrate, in molecular electronics applications[18], but also parallel to the surface plane, between the molecular π systems[19]. In this respect, terpyridine-based metal complexes are

quite promising functional species to be incorporated in a monolayer. They are good linkers groups as they:

- Are redox-active species.
- Terpyridine ligands may coordinate various metal cations and producing stable complexes (e.g. Ru(II) and Os(II) cations)[20].
- In most cases, these complexes are also photoactive[21][22] and this may add important properties to the organised assemblies.

One of the problems to be addressed is the lateral spacing of the ligand groups, since they are intended to accommodate large, sterically hindered and often intrinsically charged species. A way of overcoming this difficulty is that of "diluting" the component carrying the active group with another component acting as a lateral spacer.

The central aspect of this thesis was the synthesis and characterisation of molecular metal complexes containing functional groups, acting as molecular chips that may be used to connect the metal complex to a solid surface.

Examples of these functional groups are: SH, COOH, pyridyl groups. Self-assembled monolayers of terpyridine thiol-substituted complexes onto gold and other surface have been the object of extensive research over the last decade [23][24][5] (see Figure 5.4).

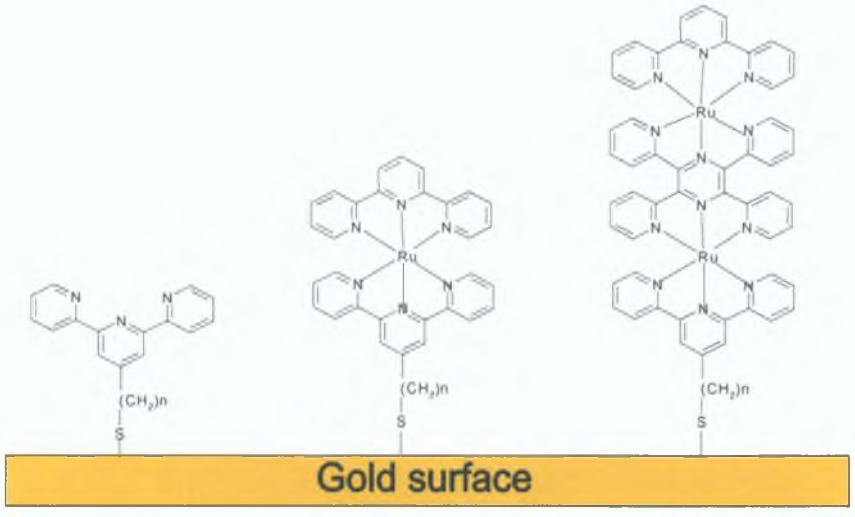

Figure 5.4: Example of self-assemble monolayers of thiol Ru (II) terpyridine complexes onto gold surface

The use of these modified surfaces ranges from fundamental examinations concerning the structure of the layers and thermodynamics and kinetics of adsorption to including sensors[25] and molecular[26] and electronic devices[27]. The presence of electroactive centres connected to the thiol group facilitates characterisation of the attached species by the use of electrochemical techniques such as cyclic voltammetry[28][29]. The free ligand as well as (tpy) - SH containing metal complexes, adsorbs strongly on to gold electrode surfaces; in the case of the metal complexes, they retain their redox-active responses at potentials very close to those of nano adsorbing analogues in homogeneous solution.

The aim of the Chapter is to describe the synthetic investigated towards the preparation of monometallic complexes of ruthenium and cobalt in which the metal centre is coordinated to terpyridinyl linkers containing a thiol end group, which confers high absorbility onto gold surfaces. The synthesis of thiol compounds using Suzuki coupling reactions has been investigated.

Two approaches have been followed for this purpose:

- Modification of bromo functionalised terpyridine ligands.
- Modification of bromo functionalised terpyridine complexes (ruthenium and cobalt metal centre).

Modification of the bromide into the thiol group has been attempted using 1-mercapto-4-boronic acid benzene, 1-methyl-mercapto-4-boronic acid benzene and new boronic compounds synthesised in this thesis:

- 4-(4,4,5,5-tetramethyl-1,3,2-dioxaborolan-2-yl)-thiophenol.
- [4-[[(1,1-dimethylethyl)dimethylsilyl]thio]phenyl]-boronic acid.
- 4,4,5,5-tetramethyl-2 [4-(1,1- dimethylethyl) dimethylsilyl) phenyl]-1,3,2 – dioxaborolane.

These boron compounds have been reacted with (tpy-ph-Br), $[Ru(tpy)(tpy\text{-}ph\text{-}Br)]^{2+}$ and $[Co(tpy\text{-}ph\text{-}Br)_2]^{2+}$ (Synthetic procedures are described in Section 5.2).

5.2 Synthetic methods

5.2.1 General

All synthetic reagents were of commercial grade and no further purification was employed. All solvents were used as purchased from Aldrich. Column chromatography was performed using neutral activated aluminium oxide or silicon oxide (35–70 μm).

5.2.2 Synthesis of starting materials

The synthesis of (tpy-ph-Br) the complexes $[Ru(tpy\text{-}ph\text{-}Br)(tpy)][PF_6]_2$ and $[Co(tpy\text{-}ph\text{-}Br)_2][PF_6]_2$ are reported in Chapter 2. Starting materials as 1 - mercapto - 4 - boronic acid benzene and 1- methyl - mercapto - 4 - boronic acid benzene were purchased from Aldrich and used without any further purification.

First procedure used for the preparation of (tpy-ph-SH) was a modification of the synthesis reported for similar ligands by Abruna and Maskus[30]. All the others boronic compounds described in this Chapter and used for Suzuki coupling reactions were synthesised using a modified literature procedure [31]. Suzuki coupling reaction conditions were investigated to prepare both the ligands (tpy-ph-ph-SH) and (tpy-ph-ph-SCH_3) as described in Section 5.5.

5.2.3 Attempted synthesis of 4' – (4''' – mercaptophenyl) – 2,2': 6',2'' – terpyridine. (tpy-ph-SH) (1)

Two reaction steps have been carried out for this synthesis;

1) Preparation of intermediate thiouronium salt (A')

2) Hydrolysis of (A') salt to give the SH group.

Step 1: Synthesis of intermediate thiouronium salt (A') (see Figure 5.6)

(tpy-ph-Br) (410 mg, 1.1 mmol), and thiourea (10.0 mg, 0.10 mmol), were heated at reflux in ethanol (10 cm^3) for 24 h. The solvent was evaporated and the residue dissolved in hot ethanol (5 cm^3). Water (1cm^3) and 37% HCl (1 cm^3) were added and the solution was cooled overnight in the refrigerator. The solution was filtered and white crystals were obtained. NaOH 3M (10 cm^3) and ethanol (5 cm^3) were purged under nitrogen for 15 min and then heated at reflux with the white solid obtained after

filtration. After for 4 hours, the solution was cooled and neutralised with H_2SO_4 (1M). The reaction mixture was extracted with CH_2Cl_2 and the extract was dried with Na_2SO_4. The solvent was evaporated and the product was recrystallised twice from chloroform to yield the product A'. Yield: 4.0 mg, 10%.

^{1}H-NMR (DMSO): 9.30 (s, $2NH_2$), 8.70 (d, H^6), 8.63 (d, H^3), 8.32 (d, $H^{3'}$), 7.80 (t, H^4), 7.30 (t, H^5)

5.2.4 Attempted synthesis of [4' – (4''' – mercapto phenyl) benzene] – 2,2': 6', 2" – terpyridine. (tpy-ph-ph-SH) *(2).*

(Reactions 1/11, see Table 5.1)

(tpy-ph-Br) (100 mg, 0.30 mmol), 1-mercapto-4-boronic acid benzene (52.0 mg, 0.40 mmol), and potassium carbonate (428 mg, 3.1 mmol), were mixed in DMF (10 cm^3), and the solution was deaerated by bubbling argon, for 20 minutes. A 5 mol% of a Pd catalyst was added and the reaction was stirred and heated to 80 °C, under nitrogen. The DMF was removed under vacuum adding toluene. The crude solid was recrystallised from ethanol/H_2O. Yield: 70.1 mg.

^{1}H-NMR (DMSO) of the product obtained: 8.66 (d, H^6), 8.63 (s, $H^{3'}$) 8.59 (d, H^3) 7.82 (td, H^4), 7.72 (d, H^β), 7.57 (d, H^α), 7.30 (m, H^5).

5.2.5 Attempted synthesis of compound (4): [4'–(4'''–methyl mercapto phenyl)benzene]–2,2': 6', 2" - terpyridine. (tpy-ph-ph–SCH_3) (4)

(Reactions 31/57 see Table 5.3)

(tpy-ph-Br) (100 mg, 0.30 mmol), 1-methyl mercapto-4-boronic acid benzene (67.0 mg, 0.40 mmol) and potassium carbonate (497 mg, 3.6 mmol), were mixed in DMF (10 cm^3) and the solution was deaerated by bubbling argon, for 20 minutes. A 5 mol% of Pd catalyst was added and the reaction was stirred and heated to 80 °C, under nitrogen. The DMF was removed under vacuum adding toluene. The crude solid was recrystallised from ethanol/H_2O. Yield: 67.0 mg.

^{1}H-NMR (DMSO) of the product obtained: 8.66 (d, H^6), 8.63 (s, $H^{3'}$) 8.59 (d, H^3) 7.82 (td, H^4), 7.72 (d, H^β), 7.57 (d, H^α), 7.30 (m, H^5).

5.3. Synthesis of new boronic acid compounds

Boron compounds as (6), (7), (8), (9) and (10) were used as starting material for Suzuki coupling reactions and were synthesised by using modification of a literature procedure[31]. Same procedure was followed to attempt the synthesis of the compounds (11) and (12) (see structures in Figure 5.11). The ^{1}H-NMR of these compounds is shown in Appendix I.

5.3.1 Synthesis of 4-(4,4,5,5-tetramethyl-1,3,2-dioxaborolan-2-yl)-thiophenol (6) (see Figure 5.12)

To a solution of 1-mercapto-4-boronic acid benzene (300 mg, 2.0 mmol) in dry THF (10 cm^3), was added pinacol (224 mg, 1.9 mmol). The solution was stirred for 30 minutes and dried with sodium sulfate. After filtration and evaporation of the volatiles, the residue was purified by chromatography column on silica gel in dichloromethane to afford white crystals. Yield: 270 mg, 60%. Anal. Calcd. $C_{12}H_{17}O_2B_1S_1$ C: 61.04%; H: 7.26 %. Anal. Found: C: 61.05%; H: 7.23 %.

^{1}H-NMR ($CDCl_3$) of the product: 7.60 (d, H^{α}), 7.20 (d, H^{β}), 3.45 (s, SH), 1.35 (s, $4CH_3$ pinacol group). See spectrum Figure 16, Appendix I.

5.3.2 Synthesis of [4-[[(1,1-dimethylethyl)dimethylsilyl]thio]1-bromo]benzene *(7)* *(see Figure* 5.13)

4-mercapto-1-bromo benzene (2.00 g, 10.0 mmol) was dissolved in dry THF (20 cm^3). NaH (0.28 g, 10.0 mmol) was added at 4 °C. After 10 minutes, dimethyl – terbutyl – silyl chloride (2.40 g, 20.0 mmol) was added to the reaction mixture and stirred for 14 hours at room temperature. The solution was then filtered over Celite and the solvent removed under pressure. A yellow oil was then obtained and purified by column chromatography in dichloromethane. The fraction isolated afforded white crystals. Yield: 1.70 g, 53%. Anal. Calcd. $C_{12}H_{19}S_1Br_1Si_1$ C: 47.51%; H: 6.31 %. Anal. Found: C: 47.42%; H: 6.15 %. ^{1}H-NMR ($CDCl_3$) of the product: 7.30 (d, H^{α}), 7.10 (d, H^{β}), 0.80 (s, $3CH_3$), 0.2 (s, $2CH_3$). See spectrum Figure 17, Appendix I.

5.3.3 [4-[[(1,1-dimethylethyl)dimethylsilyl]thio]phenyl]-boronic acid *(8) (see Figure 5.14)*

Under Argon, a solution of compound *(7)* (1.90 g, 6.0 mmol), in dry THF (15 cm^3), was stirred at -78°C and triisopropyl borate (7.52 cm^3, 32.6 mmol) and N-butyl lithium (4.01 cm^3, 2.5 M in n-hexane, 10.0 mmol), was added dropwise. The mixture was stirred at –78 °C for 2 hours and then at –20 °C for 2 hours, finally overnight at room temperature. A white solution was obtained. Water (15 cm^3) was added and the mixture was concentrated to one third under reduced pressure. Extraction was performed with diethyl ether and the organic layer was washed with water, dried (sodium sulphate) and concentrated under reduced pressure. Recrystallisation using diethyl ether/pentane afforded white crystals. Yield: 810 mg, 49%. Anal. Calcd. $C_{12}H_{21}S_1B_1O_2Si_1$ C:53.73%; H:7.89%. Anal. Found: C: 53.45%;.H:8.04 %. ^{1}H-NMR ($CDCl_3$) of the product: 7.60 (d, H^{α}), 7.20 (d, H^{β}), 0.80 (s, $3CH_3$), 0.2 (s, $2CH_3$). ^{11}B-NMR showed a signal at 20 ppm. See spectrum Figure 18, Appendix I.

5.3.4 Synthesis of 4,4,5,5-tetramethyl-2-[4-(1,1 dimethylethyl)dimethylsilyl)phenyl]-1,3,2-dioxaborolane *(9) (see Figure 5.15)*

Two different methods were attempted for the synthesis of this compound:

Method 1: Attempted synthesis of (9) (see Figure 5.15)

To a solution of (8) (303 mg, 1.10 mmol) in THF (10 cm^3), was added 2 equivalent of pinacol (260 mg, 2.20 mmol). The solution was stirred for 1 hours at room temperature and dried with sodium sulfate. After filtration and evaporation of the volatiles, the residue was purified by chromatography on silica gel in dichloromethane. The signals of the dimethyl-terbutyl-silyl group were absent in the ^{1}H-NMR of the product obtained ($CDCl_3$): 7.60 (2H, d), 7.20 (2H, d), 1.3 (12H, s). For further details see Section 5.5.

Method 2 synthesis of (9) (see Figure 5.16)

To a solution of *(6)* (702 mg, 3.0 mmol) in dry THF (10 cm^3), an excess of NaH (79 mg, 3.3 mmol) was added at 4°C. After 10 minutes, dimethyl-terbutyl-silyl chloride (678 mg, 4.5 mmol) was added and the solution was stirred for 14 hours at room temperature.The reaction mixture was then filtered over Celite and the solvent

removed with rotary evaporator to afford a product the was extracted with dichlorometane/H_2O and dried with sodium sulphate. The solvent was then evaporated and white crystals have been obtained. Yield: 610 mg, 58%.

Anal. Calcd. $C_{18}H_{31}S_1Si_1B_1O_2$ C:61.70%; H:8.92 %. Anal. Found: C: 61.54%; H: 9.01 %. ^{1}H-NMR ($CDCl_3$) of the product: 7.60 (d, H^{α}), 7.20 (d, H^{β}), 1.35 (s, $4CH_3$ pinacol group), 0.78 (s, $3CH_3$), 0.2 (s, $2CH_3$). See spectrum Figure 19, in Appendix I.

5.3.5 [4-[(triphenylmethyl)thio][(1-bromo)]benzene *(10) (see Figure 5.17)*

Under Argon, 4-mercapto-1-bromo benzene (2.00 g, 10.0 mmol) was dissolved in dichloromethane. Pyridine (840 mg, 10.0 mmol), was added to the solution and after 10 minutes, triphenyl-methyl-chloride (2.95 g, 10.0 mmol). The reaction mixture was then stirred for 4 hours under reflux. The product was purified with column chromatography in dichloromethane to afford a pure product. Yield: 2.51 g, 55%. Anal. Calcd. $C_{25}H_{19}S_1Br_1$ C: 69.61%; H: 4.44 %. Anal. Found: C: 69.35%; H; 4.53 %. ^{1}H-NMR ($CDCl_3$) of the product: 7.40-7.20 (m, 15H phenyl group), 7.13 (d, H^{α}), 6.70 (d, H^{β}), 3.45. See spectrum Figure 20, Appendix I.

5.3.6 Attempted synthesis of [4-[(triphenylmethyl)thio]phenyl]-boronic acid *(11) (Figure 5.18)*

A solution of *(10)* (517 mg, 1.2 mmol), in dry THF (20 cm^3), was stirred under Argon at -78°C and triisopropyl borate (1.39 cm^3, 6.0 mmol), was added. Subsequently N-butyl lithium (0.742 cm^3, 2.5 M in n-hexane, 1.9 mmol), was added dropwise. The mixture was stirred at –78 °C for 2 hours and then at –20 °C for 2 hours, finally overnight at room temperature. Water (20 cm^3) was added and the mixture was concentrated to one third under reduced pressure. Extraction was performed with diehyl ether and the organic layer was washed with water, dried (Na_2SO_4) and concentrated under reduced pressure. A pale yellow oil was obtained. Recrystallisation from diethyl ether/pentane afforded a white product. Yield: 207 mg. ^{1}H-NMR ($CDCl_3$) of the product obtained: 7.43-7.20 (m, 15H phenyl group), 7.10 (d, H^{α}), 6.70 (d, H^{β}), 3.45 (s, SH).

For further details see Section 5.5.

5.3.7 Attempted synthesis of 4,4,5,5-tetramethyl-2-[4-[(triphenylmethyl) thio]phenyl]-1,3,2-dioxaborolane *(12) (see Figure 5.19)*

Compound (6) (188 mg, 0.80 mmol) was taken up in DCM (10 cm^3). Pyridine (63.0 mg, 0.80 mmol) was added to the solution and afterwards triphenylmethylchloride (223 mg, 0.80 mmol). The reaction mixture was stirred at room temperature for 4 hours. Water was then added to the solution and the organic layer was separated from the water layer. The organic layer was then dried over Na_2SO_4 and the solvent removed under vacuum pressure. The residue was purified by chromatography on silica gel using dichloromethane as eluent.

Yield: 180 mg. ^{1}H-NMR ($CDCl_3$): 7.10 (d, H^{α}), 6.70 (d, H^{β}), 2.00 (s, $4CH_3$ pinacol group). Further details are shown in Section 5.5.

5.4. Attempted synthesis of thiol containing metal complexes

Suzuki coupling reactions were also carried out using ruthenium and cobalt terpyridine complexes, as described in this Section.

5.4.1 Attempted synthesis of $[Ru(tpy)(tpy\text{-}ph\text{-}ph\text{-}SH)][PF_6]_2$ *(3) (see Figure 5.8)*

Method 1 (Reactions 12/30, see Table 5.2)

In a 10 cm^3 schlenk tube, $[Ru(tpy)(tpy\text{-}ph\text{-}Br)][PF_6]_2$ (100 mg, 0.10 mmol), 1-mercapto-4-boronic acid benzene (46 mg, 0.30 mmol), and potassium carbonate (152 mg, 1.1 mmol), were mixed in DMF (15 cm^3), and the solution was deaerated by bubbling argon, for 20 minutes. A 5 mol% of a Pd catalyst was added. and the reaction was stirred and heated at 80 °C, under nitrogen. Toluene was added and DMF was removed under vacuum. The crude solid was purified by column chromatography (silica), using as eluent acetonitrile-saturated aqueous NaCl-H_2O (14:2:1 volumetric ratios). Yield: 60.0 mg. ^{1}H-NMR (d^3-acetonitrile) of the product obtained: 9.10 (s, $H^{3'}$), 8.81 (d, H^{β}), 8.69 (d, H^3), 8,55 (d, H^6), 8.42 (t, $H^{4''}$), 8,18 (d, H^{α}), 7.90-8.00 (m, H^4, $H^{3'''}$, $H^{3''}$), 7.48 (d, $H^{2'''}$), 7.40 (d, $H^{5'''}$), 7.20 (m, H^5, $H^{4'''}$).

Method 2 (Reactions 77/85, see Table 5.5)

A solution of $[Ru(tpy)(tpy\text{-}ph\text{-}Br)][PF_6]_2$ (101 mg, 0.10 mmol), compound *(6)* (24 mg, 0.10 mmol) and sodium carbonate (21 mg, 0.20 mmol), were mixed in DMF (10 cm^3), and the solution was deaerated by bubbling argon, for 20 minutes. A 5 mol% of a Pd catalyst was added and the reaction was stirred and heated at 80 °C, under nitrogen. Toluene was added and DMF was removed under vacuum. The crude solid was purified by column chromatography (silica), using as eluent acetonitrile-saturated aqueous NaCl-H_2O (14:2:1 volumetric ratios). Yield: 69.0 mg.

^{1}H-NMR (d^3-acetonitrile) of the product obtained: 9.10 (s, $H^{3'}$), 8.81 (d, H^{β}), 8.69 (d, H^3), 8,55 (d, H^6), 8.42 (t, $H^{4''}$), 8,18 (d, H^{α}), 7.90-8.00 (m, H^4, $H^{3'''}$, $H^{3''}$), 7.48 (d, $H^{2'''}$), 7.40 (d, $H^{5'''}$), 7.20 (m, H^5, $H^{4'''}$).

5.4.2 Attempted synthesis of $[Ru(tpy)(tpy\text{-}ph\text{-}ph\text{-}SCH_3)][PF_6]_2$

(5) (see Figure 5.10) (Reactions 58/76, see Table 5.4)

$[Ru(tpy)(tpy\text{-}ph\text{-}Br)][PF_6]_2$ (100 mg, 0.10 mmol), 1-methyl-mercapto-4-boronic acid benzene (50 mg, 0.30 mmol), and potassium carbonate (42 mg, 0.30 mmol), were mixed in DMF (15 cm^3), and the solution was degassed. A 5 mol % of Pd catalyst was added. The reaction was heated during at 80 °C, under nitrogen. The DMF was removed under vacuum with adding toluene The crude solid was purified by column chromatography (silica), using as eluent acetonitrile-saturated aqueous NaCl-H_2O (14:2:1 volumetric ratios). Yield: 64.0 mg.

^{1}H-NMR of the product obtained (d^3-acetonitrile): 9.10 (s, $H^{3'}$), 8.81 (d, H^{β}), 8.69 (d, H^3), 8,55 (d, H^6), 8.42 (t, $H^{4''}$), 8,18 (d, H^{α}), 7.90-8.00 (m, H^4, $H^{3'''}$, $H^{3''}$), 7.48 (d, $H^{2'''}$), 7.40 (d, $H^{5'''}$), 7.20 (m, H^5, $H^{4'''}$).

5.4.3 Attempted synthesis of $[Ru(tpy)(tpy\text{-}ph\text{-}ph\text{-}R)[PF_6]_2$ *(13) (see Figure 5.20)*

(R = dimethyl-terbutyl-silyl group).

Method A *(Reactions 77/85, see Table 5.5)*

Compound *(8)* (40.1 mg, 0.20 mmol) and $[Ru(tpy)(tpy\text{-}ph\text{-}Br)][PF_6]_2$ (109 mg, 0.10 mmol) were heated under Argon, in presence of Na_2CO_3 (32.0 mg, 0.30 mmol) and Pd catalyst (5 mol %). The reaction was heated at 85°C. A minimum amount of DMF

was added to the reaction mixture to dissolve completely the starting material. The solution was then cooled and H_2O was added. A dark red product precipitated and collected by vacuum filtration. The crude solid was purified by column chromatography (silica), using as eluent acetonitrile-saturated aqueous NaCl-H_2O (14:2:1 volumetric ratios). Yield: 97.0 mg.

^{1}H-NMR of the product obtained (d^3-acetonitrile): 9.10 (s, $H^{3'}$), 8.81 (d,$^{\beta}$), 8.69 (d, H^3), 8,55 (d, H^6), 8.42 (t, $H^{4''}$), 8,18 (d, H^{α}), 7.90-8.00 (m, H^4, $H^{3'''}$, $H^{3''}$), 7.48 (d, $H^{2'''}$), 7.40 (d, $H^{5'''}$), 7.20 (m, H^5, $H^{4'''}$).

Method B *(Reactions 77/85, see Table 5.5)*

Compound *(9)* (19.0 mg, 0.10 mmol) and [Ru(tpy)(tpy-ph-Br)][PF_6]$_2$ (50.1 mg, 0.10 mmol) were heated under Argon, in presence of Na_2CO_3 (11.0 mg, 0.10 mmol) and Pd catalyst (5 mol %). The reaction was heated at 85°C. The Ruthenium complex was dissolved in toluene; a minimum amount of DMF was added to the reaction mixture to dissolve completely the starting material. The solution was cooled adding H_2O a red-brownish precipitate appeared. It was filtered by vacuum filtration. The crude solid was purified by column chromatography (silica), using as eluent acetonitrile-saturated aqueous NaCl-H_2O (14:2:1 volumetric ratios). Yield: 31.0 mg,.

H^1-NMR of the product (d^3-acetonitrile): 9.10 (s, $H^{3'}$), 8.81 (d, H^{β}), 8.69 (d, H^3), 8,55 (d, H^6), 8.42 (t, $H^{4''}$), 8,18 (d, H^{α}), 7.90-8.00 (m, H^4, $H^{3'''}$, $H^{3''}$), 7.48 (d, $H^{2'''}$), 7.40 (d, $H^{5'''}$), 7.20 (m, H^5, $H^{4'''}$).

5.4.4 Attempted synthesis of [Co(tpy-ph-ph-SH)$_2$][PF_6]$_2$ *(14)*

(see Figure 5.21) (Reactions 86/94, see Table 5.6)

To a solution of Na_2CO_3 (95.0 mg, 0.90 mmol) compound *(6)* (94.0 mg, 0.40 mmol) and [Co(tpy-ph-Br)$_2$][PF_6]$_2$ (360 mg, 0.30 mmol) were added. The solution was aereated for 20 minutes by bubbling argon. Pd catalyst was added (5 mol %) and the solution was stirred and heated at 85°C, under argon. The solution was allowed cool to room temperature and then extracted with CH_2Cl_2 and water.

The resulting dark red product was filtered and purified by column chromatography (silica), using as eluent acetonitrile-saturated aqueous NaCl-H_2O (14:2:1 volumetric ratios). Yield: 243 mg.

^{1}H-NMR of the product obtained (d^3-acetonitrile): 8.83 (s, $H^{3'}$), 8.78 (d, H^6), 8.69 (d, H^3), 8.15 (t, H^4), 7.90 (d, H^β), 7.82 (d, H^α), 7.48 (t, H^5).

5.4.5 Attempted synthesis of $[Co[(tpy\text{-}ph\text{-}ph\text{-}R)_2]][PF_6]_2$. *(14)*

(see Figure 5.21)

(R = dimethyl-terbutyl-silyl group).

Method A (Reactions 86/94, see Table 5.6)

Compound *(8)* (107 mg, 0.40 mmol) in toluene and $[Co(tpy\text{-}ph\text{-}Br)_2][PF_6]_2$ (360 mg, 0.30 mmol) dissolved in the minimum amount of DMF were mixed under argon, in presence of Na_2CO_3 (95.0 mg, 0.90 mmol). The solution was left under Argon for 20 minutes. Pd catalyst (5mol %) was added and the solution stirred and heated at 80°C. The solution was allowed cool to room temperature and then extracted with CH_2Cl_2 and water. The resulting dark red product was filtered and purified by column chromatography (silica), using as eluent acetonitrile-saturated aqueous NaCl-H_2O (14:2:1 volumetric ratios). Yield: 310 mg. ^{1}H-NMR (d^3-acetonitrile): 8.83 (s, $H^{3'}$), 8.78 (d, H^6), 8.69 (d, H^3), 8.15 (t, H^4), 7.90 (d, H^β), 7.82 (d, H^α), 7.48 (t, H^5).

Method B (Reactions 86/94, see Table 5.6)

Compound *(9)* (141 mg, 0.40 mmol) in toluene and $[Co(tpy\text{-}ph\text{-}Br)_2][PF_6]_2$ (360 mg, 0.30 mmol) dissolved in the minimum amount of DMF were mixed under argon, in presence of Na_2CO_3 (95.0 mg, 0.90 mmol). Argon was flashed into the solution for 20 minutes. Pd catalyst (5mol %) was added and the solution stirred and heated at 80°C. The solution was allowed cool to room temperature and then extracted with CH_2Cl_2 and water. The product was filtered and purified by column chromatography (silica), using as eluent acetonitrile-saturated aqueous NaCl-H_2O (14:2:1 volumetric ratios). Yield: 273 mg. ^{1}H-NMR of the product obtained (d^3-acetonitrile): 8.83 (s, $H^{3'}$), 8.78 (d, H^6), 8.69 (d, H^3), 8.15 (t, H^4), 7.90 (d, H^β), 7.82 (d, H^α), 7.48 (t, H^5).

5.5 Results and discussion

5.5.1 Discussion

Different synthetic pathways were investigated for the preparation of terpyridine and metal terpyridine complexes with - SH group, unfortunately, without success.

First procedure used for the preparation of (tpy-ph-SH) was a modification of that of Abruna and Maskus[30]. Their reaction scheme for the preparation of the ligand is shown in Figure 5.5.

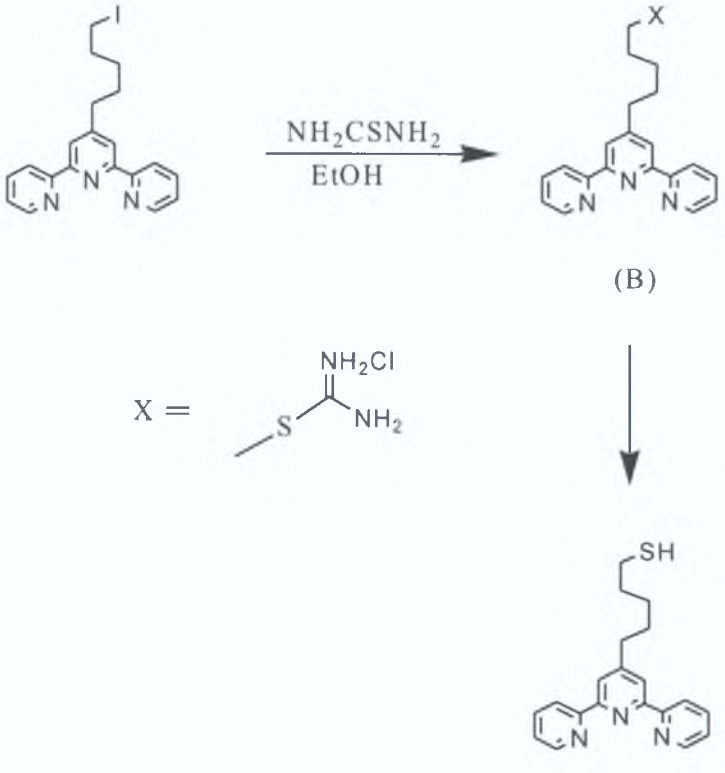

Figure 5.5: Reaction scheme for the preparation of 4'-(5-mercaptopentyl) - 2,2': 6', 2'' - terpyridine

The same procedure was followed in this thesis using (tpy-phenyl-SH) as starting material Only the synthesis of the intermediate (A^*) produced from the first step of the reaction was carried out (see Figure 5.6).

Two are the reaction steps:

- Conversion of the halide group into a thiouronium salt.
- Hydrolysis of the salt to give SH group.

The sequence follows the route for the synthesis of 4' - substituted terpyridine developed by Potts et all [32]. In this method, the thiol functionality is introduced by first converting the corresponding halide into a stable thiouronium salt, which may be stored indefinitely, followed by hydrolysis to the desired ligand (tpy-phenyl-SH). The procedure is quite long, (two 24 hours steps) and the intermediate step has a low yield.

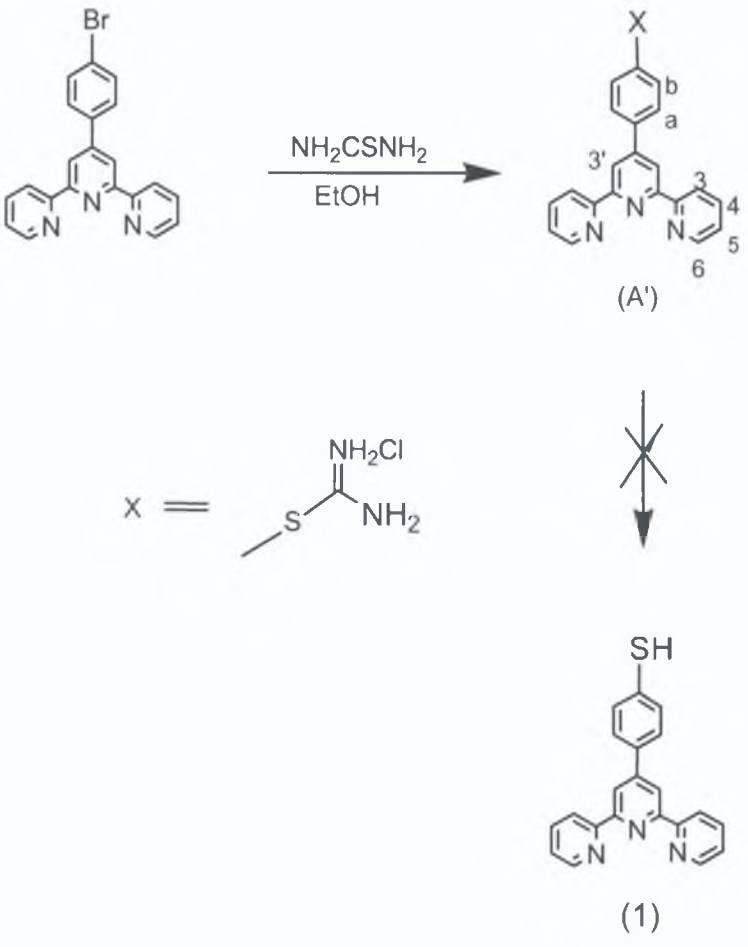

Figure 5.6: Reaction scheme for the preparation of 4'-(5-mercaptophenyl) - 2,2': 6', 2'' - *terpyridine (1)*

^{1}H-NMR measurement confirmed the presence of (A') in step 1, but many additional signals indicated the presence of undesired byproducts. A small amount of (A') was obtained after recrystallisation in chloroform (10%). The quite low yield of the thiouronium salt did not permit continuation onto the next step. It was observed that terpyridine with substituent phenyl halide in position 4', (instead of a chain, as described in Abruna's ligand, Figure 5.5), completely changed the reactivity of the terpyridine system. The conversion of the halide group into the thiouronium salt results in more reactions than just the desired one. This may be attributed to electron interactions of the phenyl group during the conversion of the bromide group into the thiouronium salt (A'). To improve the conditions for the preparation of thiol compounds, palladium catalysed, Suzuki coupling reactions have been investigated.

During the last decade, Pd-catalysed coupling of aryl halides and organoboron acid has undergone rapid development[32]. It has been suggested that these new synthetic methods allow effective and rapid reactions under mild conditions[33][34]. The palladium catalysed Suzuki cross-coupling reactions between aryl boronic acids and aryl halides have proved to be a popular and versatile method the formation of the carbon-carbon single bonds of biaryls[35]. Organoboron reagents exhibit greater functional group compatibility than organozinc or Grignard reagents. Moreover, the innocuous nature of boronic acids, which are generally non-toxic and thermally air- and moisture-stable, is a practical advantage of the Suzuki reaction relative to other coupling processes. In recent years, several thermally stable palladium catalysts have been successfully used for the Suzuki reaction[36], but most of the results, which have been described with these catalysts, were obtained for the coupling of aryl halides. However, relatively few results have been reported for the coupling of benzylic halides. Most of the results described involve drastic conditions, specific ligands and popular but unstable catalysts [37][38][39]. In addition, the coupling conditions tend to vary widely depending on the steric and electronic properties of the substrates and often have to be individually optimised. To be successful with Suzuki coupling reactions it is important to develop a set of working conditions: the appropriate solvent, base and catalyst and find out the best stoichiometric ratio for the reagents to perform the reaction. Several groups have used different substituted phenylboronic acids in the last few years. In particular, Zhuravel and Nguyen[32], found a very efficient method for the preparation of 3 – arylsalicylaldehydes by

palladium-catalysed cross coupling reactions of arylboronic acids and several 3-bromo functionalised aldehydes.

In this thesis, 1-mercapto-4-boronic acid benzene, commercial available, was the first boronic acid used to react with the terpyridine bromo functionalised compounds.

5.5.2 Suzuki coupling reactions: (tpy-ph-Br) as starting material

Firstly, cross-coupling Suzuki reactions between the ligand (tpy-ph-Br) and 1-mercapto-4-boronic acid benzene, were investigated, using modified literature procedures[40] (see Figure 5.7).

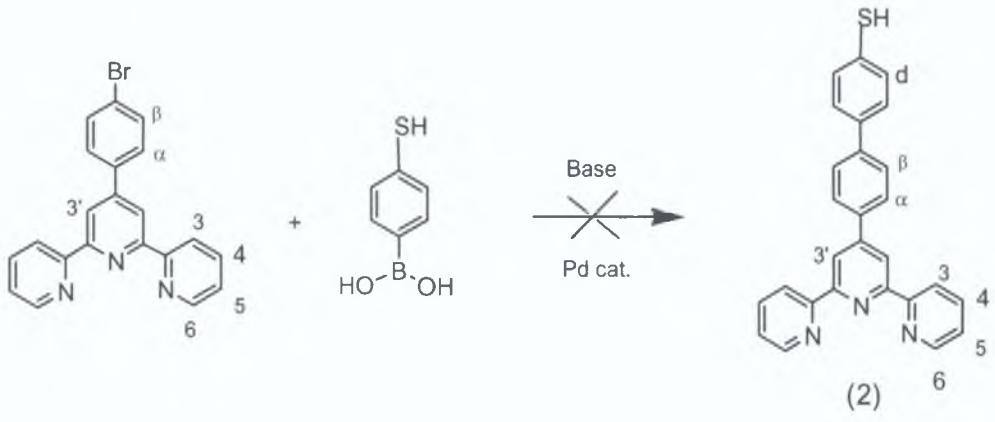

Figure 5.7: Scheme of Suzuki coupling reaction between (tpy-ph-Br) and 1-mercapto-4-boronic acid benzene

Reactions were carried out in a range of solvents using 1 equivalent of ligand and 1 equivalent of boronic acid in presence of an excess of base (K_2CO_3). Two different catalyst were tested: Pd $(PPh_3)_4$ and Pd $(OAc)_2$. The experimental conditions are shown in Table 5.1.

In the course of the investigations, three solvent schemes were used:

- Toluene/H_2O.
- DMF.
- Toluene.

The second solvent gave the best results since mostly terpyridine ligand is completely soluble in DMF. No formation of any product was observed after 4, 8 and 12 hours (TLC in acetonitrile-saturated aqueous NaCl-H_2O, 14:2:1 volumetric ratios). The reaction was stopped after 24 hours and the product obtained was purified using a chromatography column in silica gel. A red spot was isolated and the ^{1}H-NMR spectrum in DMSO suggested that signal of the starting material (tpy-ph-Br), was still present and in particular H^{β} and H^{α} peaks do not shift as was be expected when changing Br into a phenyl system.

In addition, no signals of hydrogen phenyls signals were observed. All these elements suggested that there was no formation of C-C bond between the two-phenyl groups involved in the reaction. A wide range of conditions have then been screened and these are listed below in Table 5.1

REACTION	CATALYST	BASE	SOLVENT	TEMP. (°C)	TIME (h)
1	$Pd(PPh_3)_4$	K_2CO_3	DMF	80	27/30
2	$Pd(PPh_3)_4$	K_2CO_3	DMF	80	48/72
3	$Pd(PPh_3)_4$	K_2CO_3	TOLUENE	60	24
4	$Pd(PPh_3)_4$	K_2CO_3	TOLUENE	60	48/72
5	$Pd(PPh_3)_4$	K_2CO_3	DMF/H_2O	90	30
6	$Pd(PPh_3)_4$	K_2CO_3	DMF/H_2O	90	48/72
7	$Pd(OAc)_2$	K_2CO_3	DMF/H2O	90	24
8	$Pd(OAc)_2$	K_2CO_3	DMF/H2O	90	48/72
9	$Pd(OAc)_2$	K_2CO_3	TOLUENE	80	27/30
10	$Pd(OAc)_2$	K_2CO_3	TOLUENE	80	48
11	$Pd(OAc)_2$	K_2CO_3	TOLUENE	80	72

Table 5.1: Suzuki coupling reaction conditions for reaction between (tpy-ph-Br) and 1-mercapto-4-boronic acid benzene

The reaction was also carried out for longer periods: 48 and 72 hours, at 80 /90 °C, in different solvents and using two different Pd catalysts, but no coupling was observed. Only the seven signals for the terpyridine bromo compounds were identified in the ^{1}H-NMR (DMSO) spectrum: at 8.66 and 8.63 ppm H^6 and $H^{3'}$; H^3 at 8.59 ppm; H^4 at 7.82; at 7.72 and 7.57 ppm, respectively H^{β} and H^{α}, finally, a triplet at 7.30 ppm for H^5. No evidence of any hydrogen signals from the phenyl group H^c and H^d was observed in the spectrum and also no signal of free thiol in the area between 3 and 4 ppm. It has been suggested that the SH group is very unstable and it probably reacts quite easily to form homo-coupled products.

5.5.3 Suzuki coupling reactions: [Ru(tpy)(tpy-ph-Br)][PF$_6$]$_2$ as starting material

The complex [Ru(tpy)(tpy-ph-Br)[PF_6]$_2$ has also been also used as a starting material and reacted with 1-mercapto-4-boronic acid benzene (see below Figure 5.8).

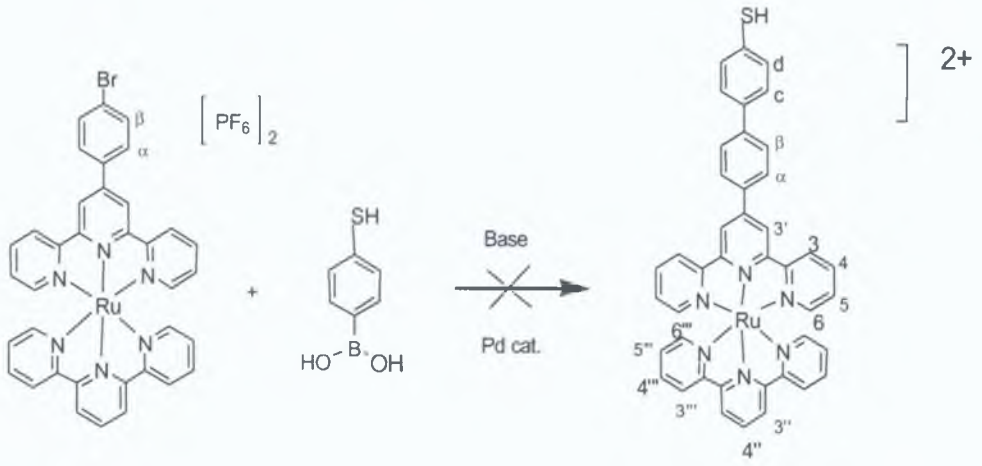

(3)

Figure 5.8: Scheme of Suzuki coupling reaction between Ru(tpy)(tpy-ph-Br)[PF_6]$_2$. and 1-mercapto-4-boronic acid benzene

Unfortunately also with the ruthenium terpyridine complex, no positive results were obtained. No signal for a SH group at 3-4 ppm, has been observed. The ^{1}H-NMR spectrum of the product shows the characteristic signals of the ruthenium starting material: two doublets at 8.69 and 8.55 ppm respectively for H^3 and H^6, two triplets for H^4 at 7.80 and for H^5 at 7.40 ppm and a singlet for $H^{3''}$ at 9.10 ppm. No shift has been observed for the hydrogen H^{β} and H^{α}; this does not suggest the presence of a

second phenyl group instead of the bromide. The ^{1}H-NMR of the rough product shows triplets at 7.56, 7.48 and 7.28 ppm, none of which may be attributed to the two hydrogen H^{c} and H^{d} of the phenyl boronic acid. Using the reaction procedure shown in fig. 5.8, several conditions were then tested and these are listed below in Table 5.2.

REACTION	CATALYST	BASE	SOLVENT	TEMP. (°C)	TIME (h)
12	$Pd(PPh_3)_4$	K_2CO_3	DMF	80	27/30
13	$Pd(PPh_3)_4$	K_2CO_3	DMF	80	48
14	$Pd(PPh_3)_4$	K_2CO_3	DMF	80	72
15	$Pd(PPh_3)_4$	Na_2CO_3	DMF	80	24/30
16	$Pd(PPh_3)_4$	Na_2CO_3	DMF	80	48
17	$Pd(PPh_3)_4$	Na_2CO_3	DMF	80	72
18	$Pd(PPh_3)_4$	K_2CO_3	DMF	80	72
19	$Pd(PPh_3)_4$	K_2CO_3	TOLUENE	60	27/30
20	$Pd(PPh_3)_4$	K_2CO_3	TOLUENE	60	48
21	$Pd(PPh_3)_4$	K_2CO_3	TOLUENE	60	72
22	$Pd(OAc)_2$	K_2CO_3	DMF/H_2O	90	30
23	$Pd(OAc)_2$	K_2CO_3	DMF/H_2O	90	48
24	$Pd(OAc)_2$	K_2CO_3	DMF/H_2O	90	72
25	$Pd(OAc)_2$	Na_2CO_3	DMF/H2O	90	24/30
26	$Pd(OAc)_2$	Na_2CO_3	DMF/H2O	90	48
27	$Pd(OAc)_2$	Na_2CO_3	DMF/H2O	90	72
28	$Pd(OAc)_2$	K_2CO_3	TOLUENE	80	27/30
29	$Pd(OAc)_2$	K_2CO_3	TOLUENE	80	48
30	$Pd(OAc)_2$	K_2CO_3	TOLUENE	80	72

Table 5.2: Suzuki coupling reaction conditions for reaction between Ru(tpy)(tpy-ph-Br)$[PF_6]_2$ and 1-mercapto-4-boronic acid benzene

Reactions were carried out at 60°C, 80°C and 90°C, using different catalysts and different solvents. Two different catalysts have been screened: Pd $(PPh_3)_4$ and Pd $(OAc)_2$ and three different solvents: DMF, a mixture of DMF/water and toluene.

Reactions in toluene show some technical problems, such as poor solubility of the starting material. This problem was solved using DMF or a mixture of DMF/H_2O. After 24 /30 hours, the percentage of starting material remaining was 58%. After 48 hours the percentage decreased from 58 to 45% and the NMR spectrum, confirmed the presence of new signals (multiplet) between 7.20 and 7.45 ppm, but coupling did not occur even on prolonged heating for 72 hours for any of the reaction condition shown in Table 5.2. The multiplets (2 triplets and doublets) between 7.20 and 7.50 ppm suggest that biphenyl compounds were produced probably from competitive homocoupling reactions involved phenyl boronic acid. This suggests that the limiting factor for reactions with 1-mercapto-4-phenyl-boronic acid is the use of an unprotected thiol which may decompose and form disulphide bonds. Possible evidence for this is the presence of multiplets at 7.23 and 7.35 ppm and eventually thioether linkages.

5.5.4 Suzuki coupling reactions: (tpy-ph-Br) and protected thiol boronic acid

To overcome the problem of the decomposition of the unprotected free thiol 1-mercapto-4-boronic acid benzene, 1-methyl-mercapto-4-boronic acid benzene was used as starting material. The ligand (tpy-ph-Br) was reacted with the protected boronic acid (see Figure 5.9) under the same conditions investigated for the unprotected analogue.

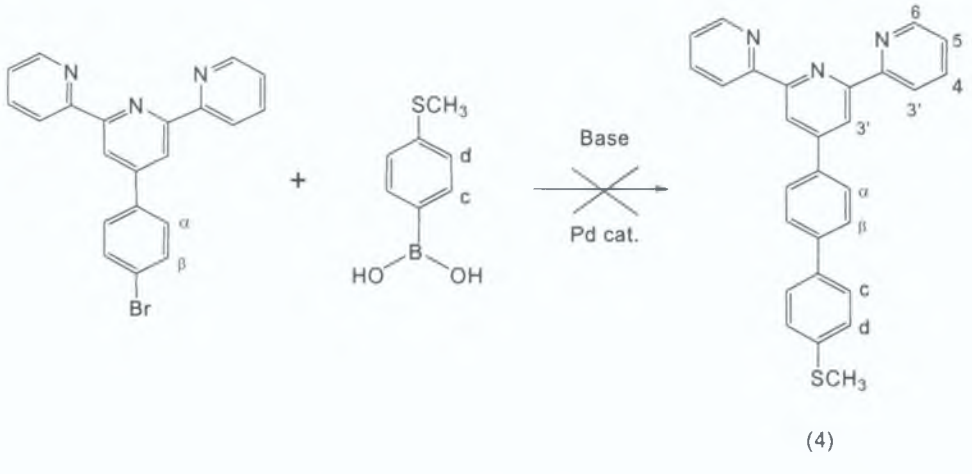

(4)

Figure 5.9: Scheme of Suzuki coupling reaction between (tpy-ph-Br) and and 1-methyl-mercapto-4-boronic acid benzene

The reaction was carried, using 1 equivalent of terpyridine ligand and a slight excess of boronic acid (1.1 equivalents) and an excess of base (12 equivalents of K_2CO_3 or Na_2CO_3). Two different catalyst were tested: Pd $(PPh_3)_4$ and Pd $(OAc)_2$ In Table 5.3 the reaction conditions used for Suzuki coupling reactions between the ligand (tpy-ph-Br) and 1-methyl - mercapto-4-boronic acid benzene are listed.

REACTION	CATALYST	BASE	SOLVENT	TEMP. (°C)	TIME (h)
31	$Pd(PPh_3)_4$	K_2CO_3	DMF	80	24
32	$Pd(PPh_3)_4$	K_2CO_3	DMF	80	48
33	$Pd(PPh_3)_4$	K_2CO_3	DMF	80	72
34	$Pd(PPh_3)_4$	Na_2CO_3	DMF	80	24
35	$Pd(PPh_3)_4$	Na_2CO_3	DMF	80	48
36	$Pd(PPh_3)_4$	Na_2CO_3	DMF	80	72
37	$Pd(PPh_3)_4$	K_2CO_3	TOLUENE	60	24
38	$Pd(PPh_3)_4$	K_2CO_3	TOLUENE	60	48
39	$Pd(PPh_3)_4$	K_2CO_3	TOLUENE	60	72
40	$Pd(PPh_3)_4$	Na_2CO_3	TOLUENE	60	48
41	$Pd(PPh_3)_4$	Na_2CO_3	TOLUENE	60	72
42	$Pd(OAc)_2$	K_2CO_3	DMF/H_2O	90	24/30
43	$Pd(OAc)_2$	K_2CO_3	DMF/H_2O	90	48
44	$Pd(OAc)_2$	K_2CO_3	DMF/H_2O	90	72
45	$Pd(OAc)_2$	Na_2CO_3	DMF/H_2O	90	24/30
46	$Pd(OAc)_2$	Na_2CO_3	DMF/H_2O	90	48
47	$Pd(OAc)_2$	Na_2CO_3	DMF/H_2O	90	72
48	$Pd(OAc)_2$	K_2CO_3	DMF	60	24/30
49	$Pd(OAc)_2$	K_2CO_3	DMF	60	48
50	$Pd(OAc)_2$	K_2CO_3	DMF	60	72
51	$Pd(OAc)_2$	Na_2CO_3	DMF	60	24/30
52	$Pd(OAc)_2$	Na_2CO_3	DMF	60	48
53	$Pd(OAc)_2$	Na_2CO_3	DMF	60	72
54	$Pd(OAc)_2$	K_2CO_3	TOLUENE	80	24/30
55	$Pd(OAc)_2$	K_2CO_3	TOLUENE	80	48
56	$Pd(OAc)_2$	Na_2CO_3	TOLUENE	80	24/30
57	$Pd(OAc)_2$	Na_2CO_3	TOLUENE	80	48

Table 5.3: Suzuki coupling reaction conditions for reaction between (tpy-ph-Br) and 1-methyl-mercapto-4-boronic acid benzene

The solution was first carefully deaerated with argon, for 20 minutes before adding the catalyst. In the course of the preparation, three solvent schemes were used: toluene, DMF, DMF/H_2O. In the DMF/H_2O mixture, the ligand showed very good solubility. The reaction was carried out at 80 °C for 24, 48 and 72 hours. However, the same results were obtained as observed for the unprotected mercapto boronic acid (see reaction scheme Figure 5.7). Initially the reaction was stopped after 24 hours and the product obtained was purified using a chromatography column in silica gel (TLC in acetonitrile-saturated aqueous NaCl-H_2O, 14:2:1 volumetric ratios). A red spot was isolated and the ^{1}H-NMR spectrum in DMSO suggested that the starting material (tpy-ph-Br) was still present and that in particular H^{β} and H^{α} signals do not shift as it expected changing the Br into a phenyl system. No signals for the hydrogen phenyls expected after coupling reaction were observed after 24 hours and after 48 hours.

5.5.5 Suzuki coupling reactions: Ru(tpy)(tpy-ph-Br)[PF_6]$_2$ and a protected thiol boronic acid

The same reactions were carried out using the complex: Ru(tpy)(tpy-ph-Br)[PF_6]$_2$, as starting material, (see reaction scheme Figure 5.10).

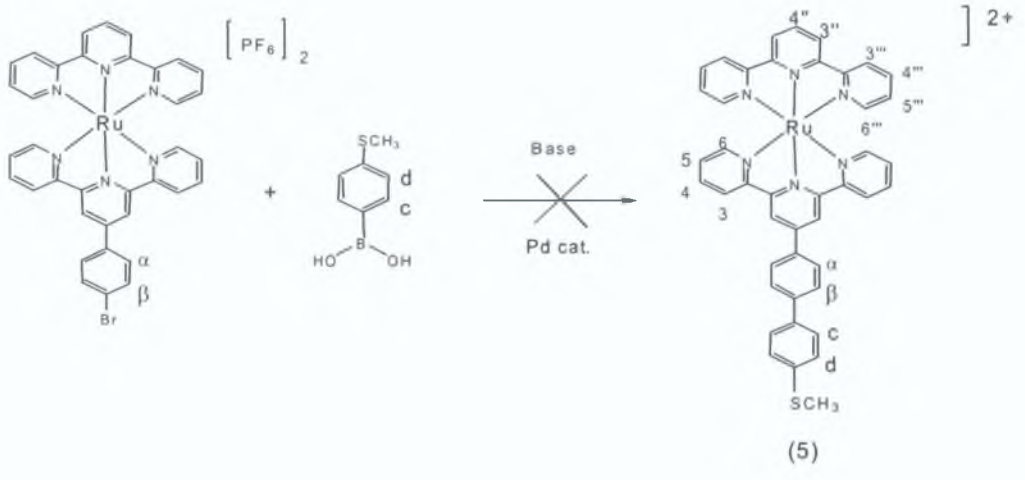

Figure 5.10: Scheme of Suzuki coupling reaction between Ru(tpy)(tpy-ph-Br)[PF_6]$_2$. and and 1-methyl-mercapto-4-boronic acid benzene

Unfortunately, also using the ruthenium terpyridine complex, no positive results were obtained. Only the characteristic signals of the ruthenium complex starting material have been observed in the ^{1}H-NMR spectrum: two doublet at 8.69 and 8.55 ppm respectively for H^3 and H^6, two triplet for H^4 at 7.80 and for H^5 at 7.40 ppm and a singlet for $H^{3'}$ at 9.10 ppm. Using the reaction reported in Figure 5.10, several conditions have been tested and they are reported below in Table 5.4.

REACTION	CATALYST	BASE	SOLVENT	TEMP. (°C)	TIME (h)
58	$Pd(PPh_3)_4$	K_2CO_3	DMF	80	27/30
59	$Pd(PPh_3)_4$	K_2CO_3	DMF	80	48
60	$Pd(PPh_3)_4$	K_2CO_3	DMF	80	72
61	$Pd(PPh_3)_4$	Na_2CO_3	DMF	80	24/30
62	$Pd(PPh_3)_4$	Na_2CO_3	DMF	80	48
63	$Pd(PPh_3)_4$	Na_2CO_3	DMF	80	72
64	$Pd(PPh_3)_4$	K_2CO_3	DMF	80	72
65	$Pd(PPh_3)_4$	K_2CO_3	TOLUENE	60	27/30
66	$Pd(PPh_3)_4$	K_2CO_3	TOLUENE	60	48
67	$Pd(PPh_3)_4$	K_2CO_3	TOLUENE	60	72
68	$Pd(OAc)_2$	K_2CO_3	DMF/H_2O	90	30
69	$Pd(OAc)_2$	K_2CO_3	DMF/H_2O	90	48
70	$Pd(OAc)_2$	K_2CO_3	DMF/H_2O	90	72
71	$Pd(OAc)_2$	Na_2CO_3	DMF/H20	90	24/30
72	$Pd(OAc)_2$	Na_2CO_3	DMF/H20	90	48
73	$Pd(OAc)_2$	Na_2CO_3	DMF/H20	90	72
74	$Pd(OAc)_2$	K_2CO_3	TOLUENE	80	27/30
75	$Pd(OAc)_2$	K_2CO_3	TOLUENE	80	48
76	$Pd(OAc)_2$	K_2CO_3	TOLUENE	80	72

Table 5.4: Suzuki coupling reaction conditions for reaction between Ru(tpy)(tpy-ph-Br)$[PF_6]_2$ and 1-methyl-mercapto-4-boronic acid benzene

The reaction described in fig. 5.10 was carried out at 60°C, 80°C and 90°C, using different Pd catalysts and different solvents to optimise the reaction conditions. No differences between $Pd(OAc)_2$ and $Pd(PPh_3)_4$ have been observed. Difficulties with the solubility of the ruthenium complex suggested DMF and the mixture DMF / H_2O as the best solvents for the reaction.

The solution was stirred and heated for 24, 48 and 72 hours, but no considerable differences have been found. The methyl-protected group does not seem to improve the reaction. It seems that under these conditions, cross coupling reaction is taking place.

5.6. Synthesis of new protected thiol boronic acid compound for Suzuki coupling reactions

Two hypotheses have been suggested to explain the above results:

- Firstly the Pd catalyst may quickly decompose and the decomposition reaction becomes competitive with the cross-coupling process. In this case, the absence of hydrogens H^c and H^d (hydrogens of the boronic acid), may be easily justified
- Secondly the Pd catalyst may quickly react with free terpyridine ligand to give ligand exchange. Under these conditions, the catalyst is deactivated and no coupling mechanism is favoured. In spite of that, several Pd catalysed Suzuky cross-coupling reactions between organoboron acids and aryl halides have proved to be quite effective methods for making the C-C single bonds of biaryls compounds.
- Thirdly the rather limited number of commercially available boronic acids may represent one limit of carrying out these reactions. For that reason, novel protected thiol boronic compounds have been synthesised. For example, t-butyldimethylsilane and triphenylmethyl groups have been bond to the sulphur atom, to form novel boronic acids.

Three novel boronic compounds (see Figure 5.11): 4-[(Dimethyl – terbutyl – silyl) thio]–boronic acid benzene, 4-[(Dimethyl – terbutyl – silyl) thio] –pinacol boronic acid benzene and 4-(mercapto)-1-pinacol boronic acid benzene have been isolated and the synthetic procedures are described in Section 5.3. The advantage of these groups is that they could easily be protected simply by adding CF_3COOH [33]. The synthesis of two others boronic compounds has been investigated: 4-[(triphenylmethyl) thio] – phenyl boronic acid (11) and 4,4,5,5-tetramethyl-2-[4-[(triphenylmethyl) thio]phenyl]-1,3,2-dioxaborolane (12), but unfortunatly it was impossible to isolate pure products. These novel protected boronic acids compounds

(Figure 5.11) were reacted with $[Ru(tpy\text{-}ph\text{-}Br)(tpy)][PF_6]_2$ and $[Co(tpy\text{-}ph\text{-}br)_2][PF_6]_2$ complexes, under Suzuki coupling conditions.

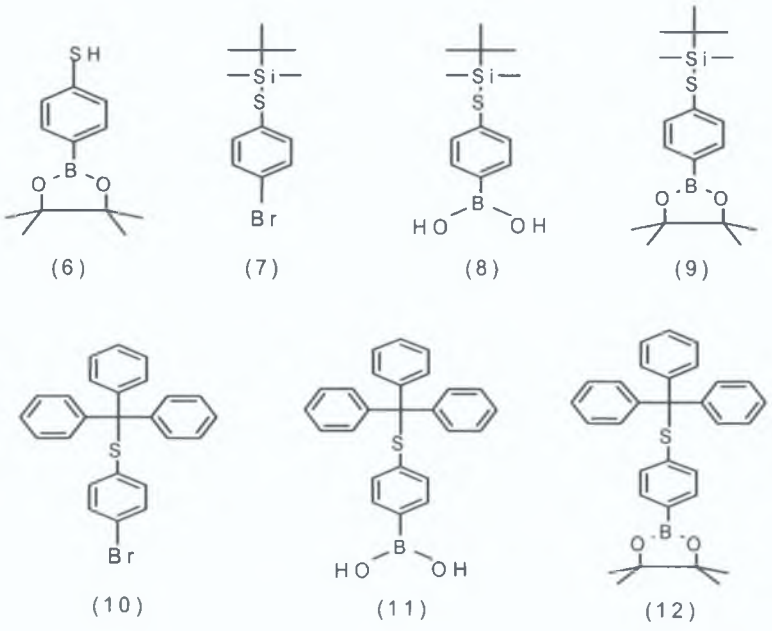

Figure 5.11: Structures of protected boronic acid prepared

5.6.1 Synthesis of 4-(4,4,5,5-tetramethyl-1,3,2-dioxaborolan-2-yl)-thiophenol (6)

4-(4,4,5,5-tetramethyl-1,3,2-dioxaborolan-2-yl)-thiophenol has been synthesised by reacting 1 equivalent of 1-mercapto-4-boronic acid benzene and a slight excess (1.1 equivalent) of pinacol in dry THF solution (see Figure 5.12).

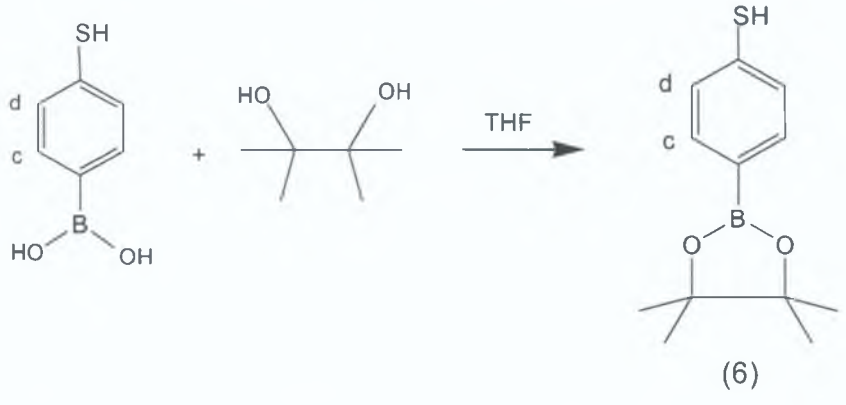

Figure 5.12: Reaction scheme for the synthesis of 4-(4,4,5,5-tetramethyl-1,3,2-dioxaborolan-2-yl)-thiophenol

Purification of the product was carried out by column chromatography in silica gel using dichloromethane as eluent. A pink band was isolated to afford white pure crystals. Synthesis and characterisation are described in Chapter 5.2.

5.6.2 Synthesis of [4 - [[(1,1-dimethyl ethyl) dimethyl silyl]thio]1 - bromo] benzene (7)

The synthesis of the starting material: 4-[(Dimethyl – terbutyl – silyl) thio]-1-bromo benzene was initially quite problematic. Several conditions were investigated, but finally resulting in dry THF, 1 equivalent of 4-mercapto-1-bromo benzene, 1.5 equivalent of Dimethyl-terbutyl-silyl chloride and a slight excess of NaH (see reaction scheme Figure 5.13) was used as the preferred method.

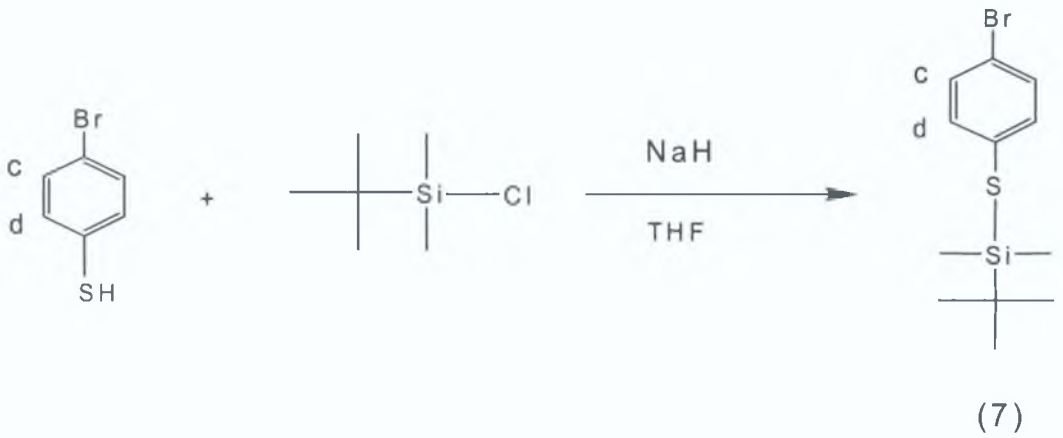

(7)

Figure 5.13: Reaction scheme for the synthesis of 4-[(Dimethyl – terbutyl – silyl) thio]-1-bromo benzene

The reaction mixture was stirred at room temperature for 14 hours. A yellow oil was obtained and distillation at 90 °C was carried out to purify the product. A dark yellow gum was obtained, since the product decomposed during the distillation process. However, when the product was purified by column chromatography in dichloromethane, white crystals were obtained.

5.6.3 Synthesis of compound (8): [4-[[(1,1-dimethylethyl)dimethylsilyl]thio]phenyl]-boronic acid

[4-[[(1,1-dimethylethyl)dimethylsilyl]thio]phenyl]-boronic acid (8) has been synthesised by reacting compound (7) with triisopropyl borate in dry THF solution as shown in Figure 14.

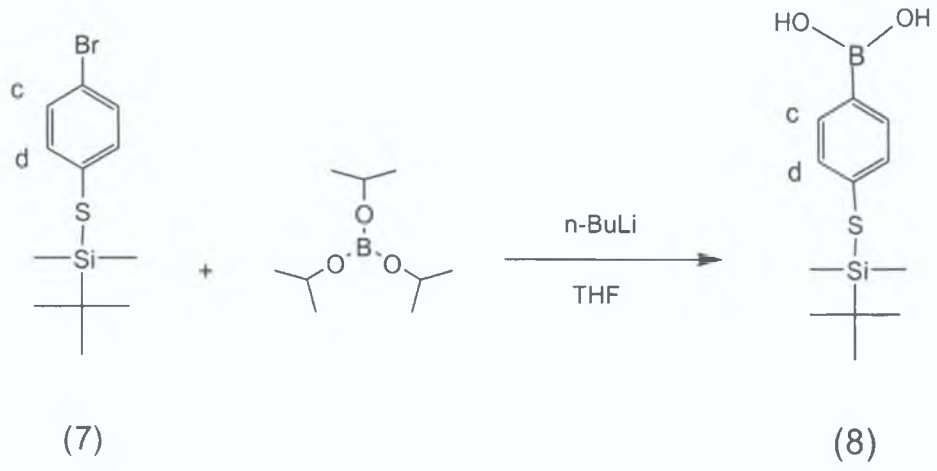

Figure 5.14: Reaction scheme for the synthesis of [4-[[(1,1-dimethylethyl)dimethylsilyl]thio]phenyl]-boronic acid

1 equivalent of the pure product (7) was reacted under argon, with 5.20 equivalent of triisopropyl borate in dry THF in the presence of N-butyl lithium (see Figure 5.14). The first step of the reaction was carried out at –78 °C, under stirring, for 2 hours, then, the reaction mixture was stirred at -20°C, for an another couple of hours. The product obtained was extracted with diethyl ether/H_2O; the organic phase was washed, dried and concentrated. Recrystallisation from diethyl ether/pentane did not afford the pure product. A different procedure was then investigated. Instead of adding triisopropyl borate to 4-mercapto-1-bromo benzene, n-butyl lithium was slowly added dropwise and only afterwards, triisopropyl borate was added.

Using this procedure, a yellow oil was obtained and recrystallisation from diethyl ether/pentane did afford white small crystal of pure product.

5.6.4 Synthesis of 4,4,5,5-tetramethyl-2 [4-(1,1-dimethylethyl) dimethylsilyl) phenyl]-1,3,2 - dioxaborolane (9)

Two different procedures have been investigated for the synthesis of 4,4,5,5-tetramethyl-2 [4-(1,1- dimethylethyl) dimethylsilyl) phenyl]-1,3,2 - dioxaborolane (9). In the first reaction, the protected thiol boronic acid was reacted with pinacol (ratio 1:2), in THF, under stirring, for 1 hour at room temperature (see Figure 5.15). Column chromatography in silica gel, using dichloromethane as eluent, did not afford any pure product. The ^{1}H-NMR of the fraction isolated does not show any evidence for the presence of the 15 H of the Dimethyl – terbutyl – silyl group.

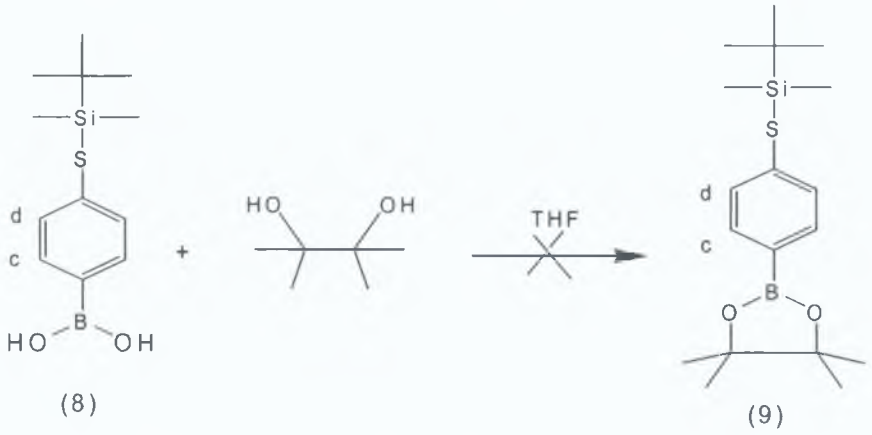

Figure 5.15: Reaction scheme for the attempted synthesis of 4,4,5,5-tetramethyl-2 [4-(1,1- dimethylethyl) dimethylsilyl) phenyl]-1,3,2 - dioxaborolane

The second procedure investigated, afforded the desired product. 1 equivalent of the pinacol protected boronic acid was reacted with 1.5 equivalent of Dimethyl-terbutyl-silyl chloride, in presence of a slight excess of NaH. The same reaction conditions described for the synthesis of (7) were used to prepare 4,4,5,5-tetramethyl-2 [4-(1,1-dimethylethyl) dimethylsilyl) phenyl]-1,3,2 – dioxaborolane (see reaction scheme in Figure 5.16).

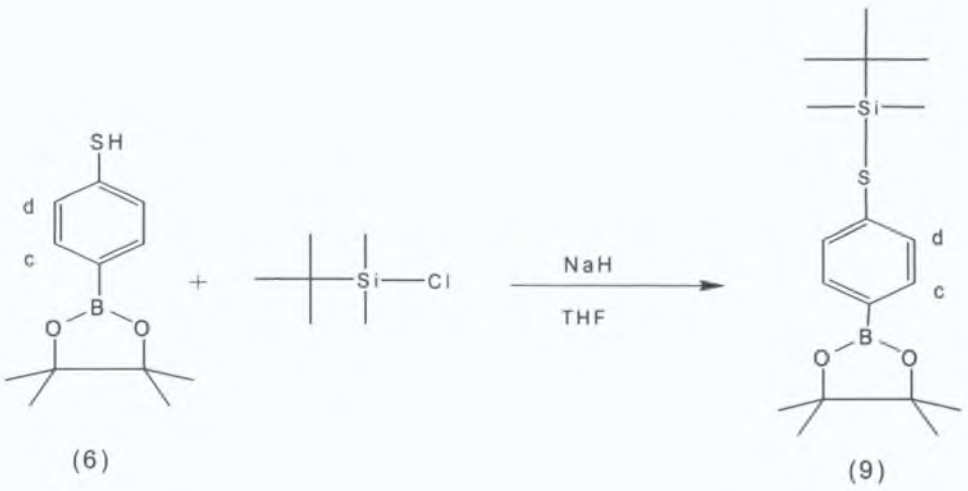

Figure 5.16: Reaction scheme for the synthesis of 4-[(Dimethyl – terbutyl – silyl) thio]–pinacol boronic acid benzene

5.6.5 Attempted synthesis of compound: [4-[(triphenylmethyl)thio]phenyl]-boronic acid (11)

Synthesis of another boronic compound has been investigated but no pure product could be isolated. The staring material 4-[(triphenylmethyl) thio]-1-bromo benzene (10) was synthesised from 1 equivalent of 4-mercapto-1-bromo benzene, 1 equivalent of triphenyl-methyl chloride and 1 equivalent of pyridine (see below Figure 5.17)

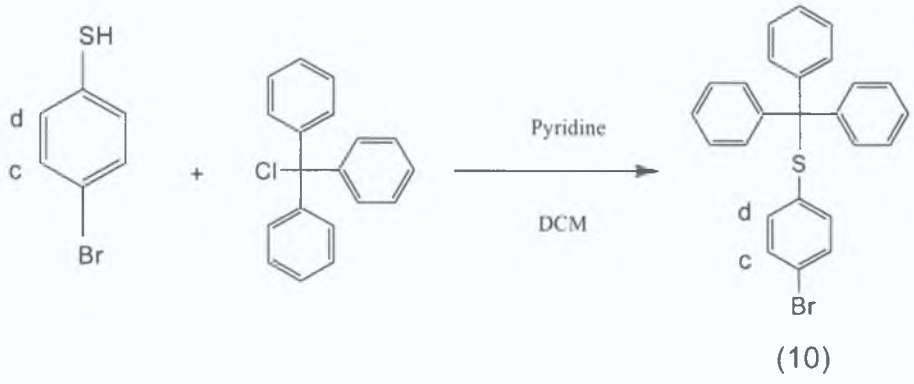

Figure 5.17: Reaction scheme for the synthesis of [4-[(triphenylmethyl)thio][(1-bromo)]benzene

Purification of the compound (10) obtained from the reaction, was carried out by column chromatography in silica gel, using dichloromethane as eluent. In Figure 5.18 the reaction scheme for the synthetic approach used for the preparation of 4-[(triphenylmethyl) thio] – phenyl boronic acid is outlined.

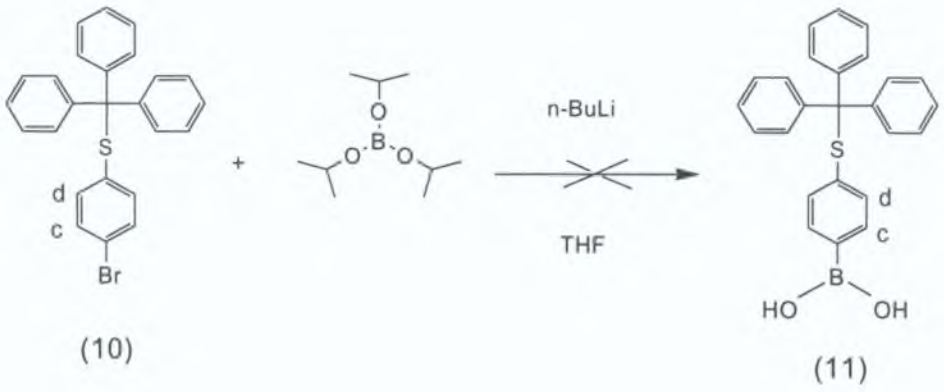

Figure 5.18: Reaction scheme for the synthesis of [4-[(triphenylmethyl)thio]phenyl]-boronic acid

The conditions described are the same as described for the synthesis of compound (8) (see Figure 5.14). 1 equivalent of pure compound (10) was reacted under argon, with 5.20 equivalent of triisopropyl borate in dry THF. N-butyl lithium was slowly added dropwise and only afterwards, triisopropyl borate was added. The first step of the reaction was carried out at –78 °C, under stirring, for 2 hours, then, the reaction mixture was stirred at -20°C, for two hours. A pale yellow oil was obtained and recrystallisation from diethyl ether/pentane did afford white small crystal of pure product.

5.6.6 Attempted synthesis of 4,4,5,5-tetramethyl-2-[4-[(triphenylmethyl) thio]phenyl]-1,3,2-dioxaborolane (12)

Synthesis of the above boronic compound used, was also investigated but no pure product could be isolated. Reaction scheme is described in Figure 5.19.

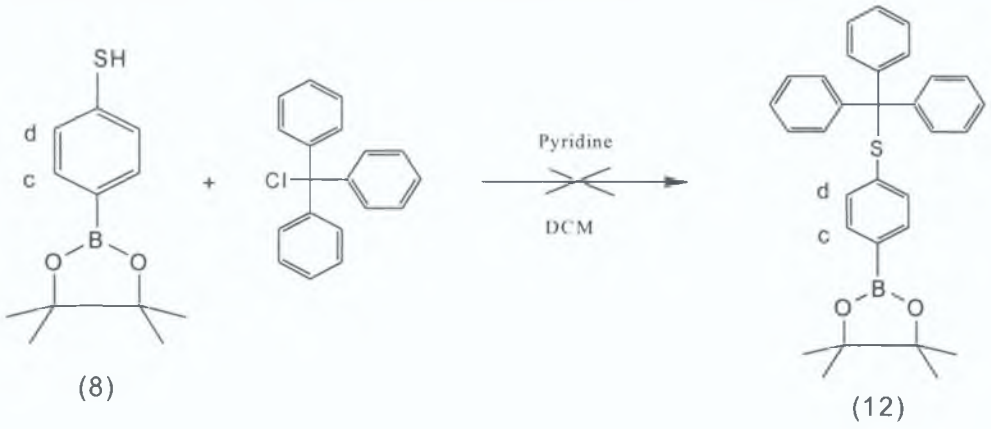

Figure 5.19: Reaction scheme for the synthesis of 4,4,5,5-tetramethyl-2-[4-[(triphenylmethyl) thio]phenyl]-1,3,2-dioxaborolane

The product obtained after extraction from diethyl ether/H_2O was purified by column in dichloromethane. The ^{1}H-NMR of the fraction isolated does not show signals of the 15 hydrogen atoms of the phenyls, but only the signals of the H^{β} and H^{α} of the phenyl boronic group and the 12 H of the pinacol group.

5.7. Attempted synthesis of Ru(II) and Co(II) modified complexes

Compounds (6), (8) and (9), have been employed for Suzuki coupling reactions and were reacted with tepryridine metal complexes, $[Ru(tpy\text{-}ph\text{-}Br)(tpy)][PF_6]_2$ and $[Co(tpy\text{-}ph\text{-}Br)_2][PF_6]_2$. The reaction investigated for $[Ru(tpy\text{-}ph\text{-}Br)(tpy)][PF_6]_2$ is reported below in Figure 5.20. General synthetic procedures are described in Section 5.4.

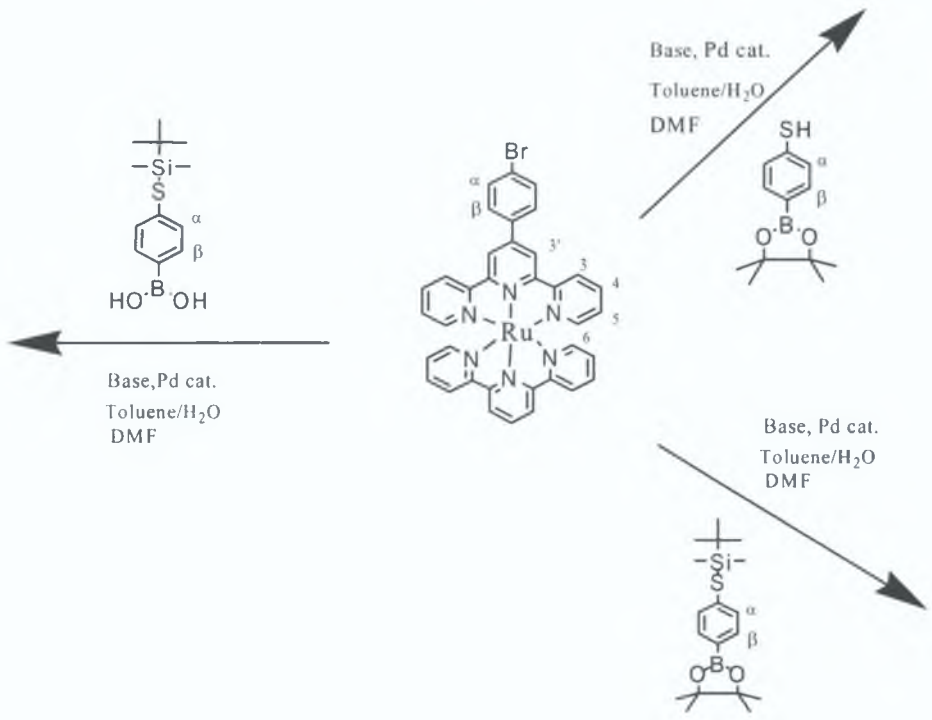

Figure 5.20: Scheme of Suzuki coupling reaction using [Ru(tpy)(tpy-ph-Br)[PF6]2 and boronic compounds (6), (8) and (9)

The boronic compounds were reacted with $[Ru(tpy)(tpy\text{-}ph\text{-}Br)][PF_6]_2$ complex, under the conditions described in Table 5.5. The same reactions have been investigated using the cobalt complex: $[Co(tpy\text{-}ph\text{-}Br)_2][PF_6]_2$, which was obtained by reacting 1 equivalent of $CoCl_2$ $6H_2O$ and 2 equivalents of (tpy-ph-Br) in a mixture

of EtOH/H_2O solution and finally precipitate from a saturated solution of NH_4PF_6. Synthetic procedures for Suzuki coupling using $[Co(tpy\text{-}ph\text{-}Br)_2][PF_6]_2$, complex as starting material, are described in Figure 5.21.

REACTION	CATALYST	BASE	SOLVENT	TEMP. (°C)	TIME (h)
77	$Pd(PPh_3)_4$	Na_2CO_3	DMF/H_2O	80	24/30
78	$Pd(PPh_3)_4$	Na_2CO_3	DMF/H_2O	80	48
79	$Pd(PPh_3)_4$	Na_2CO_3	DMF/H_2O	80	72
80	$Pd(OAc)_2$	Na_2CO_3	DMF/H_2O	60	24/30
81	$Pd(OAc)_2$	Na_2CO_3	DMF/H_2O	60	48
82	$Pd(OAc)_2$	Na_2CO_3	DMF/H_2O	60	72
83	$Pd(OAc)_2$	Na_2CO_3	DMF/H_2O	80	24/30
84	$Pd(OAc)_2$	Na_2CO_3	DMF/H_2O	80	48
85	$Pd(OAc)_2$	Na_2CO_3	DMF/H_2O	80	72

Table 5.5: $[Ru(tpy)(tpy\text{-}ph\text{-}Br)[PF_6]_2$ and novel boronic compounds (6), (8), (9): Suzuki coupling reaction conditions

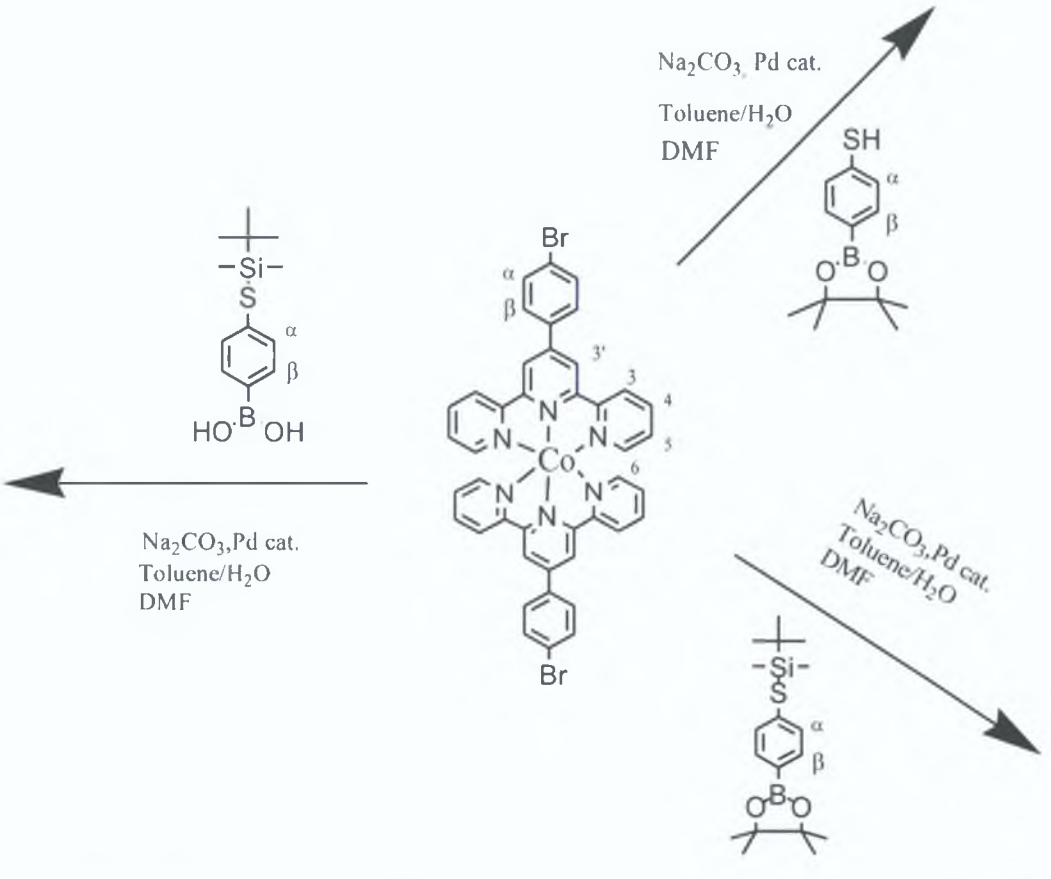

Figure 5.21: Scheme of Suzuki coupling reaction using $[Os(tpy\text{-}ph\text{-}Br)_2[PF_6]_2$ and boronic compounds (6), (8) and (9)

The three novel boronic compounds (6), (8) and (9), were reacted with the cobalt complex, under the conditions described in Table 5.6.

REACTION	CATALYST	BASE	SOLVENT	TEMP. (°C)	TIME (h)
86	$Pd(PPh_3)_4$	Na_2CO_3	DMF/H_2O	80	24/30
87	$Pd(PPh_3)_4$	Na_2CO_3	DMF/H_2O	80	48
88	$Pd(PPh_3)_4$	Na_2CO_3	DMF/H_2O	80	72
89	$Pd(OAc)_2$	Na_2CO_3	DMF/H_2O	60	24/30
90	$Pd(OAc)_2$	Na_2CO_3	DMF/H_2O	60	48
91	$Pd(OAc)_2$	Na_2CO_3	DMF/H_2O	60	72
92	$Pd(OAc)_2$	Na_2CO_3	DMF/H_2O	80	24/30
93	$Pd(OAc)_2$	Na_2CO_3	DMF/H_2O	80	48
94	$Pd(OAc)_2$	Na_2CO_3	DMF/H_2O	80	72

Table 5.6: $[Co(tpy\text{-}ph\text{-}Br)_2[PF_6]_2$ and novel boronic compounds (6), (8), (9): Suzuki coupling reaction conditions

Under the same conditions, no relevant different behaviour has been observed using two different metal centre systems. The reactions were carried out in DMF/H_2O at 80 °C, using 1 equivalent of ligand and 1 equivalent of boronic acid in presence of an excess of base (Na_2CO_3). Two different catalyst have been tested: Pd $(PPh_3)_4$ and Pd $(OAc)_2$. At the very first step of the reaction, the solution was carefully degassed for 20 minutes before adding the catalyst. The ruthenium complex did not show big problems of solubility, whereas different behaviour for the cobalt compound was observed. It required stirring and heating for 30 minutes before dissolving completely in DMF. No formation of any product was observed after 4, 8 and 12 hours (TLC in acetonitrile-saturated aqueous NaCl-H_2O (14:2:1 volumetric ratios). Initially, the reaction was stopped after 24 hours and the product obtained was purified using chromatography on silica gel. A red spot was then isolated. Even using three different boronic compounds, some common result have been observed: the ^{1}H-NMR (DMSO) spectra of the isolated fraction always showed the presence of the starting material (metal terpyridine complex). After reaction with the Ru (II) complex no shift of the signals of (tpy-ph-Br) have been observed; 9.10 (s, $H^{3'}$), 8.81 (d,H^{β}), 8.69 (d, H^3), 8,55 (d, H^6), 8,18 (d, H^{α}), 7.90 (m, H^4), 7.20 (m, H^5). No signals of the second phenyl, as expected from the introduction of C-C coupling reaction, have been

observed. Similar results have been observed for the cobalt complex; the ^{1}H-NMR showed clearly the signal of the starting material. In particular, it was noticed that by using 4-(mercapto)-1-pinacol-boronic acid benzene, no signal of the free SH (singlet between 2 and 3.5 ppm) has been observed. This confirmed what was reported for reactions carried out with 1-mercapto-4-boronic acid benzene (Figure 5.7 and 5.8); the SH group can not perform Suzuki coupling reactions, under the conditions investigated; it has been suggested that SH group, because of its high instability, reacts quickly, probably to make disulphide bonds or others possible compounds as thioethers through solvent interactions, but does not give any contribution for the formation of C-C bond expected after coupling reactions.

Different problems have been observed using the protecting group dimethyl-terbutyl-silyl for the thiol boronic acid. Unfortunately reactions between ruthenium or cobalt complex and compounds (6), (8) and (9) did not afford the expected product. It has been suggested that the protecting group can quickly react with the base Na_2CO_3 and in this case it will not act as an ideal protected group for the Suzuki coupling. Also the catalyst may be involved in collateral reactions, more competitive then the Suzuki coupling and it may easily been deactivated (hypothesis also postulated for the methyl protected boronic acid). The ^{1}H-NMR (acetonitrile) showed signals of the starting material: 9.10 (s, $H^{3'}$), 8.81 (d, H^{β}), 8.69 (d, H^3), 8.55 (d, H^6), 8.42 (t, $H^{4''}$), 8.18 (d, H^{α}), 7.20 (m, H^5). Other signal identified as multiplets appeared at 7.20 and 7.45 ppm, and they were attributed to some of the hypothetical secondary reactions that seem to be involved with the protected group. These peaks disappeared after purification with column chromatography. The same procedure has been used for the reaction between the cobalt complex and the (8) and (9) compounds. After chromatography column in silica gel the product showed a similar ^{1}H-NMR (d^3-acetonitrile): 8.83 (s, $H^{3'}$), 8.78 (d, H^6), 8.69 (d, H^3), 8.15 (t, H^4), 7.90 (d, H^{β}), 7.82 (d, H^{α}), 7.48 (t, H^5). Even in this case for the rough product few multiplets peaks have been observed in the range of 7.10 and 7.40 ppm, but they disappeared completely after purification with column chromatography.

5.8 Conclusion

Several Suzuki coupling reactions have been investigated unfortunately without success. The (tpy-ph-Br) system as a free ligand and in different metal complexes

systems has been reacted with a number of boronic acid compounds. Only two of the boronic compounds used for in this thesis are commercially available form Sigma Aldrich: 1-mercapto-4-boronic acid benzene and the 1-methyl-4-mercapto-bornic acid benzene; all the others compounds have been synthesised and characterised as showed in Section 5.2. No formation of C-C bond as a consequence of cross coupling reactions has been observed under the conditions investigated.

It has been suggested that no free thiol group could be consider ideal group for these type of Suzuki coupling. Two different boronic compounds containing free SH group have been used: 1-mercapto-4-boronic acid benzene and 4-(4,4,5,5-tetramethyl-1,3,2-dioxaborolan-2-yl)-thiophenol. Same behaviour has been observed for these compounds; it seems that they react very quickly to make disulphide bonds, thioethers compounds and secondary products due to solvent interactions. The presence of byproducts has been confirmed from ^{1}H-NMR spectrum (see discussion Section 5.5). Unfortunately the instability of the thiol group was not the only problem observed for these reactions.

Using protected thiol boronic acid, (for example CH_3 group), no cross coupling was observed. I was supposed that Pd catalyst may be deactivated at the very beginning of the reaction and it may be involved in some other reactions such as ligand-exchange, which were favoured with respect to the coupling one. That hypothesis can explain the presence of pure starting material always observed at the end of every reaction.

The dimethyl-terbutyl-silyl - thiol protected group, was investigated because it supposed to be easily deprotected group[31]; however no one of the Suzuki coupling reactions attempted did afford the expected product. It has been suggested that it may react quite easily with the base Na_2CO_3 (see further discussion in Section 5.7).

The most difficult aspect of the work presented in the Chapter was the search for the right conditions for cross coupling reactions. Several different conditions may be explored they involve the choice of a set of different catalysts, bases (for example, NEt_3), and a range of different protected boronic acid.

5.9 Bibliography

[1] Bigelow, W. C., Pickett, D. L., Zisman,W. A., J.Colloid. Sci., *1946*, 1, 513.

[2] Shafrin, E. G., Zisman, W. A., J.Colloid. Sci., *1949,* 4, 571.

[3] Allara, D. L., Nuzzo, R. G., Langmuir, *1985*, 1, 45.

[4] Sagiv, J., J. Am. Chem. Soc., *1980*, 102, 92.

[5] Ulman, A., An Introduction to Ultrathin Organic Films, Langmuir - Blodgett, Academic Press, *1991.*

[6] Troughton, E. B., Bain, C. D., Whitesides, G. M., Nuzzo, R. G., Allara, D. L., Porter, M. D., Langmuir *1988*, 4, 365.

[7] (a) Nuzzo, R. G., Zegarski, B. R., Dubois, L. H., J. Am. Chem. Soc., *1997,* 109, 733. (b) Bain, C. D., Troughton, E. B., Tao, Y. T., Evall, J., Whitesides, G. M., Nuzzo, R. G., J. Am. Chem. Soc., *1989*,111, 321.

[8] (a) Kane, R. S., Takayama, S., Ostuni, E., Ingber, D. E., Whitesides, G. M., Biomaterials, *1999*, 20, 2363. (b) Gasper, S., Schuhmann, W., Lauerll, T., Csoregi, E., Rev. Anal. Chem., *2002*, 21, 245. (c) Gooding, J. J., Mearns, F., Yang, W.R., Liu, J. Q., Electroanalysis *2003*, 15, 81.

[9] (a) Kim, Y. T., McCarley, R. L., Bard, A. J., J. Phys. Chem., *1992*, 96, 7416.(b) Obeng, Y. S., Laing, M. E., Friedly, A. C., Yang, H. C., Wang, D., Thustrup, E., W., Bard, A. J., Michl, J. J. Am. Chem. Soc., *1992*, 114, 9943.

[11] Young, C. Y., Pindak, R., Clark, N. A., Meyer, R. B., Phys. Rev. Lett. *1978*, 40, 773.

[12] Ulman, A., Scaringe, R., Langmuir, *1992*, 8, 894.

[13] (a) Pearson, R. G., Songstand, J., J. Am. Chem. Soc., *1967*, 89, 1827. (b) Pearson, R. G., J. Chem. Educ., *1968*, 45, 581, 643.

[14] (a) Kang, J. F., Liao, S., Jordan, R., Ulman, A., J. Am. Chem. Soc. *1998*, 120, 9662. (b) Kang, J. F., Ulman, A., Liao, S., Jordan, R., Langmuir, *1999*, 15, 2095.

[15] (a) Sabatani, E., Cohen-Boulakia, J., Bruening, M., Rubinstein, I., Langmuir, *1993*, 9, 2974.

[16] (a) Hsung, R. P., Babcock, J. R., Chidsey, C. E., Sita, L. R., Tetrahedron Lett., *1995*, 36, 4525. (b) Hsung, R., Chidsey, C. E., Sita, L. R., Organometallics, *1995*, 14, 4808.

[17] (a) Ulman, A., Chem. Rev., *1996*, 96, 1533. (b) Bishop, A. R., Nuzzo, R. G., Curr. Opin. Colloid. Interface Sci. *1996*, 1, 127.

[18] Ulman, A., Self-Assembled Monolayers of Thiols, Thin. Films Vol.24, Academic Press., San Diego, *1998*.

[19] Holmlin, R. E., Haag, R., Chabinye, M. L., Ismagilove, R. F., Cohen, A. E., Terfort, A., Rampi, M. A., Whitesides, G. M., J. Am. Chem. Soc., *2001*, 123, 5073.

[20] Garnier, F., Acc. Chem. Rev., *1999*, 32, 209.

[21] Loiseau, F., Di Pietro, C., Serroni, S., Campagna, A., Licciardello, A., Manfredi, G., Pozzi, G., Quici, S., Inorg. Chem., *2001*, 40, 6901.

[22] (a) Balzani, V., Juris, A., Venturi, S., campagna, A., Serroni, S., Chem. Rev., *1996*, 96, 759. (b) Berigelletti, F. and Flamigni, L., Chem. Soc. Rev. *2000*, 29, 1.

[23] (a) Yang, Z., Engquist, I., Wirde, M., Kauffmann, J. M., Gelius, U., Liedberg, R., Langmuir, 1997, 13, 3210. (b) Kang, J. F., Ulman, Jordan, R., Kurth, D. G., Langmuir, *1999*, 15, 5555.

[24] Swalen, J.D., Allara, D.L., Amdrade, J.D., Chandross, E.A., Garoff, S., Isrealachvili, J., McCarthy, T.J., Murray, R., Pease, R.F., Rabolt, J.F., Wynne, K.J., Yu, H., Langmuir, *1987*, 3, 932.

[25] Whitesides, G.M., Laibinis, P.E., Langmuir, *1990*, 6, 87.

[26] Rojas, M.T., Kaifer, A.E., J.Am. Chem. Soc., *1995*, 117, 5883; Bharathi, S., Yegnaraman, V., Rao, G.P., Langmuir, *1995*, 11, 666.

[27] Steinberg, S., Tor, Y., Sabatini, E., Rubinstein, I., J. Am. Chem. Soc., *1991*, 113, 5176.

[28] Hickmann, J., Ofer, D., Laibinis, P.E., Whitesides, G.M., Wrighton, M.S., Science, *1991*, 252, 688.

[29] Chidsey, C.E., D., Science, *1991*, 251, 919.

[30] Maskus, M., Abruna, D.H., Langmuir, *1996*, 12, 4455.

[31] Brikh, A., Morin, C., Journal of Organometallic Chemistry, 581, 1999, 82.

[32] Zhuravel M.A. and Nguyen, T., Tetrahedron Letters, *2001,* 42, 7925.

[33] Littke, A. F., Dai, C.; Fu, G.C., J. Am. Chem. Soc., *2000,* 122, 4020.

[34] Wolfe, J. P., Singer, A. R., Yang, B. H., Buchwald, S. L., J. Am. Chem. Soc., *1999,* 121, 9550.

[35] (a) Hlasta, D.J., Court, J. J., Tetrahedron Letters, *1989*, 30, 1773. (b) Gros, P., Fort, Y., Caubere, P., J. Chem. Soc., Perkin Trans. 1, *1997*, 3597.

[36] (a) Furukawa, N., Shibutani, T., Matsumura, K., Fujihara, H., Tetrahedron Letters, *1986*, 27, 3899. (b) Trecourt, F., Breton, G., Bonnett, V., Mongin, F., Marsais, F., Queguiner, G., Tetrahedron Letters, *1999*, 40, 4339.

[37] Kondo, Y., Shilai, M., Uchiyama, M., Sakamoto, T., J.Chem. Soc. Perkin Trans 1, *1996*, 1781.

[38] (a) Sakamoto, T., Kondo, Murata, N., Yamanaka, H., Tetrahedron Letters, *1992*, 33, 5373. (b) Sakamoto, T., Kondo, Murata, N., Yamanaka, H., Tetrahedron Letters *1993*, 49, 9713.

[39] (a) Yamamoto, Y., Yanagi, A., Chem. Pharm. Bull. *1982*, 30, 2003. (b) Yamamoto, Y., Ouchi, H.,Tanaka, T., Chem. Pharm. Bull., *1995*, 43, 1028.

[40] Klingensmith, L.M., Leadbeater, N.E., Tetrahedon Letter 44, *2003*, 765.

Chapter 6

Final discussion, Conclusion and Future Work

Chapter 6 summarises the synthetic work presented in this thesis concerning the attempted Suzuki coupling reactions and the analysis of luminescence and electrochemistry results obtained for Ru(II) and Os(II) terpyridine complexes. The properties of the subsequent mononuclear complexes are reviewed with suggestions for future studies.

6.1 Introduction

Electronic energy transfer lies at the heart of important natural phenomena such as photosynthesis[1] and practical applications such as spectral sensitisation[2]. The possibility of governing the direction of electronic energy transfer in supramolecular arrays may open the way to the design of photochemical molecular devices that may perform a variety of useful functions[3]. Individual molecules and nanoparticles may in the future perform functions in electronic circuitry currently performed by semiconductor devices. Molecular or nanoscale building blocks are hundreds of times smaller than the smallest features that can conceivably be attained using present semiconductor technology.

One of the scientific objectives of the S.U.S.A.N.A. (Supramolecular Self-Assembly of Interfacial Nanostructures) project is the preparation of switchable tunnelling junctions in which nanoparticles are linked via molecular bridges whose electron transfer barrier properties can be chemically, electrochemically or photophyisically switched. Transition metal complexes containing aromatic ligands are attractive candidates for excited state electron transfer processes in fluid solution. These complexes have octahedral structure and may be obtained with a variety of transition metal ions. In particular, in the course of this study, tridentate terpyridine type ligands have been used to obtain ruthenium, osmium and cobalt complexes capable of playing the role of photosensitizers in covalently – linked multicomponent systems. Although $[M(tpy)_2]^{2+}$ type complexes exhibit less favourable photophysical properties compared with $[M(bpy)_3]^{2+}$. The terpyridine systems were chosen because of their symmetry properties:

- $[M(tpy)_2]^{2+}$ complexes are achiral contrary to what happens for $[M(bpy)_3]^{2+}$.
- Two substituents on $[M(bpy)_3]^{2+}$ complexes may give rise to triads with cis-type geometrical arrangements, without possibility of control, whereas substituents in the 4' - positions of $[M(tpy)_2]^{2+}$ lead to triads where the two substituents lie in opposite directions with respect to the photosensitizer (trans-type arrangement).

As already mentioned in Chapter 1, in the course of this study, different approaches have been investigated:

1 Synthesis of metal complexes with thiol end group and pyridine group in terpyridine ligands.
2 Electrochemical control: low oxidation and potentials; use of osmium as metal centre to improve redox properties of the complexes.

Thiol end groups that have been well recognised as convenient systems to control charge transfer at metal electrodes [4], especially because of their flexibility in the design of molecular structures (several self-assembled monolayers have been studied [5-6] in the last few years). Synthesis of thiol - terpyridine complexes have been attempted starting from 4' - (4-bromo-phenyl) 2,2'; 6', 2" - terpyridine (tpy-ph-Br) and boronate groups by a palladium – catalysed Suzuki coupling reactions. Pyridyl groups have been used as substituents in terpyridine complexes. In particular, Ru(II) and Os(II) mixed complexes with 4' - (pyrid-4-yl) 2,2'; 6', 2" - terpyridine (py-tpy) have been synthesised and fully characterised in this thesis.
Finally, Ru(II) and Os(II) terpyridine complexes incorporating tetrazole ligand [2,6-bis-([1,2,3,4]tetrazol-5-yl)pyridine] (H_2L3) has been investigated to improve the photophysical properties of this class of complexes; in particular, Osmium was used as metal centre to improve the redox properties of the complexes (low oxidation and potentials).

6.2 Discussion

6.2.1 Attempted synthesis of thiol terpyridine complexes: linkers for self-assembled monolayers

The goal of this project was the synthesis of compounds capable of acting as junctions in which nanoparticles are linked via molecular bridges, whose electron transfer barrier properties can be used as chemical switches (see Figure 6.1).

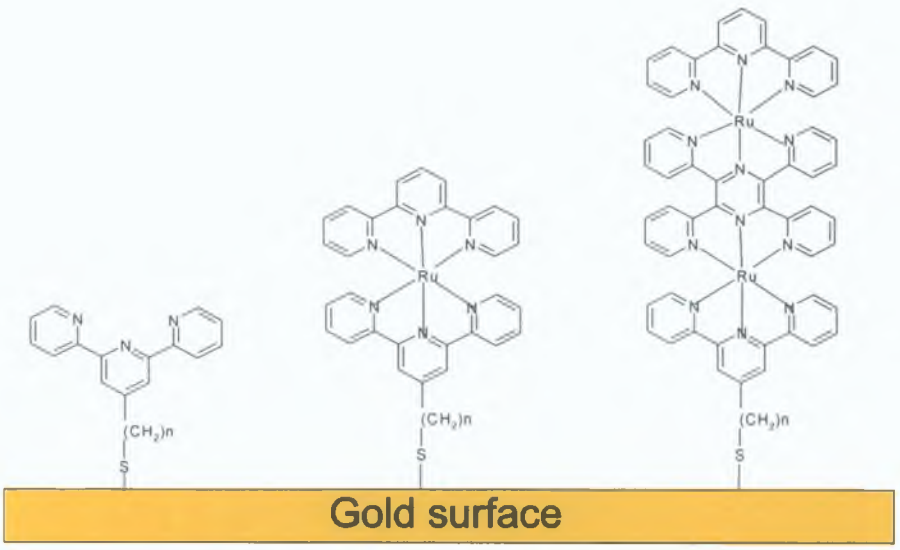

Figure 6.1: Ideal self-assembled monolayer of attempted thiol terpyridine compounds onto gold surface

As described in Chapter 5, synthetic methods for incorporating thiol functional groups to metal terpyridine complexes have been investigated. Using (tpy-ph-Br) and [Ru(tpy-ph-Br)(tpy)][PF_6]$_2$ and [Co(tpy-ph-Br)$_2$][PF_6]$_2$, as starting materials, the Suzuki coupling reaction has been attempted. The bromide compounds have been reacted with different types of boronic acid benzene: 1-mercapto-4-boronic acid benzene; 1-methyl-mercapto-4-boronic acid benzene, commercially available and a series of new substituted boronic compounds synthesised in this thesis: [4-[[(1,1-dimethylethyl)dimethylsilyl]thio]phenyl]-boronic acid; 4-(4,4,5,5-tetramethyl-1,3,2-dioxaborolan-2-yl)-thiophenol and 4,4,5,5-tetramethyl-2-[4-(1,1-dimethylethyl)dimethylsilyl)phenyl]-1,3,2dioxaborolan. No formation of C-C bond as a consequence of cross coupling reactions has been observed under the conditions investigated. Because of its high reactivity, free thiol substituted boronic compounds may not be used as starting material for the Suzuki coupling. It has been observed that SH decomposes very quickly to give disulphide and thioethers and secondary products via solvent interactions. The presence of secondary products (new signals in the range of 4-7 ppm) was confirmed with analysis of ^{1}H-NMR signals, by comparing the spectrum of the product with spectra of the staring materials. Unfortunately the instability of the thiol group was not the only problem observed during the attempted reactions. Two different

Pd catalysts and two different bases such as K_2CO_3 and Na_2CO_3, were used, without any successful.

Using protected thiol boronic acid as SCH_3 or [1,1 – dimethylethyl)dimethylsilyl] thiol, no cross coupling mechanism was observed and two different hypothesis have been formulated:

- The Pd catalyst may be deactivated at the very beginning of the reaction and may be involve in a reaction as ligand-exchange.
- When working in basic condition, interactions with the base Na_2CO_3 may occur.

To continue with Suzuki coupling reactions, many different conditions may be explored; choosing a different set of catalysts, bases (for example, NEt_3 instead of Na_2CO_3 and K_2CO_3), and new protected boronate species which can favourite cross coupling mechanism in comparison with all the other possible reactions involved.

6.2.2 Ru(II) and Os(II) terpyridine complexes: luminescence and electrochemistry

Investigation carried out on [M(tpy-X)(tpy-Y)] complexes (where X and Y are substituents in the positions 4' of the 2,2': 6', 2" – terpyridine) have shown that electron – donating (D) or electron – accepting (A) substituents may cause changes in the luminescence and electrochemical properties, whereas slight differences have been observed in the absorption spectra.

By studying the luminescence of Ru(II) and Os(II) terpyridine complexes general trends have been observed:

- The energy of the emission maximum decreases regardless of the electron accepting and donating nature of the substituent.
- Osmium terpyridine complexes are strong emitters at room temperature, whereas the analogous ruthenium complexes show strong emission only at 77 K in rigid matrix (solution of EtOH/MeOH 4/1).

As shown in Chapter 5, tetrazolate ligand is a good σ-donor and gives electron density to the metal centre (consequence red shift in the MLCT band) and vice versa, ligands such as (tpy-ph-Br) and (py-tpy) increase the electron withdrawing nature of the ligand and reduce the electron density on the metal.

Both complexes [Ru(tpy-ph-Br)(L3)(H_2O)] and [Os(tpy)(L3)(H_2O)] showed strong luminescent, with λ = 628 nm and λ = 717 nm respectively. At 298 K the luminescence lifetimes of these complexes are between 40 and 65 ns. The presence of the negatively charged ligands results in a destabilisation of the ground state and in a decrease in energy of the ^{3}MLCT based luminescence in comparison with the prototype $[Ru(tpy)_2]^{2+}$ and $[Os(tpy)_2]^{2+}$. However, despite the reduction in the energy gap, the emission lifetimes of the heteroleptic complexes are greater than the parent complexes. The substitution of a terpyridine ligand with a tetrazole moiety, dramatically extends the lifetime of the ^{3}MLCT excited states: 42 ns for [Ru(tpy-ph-Br)(L3)(H_2O)] whereas for $[Ru(tpy)_2]^{2+}$ is (0.25 ns). Similar behaviour has been noted for the analogues osmium complex. The lifetime extends from 40 ns in the $[Os(tpy)_2]^{2+}$ to 65 ns in the [Os(tpy)(L3)(H_2O)]. The protonation of one or both rings results in an increase in the emission energy. This fact is explained by a stabilisation of the ground state since the protonated ligand are weaker σ – donors than their deprotonated analogues. The effect of strong σ – donors is to raise the ligand field stabilisation energy. This results in an increase of the M(e_g) energy and consequently an increase in the ^{3}MLCT - ^{3}MC energy gap.

The different ligands used effect the energy of the emission bands, on passing from 618 nm for $[Ru(tpy)_2]$ $[PF_6]_2$, to 636 nm for [Ru(py-tpy)(tpy-ph-Br)]$[PF_6]_2$, and from 626 nm for [Ru(tpy)(tpy-ph-Br)]$[PF_6]$ to 624 nm for [Ru (tpy-ph-Br)(L3)(H_2O)]. (tpy-ph-Br) and (py-tpy) ligands increase the electron withdrawing nature of the ligand and reduce the electron density on the metal centre. Similar behaviour has been observed for osmium complexes, on passing from λ = 712 nm for $[Os(tpy)_2][PF_6]_2$, to λ = 746 nm for [Os(py-tpy)(tpy-ph-Br)]$[PF_6]_2$ and from λ = 714 nm for [Os(tpy)(tpy-ph-Br)]$[PF_6]_2$ to λ = 748 nm for $[Os(py\text{-}tpy)_2][PF_6]_2$. This behaviour may be easily explained. by observing the

nature of the ligands, σ-donor, or π-acceptor, as described for analogous ruthenium complexes.

Complex	Absorption	*Emission (r.t.)*		*Emission (77K)*
	λ, nm	λ, nm	τ^a, ns	λ, nm
$[Ru(tpy)_2][PF_6]_2$	474		0.25	618
$[Ru(tpy)(tpy\text{-}ph\text{-}Br)][PF_6]_2$	490	631		626
[Ru[2,6-(2,3-ph-4-CH_3-pyrazol)py](tpy)$[PF_6]_2$	486			602
$[Ru(tpy\text{-}ph\text{-}Br)(L3)(H_2O)]$	485	628	42	624
$[Ru(py\text{-}tpy)(tpy\text{-}ph\text{-}Br)][PF_6]_2$	495			636
$[Ru(py\text{-}tpy)_2][PF_6]_2$	498			670
$[Os(tpy)_2][PF_6]_2$	477, 657	712		689
$[Os(tpy)(tpy\text{-}ph\text{-}Br)][PF_6]_2$	488	714	144	
[Os[2,6-(2,3-ph-4-CH_3-pyrazol)py](tpy)$[PF_6]_2$	490	718	55	
$[Os(tpy)(L3)(H_2O)]$	478	698	64	
$[Os(py\text{-}tpy)(tpy\text{-}ph\text{-}Br)][PF_6]_2$	498	746		
$[Os(py\text{-}tpy)_2][PF_6]_2$	502	748	62	

Table 6.1: Absorption and luminescence data for ruthenium and osmium terpyridine complexes; (a): *Luminescence emission lifetime in deaerated acetonitrile*

Electrochemical behaviour shows that:

- Electron accepting groups stabilise the LUMO π* ligand orbitals more than the HOMO $\pi(t_{2g})$ metal orbital.
- Electron – donor groups destabilised the HOMO $\pi(t_{2g})$ metal orbitals more than the LUMO π* ligand orbitals.

The cyclic voltammetric data for the monomeric complexes investigated, exhibited one metal-based oxidation at positive potentials corresponding to the

M(II/III) couple. In the negative region, the redox processes observed were sequential ligand based reductions.

Complex	E° (V vs Ag/Ag^+)*		
$[Ru(tpy)_2][PF_6]_2$	+1.23	-1.25	-1.51
[Ru (py-tpy)$_2$][PF_6]$_2$	+1.07	-1.44	-1.68
[Ru(tpy)(tpy-ph-Br)][PF_6]$_2$	+1.06	-1.44	-1.69
[Ru(py-tpy)(tpy-ph-Br)][PF_6]$_2$	+1.04	-1.52	-1.80
[Ru(tpy-ph-Br)(L3)(H_2O)]	+1.02	-1.21	
[Ru[2,6-(2,3-ph-4-CH_3-pyrazol)py](tpy)[PF_6]$_2$	+1.08	-1.57	-1.79
[Os(tpy)$_2$][PF_6]$_2$	+0.73	-1.47	-1.76
[Os(py-tpy)$_2$][PF_6]$_2$	+0.67	-1.43	-1.70
[Os(tpy)(tpy-ph-Br)][PF_6]$_2$	+0.65	-1.44	-1.75
[Os(py-tpy)(tpy-ph-Br)][PF_6]$_2$	+0.63	-1.53	-1.87
[Os(tpy)(L3)(H_2O)]	+0.40	-1.33	-1.75
[Os[2,6-(2,3-ph-4-CH_3-pyrazol)py](tpy)[PF_6]$_2$	+0.48	-1.65	

Table 6.2: Formal potentials for ruthenium and osmium terpyridine complexes at a platinum electrode in a 0.1M acetonitrile solution of $TBABF_4$. (*) calibrated versus Ferrocene – Ferrocenium.

The oxidation potentials for ruthenium complexes appear as one electron reversible process in a range between 1.02 V and 1.23 V. By adding (py-tpy) and (tpy-ph-Br) ligands instead of the terpyridine group, the oxidation potential shift to less positive values compare with the prototype $[M(tpy)_2]^{2+}$.

For ruthenium complexes, the least positive potential has been observed for [Ru(tpy-ph-Br)(L3)(H_2O)], E = +1.02 V, followed by [Ru(py-tpy)(tpy-ph-Br)][PF_6]$_2$, with E = = + 1.04 V and [Ru(tpy)(tpy-ph-Br)][PF_6]$_2$ E = + 1.06 V. The terpyridine π^* levels are lower than those of the tetrazole based ligands. The metal based oxidation potential of the deprotonated complex is lower than that observed for the prototype. This is in agreement with the spectroscopic data and can be explained by the stronger σ – donor properties of the tetrazole group. The presence of strongly electron releasing groups results in a stabilisation of the

ruthenium (II) state and a shift of the oxidative process to less positive potential. The first reduction potentials for [Ru(tpy-ph-Br)(L3)(H_2O)], observed at - 1.21 V, is assigned as being tpy based. In the same way, electron-releasing substituents shift the reductive processes to more negative potentials, as observed for the ruthenium compounds. The redox potentials for the prototype $[Ru(tpy)_2]^{2+}$ appear at –1.25 V and –1.51 V, whereas all the ruthenium complexes show first redox potential between –1.31 V and – 1.57 V and the second redox potential between – 1.68 V and – 1.79 V.

Osmium complexes are oxidised at less positive potentials than the Ru(II) complexes, whereas the redox potentials did not show considerable differences. For osmium compounds the oxidation potentials are observed in a range between + 0.40 V and + 0.73 V, whereas the one electron ligand based reductions are observed between – 1.33 V and - 1.65 V for the first redox process and – 1.70 V and – 1.87 V for the second redox process. As already shown for ruthenium complexes, the least positive potential has been observed for [Os(tpy-ph-Br)(L3)(H_2O)], E = +1.02 V, followed by [Ru(py-tpy)(tpy-ph-Br)]$[PF_6]_2$, with E = =1.04 V and [Ru(tpy)(tpy-ph-Br)]$[PF_6]_2$ E = 1.06 V. This behaviour confirms what was anticipated at the beginning of this Section: the ground state of the mixed ligand complexes is destabilised with respect to the homoleptic tpy complexes. This results in a lowering of the metal based oxidation potential and raising the HOMO energy in comparison with the prototype parent. Another effect is the increase in back – bonding to the terpyridine ligand (t_{2g} π^*_{tpy}) and consequently lowering in the terpyridine based LUMO energy. A lowering in the HOMO – LUMO energy gap is observed as a lowering in the energy of the ^{3}MLCT emission.

6.3 Future work

The development of molecular wires or rods where photoactive and electroactive termini are linked by large size bridging molecular units may open new paths in the field of storage and utilisation of light energy[7-10]. In such types of molecular species, it should be possible to drive electrons and / or energy transfer processes

over nanometre distances by the use of light. An interesting continuation of this thesis may involve the preparation of systems containing two or three terpyridine complex units, linked by different spacers (for example phenyl group as shown in Figure 6.2). Combination of the metals ruthenium and osmium has already been investigated with a few interesting examples [11]. Energy and also electron transfer processes make such complex-arrays interesting for use as molecular wires. Starting from a dyad with directly connected terpyridines, various spacer groups may be introducing in the molecular system, allowing the photo-physical properties of the corresponding complexes to be fine-tuned. From the synthesis of ruthenium / osmium dyads, an energy transfer from the ruthenium to the osmium may be observed in the products and as a consequence luminescence may be enhance when compared the products to the homoleptic complexes. Adjustment and fine-tuning of the optical properties may be achieved by introducing donor or acceptor groups into the terminal ligands[12].

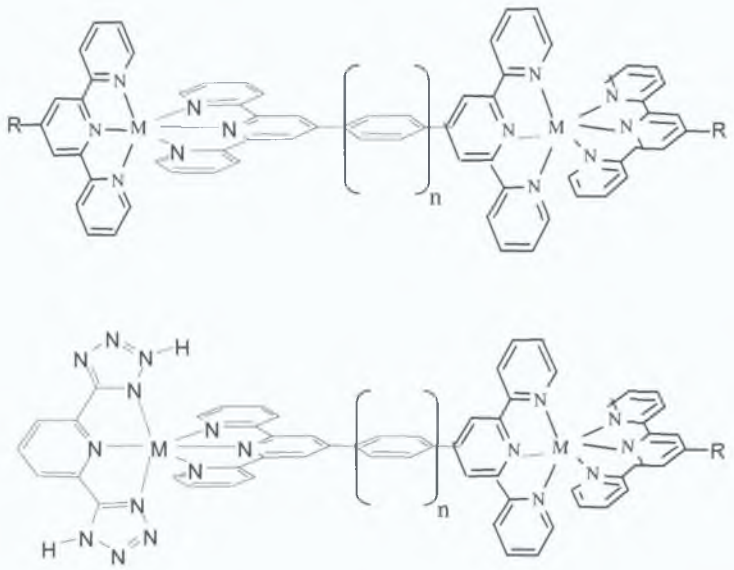

Figure 6.2: Example of possible homo or hetero-nuclear incorporating phenyl spacer (M = ruthenium or osmium, R = pyridine, phenyl-Br)

Multinuclear terpyridine complexes are promising compounds for future applications in optical nano-devices and solar cells. The field of devices and molecular switches, where electrochemical or optical activities may be switched simply and reversibly, are of special importance. Different approaches to tunable

metal complex arrays may include the incorporation of complexing moiety such as bipyridine within the bridging ligand or others aromatic groups as phenyl or thiophenes group as already observed[13], which has been found to act as an insulator in homometallic ruthenium systems.

6.4 Bibliography

[1] Hader, D.P., Tevini, M., General photobiology, *1987.*

[2] Amadelli, R., Argazzi R., Bignozzi C.A., Scandola, F., J. Am. Chem. Soc., *1990*, 112, 7099.

[3] Balzani, V., Scandola, F., Supramolecular Photochemistry, *1991*, 12.

[4] Bard, A.J., Rubinstein, I., Electroan. Chem. *1996*, 12, 109.

[5] Porter, M.D., Broght, T.B., Allara, D.L., Chisday, J. Am. Chem. Soc., *1987*, 109, 3559.

[6] Xu, J., Li, H., Zhang, Y., J. Phys.Chem., *1993*, 97, 11497.

[7] Mayer, T., J. Acc. Chem. Res., *1989*, 22, 163.

[8] Wasielewski, M.R., Chem. Rev., *1992*, 92, 435.

[9] Fox, M.A., Jones, W.E., Watkins, D.M., Chem. Eng. News, *1993*, 71, 38.

[10] Gust, D., Moore, T.A., Moore, A.L., Acc. Chem. Res., *1993*, 26, 198.

[11] Sauvage, J.P., Collin, J.C., Chambron, J.C., Guillerez, S., Coudret, C., Balzani, V., Barigelletti, F., De Cola, L., Flamigni, L., Chem. Rev., *1994*, 94, 993.

[12] Barigelletti, F., Flamigni, L., Balzani, V., Sauvage, J.P., Collin, J.C., Sour, A., Constable, E.C., Thompson, A.M.W.C., J. Am. Chem. Soc., *1994*, 116, 7692.

[13] Constable, E.C., Housecroft, C.E., Schofield, E., Encinas, S., Armaroli, N., Barigelletti, F., Flamigni, L., Figgemeier, E., Vos, J.G., Chem. Commun., *1999*, 869.

Time sheet. SUSANA Training Network.

Month……June……. Year 2005……

The researcher must indicate on what days he/she was present. Normal working hours are between 9.00 and 17.00 h. Indicate any significant deviations from this.

Day		day		day	
1	Present	12	Sunday	23	Susana Meeting
2	Present	13	Present	24	Susana Meeting
3	Present	14	Present	25	Susana Meeting
4	Saturday		Present	26	Sunday
5	Sunday	16	Present	27	Present
6	Present	17	Present	28	Present
7	Present	18	Saturday	29	Present
8	Present	19	Sunday	30	Present
9	Present	20	Present	31	Present
10	Present	21	Present		
11	Saturday	22	Susana Meeting Oporto		

Researcher; Stefania Tasca **Supervisor;Han Vos**

Signature; Stefania Tasca **Signature;**

Date; July 2005 **Date;July 2005**